



The  
University  
Of  
Sheffield.

## Investigation into the Use of Polypropylene in High Speed Sintering

**By:**

Luke M Fox

A thesis submitted in partial fulfilment of the requirements for the degree of  
Doctor of Philosophy

The University of Sheffield  
Faculty of Engineering  
Department of Mechanical Engineering

September 2018



## Acknowledgements

Firstly I would like to thank my supervisor Dr Candice Majewski for her continued guidance and help throughout this research and advising me in these early stages of my career. I also want to thank Professor Neil Hopkinson for his supervision and convincing me initially to carry out a PhD in Additive manufacturing.

I would like to thank PA Consulting and in particular Dr Simon Kew and Richard Claridge, my industrial supervisors for their guidance and input as well as being so accommodating during my placement at PA. Thank you to EPSRC and the Centre for Doctoral Training in Polymers Colloids and Soft Matters. Professor Steve Armes and Dr Joe Gaunt for the additional support that the CDT offers, extra training and widening my experiences across the university. The grind of the PhD wouldn't have been the same without all the CDT students especially the guinea pigs Amy, Dom, Kat, Matt and Ste.

Thanks to all those technical staff who have helped throughout my PhD and in particular Kurt Bonser and Wendy Birtwistle, without their extensive support this work wouldn't have been possible. I would like to thank everyone in the Garden Street building who have helped in countless ways be it in technical conversations or compiling biscuit top trumps. Many thanks to the friendship group I have gained from my PhD including Ryan Brown, Rhys Williams, Ryan Seabright, Ste Knox and Alex Sickleford, and to a great housemate Isobelle Logan. Thanks to all my friends further away for their constant assistance and a special thanks to Chris Hughes for accommodation and photography as well as the rapid proof reading of Luke Baker.

Final thanks to my parents and sister who without their support and encouragement none of this would be possible.



## Abstract

Additive Manufacturing (AM) is becoming increasingly popular for production of end-use parts, partly due to their potential for mass customisation as well as costs reducing, for production to be feasible. High Speed Sintering (HSS) is a polymer AM technique developed to provide the production speeds needed to compete with Injection Moulding. There is increasing interest in the use of HSS from Fast Moving Consumer Goods (FMCG) companies, but the current range of materials is unsuitable due to high costs and limited material properties. There is therefore a need to identify more suitable HSS materials for FMCGs, and this will be addressed in this research.

A comprehensive material selection process was carried out to identify possible materials for the use of FMCGs manufactured via HSS. Processing compatibility, chemical compatibility and cost were considered in order to identify the most suitable polymer for investigation. This selection process identified polypropylene (PP) as the most likely to be suitable for production of FMCGs through the HSS process; this material was therefore chosen for investigation in this thesis.

The ability to process three separate grades of PP in the HSS process was investigated here, in order to identify any factors which lead to differences in processability and properties of parts manufactured.

The three different grades of PP tested (CP22 PP, XX00199PP and AdSint PP) demonstrated different levels of processability, with the base material type and the presence of flow additives identified as key reasons for this. The best performing grade was found to have a significantly different melt temperature and crystallinity, which is likely due to the polymer being a copolymer polypropylene, and led to increased mechanical properties. The ability to reuse unsintered material from the build area was seen to be possible, with indications that the levels of reusability may be greater than those for other HSS materials.

Key processing parameters (bed temperature, grey level and sinter speed) were found to be critical in the processing of the PP powder into part. The range at which build bed temperature could be varied was found to be material-dependent, and fell within a small window. Increasing grey level was generally found to lead to poorer mechanical properties, and sinter speed was found to affect the mechanical properties of parts, but again this relationship was dependent on the material used.

AdSint PP has been identified as the best choice of material currently for the production of FMCGs via HSS, partly through its higher mechanical properties (Ultimate Tensile Strength of 23.39 MPa, Elongation at Break of 59.33 % and Young's Modulus of 977 MPa), and partly due to its greater ease of processing.

# Table of Contents

Acknowledgements.....	i
Abstract .....	iii
Table of Contents.....	iv
List of Figures.....	xiii
List of Tables .....	xx
Chapter 1 Introduction – Additive Manufacturing.....	1
<b>1.1 Benefits and limitations of AM.....</b>	<b>2</b>
<b>1.2 Applications .....</b>	<b>2</b>
<b>1.3 Application of Additive Manufacturing for Fast Moving Consumer Goods .....</b>	<b>6</b>
<b>1.4 Additive Manufacturing techniques .....</b>	<b>6</b>
1.4.1 Vat polymerisation .....	6
1.4.2 Material extrusion .....	7
1.4.3 Material jetting.....	8
1.4.4 Binder jetting.....	9
1.4.5 Powder bed fusion.....	10
Chapter 2 Polymer powder bed fusion and applicable literature .....	13
<b>2.1 Polymer powder bed fusion techniques .....</b>	<b>13</b>
2.1.1 Laser Sintering .....	13
2.1.2 High Speed Sintering .....	14
2.1.3 Multi Jet Fusion .....	15
2.1.4 Other polymer powder bed fusion systems .....	15
2.1.5 Post processing.....	15
<b>2.2 Energy input mechanisms .....</b>	<b>16</b>

<b>2.3 Effect of energy input .....</b>	<b>18</b>
2.3.1 Lamp power.....	18
2.3.2 Bed temperature .....	19
2.3.3 Ink in HSS .....	20
2.3.4 Part orientation .....	20
<b>2.4 Materials in HSS .....</b>	<b>21</b>
2.4.1 Processing materials in HSS.....	21
2.4.2 Overview of thermoplastics .....	21
2.4.3 Polyamides .....	22
2.4.4 Important material properties .....	24
2.4.5 Materials processed in powder bed fusion .....	26
<b>2.5 Key differences between HSS and LS .....</b>	<b>27</b>
<b>2.6 Summary .....</b>	<b>28</b>
 Chapter 3 Project rationale and definition of initial focus .....	 29
<b>3.1 Project rationale and research questions .....</b>	<b>29</b>
<b>3.2 Material compatibility .....</b>	<b>30</b>
3.2.1 Chemical incompatibilities .....	30
3.2.2 Processing incompatibilities .....	31
3.2.3 Application compatibility .....	31
3.2.4 Cost analysis .....	32
3.2.5 Summary of material compatibility.....	33
<b>3.3 Polyolefins .....</b>	<b>33</b>
<b>3.4 Polypropylene.....</b>	<b>34</b>
<b>3.5 Conclusions .....</b>	<b>36</b>
 Chapter 4 Processability of a commercial polypropylene grade.....	 37
<b>4.1 Characterisation of raw materials .....</b>	<b>37</b>
4.1.1 Powder flow .....	37

4.1.2 Particle size and morphology .....	40
4.1.3 Thermal properties.....	46
4.1.4 Powder characterisation summary .....	49
<b>4.2 Part manufacture via High Speed Sintering.....</b>	<b>49</b>
<b>4.3 Identification of initial processing parameters.....</b>	<b>51</b>
4.3.1 Preheat power .....	52
4.3.2 Sinter power .....	52
4.3.3 Preheat speed.....	52
4.3.4 Sinter speed.....	53
4.3.5 Grey level.....	53
4.3.6 Build bed temperature .....	53
<b>4.4 Effect of processing parameter variation .....</b>	<b>53</b>
4.4.1 Experimental rationale .....	54
4.4.2 Build bed temperature .....	54
4.4.3 Grey level.....	55
4.4.4 Sinter speed.....	56
4.4.5 Preheat power .....	57
<b>4.5 Characterisation of parts .....</b>	<b>58</b>
4.5.1 Part size .....	58
4.5.2 Part density.....	65
4.5.3 Tensile properties.....	67
4.5.4 Melt characteristics of parts.....	72
<b>4.6 Further discussion .....</b>	<b>73</b>
<b>4.7 Summary.....</b>	<b>76</b>
 Chapter 5 The effect of powder age in High Speed Sintering of polypropylene.....	 79
<b>5.1 Introduction .....</b>	<b>79</b>
<b>5.2 Part manufacture via High Speed Sintering.....</b>	<b>79</b>
<b>5.3 Powder characterisation.....</b>	<b>81</b>

5.3.1 Powder flow .....	81
5.3.2 Particle size and morphology .....	83
5.3.3 Chemical and thermal properties.....	90
5.3.4 Powder characterisation summary .....	98
<b>5.4 Characterisation of parts .....</b>	<b>98</b>
5.4.1 Part size .....	98
5.4.2 Part density.....	99
5.4.3 Tensile properties.....	100
<b>5.5 Further discussion .....</b>	<b>101</b>
<b>5.6 Conclusions .....</b>	<b>103</b>
 Chapter 6 Processability of alternative polypropylene grade XX00199PP (pre-commercial) ...	105
 <b>6.1 Introduction .....</b>	<b>105</b>
 <b>6.2 Characterisation of raw materials .....</b>	<b>105</b>
6.2.1 Powder flow .....	105
6.2.2 Particle size and morphology .....	106
6.2.3 Thermal properties.....	108
 <b>6.3 Part manufacture via High Speed Sintering .....</b>	<b>110</b>
 <b>6.4 Identification of initial processing parameters.....</b>	<b>110</b>
6.4.1 Build bed temperature .....	111
6.4.2 Preheat power.....	112
6.4.3 Sinter power .....	112
6.4.4 Preheat speed.....	112
6.4.5 Sinter speed.....	112
6.4.6 Grey level.....	112
 <b>6.5 Effect of processing parameter variation.....</b>	<b>112</b>
6.5.1 Build bed temperature .....	113
6.5.2 Grey level.....	114
6.5.3 Sinter speed.....	115
6.5.4 Preheat power.....	115

6.5.5 Summary of the effect of processing parameter variation .....	115
<b>6.6 Part characterisation .....</b>	<b>116</b>
6.6.1 Part size .....	116
6.6.2 Part density.....	119
6.6.3 Tensile properties.....	121
<b>6.7 Further discussion .....</b>	<b>124</b>
<b>6.8 Conclusions .....</b>	<b>126</b>
 Chapter 7 Processability of alternative polypropylene grade AdSint (commercial) .....	 129
<b>7.1 Introduction .....</b>	<b>129</b>
<b>7.2 Characterisation of raw materials .....</b>	<b>129</b>
7.2.1 Powder flow.....	129
7.2.2 Particle size and morphology .....	129
7.2.3 Thermal properties.....	132
<b>7.3 Part manufacture via High Speed Sintering.....</b>	<b>135</b>
<b>7.4 Identification of initial processing parameters.....</b>	<b>135</b>
7.4.1 Build bed temperature .....	136
7.4.2 Preheat power .....	136
7.4.3 Sinter power .....	136
7.4.4 Preheat speed.....	136
7.4.5 Sinter speed.....	136
7.4.6 Grey level.....	136
<b>7.5 Effect of processing parameter variation .....</b>	<b>137</b>
7.5.1 Build bed temperature .....	137
7.5.2 Grey level.....	138
7.5.3 Sinter speed.....	139
7.5.4 Preheat power .....	139
7.5.5 Summary of the effect of processing parameter variation .....	140
<b>7.6 Characterisation of parts .....</b>	<b>141</b>

7.6.1 Part size .....	141
7.6.2 Part density.....	145
7.6.3 Tensile properties.....	148
7.6.4 Melt characteristics of parts.....	152
<b>7.7 Further discussion .....</b>	<b>156</b>
<b>7.8 Conclusions.....</b>	<b>158</b>
 Chapter 8 Discussion.....	 159
<b>8.1 Introduction.....</b>	<b>159</b>
<b>8.2 Ease of processing .....</b>	<b>159</b>
8.2.1 Thermal properties.....	159
8.2.2 Flow agent.....	160
<b>8.3 Mechanical properties of parts .....</b>	<b>167</b>
8.3.1 Part density.....	169
8.3.2 Elongation at Break .....	170
8.3.3 Ultimate Tensile Strength.....	172
8.3.4 Young's Modulus .....	173
<b>8.4 Effect of build parameters .....</b>	<b>174</b>
8.4.1 Build bed and overhead temperature.....	174
8.4.2 Grey level.....	175
8.4.3 Sinter speed.....	176
8.4.4 Preheat power.....	177
 Chapter 9 Conclusions and further work.....	 179
<b>9.1 Conclusions.....</b>	<b>179</b>
<b>9.2 Recommendations for future work .....</b>	<b>181</b>

Chapter 10 References.....185

Chapter 11 Appendix A .....191

## List of Abbreviations

3DP	Three dimensional printing
AM	Additive Manufacturing
ANOVA	Analysis Of Variance
AR	Aspect Ratio
CDLP	Continuous Digital Light Processing
CE Diameter	Circle Equivalent Diameter
CNC	Computer numerical control
COD	Coefficient of determination
$\bar{D}$	Dispersity
DLP	Digital Light Processing
DoE	Design of Experiment
DSC	Differential Scanning Calorimetry
EaB	Elongation at Break
EBM	Electron Beam Melting
ED	Energy density
EMR	Energy Melt Ratio
FDM	Fused Deposition Modelling
FMCGs	Fast Moving Consumer Goods
GPC	Gel Permeation Chromatography
HS Circularity	High Sensitivity Diameter
HSS	High Speed Sintering
IR	Infrared
LS	Laser Sintering
mg	Milligram
MJF	Multi Jet Fusion
mm	millimetre
$M_n$	Number average molecular weight
$M_w$	Weight average molecular weight
$N_2$	Nitrogen
NIR	Near-infrared
PA	Polyamide
PBF	Powder bed fusion
PE	Polyethylene
POM	Polyoxymethylene
PP	Polypropylene
s	seconds
SEM	Scanning Electron Microscopy
SD	Standard Deviation
SHS	Selective Heat Sintering
SIS	Selective Inhibition Sintering
SL	StereoLithography
SLA	StereoLithography Apparatus
SMS	Selective Mask Sintering
STL	Stereolithography (file format)

$T_g$	Glass transition temperature
TGA	Thermogravimetric analysis
$T_m$	Melt temperature
$T_r$	Recrystallisation temperature
UHMWPE	Ultra high molecular weight polyethylene
UTS	Ultimate Tensile Strength
UV	Ultraviolet
YM	Young's Modulus
$\Delta H$	Enthalpy
$\mu m$	Micron

## List of Figures

Figure 1.1 Pie chart describing the use of AM parts in industry, reproduced using the data from Wohlers Report 2017 (3).	1
Figure 1.2 An articulated AM textile, showing the impact (left) and the damage (right) of a scaled Laser Sintered textile (6).	3
Figure 1.3 Car door handle made from a single AM part (7).	3
Figure 1.4 Image of a GE LEAP jet engine fuel nozzle, which is manufactured using AM as a single part (10).	4
Figure 1.5 Futurecraft 4D shoe, which features a AM midsole made using a vat polymerisation technique by Carbon (11).	5
Figure 1.6 Examples of the customisation of Mini parts using the 'Mini Yours' service, which are manufactured using AM (12).	5
Figure 1.7 Diagram of the general vat polymerisation process where a layer of resin is cured and the process is repeated until a part is manufactured (15).	7
Figure 1.8 Diagram of the fuse deposition modelling process, where a head extrudes polymer onto the build platform to form a part (15).	8
Figure 1.9 A diagram of the material jetting process, where inkjet printheads are used to print both material for the part and support structure, these are then typically cured by a UV light source (15).	9
Figure 1.10 A diagram of the binder jetting process, where a binder liquid is printed onto the powder bed to stick the powder particles together for a single layer, this is repeated to form a part (15).	10
Figure 2.1 A representation of the LS process where a layer of powder is deposited onto the build area and then sintered by an energy source, in the case of LS this is a laser (15).	13
Figure 2.2 A diagram of the High Speed Sintering process. <b>A.</b> A powder layer is deposited on the build bed. <b>B.</b> An infrared absorbing ink is deposited selectively. <b>C.</b> An infrared lamp is used to heat the ink deposited and this causes the powder where the ink is printed to sinter creating a layer of sintered part. This process ( <b>A-C</b> ) is then repeated to produce a 3D printed part (15).	14
Figure 2.3 Modelling of the Frenkel-Eshelby model, where $a_0$ is the initial radius and $a_f$ is the final radius and $x$ is the neck radius [2].	17
Figure 2.4 Comparison between <b>(A)</b> an amorphous polymer and <b>(B)</b> a semi-crystalline polymer with crystalline and amorphous regions (64).	22
Figure 2.5 Pie chart showing the number of different LS materials available, adapted from (66), where the percentage is the number of purchasable grades of material for LS.	23
Figure 2.6. DSC trace of Nylon 12; temperature scan at 10 °C / min.	24
Figure 2.7 Image of a part, where the 'orange peel' effect is visible.	26

Figure 3.1 Flow chart showing the experimental process steps carried out for the research in this thesis.....	30
Figure 3.2 Energy trace showing the spectral output of an IR lamp used in HSS.....	31
Figure 3.3. Chart showing cost of polymer for each class of polymer with an overlaid scatter graph for the price of each specific polymer. A dotted line at 10 £ / kg is overlaid.....	32
Figure 3.4. Scatter graph showing the cost of various polymers, with red signifying polymers eliminated due to cost, yellow showing incompatibilities from process or chemical properties, blue showing polymers not suited to FMCG's, black other and green denoting polymers which can be used in the HSS process.....	33
Figure 4.1 Apparatus to measure tapped density, designed by Geca(99). The cogs lead to one rotation of the gear to lead to five taps of the density cup. ....	38
Figure 4.2 A photograph showing the equipment used to measure powder flow of CP22 PP and PA 2200 as a reference. ....	39
Figure 4.3. Elution time for powders to flow through the funnel. The error bars included are range bars. ....	40
Figure 4.4. Volume distribution against size trace showing the volumetric size distribution of PP CP 22. ....	42
Figure 4.5 Image analysis traces showing size and shape of the CP22 PP powder. (A) Circle equivalent diameter against the number distribution of powder particles. (B) Circle equivalent diameter against the volume distribution of powder particles. (C) Convexity against fraction of powder particles. (D) High sensitivity circularity against fraction of powder particles. (E) Aspect ratio against fraction of powder particles.....	44
Figure 4.6. SEM of virgin CP22 PP (A&B) used high and low magnification respectively. ....	45
Figure 4.7 Optical microscopy images of CP22 PP (A&B) using high and low magnification respectively, with the highlighted red circles showing likely glass spheres used as flow additives.....	46
Figure 4.8. DSC trace of Nylon 12; temperature scan at 10 °C / min. ....	47
Figure 4.9. DSC curve of virgin PP; temperature scan at 10 °C/min.....	48
Figure 4.10 Image showing build layout in Rapix3D from a top view showing the x and y direction..	50
Figure 4.11 Photo of parts manufactured using CP22 PP as a feedstock in HSS.....	51
Figure 4.12 Representation of a tensile test piece and rectangular block used for density calculations and labelling of the dimensions measured. ....	59
Figure 4.13 Diagram showing the effect of shrinkage and wall growth, the values of 10% shrinkage and 1 mm wall growth are arbitrary and the diagram is not to scale. The diagram demonstrates shrinkage has a larger effect on big dimensions but wall growth has more of an effect on small dimensions...	60

Figure 4.14 Plot of measured size against theoretical size against of **G3S3P4a** specimen 1, with a linear fit, the values plotted are of the overall length, tab width and gauge width. .... 61

Figure 4.15 A graph showing the effect of grey level on wall growth and shrinkage. The error bars included are range bars..... 62

Figure 4.16 A graph showing the effect of sinter speed on wall growth and shrinkage. The error bars include are range bars..... 63

Figure 4.17 A graph showing the effect of preheat power on wall growth and shrinkage. The error bars included are range bars..... 64

Figure 4.18 The effect of grey level on the density of parts. The error bars included are range bars. 65

Figure 4.19 The effect of sinter speed on the density of HSS parts. The error bars included are range bars. .... 66

Figure 4.20 The effect of preheat power on the density of HSS parts. The error bars included are range bars. .... 66

Figure 4.21 Stress strain curve of one tensile specimen in build **G3S3P4c**..... 68

Figure 4.22 The effect of grey level on tensile properties (UTS, EaB and YM). The error bars included are range bars..... 69

Figure 4.23 The effect of sinter speed on tensile properties (UTS, EaB and YM). The error bars included are range bars..... 70

Figure 4.24 The effect of preheat power on tensile properties (UTS, EaB and YM). The error bars included are range bars..... 71

Figure 4.25 Thermogravimetric Analysis trace of CP22 PP powder..... 72

Figure 4.26 DSC trace of part in G3S3P4C build..... 73

Figure 5.1 Flow chart demonstrating the process of powder age in HSS. .... 80

Figure 5.2 The effect of powder ageing on the bulk tapped density of CP22 PP powder. The error bars included are range bars..... 82

Figure 5.3 The effect of powder age on the flowability of CP22 PP powder. The error bars included are range bars..... 82

Figure 5.4 Particle size trace of aged PP powders from laser diffraction. .... 84

Figure 5.5 Particle size of ageing PP powders portrayed by the D(10), D(50) and D(90) of each powder. The error bars included are range bars..... 85

Figure 5.6 Image analysis traces showing size and shape of the various ages of CP22 PP powder. **(A)** Circle equivalent diameter against the number distribution of powder particles. **(B)** Circle equivalent diameter against the volume distribution of powder particles. **(C)** Convexity against fraction of powder

particles. <b>(D)</b> High sensitivity circularity against fraction of powder particles. <b>(E)</b> Aspect ratio against fraction of powder particles.....	89
Figure 5.7 The effect of powder age in PP powders on number average molecular weight, weight average molecular weight and dispersity.....	91
Figure 5.8 The chemical structure of A. polypropylene and B. Nylon 12. ....	91
Figure 5.9 Example of onset temperature (°C) and percentage residual for virgin CP22 PP. ....	93
Figure 5.10 The effect of powder age on decomposition temperature and residual mass. The error bars included are range bars. ....	94
Figure 5.11 DSC trace of virgin PP showing the 1st and 2nd heat and 1st cool cycle. ....	96
Figure 5.12 Melt and recrystallisation temperatures of various aged PP powders. ....	97
Figure 5.13 Melt and recrystallisation enthalpies of various aged PP powders. ....	97
Figure 5.14 The effect of powder age on shrinkage and wall growth of HSS PP parts. The error bars included are range bars. ....	99
Figure 5.15 The effect of powder age on part density. The error bars included are range bars. ....	100
Figure 5.16 The effect of powder age on tensile properties including; UTS, EaB and YM. The error bars included are range bars. ....	101
Figure 6.1 Mastersizer trace of XX00199PP. ....	106
Figure 6.2 Image analysis traces showing size and shape of the CP22 PP powder. <b>(A)</b> Circle equivalent diameter against the number distribution of powder particles. <b>(B)</b> Circle equivalent diameter against the volume distribution of powder particles. <b>(C)</b> Convexity against fraction of powder particles. <b>(D)</b> High sensitivity circularity against fraction of powder particles. <b>(E)</b> Aspect ratio against fraction of powder particles.....	107
Figure 6.3 SEM of XX00199PP (A&B) used high and low magnification respectively. ....	108
Figure 6.4 DSC curve of XX00199PP; temperature scan at 10 °C/min. ....	109
Figure 6.5 Thermogravimetric Analysis trace of XX00199PP powder. ....	110
Figure 6.6 The effect of bed temperature on shrinkage and wall growth on XX00199PP parts. The error bars included are range bars. ....	117
Figure 6.7 The effect of grey level on shrinkage and wall growth on XX00199PP parts. The error bars included are range bars. ....	118
Figure 6.8 The effect of sinter speed on shrinkage and wall growth on XX00199PP parts. The error bars included are range bars. ....	119
Figure 6.9 The effect of build bed temperature on part density of XX00199PP parts. The error bars included are range bars. ....	120

Figure 6.10 The effect of grey level on part density of XX00199PP parts. The error bars included are range bars..... 120

Figure 6.11 The effect of sinter speed on part density of XX00199PP parts. The error bars included are range bars..... 121

Figure 6.12 The effect of build bed temperature on the mechanical properties of HSS parts using XX00199PP as the powder feedstock. The error bars included are range bars..... 122

Figure 6.13 The effect of grey level on the mechanical properties of XX00199PP parts manufactured via HSS. The error bars included are range bars. .... 123

Figure 6.14 The effect of sinter speed on the mechanical properties of parts manufactured using XX00199PP via HSS. The error bars included are range bars. .... 124

Figure 7.1 Mastersizer trace of AdSint PP. .... 130

Figure 7.2 Image analysis traces showing size and shape of the CP22 PP powder. (A) Circle equivalent diameter against the number distribution of powder particles. (B) Circle equivalent diameter against the volume distribution of powder particles. (C) Convexity against fraction of powder particles. (D) High sensitivity circularity against fraction of powder particles. (E) Aspect ratio against fraction of powder particles..... 131

Figure 7.3 SEM images of AdSint PP (A&B), using high and low magnification respectively..... 132

Figure 7.4 DSC curve of AdSint PP; temperature scan at 10 °C/min..... 133

Figure 7.5 Thermogravimetric Analysis trace of AdSint PP powder..... 134

Figure 7.6 Photo of parts using AdSint PP in HSS..... 135

Figure 7.7 The effect of build bed temperature on shrinkage and wall growth of AdSint PP parts. The error bars included are range bars..... 142

Figure 7.8 The effect of grey level on shrinkage and wall growth of AdSint PP parts. The error bars included are range bars..... 143

Figure 7.9 The effect of sinter speed on the shrinkage and wall growth of AdSint PP parts. The error bars included are range bars..... 144

Figure 7.10 The effect of preheat power on the shrinkage and wall growth of AdSint PP parts. The error bars included are range bars..... 145

Figure 7.11 The effect of build bed temperature on part density of AdSint PP parts. The error bars included are range bars..... 146

Figure 7.12 The effect of grey level on the part density of AdSint PP parts. The error bars included are range bars..... 146

Figure 7.13 The effect of sinter speed on part density of AdSint PP parts. The error bars included are range bars..... 147

Figure 7.14 The effect of preheat power on part density of AdSint PP parts. The error bars included are range bars.....	147
Figure 7.15 Stress strain curve of one tensile specimen in build <b>B3G2S3P4a</b> . .....	148
Figure 7.16 The effect of build bed temperature on the mechanical properties of HSS parts using AdSint PP as the powder feedstock. The error bars included are range bars. ....	149
Figure 7.17 The effect of grey level on the mechanical properties of HSS parts using AdSint PP as a powder feedstock. The error bars included are range bars. ....	150
Figure 7.18 The effect of sinter speed on the mechanical properties of parts manufactured using AdSint PP as a powder feedstock for HSS. The error bars included are range bars.....	151
Figure 7.19 The effect of preheat power on the mechanical properties of AdSint PP parts manufactured using HSS. The error bars included are range bars.....	152
Figure 7.20 Graph showing the melt and recrystallisation temperatures and enthalpies of AdSint PP parts compared to bed temperature. ....	153
Figure 7.21 Graph showing the melt and recrystallisation temperatures and enthalpies of AdSint PP parts compared to grey level.....	153
Figure 7.22 Graph showing the melt and recrystallisation temperatures and enthalpies of AdSint PP parts compared to sinter speed. ....	154
Figure 7.23 Graph showing the melt and recrystallisation temperatures and enthalpies of AdSint PP parts compared to preheat power. ....	154
Figure 7.24 Hollow bottle manufactured using AdSint PP in HSS. ....	155
Figure 7.25 Lattice structure manufactured using HSS using AdSint PP as a powder feedstock.....	156
Figure 8.1 Image analysis traces showing size and shape of the CP22 PP, XX0199PP and AdSint PP powder to allow comparison. (A) Circle equivalent diameter against the number distribution of powder particles. (B) Circle equivalent diameter against the volume distribution of powder particles. (C) Convexity against fraction of powder particles. (D) High sensitivity circularity against fraction of powder particles. (E) Aspect ratio against fraction of powder particles.....	164
Figure 8.2 TGA results of the PP powders, showing decomposition onset temperature and residual mass. The error bars included are range bars. ....	166
Figure 8.3 Summary of the UTS and EaB of parts manufactured using different PP powders. The error bars included are range bars. ....	167
Figure 8.4 Summary of the YM and Apparent density of parts manufactured using different polymer powder feedstocks. The error bars included are range bars. ....	168
Figure 8.5 Tapped bulk density of CP22 PP, XX00199PP and AdSint PP. The error bars included are range bars.....	169

Figure 8.6 Relationship of enthalpy of melting against the EaB of parts manufactured using CP22 PP. .....	171
Figure 8.7 Relationship of enthalpy of melting against the EaB of parts manufactured using AdSint PP. .....	172
Figure 8.8 Relationship of enthalpy of melting against the UTS of parts manufactured using CP22 PP and AdSint PP. ....	173
Figure 8.9 Relationship of enthalpy of melting against YM of parts manufactured using CP22 PP and AdSint PP. ....	174

## List of Tables

Table 3.1 Mechanical properties of IM PP, data from Polymer Handbook (82, 94). .....	34
Table 4.1 Tapped bulk density of CP22 PP and PA2200 for each run and averages. Standard deviation is shown in brackets. ....	38
Table 4.2. Particle size breakdown of CP22 PP and Nylon 12. ....	41
Table 4.3 Parameters measured by image analysis and their descriptions and equations (109).....	43
Table 4.4 High Speed Sintering parameters. ....	52
Table 4.5 Build classifications and the explanation of the terms used, where the builds classified by the first two terms were then further tested. Compared to the other build classifications which were described and could not be further tested. ....	53
Table 4.6 Build parameters where build bed and overhead temperature was varied. ....	55
Table 4.7 Grey level to ink conversion. ....	55
Table 4.8 Build parameters where grey level was varied.....	56
Table 4.9 Build parameters where sinter speed was varied. ....	56
Table 4.10 Build parameters where preheat power was varied. ....	57
Table 4.11 Summary table of builds attempted, with build parameters with build name. <b>G</b> indicates the grey level, <b>S</b> sinter speed where lower <b>S</b> value indicates a higher speed and therefore less energy input and <b>P</b> the preheat power. Small letters indicate repeat at same parameter set and capitals are used where bed and overhead temperature are non-standard. Cells highlighted are the centre point repeats used. ....	58
Table 4.12 One way analysis of variance the effect of various parameters on tensile properties and shrinkage and wall growth. The result of the ANOVA is shown with tests which should significance highlighted in green and then followed by post-hoc tests to demonstrate which data sets were significantly different from each other. The numbers in the table signify the two levels of parameters examined, e.g. in grey level shrinkage 2 1 is the comparison between the data for the grey level 1 compared to the data for grey level 2.....	75
Table 5.1 Machine parameters used for the production of parts to assess the effect of powder age. ....	80
Table 5.2 The powder age of builds and the successfulness of builds at different powder ages. ....	81
Table 5.3 Particle size breakdown of different powder ages of PP. ....	84
Table 5.4 Parameters measured by image analysis and their descriptions and equations (109).....	86
Table 5.5 Parameters measured by Gel Permeation Chromatography to define molecular weight, where $M_i$ is the molecular weight of a polymer chain and $N_i$ is the number of chains of that molecular	

weight.  $M_w$  is reported as a small number of small polymer chains can have a large effect on  $M_n$  although little to no effect on the properties measured of the polymer. .... 90

Table 5.6  $M_w$ ,  $M_n$  and  $\bar{D}$  of CP22 PP powders at various powder ages. .... 90

Table 5.7 One way analysis of variance the effect of powder age on tensile properties and shrinkage and wall growth. The result of the ANOVA is shown with tests which should significance highlighted in green and then followed by post-hoc tests to demonstrate which data sets were significantly different from each other. The numbers in the table signify the two levels of parameters examined, e.g. 1U V is the comparison between powder of virgin age compared to powder of used 1 age..... 102

Table 6.1 Tapped bulk density of XX00199PP for each run and average. Standard deviation is shown in brackets. .... 105

Table 6.2 Particle size breakdown of XX00199PP. .... 106

Table 6.3 TGA results for XX00199PP including; onset temperature and residual mass. Standard deviation is shown in brackets. .... 110

Table 6.4 High Speed Sintering parameters for the attempted processing of XX00199PP. .... 111

Table 6.5 Parameter set attempted to process XX00199PP which had previously manufactured CP22 PP powder into HSS parts..... 111

Table 6.6 Build classifications and the explanation of the terms used, where the builds classified by the first two terms were then further tested. Compared to the other build classifications which were described and could not be further tested. .... 113

Table 6.7 Build parameters where build bed and overhead temperature was varied. The builds highlighted are those used for comparison of build bed temperature. .... 114

Table 6.8 Build parameters where grey level was varied. .... 114

Table 6.9 Build parameters where sinter speed was varied. The builds highlighted are those which parts were used for the comparison of sinter speed. .... 115

Table 6.10 Summary table of builds attempted, with build parameters with build name. **B** indicates the build bed temperature, **G** the grey level, **S** sinter speed where lower **S** value indicates a higher speed and therefore less energy input and **P** the preheat power. Small letters indicate repeat at same parameter set and capitals are used where bed and overhead temperature are non-standard..... 116

Table 6.11 One way analysis of variance the effect of various parameters on tensile properties and shrinkage and wall growth. The result of the ANOVA is shown with tests which should significance highlighted in green and then followed by post-hoc tests to demonstrate which data sets were significantly different from each other. The numbers in the table signify the two levels of parameters examined, e.g. in build bed temperature shrinkage 135 130 is the comparison between the data for the build bed temperature at 130 °C compared to the data for build bed temperature at 135 °C. . 125

Table 7.1 Tapped bulk density of AdSint PP for each run and average.....	129
Table 7.2 Particle size breakdown of AdSint PP. ....	130
Table 7.3 TGA results for AdSint PP, including; decomposition onset temperature and residual mass percentage.....	134
Table 7.4 High Speed Sintering parameters for the attempted processing of AdSint PP. ....	135
Table 7.5 Build classifications and the explanation of the terms used, where the builds classified by the first two terms were then further tested. Compared to the other build classifications which were described and could not be further tested. ....	137
Table 7.6 Build parameters where build bed and overhead temperature was varied. The builds highlighted are those used for comparison of build bed temperature.....	138
Table 7.7 Build parameters where grey level was varied.....	138
Table 7.8 Build parameters where sinter speed was varied. The naming notation <b>S1</b> is the fastest sinter speed and hence the least input energy from the sinter lamp in accordance with the other naming notations.....	139
Table 7.9 Build parameters where the preheat power was varied.....	140
Table 7.10 Summary table of builds attempted, with build parameters with build name. <b>B</b> indicates the build bed and overhead temperature, <b>G</b> indicates the grey level, <b>S</b> sinter speed where lower <b>S</b> value indicates a higher speed and therefore less energy input and <b>P</b> the preheat power. Small letters indicate repeat at same parameter set. Cells highlighted are the centre point repeats used. ....	141
Table 7.11 One way analysis of variance the effect of various parameters on tensile properties and shrinkage and wall growth. The result of the ANOVA is shown with tests which should significance highlighted in green and then followed by post-hoc tests to demonstrate which data sets were significantly different from each other. The numbers in the table signify the two levels of parameters examined, e.g. in build bed temperature shrinkage 114 112 is the comparison between the data for the build bed temperature at 114 °C compared to the data for build bed temperature at 112 °C. .	157
Table 8.1 Summary table of the melt and recrystallisation temperatures and enthalpies of the PP powders tested.....	159
Table 8.2 Particle size and shape information for the three PP powders tested.....	161
Table 8.3 Builds used to compare general mechanical properties of parts manufactured using CP22 PP, XX00199PP and AdSint PP via HSS.....	167
Table 8.4 The highest properties achieved for the various powders selected from the build with the highest EaB (most significant for FMCGs).The standard deviation is shown in brackets. ....	168

Table 9.1 Mechanical properties of PP in different manufacturing techniques, data from Polymer Handbook (82, 94) for IM. The LS data is from Kleijnen et al.(111). The HSS data is from this thesis, standard deviations are shown for work carried out in this thesis..... 179

Table 11.1 A list of possible polymers for the use in HSS. Polymers identified by blue show a possibility to be used in HSS, polymers identified by yellow have a reason not to be used in HSS and this reason is highlighted in orange. Information collated from (82, 84). ..... 191



## Chapter 1 Introduction – Additive Manufacturing

Additive Manufacturing (AM) is defined as the process of joining materials to make objects from 3D model data, usually layer upon layer, as opposed to subtractive manufacturing methodologies' (1). AM includes several steps with the first being the use of a computer-aided design (CAD) model of the part which includes all the geometry. This file is converted into slices, and the part is then built in a layer by layer process by definition of a number of AM technologies. The part is then removed from the machine, at which point it may undergo post-processing techniques (2).

Additive Manufacturing can allow the manufacture of parts with high complexity, which would be of high cost, if not impossible, via a traditional manufacturing technique such as Computer Numerical Control (CNC) machining or injection moulding. To be able to build complicated parts via traditional techniques expensive tooling is often required, which is often the time limiting factor when undertaking design iterations. The expense of tooling led to one of the first industrial usages of AM, where AM was used to fabricate prototypes to allow rapid manufacture of sequential design iterations, which would not be possible via a method other than AM. However one of the main themes of the industry more recently is a drive towards manufacture of end use parts via AM. Currently 33.8 % of parts manufactured are for use as functional parts (3) rising from 29.0 % in 2015 (4) while the other uses for AM parts include visual aids, patterns and education and research, as shown in Figure 1.1.

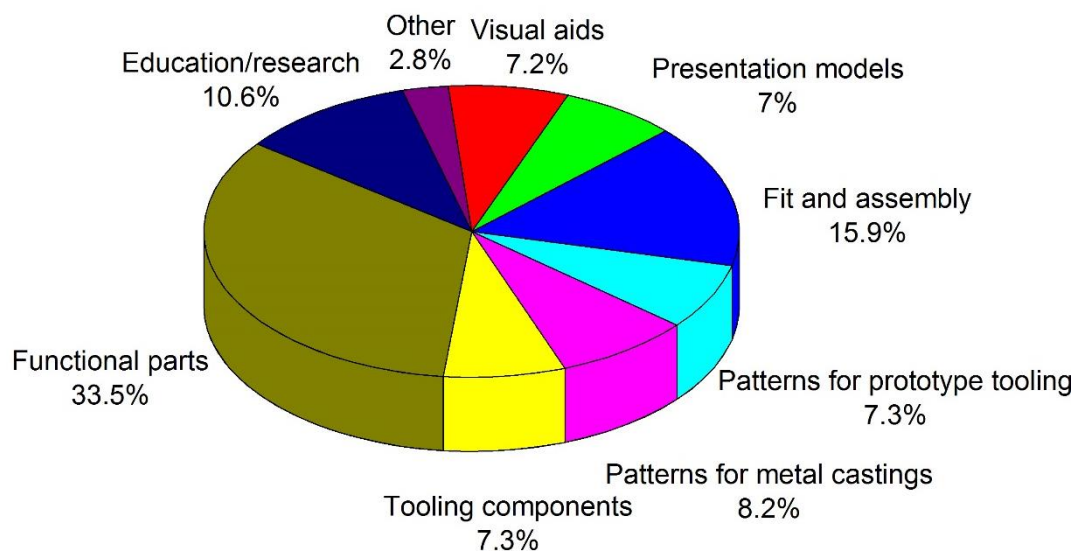


Figure 1.1 Pie chart describing the use of AM parts in industry, reproduced using the data from Wohlers Report 2017 (3).

## 1.1 Benefits and limitations of AM

AM is another manufacturing method with limitations as well as benefits in comparison to other manufacturing techniques. The key benefits of AM include:

- AM often allows complex geometries to be built which would not be possible with traditional techniques or cost of manufacture would prohibit the design
- Personalisation of parts is possible as the benefits of large mass production can be leveraged, with the ability to have each part different as no tooling is required to produce a specific part.
- Part consolidation allows the reduction of the number of parts used in a process, this can create several advantages. Many systems traditionally use several parts which are then assembled together, however AM allows a complex system to be built as a single part. The single part may increase cost, but will reduce weight and limit the number of failure points, which will in turn reduce the cost of the part and service in the long run.
- Supply chains can be redesigned to include: localised manufacture where parts are made at the location they are required and just in time production where the flexibility of AM allows the manufacture of parts when they are required and hence reducing the need for large warehouses for part or tool storage.

As with any group of technologies, there are also limitations, including:

- Material selection is currently a limitation in AM, this is due to the increased cost and restricted range in comparison to other manufacturing techniques.
- Integrity of parts is also a limitation where mechanical properties, anisotropy of parts, geometric accuracy and repeatability of production must be considered.
- Additive Manufacturing machines are often slow and build speed is reliant upon the amount of parts produced (although this is developing with new techniques). Build volume has also been low and alongside machine cost this has led to restrictions in the amount of parts that can be manufactured.
- Post processing is often required of AM parts which adds further time and cost to production in comparison to parts made via different techniques.

## 1.2 Applications

Additive manufacturing often requires different design approach in comparison to traditional techniques. AM textiles are a prime example of this where interlinking chains made of polymer can be manufactured, where the end purpose of the textiles can be for fashion or to take advantage of the mechanical properties of Nylon to manufacture stab-resistant vests (5, 6), as shown in Figure 1.2.

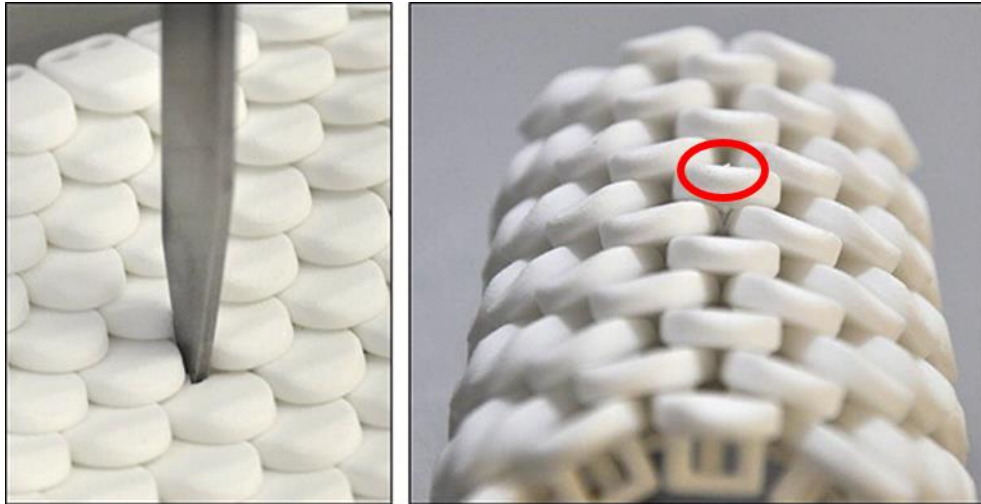


Figure 1.2 An articulated AM textile, showing the impact (left) and the damage (right) of a scaled Laser Sintered textile (6).

Additive manufacturing allows part consolidation, Hopkinson *et al.*(7) carried out research into using AM technology to produce a single part to replace an 11-piece assembly via traditional manufacturing techniques. The part studied was a car door handle as shown in Figure 1.3. This part although requiring post processing to remove excess powder from manufacture required no assembly.

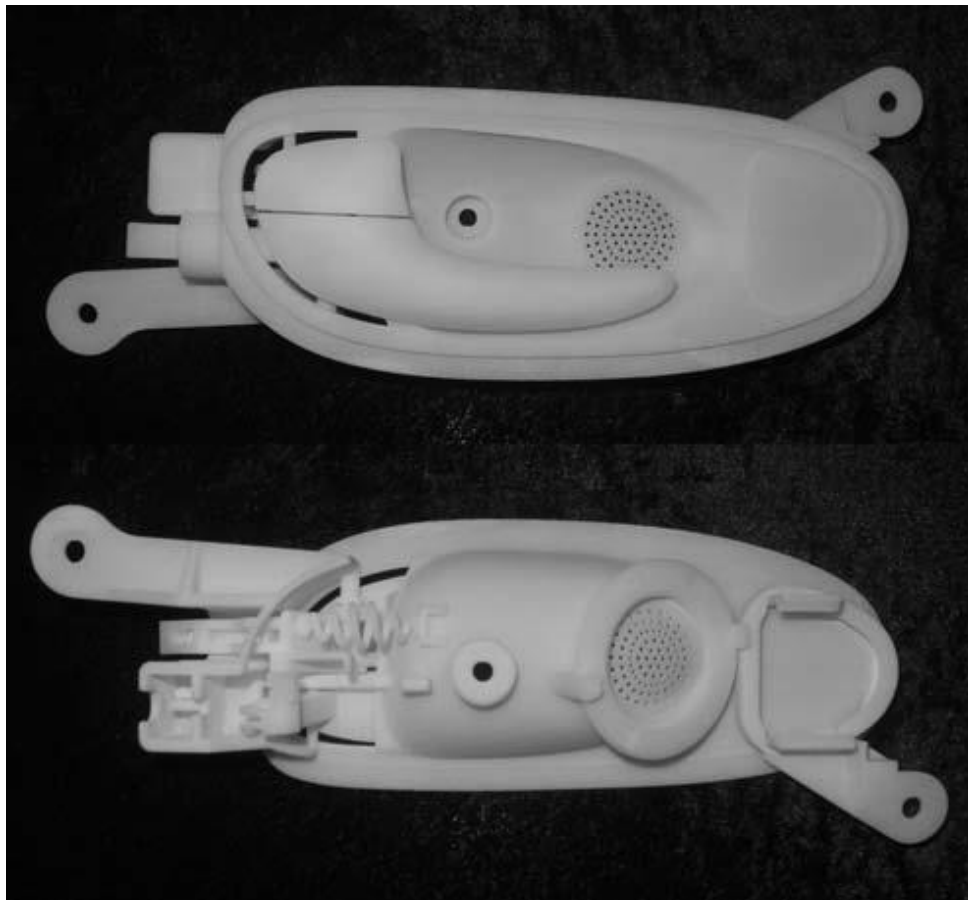


Figure 1.3 Car door handle made from a single AM part (7).

Khajavi *et al.* (8) studied the spare parts supply chain for the F-18 Super Hornet fighter jet in a comparison of current practice, which involves a centralised production versus decentralising production to on-demand part production at the location required. Although at the time of the study in 2013 it was identified that central production led to lower costs, but it was identified as AM machines become less capital intensive, quicker production cycles and more autonomous a distributed production system is more practical. Allowing the advantages of less transportation, inventory and obsolescence costs to be leveraged.

The first uses of AM in industrial applications were in prototyping and rapid tooling. However there is a large drive towards the use of AM in the production of end-use parts using the benefits of AM. Examples of AM being leveraged for the production of final parts are shown below.

Automotive companies such as Porsche are using AM in their classic cars spare part business (9) to produce spares for low production volume. The use of AM allows the production of parts without the storage or tool costs normally associated with parts on a very small production run.

GE have used metal AM to produce LEAP jet engine fuel nozzles (10), demonstrating several of the advantages of AM in the production of a part for end-use. These include: reduction of 20 parts to 1, 25 % in weight reduction and \$3 million saving in running costs per year for each plane. Other examples of metal AM for final parts are Johnson and Johnson using CT-scans to produce CAD files for the manufacture of facial implants.



*Figure 1.4 Image of a GE LEAP jet engine fuel nozzle, which is manufactured using AM as a single part (10).*

Polymer AM systems have been used widely in the production of soles for trainers. Adidas has partnered with Carbon to produce their Futurecraft 4D shoe with an AM midsole, see Figure 1.5, with the aim of 100,000 pairs manufactured by the end of 2018 (11). The midsole has a lattice structure and this structure would be very difficult to produce via a traditional manufacturing technique.

Although all of the soles currently manufactured have the same structure it is feasible and the aim of Adidas is to have mass customisable soles where the lattice is specific to the customer. Other sports manufacturers have used laser sintering, another polymer AM technique to produce soles for trainers, these include – Nike, Under Armour and New Balance.



*Figure 1.5 Futurecraft 4D shoe, which features a AM midsole made using a vat polymerisation technique by Carbon (11).*

BMW now offers a ‘Mini Yours’ service which allows a customer to personalise decorations for the Mini including interior trim and indicator inlays, see Figure 1.6 (12). AM allows the production of single customer parts which were not previously possible due to economies of scale adding unique value to the Mini in comparison to competition.



*Figure 1.6 Examples of the customisation of Mini parts using the 'Mini Yours' service, which are manufactured using AM (12).*

The drive from a large amount of companies manufacturing parts from aerospace components to consumer goods demonstrates the desire for end use AM parts. This brings various advantages including customisation, personalisation and cost reduction.

### 1.3 Application of Additive Manufacturing for Fast Moving Consumer Goods

Fast moving consumer goods (FMCGs) are inexpensive products that people usually purchase on a regular basis such as supermarket foods and toiletries (13). The sale of FMCGs is very competitive and hence packaging is an important sales technique. Therefore there is strong desire from FMCG manufactures to use AM to differentiate their products from competitors, leveraging the ability of AM to produce small runs and customisable packaging at little to no extra cost. Traditionally there is not much use of AM for the production of FMCGs, because of the need for low cost and high production volumes, but if these key aspects could be addressed there would be a large market for this.

This research will concentrate on the use of polymers. Polymers are widely used in the production of FMCGs due to the low-cost and ease of processing on high production volumes in comparison to equivalent materials such as metals.

### 1.4 Additive Manufacturing techniques

There are a wide range of AM technologies; those which can be used for the processing of polymers will be discussed below.

#### 1.4.1 Vat polymerisation

The first AM systems were available in 1987; these systems were Stereolithography Apparatus (SLA) from 3D Systems(14). Stereolithography (SL) works by using a UV-curable liquid resin in a tank which is exposed to a UV laser light source to selectively cure the resin and form a solid layer. The stage on which the first layer is cured on to is then moved away from the light source by the layer thickness specified in the build and fresh resin flows into the void which can then be cured by the light source. These steps are repeated until the part is manufactured, Figure 1.7 shows this general process. The materials used in SL are thermoset resins. The use of thermoset polymer allows advantages such as good temperature resistances and dimensional stability although has disadvantages including no ability to reshape and therefore cannot be recycled. The process may require addition of supports for some geometries and therefore often requires additional post processing to produce final parts. SL was the predominant AM process in the early years of the industry, and used in several areas including medical, electronics and automotive industries (4).

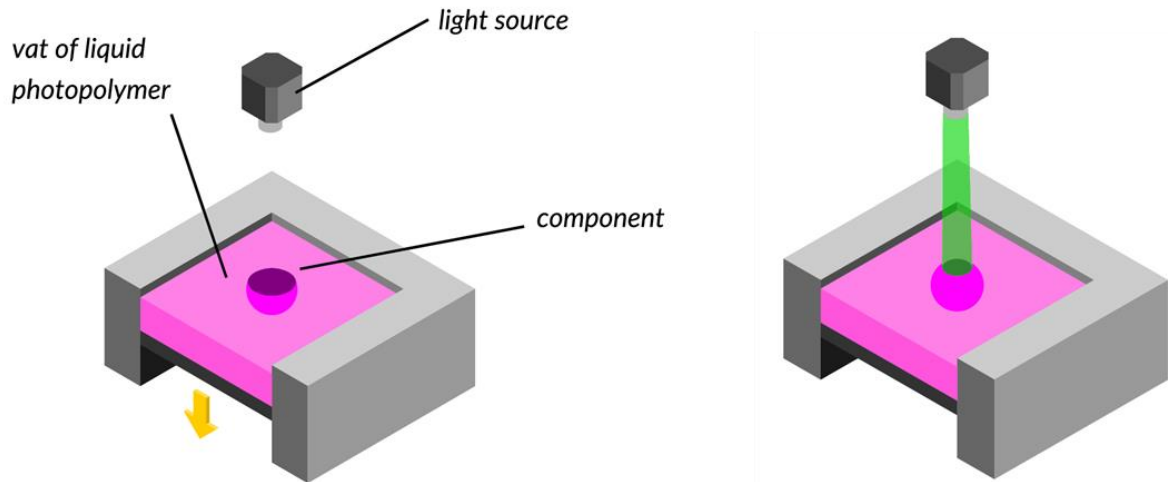


*Figure 1.7 Diagram of the general vat polymerisation process where a layer of resin is cured and the process is repeated until a part is manufactured (15).*

Newer vat polymerisation techniques include Digital Light Processing (DLP) where a projector-style unit is used to cure a single layer at once. These devices have been developed into bench-top devices, including machines by Formlabs (16). Carbon and EnvisionTEC have developed Continuous Digital Light Processing (CDLP) using an oxygen permeable membrane parts can be built continuously resulting in various advantages, especially with respect to build speed. This increase in speed has allowed the Carbon's CDLP to manufacture parts for production as demonstrated with the Adidas shoe sole discussed in Section 1.2. The development of these faster versions of SLA has led to lower cost and therefore more suitable for use in production.

#### 1.4.2 Material extrusion

Material extrusion was first developed by Stratasys, who introduced the first Fused Deposition Modelling system (FDM) in 1991(4). The systems work by extrusion of a spool of material through a heated extruder head and onto a build platform allowing material to build up on the bed to form the part. These systems were first aimed at the industrial market but were adapted for the hobbyist market before any other AM technique, with machines such as Makerbot and Lulzbot aimed at the amateur market (17).

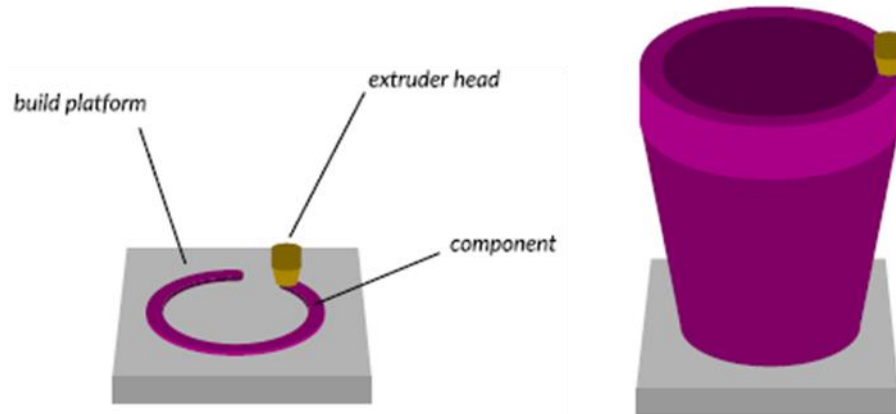


*Figure 1.8 Diagram of the fuse deposition modelling process, where a head extrudes polymer onto the build platform to form a part (15).*

With the capability of being office-friendly, a wide range of materials and machines including industrial-grade and home machines are some of the benefits of material extrusion machines. The ideal materials for FDM are amorphous thermoplastics (see 2.4.2), due to their ability to not undergo significant warpage when extruded. There are limitations to these techniques which include being slow for large cross-section parts, poor mechanical properties especially in the Z direction, requirement of supports and often a poor surface finish. FDM due to the speed caused by the process and the requirement of removing support for complicated structures, it is not suitable for mass production as slow speeds lead to high costs. Material extrusion parts are used in tooling(18), in space on the International Space Station(19) and other high-end applications.

### 1.4.3 Material jetting

In the material jetting process inkjet printheads are used to print down the droplets of the build material, as demonstrated by Figure 1.9. These materials are then typically cured by a UV light source.

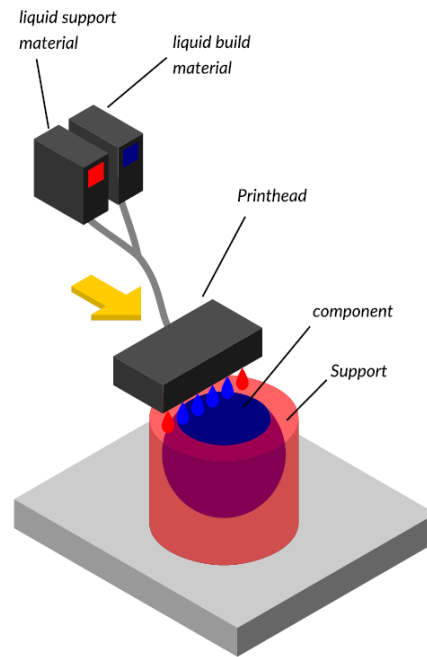


*Figure 1.9 A diagram of the material jetting process, where inkjet printheads are used to print both material for the part and support structure, these are then typically cured by a UV light source (15).*

Material jetting allows multi-material and full colour parts to be produced and can be relatively fast to produce a single part, however these resins machines are often expensive and the process is difficult to scale and hence slow for mass production. The materials used are too expensive for the use in production. Material jetting also requires supports for some complicated structures which increases material cost as well as the need for additional post-processing. Applications of material jetting include use in jewellery and dental patterns as well as prototyping due to full colour and material grading allows designers and consumers to feel and see what a final product may be.

#### 1.4.4 Binder jetting

Binder jetting involves printing down a binder to join the powder particles on the build bed. To form a single layer, new powder is then deposited on the build bed and the process is repeated until the part desired is manufactured. Similar to standard 2D printers a full colour model can be printed by using four different colour binders (cyan, magenta, yellow and clear). One type of binder jetting is three dimensional printing (3DP) and it was invented at MIT(20). The technology was licensed to several companies in different markets including Z-Corporation Inc. and ExOne(2). With Z-Corporation's machines using polymer based systems and ExOne's metal systems. In this context the polymer based systems will be discussed. The Z-Corporation machines manufacture parts designed for early concept models and product prototypes, due to poor mechanical properties. The lack of requirement for support for complicated designs as the powder acts as self-supporting is an advantage of this process compared to the other techniques discussed to this point.

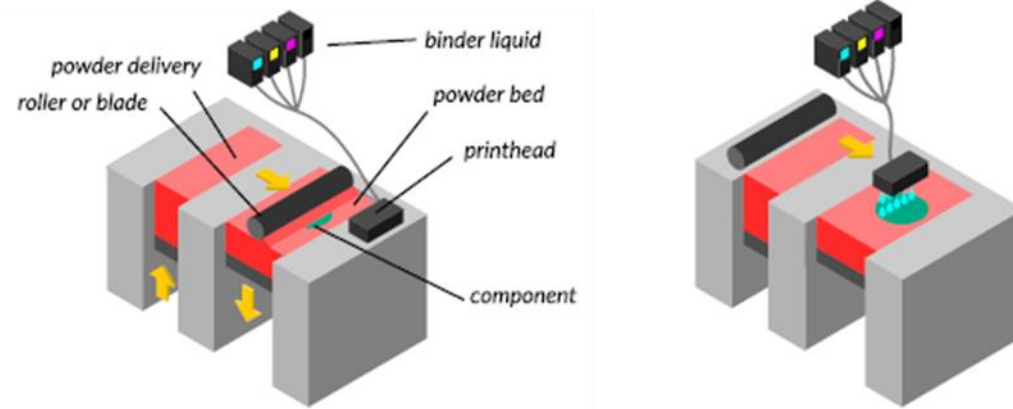


Figure 1.10 A diagram of the binder jetting process, where a binder liquid is printed onto the powder bed to stick the powder particles together for a single layer, this is repeated to form a part (15).

voxeljet's binder jetting systems print a solvent for the polymer powder (poly-(methyl methacrylate)) through a printhead to selectively bind the powder and build a part. These parts which can be up to 4000 x 2000 x 1000 mm, are relatively mechanically weak and therefore often used as moulds or patterns.

#### 1.4.5 Powder bed fusion

Powder bed fusion (PBF) processes work by selectively melting a layer of powder into the desired cross-section. While these can process a range of materials, polymer PBF processes are the focus here.

##### Polymer powder bed fusion systems

Polymer powder bed fusion systems along with binder jetting but unlike the majority of the other systems discussed do not require supports to build complex geometries. This is due to the unsintered polymer powder acting as support for the structure whilst building.

Polymer powder fusion systems use a thermoplastic polymer as the feedstock, the number of polymers available however is limited and this will be discussed further in Section 2.4. The polymer powder is sintered using heat energy to form parts.

The fastest production speeds per part for AM can be achieved through polymer PBF, this makes PBF techniques the most attractive for FMCGs. A study by Hopkinson *et al.*(21) presented a theory that stated LS could be used to manufacture parts cheaper than injection moulding for production volumes up to 14,000. In comparison to roughly 6,000 parts for SL and FDM. It should be noted though size and part complexity are major drives here as parts get smaller and more complex their suitability for manufacture using AM increases. This is due to complex injection moulding tools being expensive to manufacture. As well as the volume of a part having a larger impact on time to manufacture for a PBF

part in comparison to that of injection moulding as the packing in the build volume is critical for powder bed AM.

PBF often requires a long powder cool time after printing this however can be done offline whilst more parts are being printed minimising the effect on build time and throughput. Due to the possibility of use in production, PBF techniques will be the focus of this research from this point.



## Chapter 2 Polymer powder bed fusion and applicable literature

### 2.1 Polymer powder bed fusion techniques

As discussed in Chapter 1, the high production speeds per part that can be achieved using polymer powder bed fusion (PBF) in comparison to other AM techniques, make these methods the most attractive for FMCGs. The most common PBF techniques currently available will be discussed below.

Key advantages of PBF techniques are the lack of need for additional support structures as the unsintered powder acts as support during building, relatively high mechanical properties and the efficient production of more complex designs. However, there are some limitations to these techniques which include; slow production speeds in some cases compared to that of injection moulding, expensive and limited range of materials and difficulties in controlling the surface finish.

#### 2.1.1 Laser Sintering

Laser Sintering (LS) is the most common polymer powder bed fusion technique. LS was first developed for commercialisation in the 1980's by Carl Deckard at the University of Texas at Austin and initially launched commercially by DTM and EOS GmbH (22). LS works by a laser selectively sintering a layer of powder particles on a build bed, following which a fresh layer of powder is deposited on top of this partially sintered layer and the process is repeated until the part is complete. Figure 2.1 shows the laser sintering process.

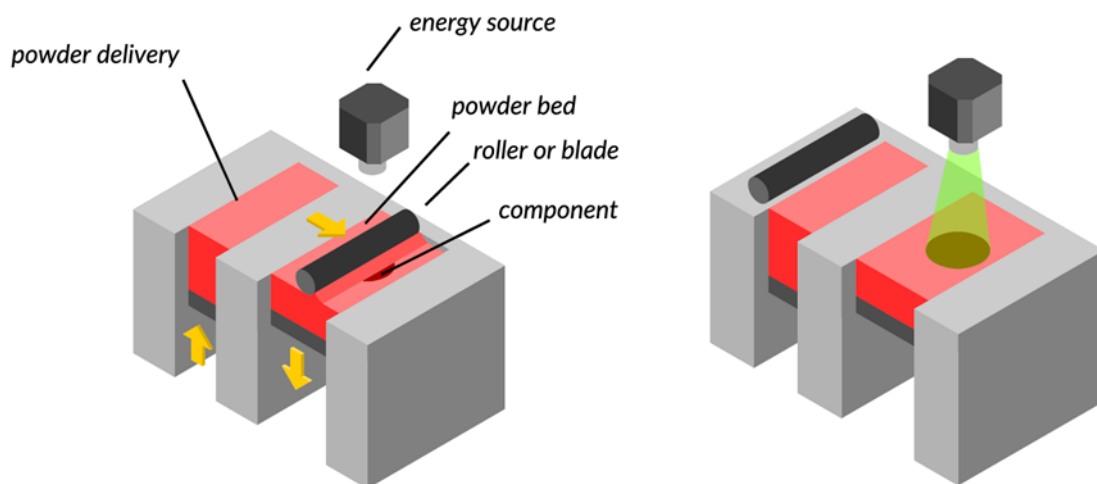


*Figure 2.1 A representation of the LS process where a layer of powder is deposited onto the build area and then sintered by an energy source, in the case of LS this is a laser (15).*

LS has been used in a variety of applications including aerospace, fashion (Figure 1.2) and automotive (Figure 1.6).

### 2.1.2 High Speed Sintering

High Speed Sintering (HSS) was first developed at Loughborough University (22, 23), to increase the speed of LS as well as to reduce the machine cost. Hopkinson *et al.* (21) made a comparison of costs of LS to injection moulding, it was identified in this work that machine costs play a major role in the overall costs of AM parts. Therefore, a clear method to reduce the cost of parts built via AM would therefore be to reduce machine costs. Laser sintering machines use an expensive laser optic system, adding both cost and complexity to the system. As the required parts get larger, or higher quantities of smaller parts are produced simultaneously, the build time increases due to a longer scanning time of the laser. One way of achieving a larger build area can be the addition of multiple lasers to the machine, however this greatly increases the cost of the machine as well as potentially introducing errors in the areas where the lasers interact.

In the HSS process (see Figure 2.2), energy to sinter is inputted to the powder via an industrial inkjet printhead and an infrared (IR) lamp. This printhead deposits an IR absorbing ink on the regions of the build bed which will be sintered. The IR lamp is then passed across the build, whereby the areas which have had the IR absorbing ink printed are heated above the melting temperature of the powder and hence sintering occurs. Ceramic infrared heaters are mounted above the build bed, the function of these heaters are to keep the powder in the build (sintered and unsintered) in the process temperature window.

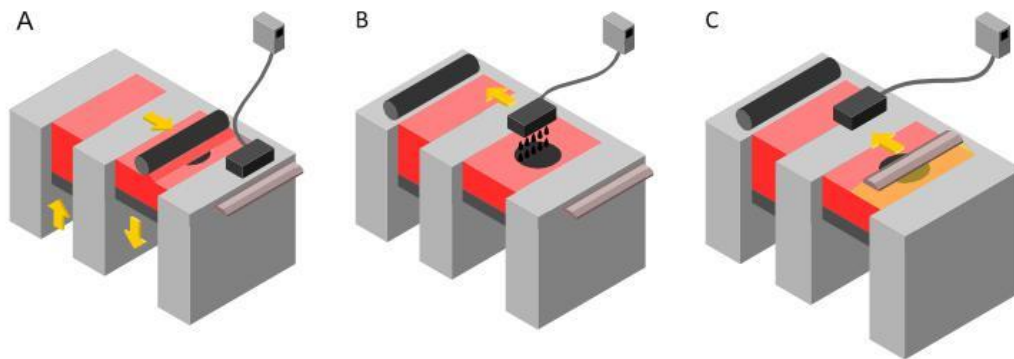


*Figure 2.2 A diagram of the High Speed Sintering process. A. A powder layer is deposited on the build bed. B. An infrared absorbing ink is deposited selectively. C. An infrared lamp is used to heat the ink deposited and this causes the powder where the ink is printed to sinter creating a layer of sintered part. This process (A-C) is then repeated to produce a 3D printed part (15).*

The printheads for each layer cover the width of the build bed area, hence the cross sectional area of the build does not affect layer time. HSS is easily scalable due to this factor, where larger build beds are accessible by increasing the number of printheads (24). Although a larger build volume allows the

production of bigger parts, its major advantage is the potential for increased quantities of smaller parts manufactured in a decreased time per part, hence reducing the cost of the part.

Due to the relatively slower method of sintering the powder in comparison to the fast and intense method of using a laser to input the energy to cause the powder to sinter, detrimental effects of high temperature spikes caused by the laser, for example oxidising the material are reduced. Solid state polycondensation of Nylon has been observed in LS where the polymer chains join and the molecular weight increases (25). Other polymers also degrade at elevated temperatures such as polyvinyl chloride breaks down into constituent components, polypropylene can degrade and decrease in molecular weight if held at increased temperatures without stabilisers.

### 2.1.3 Multi Jet Fusion

Multi Jet Fusion (MJF) is technology commercialised by Hewlett-Packard, with the first MJF systems going on sale in 2016 (3). MJF works the same as HSS but with the addition of an inhibition agent printed around the outside edge of the part (26). In 2018 HP have released a colour MJF machine where a colourless sintering agent has been used, in addition to extra printheads which print a coloured ink on the outside of parts produced.

The first MJF systems are developed to be fast with the ability to manufacture parts at speed, which is conducive with mass production. The system is modular with a printer, removable build unit and post processing station that allows minimal turn cycle time due to building whilst the previous build is cooling down out of the machine. The technique is still new in the field and currently there is little published research in the area (27, 28).

### 2.1.4 Other polymer powder bed fusion systems

Other PBF systems such as Selective Masking Sintering (SMS) (29), Selective Inhibition Sintering (SIS) (30) and Selective Heat Sintering (SHS) (31, 32) have been discussed in the literature but have little to no commercial availability, hence will not be further examined. HSS will be the focus in this research due to its faster production capability.

### 2.1.5 Post processing

At the end of a build, parts manufactured using powder bed fusion techniques remain encased in the loose powder which has acted as a support throughout the build, and this powder must be removed. Normally pressurised air or a vacuum is used to remove loose powder followed by more aggressive removal such as bead blasting to remove more rigid powder.

Whilst powder removal is regarded as a necessity to be able to produce parts, there are also other processing techniques which allow a selection of surface finishes and colours that can be selected.

These further post-processing techniques can vary from manual techniques such as hand sanding, polishing and hydrographics to automated systems such as dyeing, tumbling and chemical techniques. Although not studied in this thesis, the development of automated post-processing techniques is likely to be essential for the use of AM in a medium to high production capacity, where labour costs would be too high to allow these processes to be carried out manually.

## 2.2 Energy input mechanisms

HSS is a relatively new AM technique and hence the research in the literature is sometimes limited. At some points it is therefore useful to draw from the existing body of research in Laser Sintering. Whilst both techniques are similar, the way in which energy is inputted into the system varies.

Both High Speed Sintering and Laser Sintering include the term sintering, the terms sintering and melting are often used interchangeably when used referring to these technologies, however more specificity is required. Kruth *et al.*(33) investigated the binding mechanisms of SLS and the related technologies for metals. Identifying 4 classifications; Solid State Sintering, Chemically Induced Sintering, Liquid Phase Sintering / Partial Melting and Full Melting. In LS Liquid Phase Sintering / Partial Melting is normally observed where the border of the particle is melted but there is insignificant heat to cause the full particle to melt and the particles are then fused by the edges. Full Melting has also been demonstrated to occur in LS(34) where the complete powder particle is melted then fuses. Therefore SLS and HSS should be considered as mainly Partial melting process but Full Melting can occur.

HSS systems use an IR absorbing ink printed through a printhead which is then heated with an IR lamp, in comparison to the laser used in LS. In LS the laser scans across the build area and causes the powder hit by the laser to selectively sinter. The time the laser is in contact with individual pairs of powder particles is short, although the larger the cross-section part in a layer, the longer the layer time. In comparison HSS layer time is independent of sinter area, and the layer time is only defined by the time it takes to deposit a new layer of powder, print in the selected area and pass the lamp over to selectively sinter the layer. However, the time each pair of particles is exposed to the energy source is longer. This leads to differing kinetics for LS versus HSS, as in LS particles are exposed to a high temperature for a short time period as the laser is in contact with them. In comparison to HSS where the lamp passes over the printing area slower so a lower maximum temperature is required. A laser in LS moves across the build bed at a speed of circa 2500 mm/s (35), compared to the sintering lamp moving at circa 150 mm/s (36) for HSS. The maximum temperature reached by the polymer in HSS is currently not known.

The Frenkel-Eshelby (2.1) (37) models powder sintering relating viscosity and surface energy of the melting polymer. Figure 2.3 is an adapted diagram showing the Frenkel-Eshelby model from (38).

$$\frac{x}{a} = \left( \frac{\Gamma t}{\mu a} \right)^{1/2} \quad 2.1$$

Where  $x$  is the neck radius,  $a$  is the particle radius,  $\Gamma$  is the surface energy,  $\mu$  is viscosity and  $t$  is time (37).

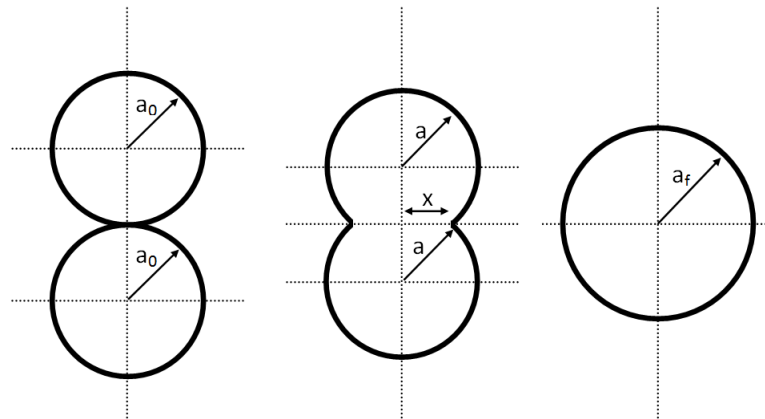


Figure 2.3 Modelling of the Frenkel-Eshelby model, where  $a_0$  is the initial radius and  $a_f$  is the final radius and  $x$  is the neck radius [2].

The application of this model in LS was demonstrated by Vasquez *et al.* (39) and the model shows that time has an effect on the sintering of polymer particles. This might suggest that particles in HSS would sinter more at the same temperature. However viscosity also affects the level of sintering, and tends to be lower at high temperatures, meaning it sinters more quickly. Although in LS particles are heated for a short time, they experience a higher temperature and hence sinter to a roughly equivalent amount to the amount observed in HSS.

LS systems use a protective atmosphere (normally  $N_2$ ) during manufacture to reduce oxidisation of powder as well as fire risk. In HSS the maximum temperature the powder encounters is lower than the scanning laser and hence this is not generally required in HSS.

HSS introduces an additional material into the process via the IR absorbing ink, some of which remains in the final part and must be assessed when used in some end-use parts. Both HSS and LS have a relatively small number of materials processed compared to more traditional manufacturing techniques, but this is more significant with HSS as discussed in Section 2.4.

## 2.3 Effect of energy input

HSS since its invention has seen the majority of research carried out on the technique investigating the effect of parameters in the process, although there has been research on dimensional accuracy (40, 41) and build orientation (42).

### 2.3.1 Lamp power

The effect of lamp power has been studied by various authors in HSS. Thomas *et al.* (43) demonstrated that increasing energy from the IR lamp led to harder powder caking causing post processing to become more difficult until it was no longer possible. Majewski *et al.* (44) observed as build bed temperature and IR lamp energy were increased Ultimate Tensile Strength (UTS), Elongation at Break (EaB) and Young's Modulus (YM) were found to increase although only two levels for each factor were examined.

In further work Majewski *et al.* (44) demonstrated that the depth of sintering which was possible is limited. With an increase in sinter lamp power a maximum depth of penetration of approximately 200  $\mu\text{m}$  was achieved and an increase in lamp energy did not lead to deeper sintering, although a higher level of sintering occurred, as demonstrated by higher shrinkage values. The reasoning given by the author for this phenomenon was sintering across the top layer of powder layer reducing the ability to sinter in z-direction, this was supported by observations seen in LS (45).

Norazman *et al.* (46) compared the difference between using two different IR lamps in the HSS process, using an elastomer. Both lamps tested were 2 kW quartz halogen IR lamps, but had different reflector coatings on the lamp. The spectral output of both lamps were then analysed and it was found that one lamp had a significantly higher irradiance (100% increase), which had the effect of increasing the energy input into the system via the IR lamp. It was found that the lamp with higher irradiance led to higher mechanical properties (UTS, EaB and YM) with a 50% increase in UTS and YM and 100 % increase in EaB and lower porosity, indicating that an increase in sinter lamp energy increases mechanical properties and decreases porosity.

Rouholamin *et al.* (47) demonstrated the effect of lamp power on various properties measured. It was shown that part density and UTS increased then plateaued as lamp power was increased. This was mirrored by the porosity measurements where the porosity decreased then plateaued with an increase in lamp energy. EaB and YM both showed a peak IR lamp energy where properties increased up to 30 % and 2,000 MPa at a power of 80 % and 90 % respectively before decreasing. The authors suggest a degradation in polymer led to the decrease in mechanical properties.

The combination of sinter lamp power and speed in HSS is similar to energy density (ED) in LS. ED is a measurement of the input energy inputted from the laser in LS and is used throughout literature (48-51) to quantify laser energy input, where a large ED value means more laser energy was used to melt the polymer powder. Equation 2.2 is the equation for ED (52) and is a general method in LS to observe the amount of energy input into the system, no analogue currently exists for HSS for HSS.

$$ED = \frac{\text{Laser Power}}{\text{Scan Speed} \times \text{Scan Spacing}} \quad 2.2$$

Khalil *et al.* (49) observed that the density of parts increased as ED was increased but decreased at the highest level tested. Starr *et al.* (50) demonstrated that to reach maximum elongation performance as well as other mechanical properties a high ED was required. It was also determined that other factors as well as ED have an effect in LS. Beal *et al.* (51) found that both laser power and scan speed which contribute to ED influence the properties of LS parts.

The effect of sinter power on the manufacture of parts has been studied previously as discussed above although this level has not been increased to a point where mechanical properties decrease, whereas this has been observed for ED (53). This may suggest this effect is not encountered in HSS, but is more likely to suggest lower temperatures in HSS.

In HSS the IR heat lamp passes across the build bed twice, once after a new layer of powder is deposited (preheat stroke) and after the IR absorbing ink is printed onto the powder surface (sinter stroke). Previous research as discussed above, has studied the effect of varying the energy input from the sinter stroke. However the preheat stroke also inputs energy into the system although it does not directly see the IR absorbing ink. The effect of this method of inputting energy into the HSS system will also therefore be studied in this research.

### 2.3.2 Bed temperature

The effect of build bed temperature was studied by Majewski *et al.* (54), where it was observed that increase in temperature led to an increase in all the mechanical properties measured (UTS, EaB, and YM). With this increase in mechanical properties the range of values obtained also increased, as demonstrating less repeatability at a higher energy input. IR lamp power was also investigated as discussed above and it was found that variation in the bed temperature had a larger effect than that of the IR lamp. It was also observed powder removal became more difficult with an increase in part bed temperature.

Starr *et al.*(50) defined a new dimensionless parameter Energy Melt Ratio (EMR) which includes the effect of bed temperature in the amount of energy input into the system. As well as taking into account the layer thickness and material properties. As discussed earlier in this section an equivalent of energy

density for HSS does not currently exist neither does one for EMR. The general principle can be applied where an increase of speed of the energy input leads to less energy and more power from the lamp means more energy into the system and these can be balanced against each other. As well as the additional factors of material, bed temperature and layer thickness also effecting the energy input required.

### 2.3.3 Ink in HSS

#### Quantity

There has been research by Noble *et al.* (55) and Ellis *et al.* (56, 57) into the effect of amount of printed ink in HSS parts using both Nylon 12 and an elastomer as powder feedstock. A trend of mechanical properties increasing with ink quantity was observed to a level and then a drop off was observed for UTS and YM, although this trend was not seen for EaB. In further work (57) the amount of ink was correlated to the crystallinity of parts produced, with an increase in ink leading to lower part crystallinity with a range of crystallinities of 23 – 28 %. The authors reason this is due to more complete melting of parts and hence lowering the crystallinity as observed by Majewski *et al.* (58) in LS and the ink not directly affecting the crystallinity but the ink increasing the energy input and causing more melting. The crystallinity of the feedstock material was found to be 47 % and (59) research showed the fully melted feedstock had a crystallinity of 25 % after cooling. As the degree of melt is increased the crystallinity of the residual part decreases until a crystallinity of 25 % is achieved after a full melt is observed. These trends were also observed for similar experiments using an elastomer as the powder feedstock. However in this work it can be observed there is a lack of reproducibility shown by the error bars which makes the trends more difficult to observe.

#### Type

Fox *et al.* (36) demonstrated the use of two different carbon black containing IR absorbing inks used in the HSS process, with a small difference in mechanical properties. The work demonstrated it was possible to use inks from different suppliers and manufacture HSS parts.

In general the literature discussed above has shown mechanical properties were increased when the input energy from various parameters were increased. Similar observations have been made in LS where ED was increased and mechanical properties increased (48, 52, 60). Increase in bed temperature has also been shown to increase density (61) and also mechanical properties (53).

### 2.3.4 Part orientation

Although not a method of energy input part orientation often has a large effect on part properties where orientation can greatly affect the surface finish (2). Ellis *et al.* (42) demonstrated in HSS that as build orientation was altered from an XY to a ZY the mechanical properties decreased (a 50 %

reduction in UTS and 75 % in EaB), as observed in LS (50, 62). Orientation can also greatly affect the number of layers in a build hence changing the build time and therefore altering the cost of part manufacture.

## 2.4 Materials in HSS

### 2.4.1 Processing materials in HSS

The HSS process uses an IR absorbing ink and an IR lamp to sinter polymer particles together to form parts layer by layer. The powder is deposited in layers onto the build bed area, with a 'typical' layer thickness of 100  $\mu\text{m}$ . The powder supply is pre-heated in the machine chamber to heat the particles near to the melting point of the material, and the required cross-section is heated above its melt temperature ( $T_m$ ) by the ink and the IR lamp. The polymer is then kept in the liquid phase and hence above the recrystallization temperature ( $T_r$ ). The area between the  $T_m$  and the  $T_r$  is referred to as the super cooling process window. This stops the effect of curling which occurs when a cool powder is placed on top of warm molten material which causes stress and the part then curls(62). Fresh pre-heated powder is deposited on build area and then selectively sintered by the laser to form another layer which is repeated until a part is fully built.

The majority of materials used in the process to date are semi-crystalline polymers, notably Nylons (see Section 2.4.5). Semi-crystalline polymers tend to have a clearly defined  $T_m$  and produce parts with relatively high mechanical properties. This is in contrast to amorphous materials which do not tend to have a clearly defined  $T_m$  and instead are heated to above the glass transition temperature ( $T_g$ ) when used in PBF. The lack of a defined  $T_m$  leads to a poor level of sintering between particles and hence the parts manufactured using amorphous powders are relatively weak. Parts using amorphous materials are therefore generally not suitable for end-use parts built via AM, and tend to be more likely to be used in investment casting and similar applications.

### 2.4.2 Overview of thermoplastics

Polymers can be divided into two major groups, thermosets and thermoplastics. A thermoset is a polymer which becomes irreversibly hardened upon being cured. A thermoplastic is a polymer which becomes plastic during heating and hardens after cooling; this process is repeatable. Elastomers can be thermosets or thermoplastics. Powder bed fusion AM techniques rely upon melting the polymer, meaning thermosets are not currently a useable set of polymers in these techniques, and this work has therefore focused on thermoplastic polymers. These can be divided into two further subsets amorphous and semi-crystalline polymers.

Amorphous polymers

Amorphous polymers do not exhibit any crystalline structures, with no polymer showing no ordered structure. The use of amorphous polymers in AM sintering techniques is mainly limited to use in master patterns that are then infiltrated to form a useful part (63). This is due to amorphous parts not undergoing the shrinkage which is present in sintering of semi-crystalline parts, allowing an accurate sized pattern to be manufactured. A comparison between amorphous polymers and semi-crystalline polymers is shown in Figure 2.4.

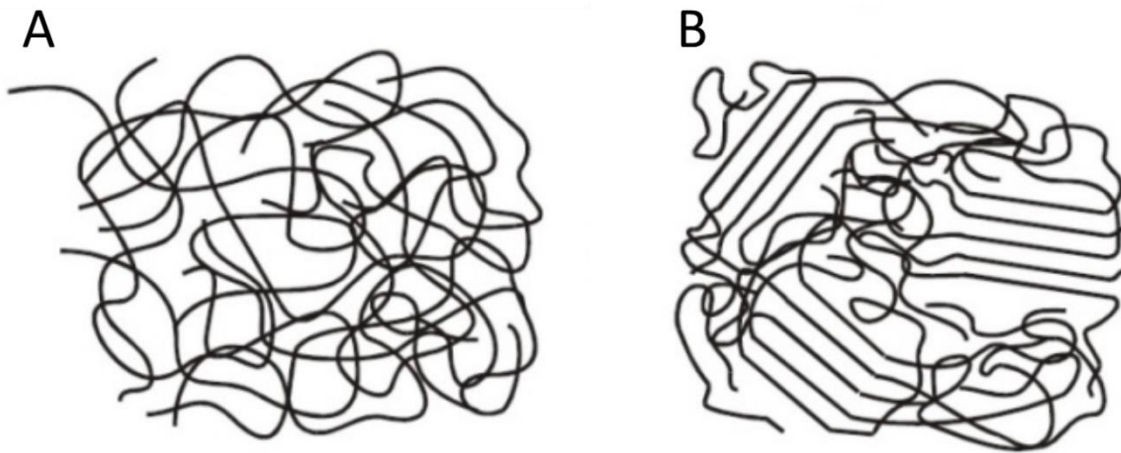


Figure 2.4 Comparison between (A) an amorphous polymer and (B) a semi-crystalline polymer with crystalline and amorphous regions (64).

Amorphous polymers possess a glass transition temperature ( $T_g$ ) but no melt temperature ( $T_m$ ) hence there is not a well-defined peak at which the polymer will sinter. The relatively high viscosity leads to a high amount of voids formed in the part, resulting in poor mechanical properties of the part. Amorphous polymers that have been sintered in LS include polystyrene, poly(methyl methacrylate) and polycarbonate(65), but these have not received substantial attention in recent times. No amorphous polymers have been processed in HSS.

Semi-crystalline polymers

Semi-crystalline polymers produce parts where the part of the structure of the polymer is highly ordered, with some amorphous sections. There is a wide range of semi-crystalline polymers including polyamides, polyolefins, acetals and acrylics.

## 2.4.3 Polyamides

Polyamides also known as Nylons are the most common LS powder feedstock, as a result of its favourable material characteristics (Section 2.4.4); however the price of polyamide powders is too

high for use in fast moving consumer goods<sup>1</sup>. The current dependency on Nylon powders is shown in Figure 2.5.

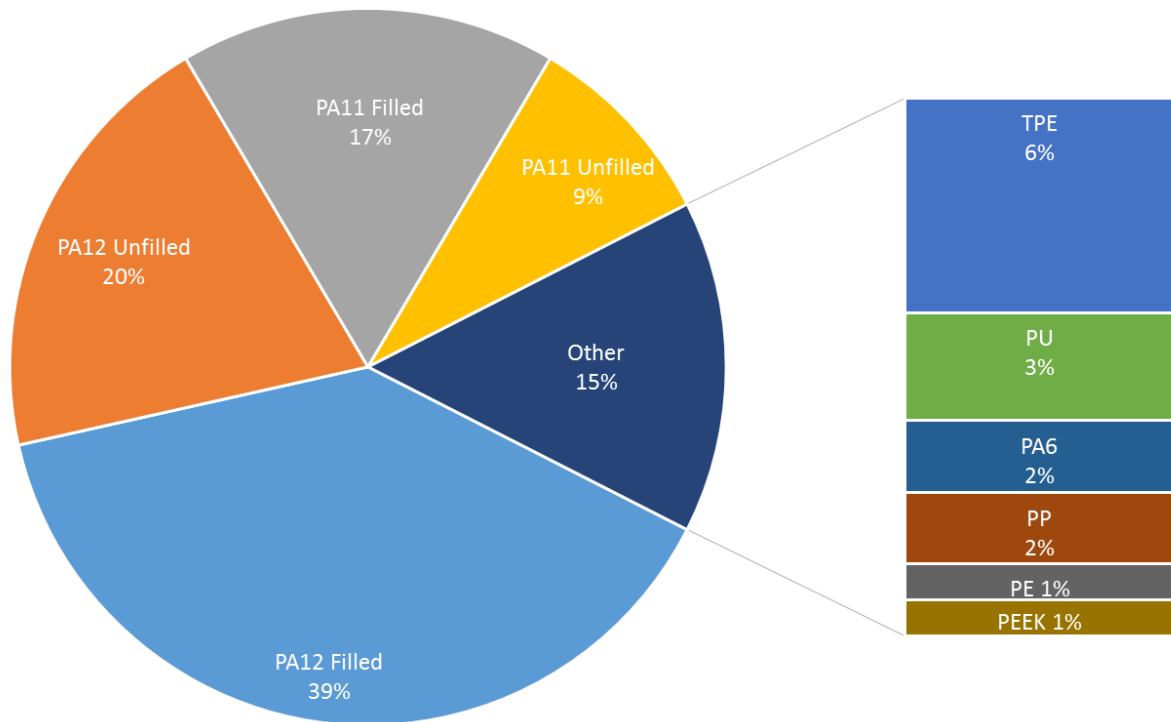


Figure 2.5 Pie chart showing the number of different LS materials available, adapted from (66), where the percentage is the number of purchasable grades of material for LS

### Polyamide 12

Polyamide/Nylon 12 is the most common polymer used in LS and HSS (65). Nylon 12 is an ideal polymer for the use in LS, due to its processability and the relatively high mechanical properties it retains after sintering.

Polyamide 12 is an engineering thermoplastic and therefore has reasonable mechanical properties for its standard applications. In some cases these already good mechanical properties can then be modified through the inclusion of a range of fillers such as glass, aluminium and carbon fibre, although this can add cost and complexity to the process.

### Other semi-crystalline polymers

Several other polymers are used in LS. These grades include Nylon 11, another polyamide. Nylon 11 is more ductile than Nylon 12 (67, 68) however its process window in PBF is smaller and hence more difficult to manufacture with. Other notable sintering polymers include polyether ether ketone, polyolefins and thermoplastic elastomers.

<sup>1</sup> Quote from EOS GmbH for 20kg of PA2200 £1,094.06 which is equivalent to £54.70 per kg, July 14.

#### 2.4.4 Important material properties

Identifying and processing other polymers in LS has been identified in literature (69-71) to be an important area to allow the growth of the PBF market. This work has been carried out by identifying the key characteristics which allow the current polymers to be processed and then identifying other possible polymers which could have these necessary properties.

##### Melt and recrystallisation characteristics

An important part of the processability of Nylons in PBF techniques are the melt and recrystallisation properties of the material. The thermal processability of Nylon is demonstrated by Differential Scanning Calorimetry (DSC), where a material is heated at a controlled rate and the amount of energy to do so is recorded. The data from the energy input allows melting and recrystallisation temperatures to be calculated. An example DSC trace for Nylon 12 is shown in Figure 2.6.

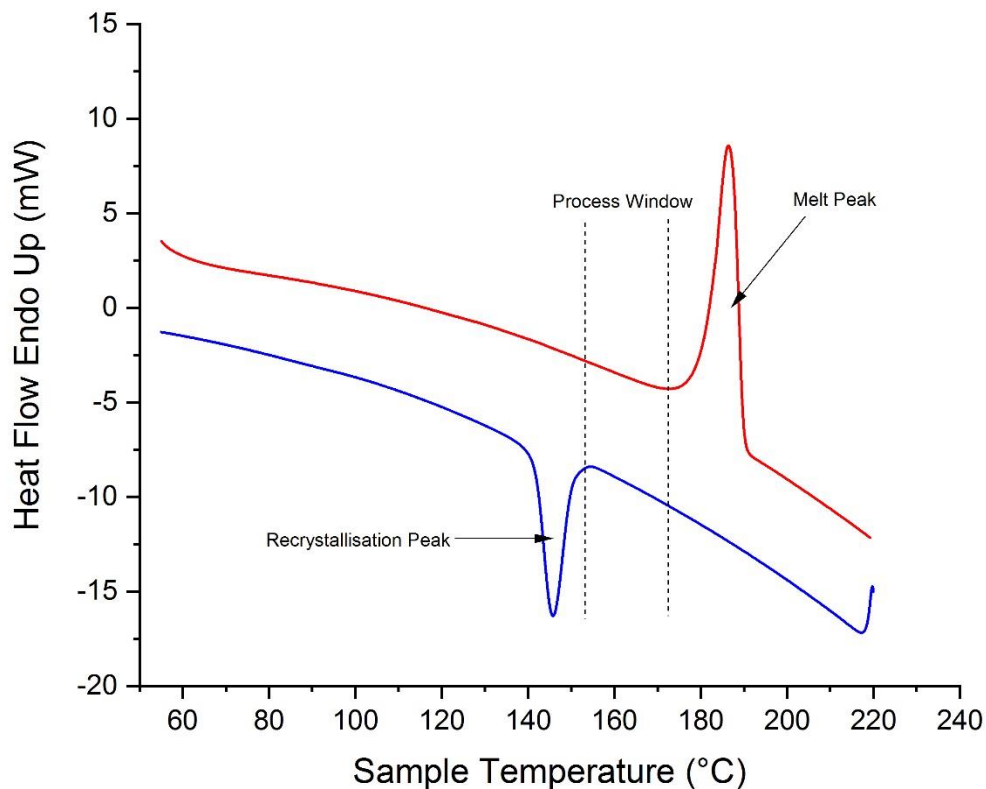


Figure 2.6. DSC trace of Nylon 12; temperature scan at 10 °C / min.

Figure 2.6 shows a well-defined and sharp melt peak and recrystallisation peak and a large gap between these for Nylon 12. This aids in creating a large process window, where the material remains in a molten state after melting but at a temperature above that at which it would recrystallise. The bed temperatures on the sintering machines are set within the process window. If the temperature is

set below this, when fresh powder recoats the build bed the hot polymer of the part cools quickly and stress is formed. The parts then curl, causing the build to fail. The alternative is the bed temperature being too high which can cause the polymer to sinter where not required, resulting in the build losing accuracy or failing.

#### Powder flow

Powder flow is critical in PBF techniques, whereby a powder must be deposited on the build bed to form an even uniform layer, before the powder is sintered (72). Powder flow is affected by multiple factors including equipment design, environment (temperature and humidity), particle shape, particle size and flow agents (additives added which are designed to aid flow). Equipment design and the operational environment are fixed in this case, and hence the impact and modification of the other parameters are required.

Work by Fu *et al.* (73) investigated the effect of powder shape and particle size on lactose powders which with respect to powder flow are analogous to polymer particles. The research demonstrated smoother and larger particles showed better flow and packing compared to rough non-spherical small particles. This has been supported by research using AM powders by Berretta *et al.* (72, 74) where particle shape and size affected the powder flow and hence the usability of the polymers. In this case additives aided the flow of the material. It was demonstrated that the grade of Nylon 12 used (PA2200) was smoother than the other types of polymer used and accounted for the superior flow.

Lexow *et al.* (75) demonstrated the grinding of a polypropylene for use in LS. The grinding processing in LS was attempted without addition of flow or any other additives, however was not possible. After the addition of additives it was then possible to manufacture parts, showing the critical use of flow agents in milled polymer powders.

#### Molecular weight

Nylon although being widely used in PBF techniques undergoes a decrease in surface properties as the previously unsintered powder is reused in the system. The change in surface finish is known as 'orange peel', and an image of a part with this degradation in the surface finish is shown in Figure 2.7.



Figure 2.7 Image of a part, where the 'orange peel' effect is visible.

A reasoning for the 'orange peel' was presented by Yusmawiza (25), where the 'orange peel' is driven by the melt viscosity and hence the molecular weight and dispersity of the polymer as these change during powder ageing, due to chemical reactions. The chemical reactions occurring are solid state polycondensation where the end groups of the Nylon polymer chains react with each other and parts of the chain, increasing the molecular weight as well as the dispersity broadening. This is due to the chemical groups in Nylon being susceptible to condensation reactions which result in the loss of water molecules. The polymer melt viscosity is a function of the molecular weight of a polymer (76), hence measuring the change of the molecular weight of a polymer gives information about any potential deterioration in surface finish. Dispersity ( $\bar{D}$ ) is a measure of the broadness of the molecular weight distribution of the polymer. Yusmawiza also demonstrated that a larger polydispersity led to a worse surface finish.

An ideal polymer for PBF would not undergo any chemical reactions which are observed in Nylons and hence the molecular weight and dispersity of the material would stay constant. Therefore, the powder would not deteriorate as the powder is reused in the PBF process.

#### 2.4.5 Materials processed in powder bed fusion

To date the published research on HSS has been carried out on two materials – Nylon and thermoplastic elastomers. Nylon 12 has been used widely in HSS process (22, 43, 44, 54). Ellis *et al.* (77) demonstrated the use of filled Nylon, Duraform<sup>®</sup> HST which is a Nylon 12 filled with fibre reinforcement. In HSS the filled material demonstrated similar EaB to LS, however showed a significant decrease in both UTS and YM although the material was processable. Ellis *et al.* (42) in further work demonstrated the use of Nylon 11 in HSS. There have been several demonstrations of the use of

elastomers in HSS (46, 56, 78, 79). The effect of additives, mechanical properties, dimensional accuracy and surface finish of the elastomer were tested, where Norazman (78) demonstrated a EaB of 265 %.

This list of materials is however reduced compared to the number of polymers used in LS, which include; Nylon 12, Nylon 11, various different filled Nylon materials, elastomers, PEEK, PP, PE, UHMWPE, POM (3, 65, 69) and is demonstrated by the number of materials available for purchase for LS, as shown in Figure 2.5. Khalil *et al.* (35) demonstrated the processability of UHMWPE in LS however other issues are encountered when processed such as warpage and high porosity. PEEK has been processed in LS demonstrating good mechanical properties (74, 80), however requires a high temperature in excess of 345 °C to process. PP has been processed in LS and will be discussed further in Section 3.4. Wegner (81) showed the processing of both PE and POM in LS was possible, however large warpage was observed of the manufactured parts. A wider range of polymers has been used in LS compared to HSS, although both techniques have been dominated by Nylons.

## 2.5 Key differences between HSS and LS

In this chapter literature from research on both HSS and LS have been used to inform further research carried out in this thesis. It is important to acknowledge the differences between HSS and LS and these will be discussed below.

In HSS the difference between in the absorption of energy in the Near Infrared (NIR) region of the ink versus the feedstock powder is critical. This is because if they are similar then when the IR lamp passes over the build bed then the ink will not lead to selective sintering but the whole bed will sinter. This requirement is not needed in LS as the energy to cause the powder to sinter is applied by limiting the area it is exposed to rather than using the absorptivity differences that HSS uses. This fundamental difference could lead to a more restrictive material selection in HSS but currently this has not been shown in literature.

As discussed in Section 2.2, the sinter kinetics are different in HSS versus LS, where HSS occurs over a longer time period in comparison to that of LS. Melt viscosity is a variable shown in Equation 2.1, melt viscosity is dependent on temperature therefore the higher maximum temperature observed in LS compared to that of HSS will lead to a lower melt viscosity in LS. But due to the time for sintering in HSS being longer than LS sintering occurs as time is also a factor in the Frenkel-Eshelby sintering model.

Another key difference in HSS and LS is the energy input mechanisms as discussed in Section 2.3, the bed temperature in both techniques is similar and has been shown to have an effect on the processing of materials. LS uses Energy density including laser power, scan speed and scan spacing to adjust the

input energy from the laser. Whereas HSS uses lamp power and speed on the sinter and preheat strokes as well as the amount of ink used to absorb the energy used for sintering.

## 2.6 Summary

This chapter has investigated the important differences between HSS and LS and their respective methods of energy input to cause the polymer powder to sinter. The different parameters which will be assessed later in this research have also been discussed as has their effect on part properties. The bed temperature and sinter power has been shown to be critical in HSS as well as LS and therefore will be varied in this research. Specifically in HSS the amount of sintering ink used (grey level) has been shown to affect the part properties therefore this parameter will also be studied. Preheat power will also be studied as it is another method of inputting energy into the system.

Nylon 12 has been investigated widely in PBF and the factors to which it is a good polymer in these processes have been identified and will be used later in this research to compare to other polymers.

## Chapter 3 Project rationale and definition of initial focus

### 3.1 Project rationale and research questions

HSS been shown to have the production speeds which could allow for manufacture of Fast Moving Consumer Goods (FMCGs), see Chapter 2. However, for this goal to be achievable it is necessary for a wider range of materials to be identified, which can provide a range of properties at a price point conducive to large scale Additive Manufacturing (AM).

The aim of this work is to establish the feasibility of manufacturing HSS parts using a more economical alternative to polyamides as the powder feedstock. Using a less expensive material as the feedstock would allow AM to be used in the production of FMCGs, by allowing AM to be at a competitive price point in comparison to traditional techniques.

The research questions of this thesis is; can HSS use a more economical alternative material as a powder feedstock? If this is possible what are the part properties achievable and what process parameters have an effect of the manufacture and part properties? For AM to be used in production the material wastage is key and therefore is there any disadvantage of using the material feedstock repeatedly as there is with traditional powder Bed Fusion (PBF) materials? In order to answer these questions, a number of research tasks must be carried out.

- Identify criteria required for suitability as a HSS feedstock for FMCGs.
- Using these criteria, identify one or more suitable materials.
- Perform initial trials to ensure processability in HSS.
- If suitable, perform more in-depth experiments to determine achievable mechanical properties and effect of processing parameters.
- Cost and sustainability are crucial for FMCGs, this in turn means reuse of excess powder is critical, hence the effect of powder ageing will be studied.
- Attempt to identify key performance indicators for powder/material to ensure suitability for HSS.

A summary of experimental process which will be used in this thesis is shown in Figure 3.1.

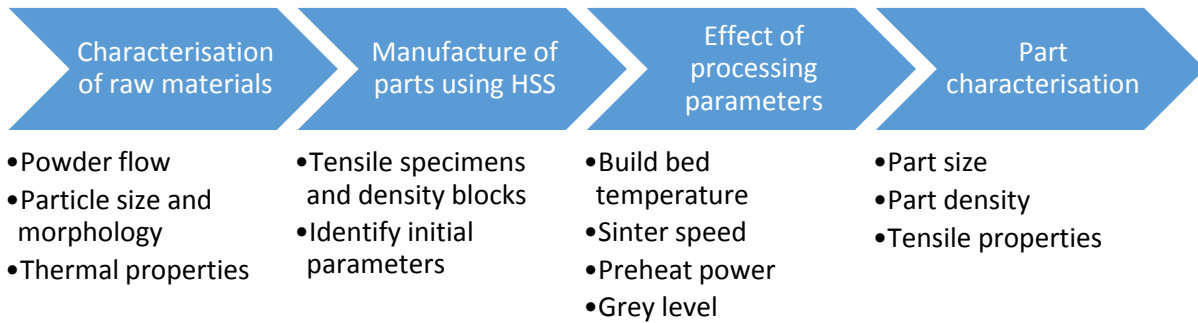


Figure 3.1 Flow chart showing the experimental process steps carried out for the research in this thesis.

### 3.2 Material compatibility

This work will concentrate on semi-crystalline polymers because of the benefits identified in Section 2.4. Research has been conducted to identify ‘commodity thermoplastics’. There are several key criteria which must be met when considering suitable materials to be further studied in this research; these are chemical (3.2.1), processing (3.2.2) and application compatibility (3.2.3) as well as cost analysis (3.2.4). The materials investigated are listed in Appendix A.

#### 3.2.1 Chemical incompatibilities

Chemical incompatibilities were identified as key criteria for polymers to be used in the HSS process. For example, polyvinylchloride decomposes at 140 °C which is below its melt point and is therefore not appropriate for a sintering technique.

Another chemical incompatibility identified relates to the use of an IR emitting lamp and absorbing ink to provide heat energy to the system to cause the polymer to sinter where required on the build bed. However if the polymer itself absorbs strongly in the same region of the electromagnetic spectrum (800 – 1700 nm, see Figure 3.2), it will also sinter in un-printed regions, causing the whole bed to sinter and fail.

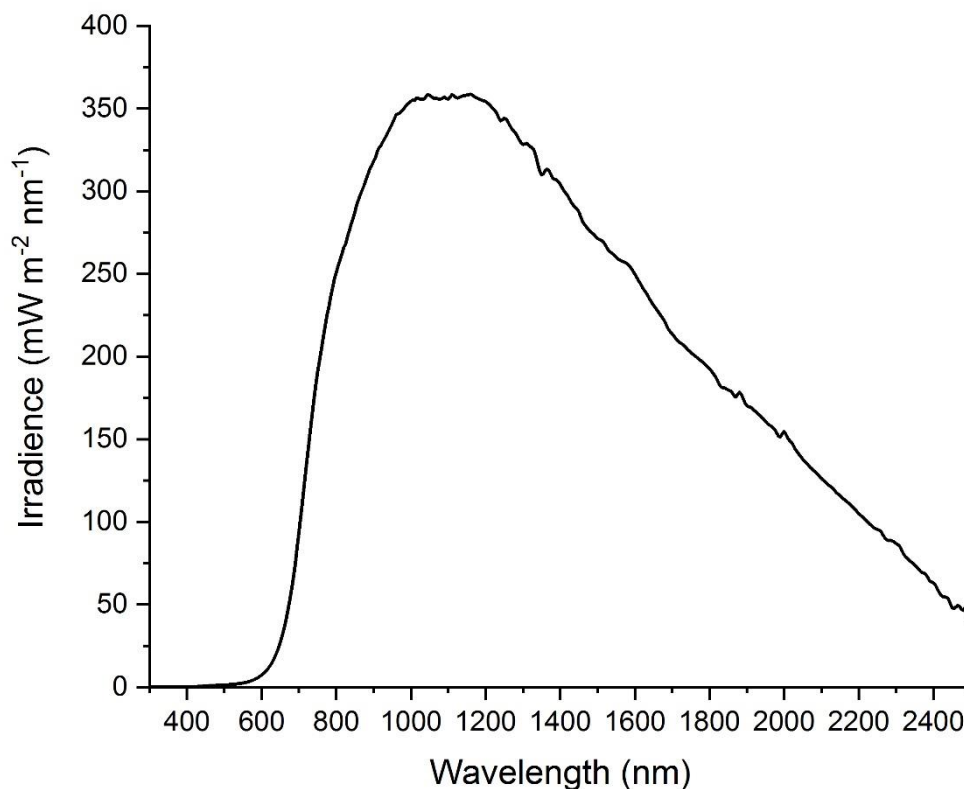


Figure 3.2 Energy trace showing the spectral output of an IR lamp used in HSS.<sup>2</sup>

### 3.2.2 Processing incompatibilities

Some polymers cannot be processed by the current HSS machine due to the melting point of the polymer being too high for the HSS machine used in this research. The current system can reach a bed temperature of roughly 200 °C, meaning any material with a  $T_m$  of above 210 °C cannot be processed. This includes Nylon 6 and Nylon 66, both of which with a melting point above 220 °C (82).

### 3.2.3 Application compatibility

Amorphous materials were ruled as incompatible with the project due to the poor mechanical properties (see 2.4.2), this would therefore require a further step to infiltrate the polymer to acquire suitable properties and hence make financially unviable.

Elastomeric materials were eliminated due to the materials' properties not being suited to the production of fast moving consumer goods packaging although they have previously been processed via HSS (78, 83).

<sup>2</sup> Spectral output provided by lamp supplier, Victory Lighting UK Ltd.

### 3.2.4 Cost analysis

The 'commodity thermoplastics' were identified, then the cost of each thermoplastic was obtained from statistics of the price of 'commodity thermoplastics' (84) and converted to £ per kg from U.S. cents per pound. The prices were obtained for a purchase of large quantities of powder, as these are public commodity prices. A list of these polymers were identified and described in Appendix A. The prices obtained are for non-processed polymer in pellet form, therefore costs would be higher to obtain a polymer that could be used in AM. The processing costs of polymers from pellet to powder may vary for different materials as some would be polymerised to a powder directly whereas others would require grinding post polymerisation. However for this piece of work only the bulk pellet prices were available.

All 'commodity thermoplastics' were analysed but for ease of interpretation they were grouped into classes. In Figure 3.3 the bars represent the average cost of the class, whereas the scatter points are the specific polymer price point. A maximum price cut-off was set at 10 £/kg; anecdotally this is an absolute limit for the production of FMCGs, although cost would ideally be lower. This limit also allows a large range of thermoplastics to be examined, and allows any polymer which could be feasibly used in the production of FMCGs to be included in further analysis of compatibility with HSS for this application.

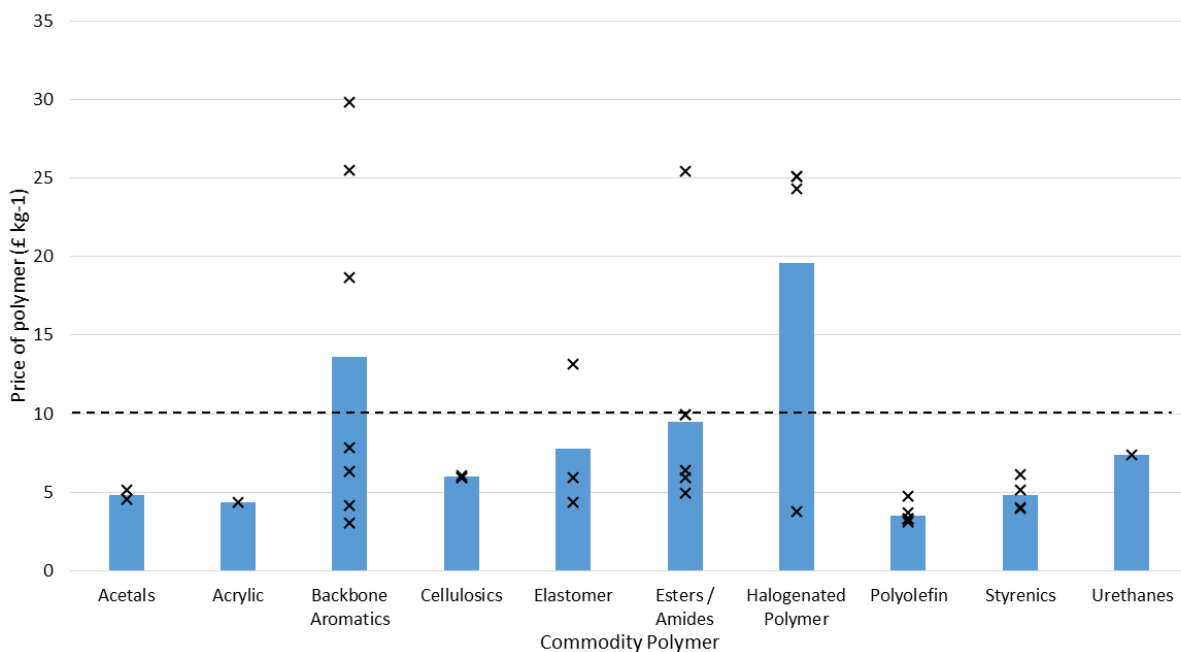


Figure 3.3. Chart showing cost of polymer for each class of polymer with an overlaid scatter graph for the price of each specific polymer. A dotted line at 10 £ / kg is overlaid.

### 3.2.5 Summary of material compatibility

'Commodity thermoplastics' were analysed using the criteria of chemical, processing and application compatibility as well as cost analysis. This research is summarised in Figure 3.4, where the polymers which can be used in HSS are denoted by the green marker. This is in comparison to the red markers denoting too high cost (3.2.4), yellow denoting either process or chemical incompatibilities (3.2.1 - 3.2.2), blue not appropriated due to application (3.2.3) and black as other (e.g. possible chemical incompatibilities with lack of supply of processable material in the correct form). The polymers denoted with a black mark were backbone aromatics. These may be processable but due to their ability to absorb strongly in the same region of the electromagnetic spectrum as the sinter lamp emits, as described in Section 3.2.1, the processability of these materials is likely to be problematic, therefore were excluded from further investigation.

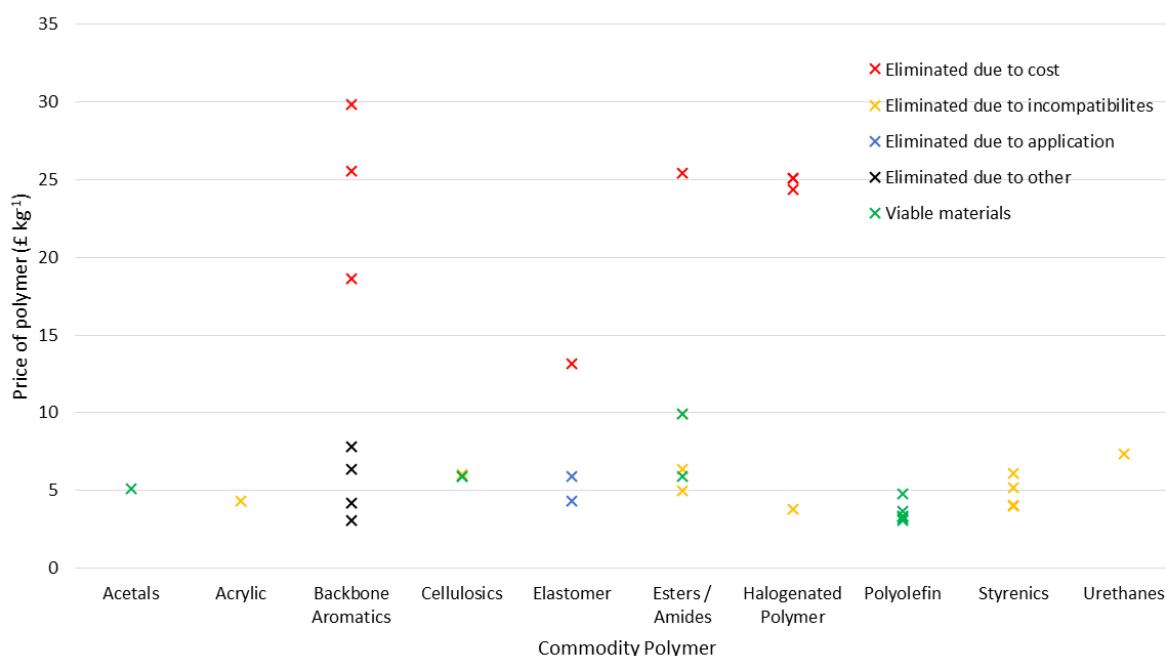


Figure 3.4. Scatter graph showing the cost of various polymers, with red signifying polymers eliminated due to cost, yellow showing incompatibilities from process or chemical properties, blue showing polymers not suited to FMCG's, black other and green denoting polymers which can be used in the HSS process.

### 3.3 Polyolefins

After assessing compatibility according to each of these criteria, the remaining polymers were polyolefins, acetals and cellulose. There is also a lack of supply of material in the correct form made from acetal or cellulose suitable for PBF. Furthermore, polyolefins are substantially better understood in LS (85-87), polyolefins include polyethylene (PE) (49, 85, 88) and polypropylene (PP) (89-92), with PP showing the greatest success. This was therefore deemed the most likely to be successful in HSS, and therefore the closest to a potentially commercially-viable solution. PP is also an ideal polymer as

it is a common polymer in the FMCG area due to the low price of the material and the relatively high mechanical properties.

### 3.4 Polypropylene

Since the beginning of this decade the research in the literature of powder PP as a material for the use in LS has greatly increased and practical examples have been shown. This increase in research is led by demand by industry to have alternative materials to Nylons, due to price and restrictions such as material properties shown by polyamides. Although polypropylene has not previously been used in HSS, in order to gain any relevant insights the use of PP in LS has been investigated.

Research by Drummer *et al.* (93) showed comparison between various polymers in LS and reference IM values. These polymers included; polyamide 12, polyether ether ketone, polyoxymethylene, high density polyethylene and polypropylene. This research displayed it was possible to sinter a PP powder with mechanical properties similar to injection moulded specimens for the Young's Modulus (YM) and Ultimate Tensile Strength (UTS), but significantly reduced for Elongation at Break (EaB). EaB values of 4 % were found for LS, compared to in excess of 50 % for IM specimens, see Table 3.1. Drummer *et al.* suggested that these poor values for EaB were caused by long sintering times leading to high crystallinity, a coarse surface and residual porosity of the parts. Another possible reason for lower EaB values than IM is the lack of shear in LS and the vast majority of AM techniques. The shear in IM especially across thin sections (for example the gauge length in a tensile test specimen) can lead to chain alignment and hence a part with a higher EaB as chains are trying to move past each other. This is in contrast to the more random orientation observed in AM as there is no shear to cause the chains to align.

Table 3.1 Mechanical properties of IM PP, data from Polymer Handbook (82, 94).

Material	UTS (MPa)	EaB (%)	YM (MPa)
Injection Moulded PP	35.5	150	1380

Various other researchers have investigated the use of PP in LS. Wegner (81) similar to Fiedler *et al.* showed that it would be possible to use several materials as feedstocks for LS, using Differential Scanning Calorimetry (DSC) and hence the process window of the materials. The research then went on to process a pre-commercial grade of PP designed for LS by ROWAK on two different LS machines. The research demonstrated a difference in material properties using different LS machines but that PP was processable in both. The highest values of EaB obtained in this research were roughly 15 % which is comparable to values obtained for Nylons on the same machine (95). This was an important result showing the possibility of PP demonstrating comparable material properties to an expensive

Nylon 12 material. Further research by Wegner *et al.* (90) showed the ageing effects of the same PP in LS. Virgin, refreshed and once used powder was used in the processing, with little effect of powder age on part density, YM and UTS, although EaB decreased as powder was aged.

Zhu *et al.* (89) studied a low iso-tacticity PP provided by Trial Corporation Japan, the powder properties were studied and then processed in laser sintering. The PP powder was a near spherical shape and smooth, an indication of a non-milled PP. The research reported a maximum UTS value of 19.9 MPa but no EaB was reported so this cannot be commented on. Figures of complex geometries were also published showing the ability to manufacture consumer parts and not purely tensile specimens. Further work by Zhu *et al.* (96) using the same polymer feedstock, showed a comparison between LS and IM, this research demonstrated an EaB of 122 % was achievable for LS PP parts. This was a significant increase compared to other research published. However this remains a large decrease compared to the 609 % achieved from IM parts. The PP used in this research is by far the best performing PP in currently published research with respect to mechanical properties. However the spherical nature and the smoothness of the powder particles in the manufacture of the powder is likely not to be the same as in the manufacture of traditional commodity PP and more akin to techniques used for AM grades of polyamides, which are precipitation polymerisation where monomer is polymerised directly into a powder by precipitating out after polymerisation (97). As discussed in Section 2.4.4, this would lead the powder to have a better native flowability without the need for additives.

Research into a commercially available PP (CP22 PP) for LS was also conducted by Kleijnen *et al.* (91), where the study investigated the effect of a nucleating agent added to the powder in LS. The addition of a nucleating agent to PP was investigated in traditional manufacturing techniques, with the benefit of reducing shrinkage caused by crystallisation. The addition of a nucleating agent may however cause recrystallisation of the polymer in the LS and HSS processes, reducing the process window. Kleijnen *et al.* work shows little benefit of a nucleating agent at a low and ideal energy density but demonstrates a plateau of mechanical properties at higher energy densities compared to the decrease of the pure CP22 PP. The maximum tensile values published were a UTS of 12.5 MPa, EaB of 1 % and YM of 1900 MPa. In summary Kleijnen *et al.* demonstrated the optimal tensile properties for CP22PP were obtained at the lowest energy densities published. In comparison to Table 3.1 it is clear this grade of PP and other PP designed for laser sintering have substantially lower EaB than IM specimens.

Other work has included the use of blends of polymers where PP and other higher performance polymers were mixed to manufacture AM parts (98); however this technique had little success and was at greater cost.

As shown previous in Chapter 2 there are similarities between HSS and LS but there are also key differences. The work reviewed in this Section shows how PP has been processed previously in LS. LS has shown it is possible to process PP in PBF. One of the major differences between the techniques is the use of an infrared absorbing ink and an IR lamp rather than a laser to cause the powder to sinter. Polypropylene as it does not strongly absorb in the same region as the sintering lamp, has a good probability of being processable in HSS.

### 3.5 Conclusions

This chapter has shown a comprehensive examination of various commodity thermoplastics for their possible use in HSS. Polypropylene was identified as an ideal material for the production of fast moving consumer goods via HSS, due to its cost and processing compatibilities. At the current time there is no published research regarding the use of PP as a powder for use in HSS, meaning work in this area will be completely novel.

Literature identified in Section 3.4 shows that PP can be processed in LS with certain limitations but that the specific grade has an effect and therefore different grades of PP will be examined in this thesis. Hence the remainder of this thesis will focus on the use of commercially and developmental grades of PP in HSS.

## Chapter 4 Processability of a commercial polypropylene grade

The objective of the work described in this chapter is to provide an initial understanding of the behaviour of polypropylene in HSS. The material feedstock selected was a commercially available PP (CP22 PP) purchased from Diamond Plastics, which has been previously processed in Laser Sintering (91). As discussed in Chapter 3, PP has not previously been processed in HSS. However, the ability to process this material in Laser Sintering (LS) was considered an indication of potential for use in HSS. The work examines the effect of processing parameters in the HSS process on various properties of the parts manufactured.

### 4.1 Characterisation of raw materials

Before attempting High Speed Sintering (HSS), the CP22 powder was fully characterised according to existing practices in powdered-polymer AM. In some cases these results have been compared with Nylon-12, the most documented polymer sintering material, and in others these results will be used to compare with other PP grades in later sections.

#### 4.1.1 Powder flow

Powder flow is critical in powder bed fusion AM as a consistent even powder layer is required to be able to manufacture reproducible parts, hence powder flow and density will be examined below.

**Tapped Density.** The tapped bulk density of a powder gives an indication of the potential density of the powder bed. A higher tapped density may allow a more dense part to be produced when sintered, whereas a lower value may indicate poor powder packing. The bulk density was measured by quantifying the tapped density of the material using the apparatus as described by Geca(99), where the measurement of density was based upon a document published by U.S. Pharmacopeia(100). The method used was performed as follows:

- A 100 ml measuring cup was used with an extension piece that doubled the volume of the cup, the cup was then filled with powder.
- The cup was then placed on a mechanical platform (see Figure 4.1) that allows the operator to tap the cup by 10 mm per tap, this was tapped 500 times.
- The extension sleeve was then removed and the excess compacted material was scraped off, leaving 100 ml of powder remaining.
- This remaining powder was then weighed on an OHAUS Pioneer PA64C Analytical Balance and the tapped density was calculated. This test was repeated three times for each powder. The apparatus used is shown in Figure 4.1.

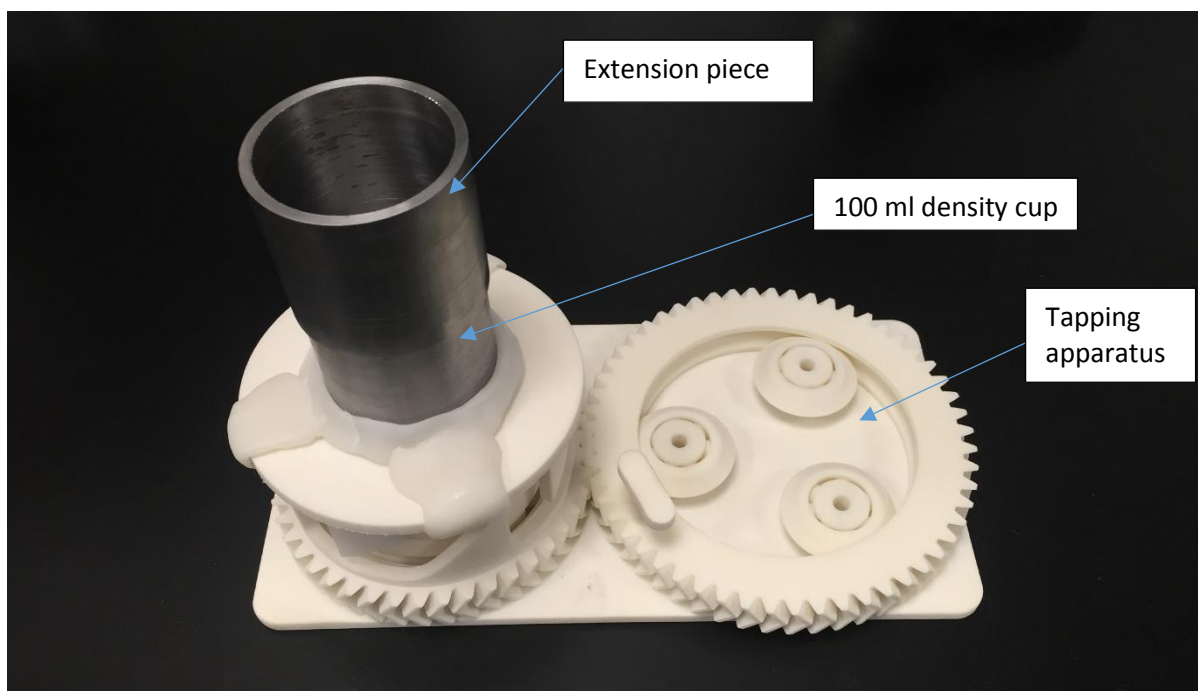


Figure 4.1 Apparatus to measure tapped density, designed by Geca(99). The cogs lead to one rotation of the gear to lead to five taps of the density cup.

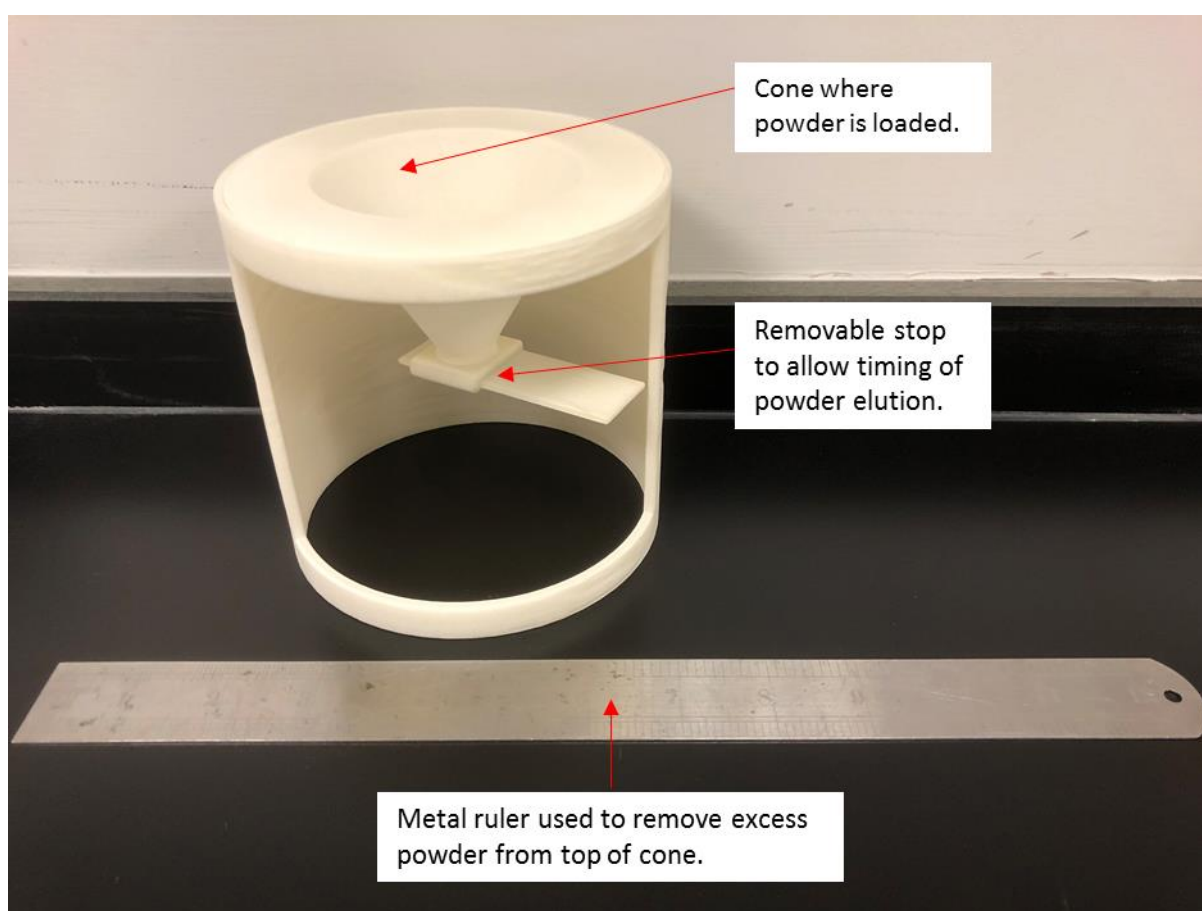
The tapped density of the virgin CP22 was  $0.47 \text{ gcm}^{-3}$ . The tapped bulk density of PA2200 is  $0.52 \text{ gcm}^{-3}$ , similar to the reported bulk density without tapping reported by EOS of  $0.45 \text{ gcm}^{-3}$ (68), Table 4.1 shows results of individual runs. These values are comparable and indicate a similar packing of the build bed before sintering. Whilst this is not an exact quantification of the packing of the powder in the bed in the HSS machine it is a useful comparative measure.

Table 4.1 Tapped bulk density of CP22 PP and PA2200 for each run and averages. Standard deviation is shown in brackets.

Run	Density of CP22 PP ( $\text{gcm}^{-3}$ )	Density of PA2200 ( $\text{gcm}^{-3}$ )
1	0.467	0.517
2	0.468	0.519
3	0.466	0.517
<b>Average</b>	<b>0.47 (0.001)</b>	<b>0.52 (0.004)</b>

**Powder Flow.** Good powder flow is required in order to deposit an even layer of the required thickness onto the powder build bed throughout the process. Quantifying any change in powder flow is therefore critical to help predict whether the polymer may be suitable to be used in the sintering process. Two traditional methods of measuring powder flow are Carney and Hall flow (101), however these methods are not used in assessing the flowability of powders for polymer powder bed fusion techniques (87, 102, 103), due to the poor flow of polymers through a Hall or Carney funnel. A method

of measuring powder similar to Hall and Carney flow was developed using a larger orifice to allow the testing of a powder polymer (104), whereby a cone is loaded with powder (without compression) and the time for the powder to elute through the orifice of the cone is recorded, Figure 4.2. A Nylon printed cone was used this equipment was used as it had been used in previous research, it should be noted that the rough surface of the cone leads to the powder not flowing in the cone as well as a machined metal cone as used in a Hall or Carney flow test. Although not fully representative of behaviour within the HSS system at elevated temperature, these results can provide a useful comparison for benchmarking. For each powder sample five runs were carried out. The test method itself is affected by conditions and user; for this reason the testing was carried out by the same scientist on the same day at 19 °C and 41 % humidity.



*Figure 4.2 A photograph showing the equipment used to measure powder flow of CP22 PP and PA 2200 as a reference.*

Powder flow can be affected by several different factors including: powder size, size distribution, shape and any extra additives. However, it is often the overall effect of these contributing factors which is most relevant. As discussed above, the flowability of the CP22 powder was measured using a

customised flow test; results of this are shown below in Figure 4.3 with a value for PA2200 (Nylon-12) powder shown for comparison.

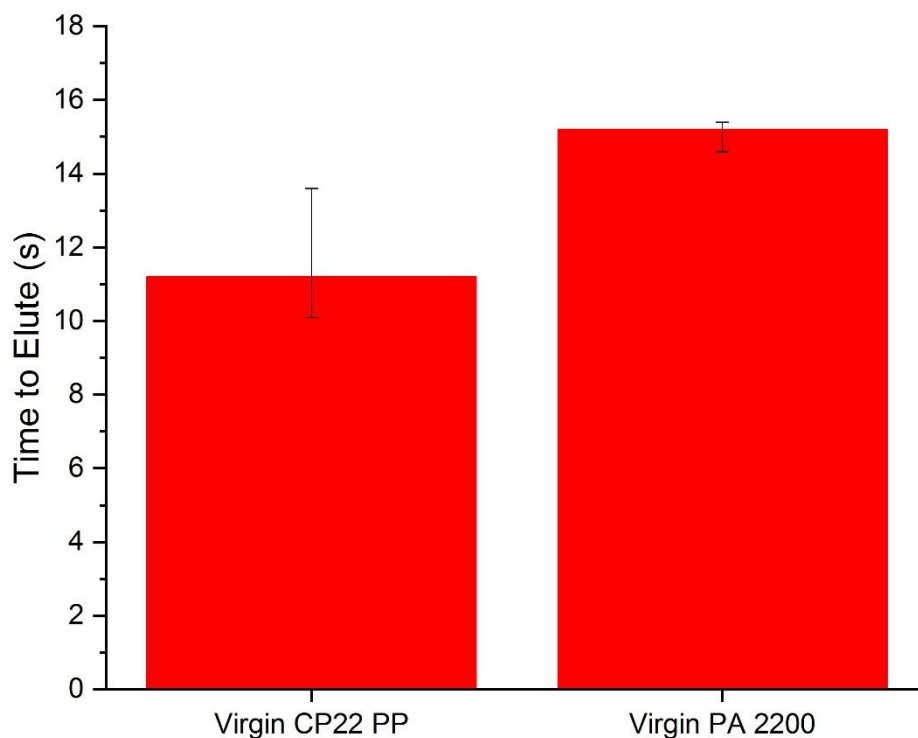


*Figure 4.3. Elution time for powders to flow through the funnel. The error bars included are range bars.*

As seen in Figure 4.3 the variability in the powders was larger for the CP22 PP than for the PA2200. It can also be seen that the polypropylene (11.2 s) flows more freely than the Nylon powder (15.2 s). This provides an indication that the PP powder is likely to provide a comparable level of powder bed filling.

Hausner ratio is often used as an indication of powder flow (103, 105, 106). Hausner ratio is the ratio of the tapped density over freely settled apparent density (107), where a value of over 1.25 is an indication of poor flowability. The Hausner ratio was not studied in this thesis but as described above an experimental method was used to measure powder flow.

#### 4.1.2 Particle size and morphology

Particle size and shape have an effect of powder flow and packing of powder, as well as the distribution of these. Therefore it is important to characterise the shape and size of the powders used.

**Particle size analysis.** A mastersizer measures particle size by laser diffraction. A laser light passes through the sample cell and larger particles cause the light to diffract less than smaller particles. The mastersizer is a volume based measurement and in the processing of the data particles are assumed as spherical, as seen in Figure 4.6 this is not always the case. Being a volume-based measurement the graph is skewed towards a larger size, as one large particle has several times the volume of smaller particles. In light diffraction larger particles also diffract the light more than smaller ones hence a larger signal is produced.

A Malvern Mastersizer 3000 with a Hydro EV wet dispersion unit attached was used to measure the particle size of the powder via laser diffraction. The settings used were standard for particles of the size expected, these were as follows. A HeNe laser at 633 nm and a LED operating at 470 nm were used to size the powder particles dispersed in water. The stirring and sonication were set to maximum at 3500 rpm and 100 % respectively for 900 s before being adjusted to 200 rpm and 40 % during data collection. The refractive index used for PP was 1.490(108) and the absorption index set to 0.01. These variables are then used in a Mie scattering model to calculate the particle size from the scattering data. Each measurement consisted of 10 measurements averaged using a single sample and this was repeated three times for each material. The Mastersizer was automatically aligned before each measurement and was cleaned by rinsing three times with de-ionised water.

Table 4.2 shows the size of the powder particles, where the D10 acts as a representation of the fines present in the feedstock as it is the largest particle in the smallest 10 % of particles in the powder. The D90 gives an indication of the largest particles present as it is the largest particle present in the smallest 90 % of particles and the D50 gives a mean average particle size of the powder. Comparison between the Nylon and PP particle size shows there are significantly more small particles in the PP powder which would suggest worse powder flow. Figure 4.4 is a trace of the size distribution of CP22 PP powder.

*Table 4.2. Particle size breakdown of CP22 PP and Nylon 12.*

Material	D (10) ( $\mu\text{m}$ )	D (50) ( $\mu\text{m}$ )	D (90) ( $\mu\text{m}$ )
CP22 PP	11.0	39.9	82.8
Nylon 12	33.3	54.5	84.3

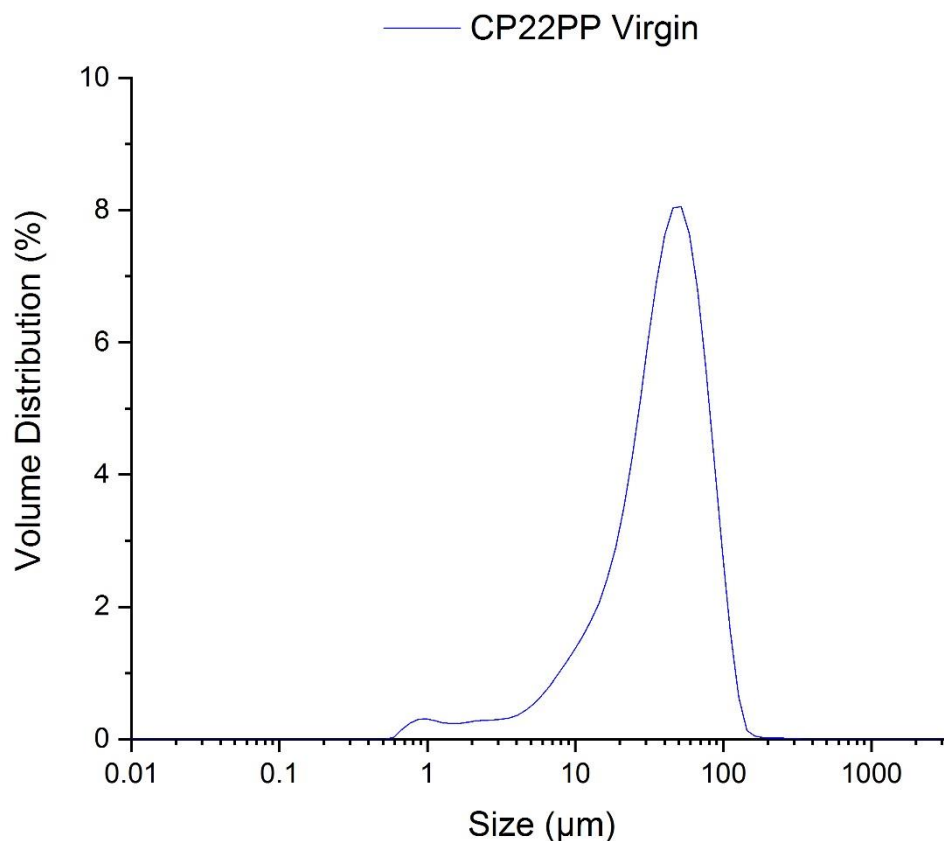


Figure 4.4. Volume distribution against size trace showing the volumetric size distribution of PP CP 22.

**Particle size and particle shape image analyser.** Image analysis can be used to measure powder particle shape and size of CP22 PP. A Malvern Morphologi G3 was used to analyse particles to examine their size and shape via image analysis. The Morphologi G3 uses a dry dispersion unit (SPD1300) to deposit powder particles onto a glass plate, which is then automatically imaged using a microscope. In excess of 8500 powder particles were taken for each sample. The Morphologi software then analyses each powder particle to produce various parameters for each sample. The parameters examined in this work are shown and described in Table 4.3, with results shown in Figure 4.5.

Table 4.3 Parameters measured by image analysis and their descriptions and equations (109).

Measured Variable	Description	Equation
Circle Equivalent Diameter (CE Diameter) - Number Distribution	Diameter of a circle with the same area as the projected area of the particle image measured as a number distribution (number of particles).	
Circle Equivalent Diameter (CE Diameter) - Volume Distribution	Diameter of a circle with the same area as the projected area of the particle image measured as a volume distribution (the volume contribution of the particles). This is similar to traces obtained via laser diffraction.	
Convexity	A measurement of how 'spiky' a particle is, as the value tends to zero the particle becomes more 'spiky'. Hence as the value tends to 1 the particle is smoother.	$\text{Convexity} = \frac{\text{Convex hull perimeter}}{\text{Perimeter of particle}}$
High Sensitivity Circularity (HS Circularity)	The ratio of a particle area to the square of its perimeter, where a perfect circle has a HS Circularity of 1 and a narrow rod has a HS circularity of near 0.	$\text{HS Circularity} = \frac{4 \times \pi \times \text{Area}}{\text{Perimeter}^2}$
Aspect Ratio (AR)	The ratio of width to length of the particle measured.	$\text{AR} = \frac{\text{Width}}{\text{Length}}$

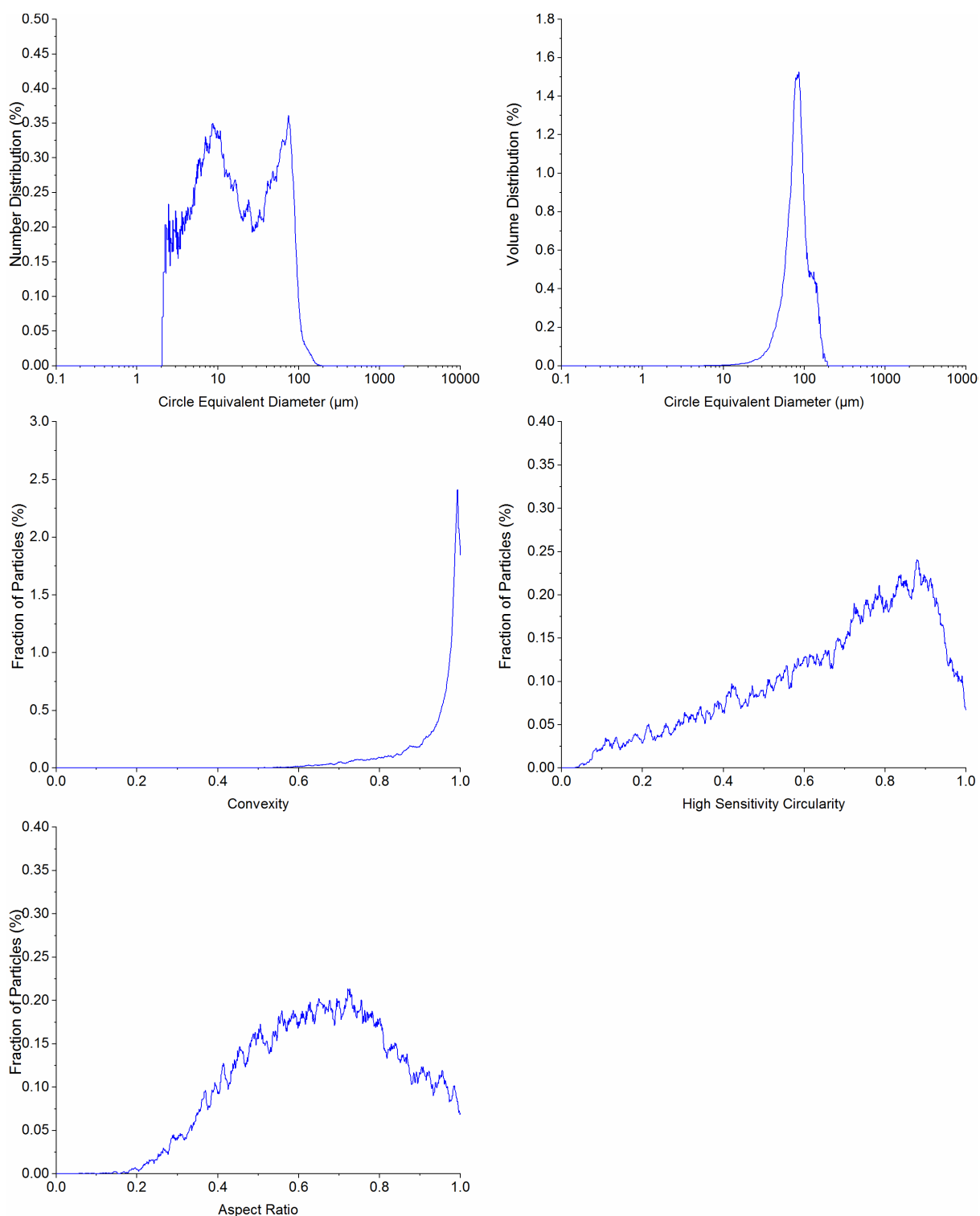


Figure 4.5 Image analysis traces showing size and shape of the CP22 PP powder. (A) Circle equivalent diameter against the number distribution of powder particles. (B) Circle equivalent diameter against the volume distribution of powder particles. (C) Convexity against fraction of powder particles. (D) High sensitivity circularity against fraction of powder particles. (E) Aspect ratio against fraction of powder particles.

There is a large difference between the volume of the particles versus the number of particles. The number distribution has a large amount of small particles not obvious in the laser diffraction particle size trace, the volume distribution does show a good correlation to the laser diffraction trace, see Figure 4.4. The convexity value indicates a smooth powder. The HS Circularity shows there are particles with a wide range of circularity with the AR distribution the powder is shown to be non-spherical. These graphs of size and shape will allow comparison to other polypropylenes and aid in understanding any differences in the flow characteristics of the materials.

**Scanning Electron Microscopy (SEM).** The use of SEM allows the study of powders at a smaller length scale in comparison to optical microscopy. SEM allows the surface texture of the powder to be investigated. SEM was conducted using a Philips XL 30S FEG SEM and a Cambridge Instruments Ltd S240 SEM. However the same method was used for both and will be described subsequently. Powder samples were placed on carbon tape to form a mono-layer on the SEM stub and then sputter-coated with a thin layer of gold, thus minimising charging of the sample during imaging. The typical operating voltage of the beam was 10 kV.

Figure 4.6 shows SEM images of CP22 PP powder at low and high magnification. The uneven shape of the polypropylene suggests the powder has been milled, whereas the smooth spheres observed are likely to be glass spheres added as flow agent (110).

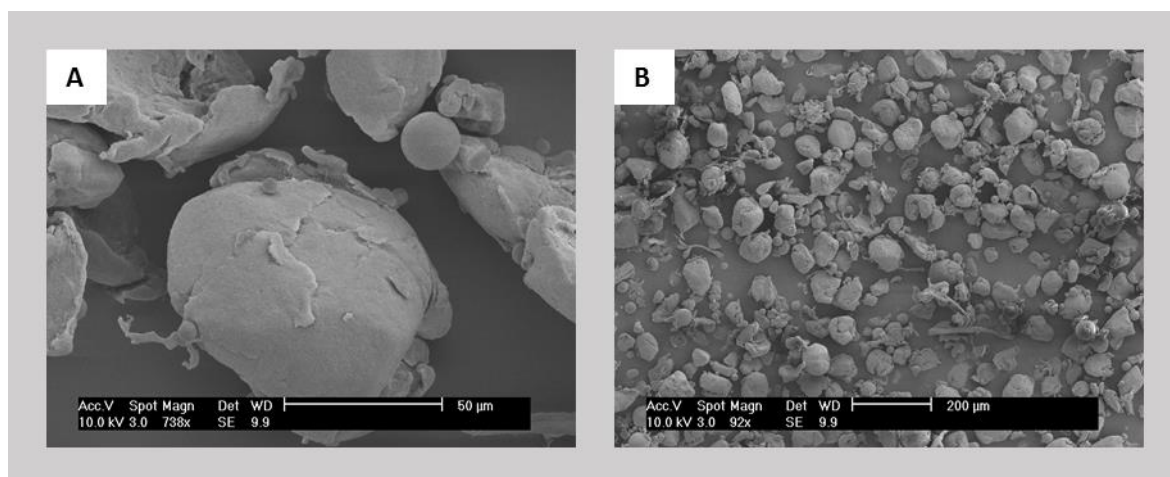
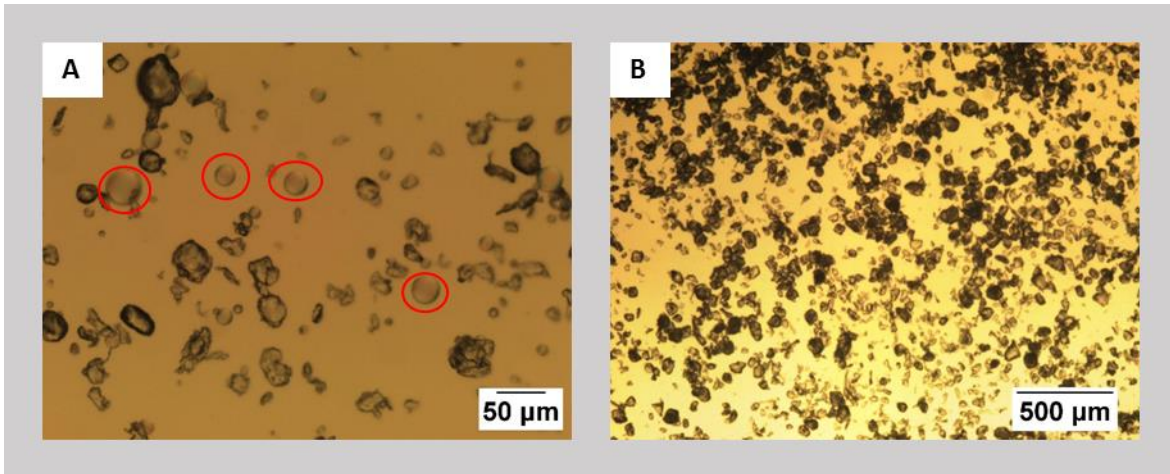


Figure 4.6. SEM of virgin CP22 PP (A&B) used high and low magnification respectively.

**Optical Microscopy.** Microscope images were obtained using an Olympus BX50 microscope using a VisiCam 10.0. Scale bars were calculated using a graticule calibration slide with an accurate scale which allows scale bars to be added to microscope images. A small amount of powder was placed onto a glass microscope slide and back lit from below to produce microscope images, as shown in Figure 4.7



*Figure 4.7 Optical microscopy images of CP22 PP (A&B) using high and low magnification respectively, with the highlighted red circles showing likely glass spheres used as flow additives.*

The powder flow tests indicate a good powder flow. However the size and shape information indicates the opposite, as there is a large amount of small powder particles. As well as a large contribution from particles of non-spherical shape which also reduce powder flow (72). SEM images as shown in Figure 4.6 show a large quantity of fines, supported by the image analysis shown in Figure 4.5. The fines are generated from the manufacture of the PP powder due to grinding. These differences however can potentially be rectified by the addition of powder flow additives to allow the powder to fit the requirements for flow in the process. Evidence of the presence of additives is shown in the SEM and optical microscope images in Figure 4.6 and Figure 4.7, where glass has been added to aid the flow properties.

#### 4.1.3 Thermal properties

The thermal properties of a powder for use in HSS are critical as they determine the optimum parameters to be used. These thermal properties can be studied as below to be able to predict initial parameters to be used in HSS.

**Differential Scanning Calorimetry (DSC).** DSC can be used to determine both the melt and recrystallisation temperature of the powder examined. The melt and recrystallisation temperatures form a process window in which the machine can process the powder into AM parts. Figure 4.8 shows a DSC trace for a Nylon material, showing a clear melt peak, recrystallisation peak and process window.

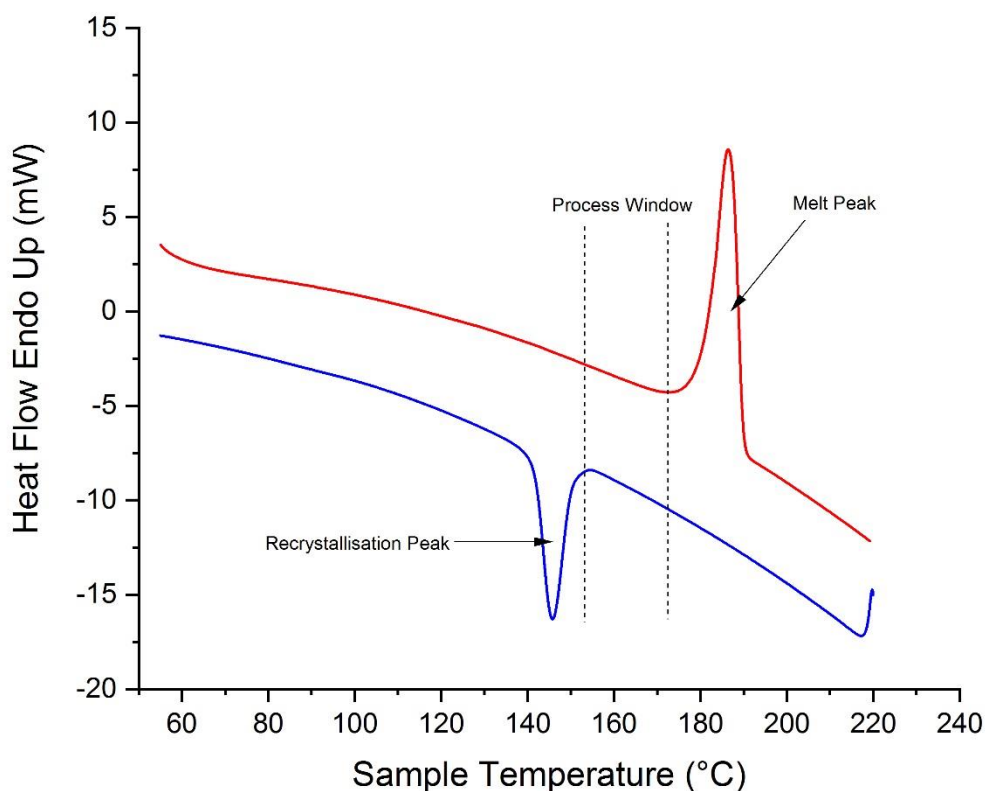


Figure 4.8. DSC trace of Nylon 12; temperature scan at 10 °C / min.

DSC was used to quantify the melt and recrystallisation temperatures for the powder, using a PerkinElmer DSC 8000. A sample 7 mg  $\pm$  2 mg was placed in an aluminium sample pan. This pan was then crimped and placed in the DSC sample furnace with an empty crimped sample pan placed in the reference surface. The samples then underwent a temperature cycle as follows:

1. Held at 20 °C for 1 min.
2. Heated from 20 °C to 200 °C at 10 °C/min.,
3. Held at 200 °C for 1 min.,
4. Cooled from 200 °C to 20 °C at 10 °C/min.,

This temperature cycle was chosen as 10 °C/min is a standard rate used in literature (111) and 20 °C to 200 °C were selected as this meant temperatures from room temperature to above melt temperature would be examined without becoming so hot that degradation of the polymer started. The hold steps were used to ensure the full temperature range was obtained. The peak temperatures were defined at the peak maxima and minima. An increase in recrystallisation temperature is likely to cause the powder build bed to curl due to stress. A decrease in the melt temperature would cause the

build bed to sinter in areas which were not selected to be selectively sintered. A significant increase in melt temperature could possibly cause an insufficient amount of energy input into the part to allow a full sinter and hence create poor quality parts.

The initial temperature to set the build bed can be determined from the initial DSC trace of the virgin powder, see Figure 4.9. Standard practice in LS and HSS is to aim for a set point of approximately 10 °C lower than the melt point for an initial build bed temperature.

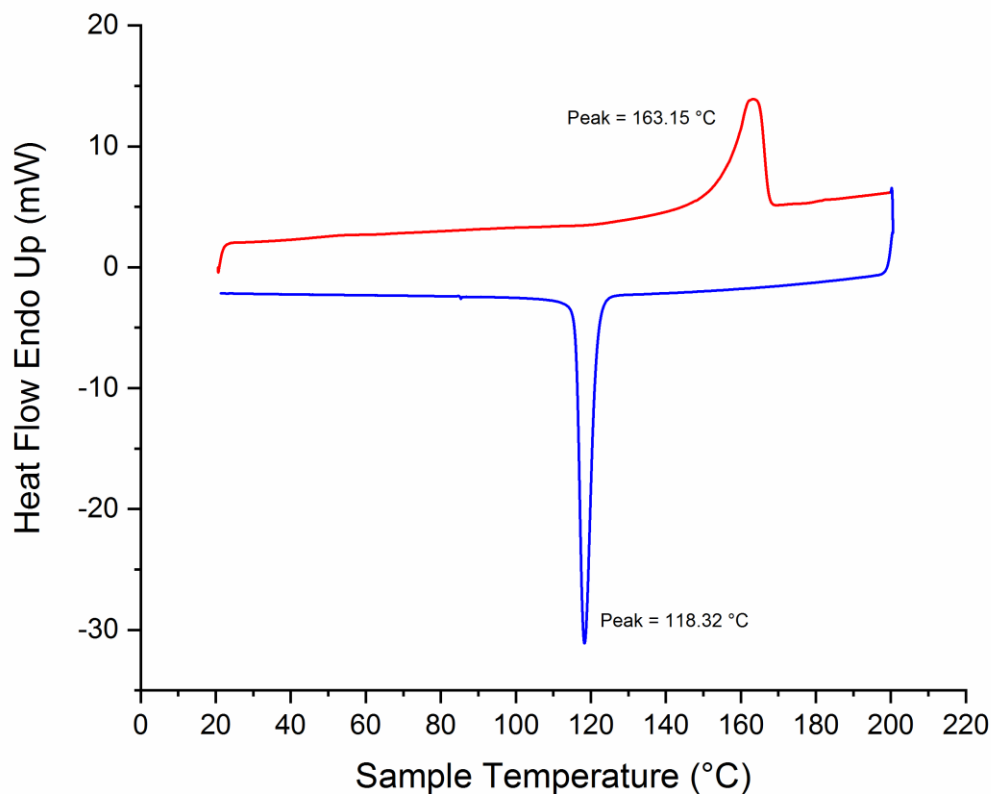


Figure 4.9. DSC curve of virgin PP; temperature scan at 10 °C/min.

The peak melt temperature of CP22PP was measured as 165.15 °C and a peak recrystallisation temperature of 118.25 °C as an average of 3 runs. These maxima and minima are calculated by differentiating the curve, where the differential is equal to zero the point is the maxima or minima. The DSC data shows there is a process window, between the melt and recrystallisation temperature of the CP22PP although the melt peak is not as sharp as measured for Nylon 12. Due to this reason the process window cannot be defined as simply by the temperature difference between the melt and recrystallisation temperatures. The broader peak shown by PP in comparison to polyamides may require the bed temperature to be set further from the peak melt temperature, because otherwise

the powder bed would begin to sinter without the IR absorbing ink. A broad peak would require a large amount of energy input to ensure a fully sintered part.

#### 4.1.4 Powder characterisation summary

The powder characterisation carried out in this section gives critical information on the processing of this material in HSS. The thermal properties as shown in Figure 4.9 demonstrate a processing window between the recrystallisation and melt temperature of CP22 PP.

The flowability of the powder indicates that an even and consistent powder layer is likely to be possible, given the many similarities with PA2200 Nylon-12 Laser Sintering material. However the size and shape information does not indicate a powder of good flow as the particle size is small and the shape non-spherical which would normally lead to poor flow. These differences however can potentially be rectified by the addition of powder flow additives to allow the powder to fit the requirements for flow in the process. Additional evidence of the presence of additives is shown in the SEM images in Figure 4.6. The addition of flow agents has previously been shown to decrease the mechanical properties of HSS parts (78), which may lead to the mechanical properties of CP22 PP being reduced.

The research carried out in this section also will provide a strong benchmark for comparison with other powders used in this thesis later and may help identify any differences in processing and part properties.

## 4.2 Part manufacture via High Speed Sintering

Parts were manufactured using voxeljet's 'alpha' VX2000 High Speed Sintering (HSS) system, based at The University of Sheffield; the process is described in Section 2.1.2. Five ASTM D638 Type I tensile test specimens were produced, with four rectangular blocks the same size as the gauge length to test density. The minimum spacing for the parts manufactured was 2 mm, in accordance with standard spacing developed for this machine. Figure 4.10 is an image of the build layout in the Rapix3D HSS software. In order to efficiently record individual samples, tensile specimens were labelled according to the position in the build volume. The build was laid out in the build volume of the HSS machine in a modelling scene with all samples built in the XY direction. Ellis *et al.* (42) demonstrated the effect of orientation on HSS parts and showed the best mechanical properties in the XY direction hence this direction is used in this research.

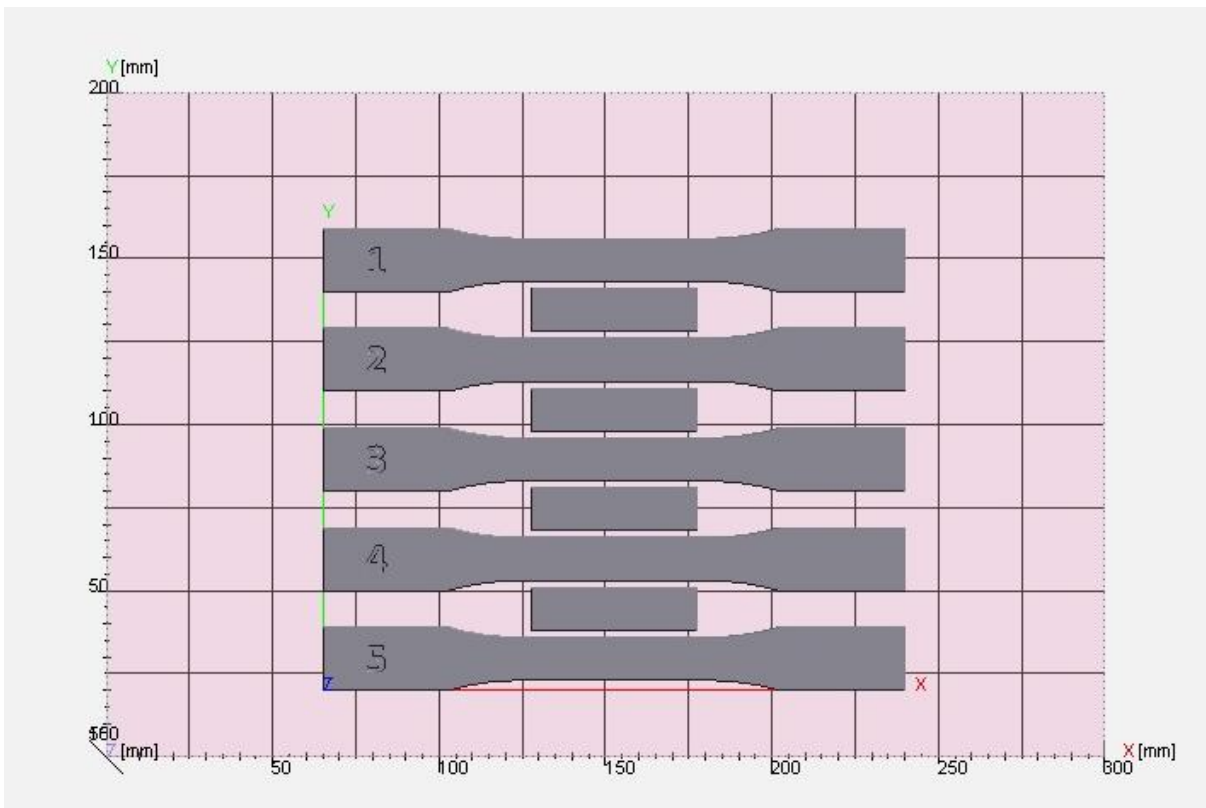


Figure 4.10 Image showing build layout in Rapix3D from a top view showing the x and y direction.

Powder was used as received according to manufacture recommendations for Laser Sintering.

The process of manufacture of parts is outlined below:

- The build stereolithography file (STL) was loaded into Rapix3D software, the HSS system control software.
- The build was then sliced before building could commence.
- A standard of 50 blank layers are added to the base of the build before the parts are manufactured. This allows thermal stability to be achieved before manufacture of parts as it leads to the lamp moving across the build bed and the target build temperature to be achieved.
- The machine was preheated for 45 minutes before build commenced.
- The build is then commenced including the 50 pad layers.
- After the build is finished, the cooling schedule was a single pad layer to complete the sinter of the final printed layer, heaters were then turned off and the machine was then allowed to cool to 100 °C, standard in HSS and LS.
- Parts were then removed from the HSS before being allowed to cool to room temperature before post-processing.

- Excess loose powder was tapped off the part and more rigid powder was removed using a Guyson Euroblast 4 where compressed air and bead blasting material (Guyson Honite Grade 16 glass media) were used.
- Excess powder which had been heated was classified as used powder and used further in this section of work as only virgin powder was used.

An image of a completed build is included for reference in Figure 4.11.



*Figure 4.11 Photo of parts manufactured using CP22 PP as a feedstock in HSS.*

### 4.3 Identification of initial processing parameters

There are several parameters which can be altered for the manufacture of HSS parts; these parameters are: preheat power, sinter power, preheat speed, sinter speed, recoater vibration, feed hopper fill duration and frequency, grey level, build bed and overhead temperature and layer thickness, see Table 4.4.

Table 4.4 High Speed Sintering parameters.

Parameter	Range
Preheat Power (%)	30 - 100
Sinter Power (%)	100
Preheat Speed (mm/s)	60
Sinter Speed (mm/s)	60 - 150
Recoater Vibration (%)	100
Feed Hopper Fill Frequency	11
Feed Hopper Fill Duration (s)	1.25
Grey level	1 – 5
Build Bed (°C)	135 - 152
Build Overhead (°C)	135 - 152
Layer Thickness (µm)	100

#### 4.3.1 Preheat power

Preheat power is a measure of the percentage voltage to the lamp on the preheat stroke in HSS. The function of this stroke is to heat the freshly deposited powder onto the build bed and reduce shrinkage caused by the deposition of this cooler powder. An initial value of 50 % was used as this is standard in HSS. Preheat power was selected as a variable to be altered throughout the research as it is a way of increasing or reducing energy into the system. The area to be sintered is covered by a single layer of powder at the point of the preheat stroke, and this preheat pass aids in inputting energy into the powder bed in addition to the overhead heaters.

#### 4.3.2 Sinter power

Sinter power is a measure of the percentage voltage to the lamp on the sinter stroke in HSS. The sinter stroke follows the printing of the infrared absorbing ink in HSS. 100 % sinter power was used throughout the builds as the lamp's spectral output is most aligned to the absorption spectra of the lamp at 100 % power. This high power also allows the sinter lamp to travel across the build bed at the fastest rate, reducing layer and hence build time, whilst still inputting the same energy input.

#### 4.3.3 Preheat speed

Preheat speed is the speed the carriage moves across the build bed for the new layer deposition as well as the preheat lamp. This speed was fixed at 60 mm/s the standard in VX200 HSS machine as at this speed a good even powder deposition was acquired.

#### 4.3.4 Sinter speed

Sinter speed is the speed at which the sinter lamp crosses the freshly printed layer. This parameter was used as a variable to change the amount of input energy into the system during the sinter stroke. After some trial work a speed of 105 mm/s was chosen to be the starting value for the sinter speed.

#### 4.3.5 Grey level

Grey level is the amount of infrared ink deposited by the printheads. The printheads used in the VX200 HSS have seven different levels of ink printable. Previous work with Nylon 12 on this machine had indicated a grey level of 2 or 3 to give good part properties. Hence for this work a grey level of 3 was selected initially to allow a greater variation around the mid-point for future builds.

#### 4.3.6 Build bed temperature

Build bed and overhead temperature is the temperature to which the build area is heated to. There are overhead ceramic heaters and pad heaters on the bottom of the build piston to maintain the temperature set. A standard rule of thumb in HSS and LS is to set the initial bed temperature to 10 °C lower than the melt temperature. This melt temperature was calculated using DSC (see 0) and found to be 163 °C, suggesting a bed temperature of 153 °C.

### 4.4 Effect of processing parameter variation

Various builds were attempted, within the range stated previously in Table 4.4. The results of the builds were classified into five categories, as shown in Table 4.5;

*Table 4.5 Build classifications and the explanation of the terms used, where the builds classified by the first two terms were then further tested. Compared to the other build classifications which were described and could not be further tested.*

<b>Classification</b>	<b>Explanation</b>
Complete	All test pieces were manufactured and post processed, then analysed.
Complete but 1 test piece failed	All but one test pieces were manufactured and post processed, the remaining pieces were then analysed. The piece that was not complete failed due to localised curl on the single piece.
Failed due to powder removal	The manufacture of parts was completed but the excess powder around the parts was sintered to the extent it could not be removed by reasonable post processing.
Failed due to build bed sintered	The build bed became fully sintered before the beginning of printing ink (during the 50 pad layers), therefore the build was abandoned at this point.
Failed due to curl	During a point of the manufacture of test pieces they underwent curl and caused the build area to fail.

Four variables were altered independently to assess the effect of build overhead and bed temperature, grey level, sinter speed and preheat power on properties.

The build name notation used is **G\_S\_P\_**, where **G** is the amount of ink used (the grey level), **S** the sinter speed where the lowest number is the fastest sinter speed and hence the least energy input and **P** the preheat power with higher number indicating higher preheat power. The lowercase letter signifies a repeat measurement and capitalised build names are used where this notation is not viable.

#### 4.4.1 Experimental rationale

Design of Experiment (DoE) is method for manipulating multiple inputs (machine parameters) to define their effect on outputs (part properties) (112). As well as demonstrating the effect of each individual parameter DoE can also show how the different inputs interact with each other to change the outputs. By using a DoE it is possible to investigate several levels of each parameter with several different parameters without the requirement for an unfeasible amount of experimentation, which would be required for a one factor at a time experimentation method.

A limitation of DoE is that an output is required for all of the experimentations for the statistical analysis to be carried out. Required experiments are those at the extremes of the parameter set i.e. the maximum energy input from all 4 factors investigated as well as the minimum energy input simultaneously. This was not possible as demonstrated latter in this Section and throughout the experimentation in this thesis, as there is balance between the energy inputs. The aim of the experimentation is not to optimise the machine parameters for processing PP in HSS, but to understand how process parameters impact build quality and part performance.

As a DoE was not a feasible method for the experimental approach, an alternative system was required. Therefore, the approach used was to fix the machine parameters at a successful mid-point parameter set and then vary one parameter at a time. Limitations of this method include the interactions between the parameters are not assessed and characterised. The results may also be limited to the localised parameter area that was examined around the starting parameter set and may not be applicable globally for a wide range of machine parameters. The experimental approach used was the most appropriate to manufacture parts which then could be analysed, this was due to the narrow process range of the materials tested in comparison the to the machine repeatability.

#### 4.4.2 Build bed temperature

Although the DSC trace suggested a build bed temperature of 153°C, initial trials at this temperature found the unsintered powder too hard to remove, and 150°C was identified as a starting point. Moving up or down by 2°C led to build failure, with only three of five builds completing successfully at 150°C.

This indicates that the material has a very limited processing window, and that the current level of machine control is not sufficient to maintain this precision. As 150°C showed the most potential for successful builds, this was selected as the set-point for all further trials.

*Table 4.6 Build parameters where build bed and overhead temperature was varied.*

Build Name	Powder Age	Grey Level	Sinter Speed (mm/s)	Preheat Power (%)	Build Bed and Overhead (°C)	Complete?
<b>A</b>	Virgin	3	105	50	148	Failed due to curl
<b>G3S3P4a</b>	Virgin	3	105	50	150	Complete
<b>G3S3P4b</b>	Virgin	3	105	50	150	Failed due to curl
<b>G3S3P4c</b>	Virgin	3	105	50	150	Complete
<b>G3S3P4d</b>	Virgin	3	105	50	150	Failed due to curl
<b>G3S3P4e</b>	Virgin	3	105	50	150	Complete
<b>B</b>	Virgin	3	105	50	152	Failed due to powder removal not possible

#### 4.4.3 Grey level

The printheads used in the VX200 HSS machine are Xaar 1002 GS6 printheads. A grey level of 1 is where the printhead ejects a single droplet to form a dot, a grey level of 2 is where the printhead ejects 2 droplets and they converge in the air to form a dot, a grey level of 3 is where the printhead ejects 3 drops of ink to form a single dot and so on. It is therefore possible to calculate the amount of ink used per the printed area and this is shown in Table 4.7.

*Table 4.7 Grey level to ink conversion.*

Grey Level of 1002 GS6 Printhead	Ink per area (pL/mm <sup>2</sup> )
1	1205
2	2411
3	3616
4	4821
5	6026

Table 4.8 demonstrates that it was possible to manufacture parts using CP22 PP in HSS at all five different ink levels tested, although the results were again somewhat inconsistent.

Table 4.8 Build parameters where grey level was varied.

Build Name	Powder Age	Grey Level	Sinter Speed (mm/s)	Preheat Power (%)	Build Bed and Overhead (°C)	Complete?
<b>G1S3P4</b>	Virgin	1	105	50	150	Complete but 1 test piece failed
<b>G2S3P4</b>	Virgin	2	105	50	150	Complete
<b>G3S3P4a</b>	Virgin	3	105	50	150	Complete
<b>G3S3P4b</b>	Virgin	3	105	50	150	Failed due to curl
<b>G3S3P4c</b>	Virgin	3	105	50	150	Complete
<b>G3S3P4d</b>	Virgin	3	105	50	150	Failed due to curl
<b>G3S3P4e</b>	Virgin	3	105	50	150	Complete
<b>G4S3P4</b>	Virgin	4	105	50	150	Complete but 1 test piece failed
<b>G5S3P4</b>	Virgin	5	105	50	150	Complete but 1 test piece failed

#### 4.4.4 Sinter speed

Sinter speed is the rate at which the infrared lamp moves across the printed build bed, meaning a faster lamp speed leads to less energy input. A series of builds were carried out by varying the sinter lamp speed from 125 mm/s to 80 mm/s. The parts produced at a speed of 80 mm/s (G3S6P4) were not suitable for tensile testing as removal of the excess powder from around the part was not possible, as it was too hard to remove.

Table 4.9 Build parameters where sinter speed was varied.

Build Name	Powder Age	Grey Level	Sinter Speed (mm/s)	Preheat Power (%)	Build Bed and Overhead (°C)	Complete?
<b>G3S1P4</b>	Virgin	3	125	50	150	Complete but 1 test piece failed
<b>G3S2P4</b>	Virgin	3	115	50	150	Complete
<b>G3S3P4a</b>	Virgin	3	105	50	150	Complete
<b>G3S3P4b</b>	Virgin	3	105	50	150	Failed due to curl
<b>G3S3P4c</b>	Virgin	3	105	50	150	Complete
<b>G3S3P4d</b>	Virgin	3	105	50	150	Failed due to curl
<b>G3S3P4e</b>	Virgin	3	105	50	150	Complete
<b>G3S4P4</b>	Virgin	3	95	50	150	Complete
<b>G3S5P4</b>	Virgin	3	85	50	150	Complete
<b>G3S6P4</b>	Virgin	3	80	50	150	Powder removal not possible

## 4.4.5 Preheat power

The final variable studied in this work was the preheat power, this is the amount of energy the bed experiences from the lamp after a new layer of powder is deposited. The builds carried out can be seen in Table 4.10. The initial percentage was set as 50 % (standard HSS practices) and the manufacture of parts with a preheat power 20 % either side of this level was attempted. The inconsistency mentioned earlier led to build **G3S3P2** unexpectedly failing due to curl and this build was therefore repeated. The **G3S3P6** build failed at higher levels of energy leading to the entire bed sintering.

Table 4.10 Build parameters where preheat power was varied.

Build Name	Powder Age	Grey Level	Sinter Speed (mm/s)	Preheat Power (%)	Build Bed and Overhead (°C)	Complete?
<b>G3S3P1</b>	Virgin	3	105	30	150	Complete but 1 test piece failed
<b>G3S3P2a</b>	Virgin	3	105	40	150	Failed due to curl
<b>G3S3P2b</b>	Virgin	3	105	40	150	Complete but 1 test piece failed
<b>G3S3P3</b>	Virgin	3	105	45	150	Failed due to curl
<b>G3S3P4a</b>	Virgin	3	105	50	150	Complete
<b>G3S3P4b</b>	Virgin	3	105	50	150	Failed due to curl
<b>G3S3P4c</b>	Virgin	3	105	50	150	Complete
<b>G3S3P4d</b>	Virgin	3	105	50	150	Failed due to curl
<b>G3S3P4e</b>	Virgin	3	105	50	150	Complete
<b>G3S3P5</b>	Virgin	3	105	60	150	Complete
<b>G3S3P6</b>	Virgin	3	105	70	150	Failed - build bed fully sintered

Table 4.11 summarises all attempted builds, with the various build parameters used.

Table 4.11 Summary table of builds attempted, with build parameters with build name. **G** indicates the grey level, **S** sinter speed where lower **S** value indicates a higher speed and therefore less energy input and **P** the preheat power. Small letters indicate repeat at same parameter set and capitals are used where bed and overhead temperature are non-standard. Cells highlighted are the centre point repeats used.

Build Name	Grey Level	Sinter Speed (mm/s)	Preheat Power (%)	Build Bed and Overhead (°C)
<b>G1S3P4</b>	1	105	50	150
<b>G2S3P4</b>	2	105	50	150
<b>G3S3P4a</b>	3	105	50	150
<b>G3S3P4b</b>	3	105	50	150
<b>G3S3P4c</b>	3	105	50	150
<b>G3S3P4d</b>	3	105	50	150
<b>G3S3P4e</b>	3	105	50	150
<b>G4S3P4</b>	4	105	50	150
<b>G5S3P4</b>	5	105	50	150
<b>G3S1P4</b>	3	125	50	150
<b>G3S2P4</b>	3	115	50	150
<b>G3S4P4</b>	3	95	50	150
<b>G3S5P4</b>	3	85	50	150
<b>G3S6P4</b>	3	80	50	150
<b>G3S3P1</b>	3	105	30	150
<b>G3S3P2a</b>	3	105	40	150
<b>G3S3P2b</b>	3	105	40	150
<b>G3S3P3</b>	3	105	45	150
<b>G3S3P5</b>	3	105	60	150
<b>G3S3P6</b>	3	105	70	150
<b>A</b>	3	105	50	148
<b>B</b>	3	105	50	152

## 4.5 Characterisation of parts

### 4.5.1 Part size

All parts manufactured were produced from the same build file shown in Figure 4.10, meaning all parts should be nominally the same size. Any significant change in dimensions can therefore be attributed to changes in the parameters used to manufacture the parts.

Part dimensions were measured using Mituoyo CD-6" AX digital calipers. The dimensions recorded were the overall length, the tab width, gauge width and thickness of the tensile test piece and the length width and thickness of the rectangular piece used for density measurements, as shown in Figure 4.12. Three measurements were taken for each dimension and the average reported.

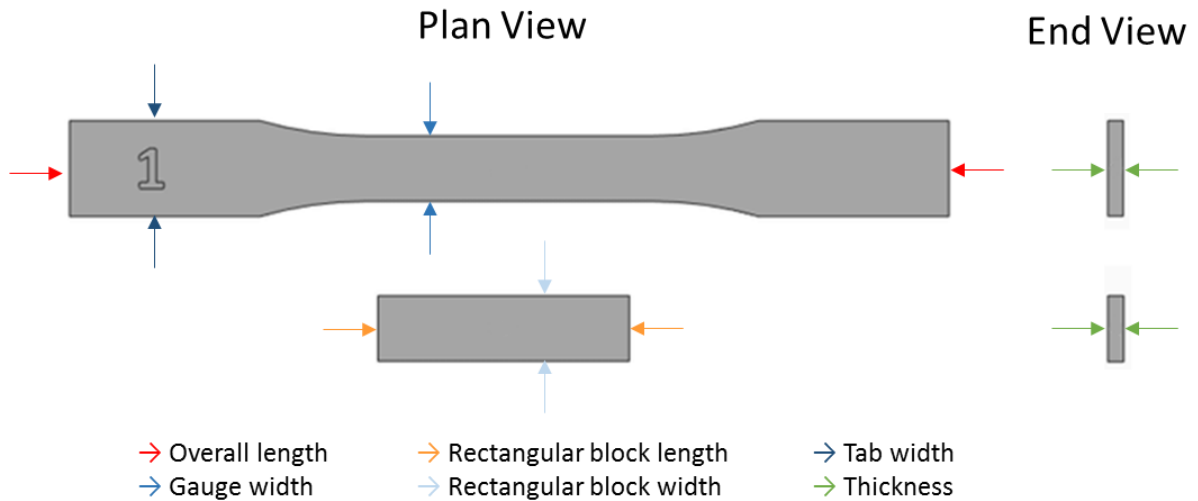


*Figure 4.12 Representation of a tensile test piece and rectangular block used for density calculations and labelling of the dimensions measured.*

There are two factors known to contribute to differences between the actual and intended dimensions of the part; shrinkage and wall growth(113). Shrinkage and wall growth are demonstrated in Figure 4.13. Shrinkage is a percentage across the part and is seen in LS at approximately 4 % for Nylons. Shrinkage is caused by the recrystallisation of the polymer leading to the part contracting in size. Wall growth is mainly seen in HSS - this value is a constant and is from each wall of the part manufactured. Wall growth leads to part size increase and is likely to be caused by two contributing factors of non-printed (by the IR absorbing ink) powder on the edges of the part overheating and sintering causing a larger part. The other potential contributor is the ink flowing to areas in which it was not printed and hence initiating the powder to melt.

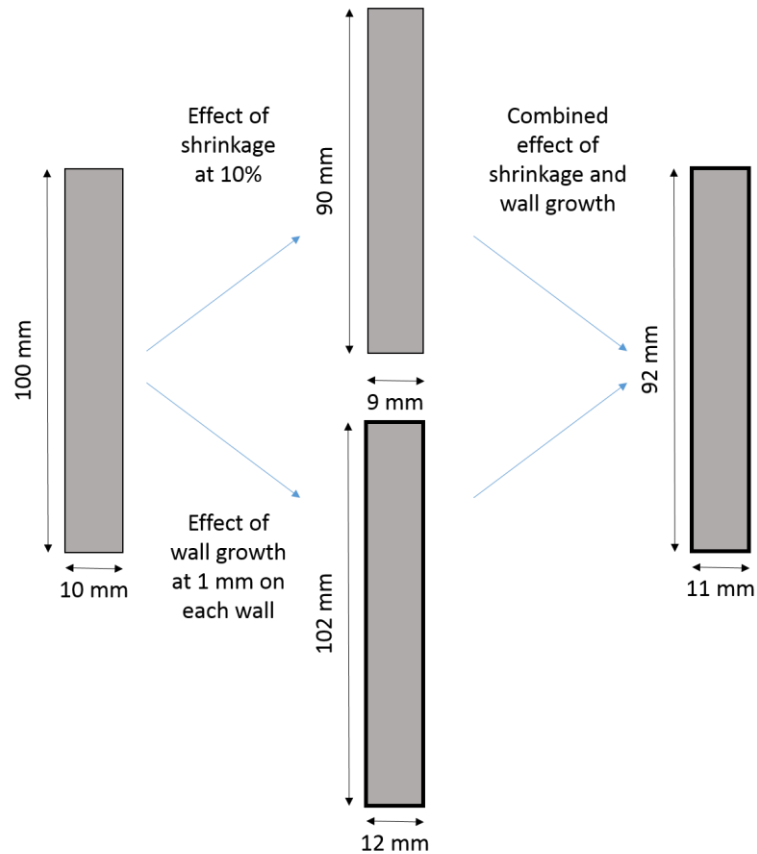


Figure 4.13 Diagram showing the effect of shrinkage and wall growth, the values of 10% shrinkage and 1 mm wall growth are arbitrary and the diagram is not to scale. The diagram demonstrates shrinkage has a larger effect on big dimensions but wall growth has more of an effect on small dimensions.

The dimensions used for calculating wall growth and shrinkage were the overall length, tab width and gauge width of the tensile specimens.

Wall growth and shrinkage were calculated for each specimen as described below then averaged and reported for each build. The steps for calculating these measurements are:

- A linear fit of the measured values against the theoretical values, this is demonstrated in Figure 4.14, where the gradient represents the shrinkage and the intercept indicates twice the wall growth (accounting for wall growth on both sides)

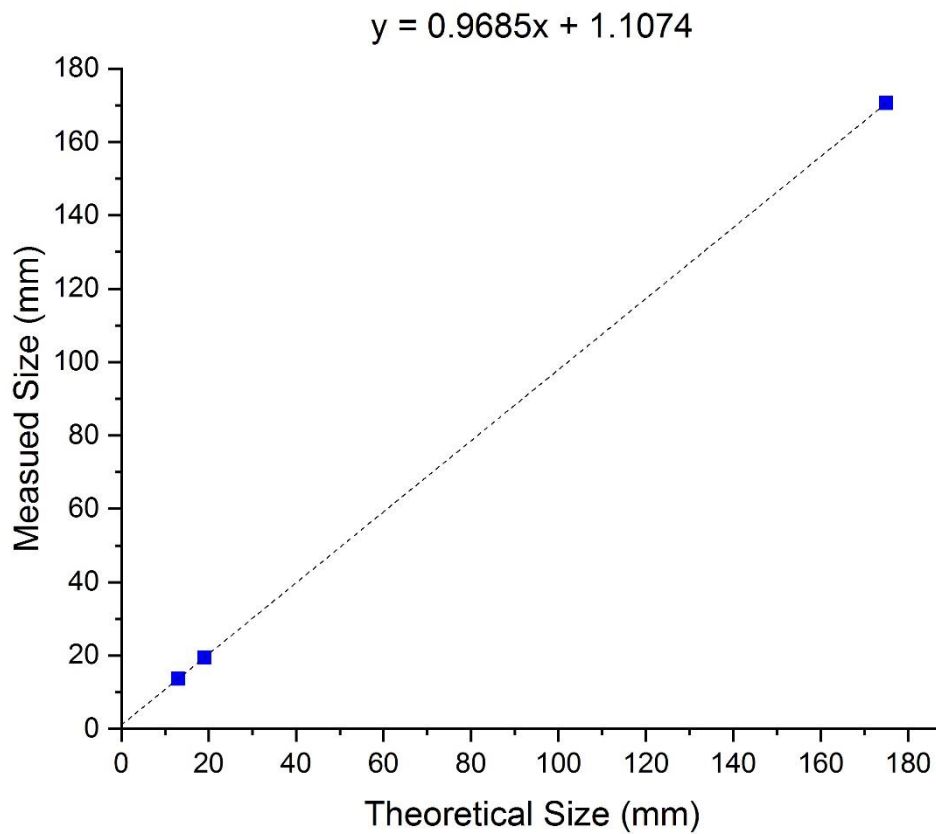


Figure 4.14 Plot of measured size against theoretical size against of **G3S3P4a** specimen 1, with a linear fit, the values plotted are of the overall length, tab width and gauge width.

- Wall growth = intercept/2
- % Shrinkage =  $(1 - \text{gradient}) \times 100$

Figures 4.15 - 4.17 demonstrate the effect of grey level, sinter speed and preheat power on wall growth and shrinkage.

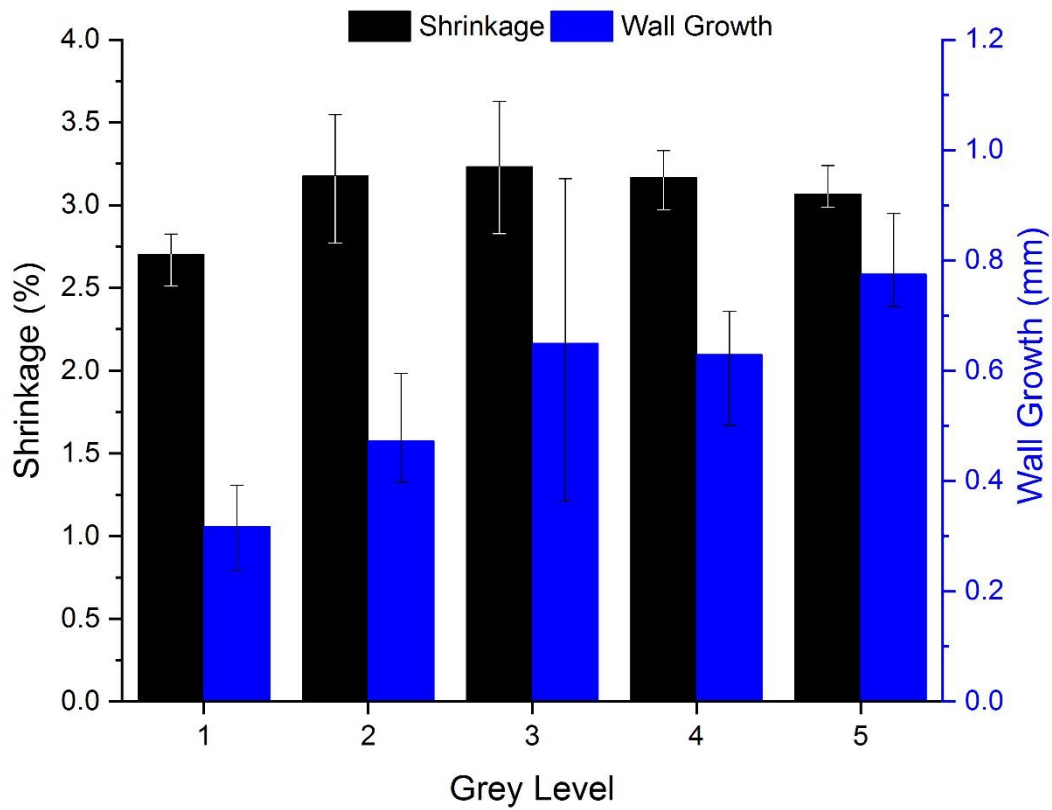


Figure 4.15 A graph showing the effect of grey level on wall growth and shrinkage. The error bars included are range bars.

The graph plotting shrinkage and wall growth against grey level (Figure 4.15) demonstrates an increase in wall growth with higher grey level. It can be observed that there is a difference in shrinkage for grey level 1 compared to the other grey levels. Large range bars are observed for grey level 3 as this is the mid-point with three times more samples measured, this is also seen in the mid-points for the other parameters.

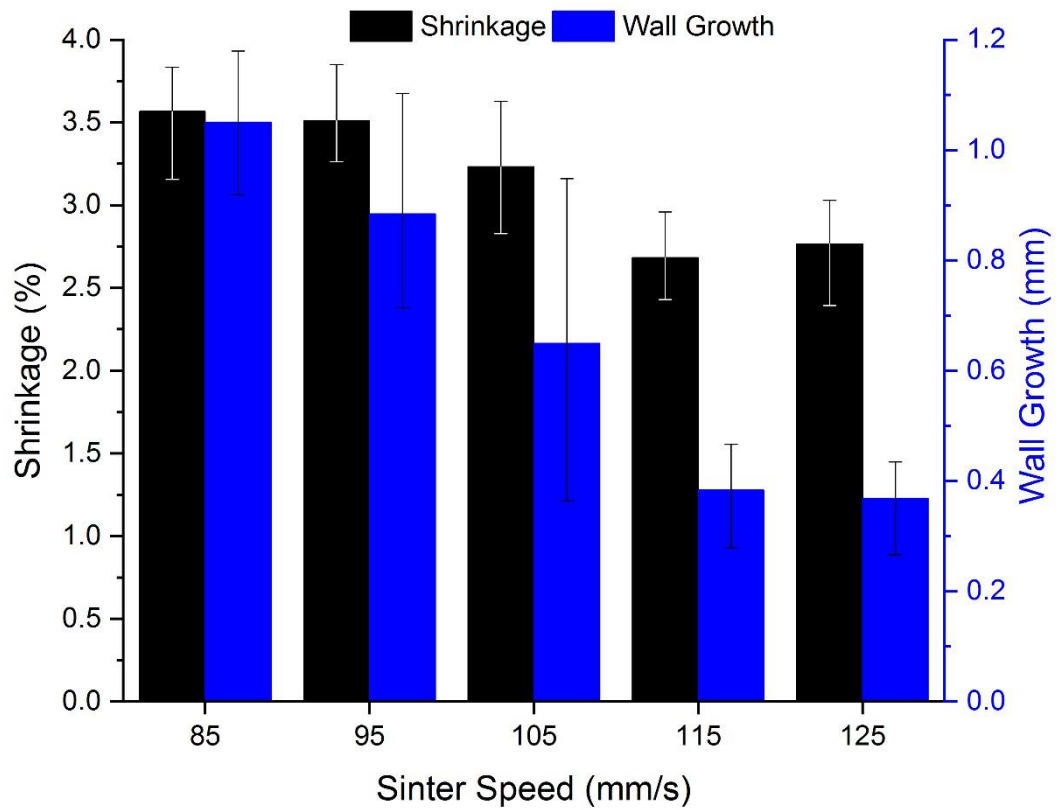


Figure 4.16 A graph showing the effect of sinter speed on wall growth and shrinkage. The error bars include are range bars.

Figure 4.16 shows that both wall growth and shrinkage decrease with an increase in sinter speed, indicating that a decrease in energy input leads to more dimensional inaccuracy.

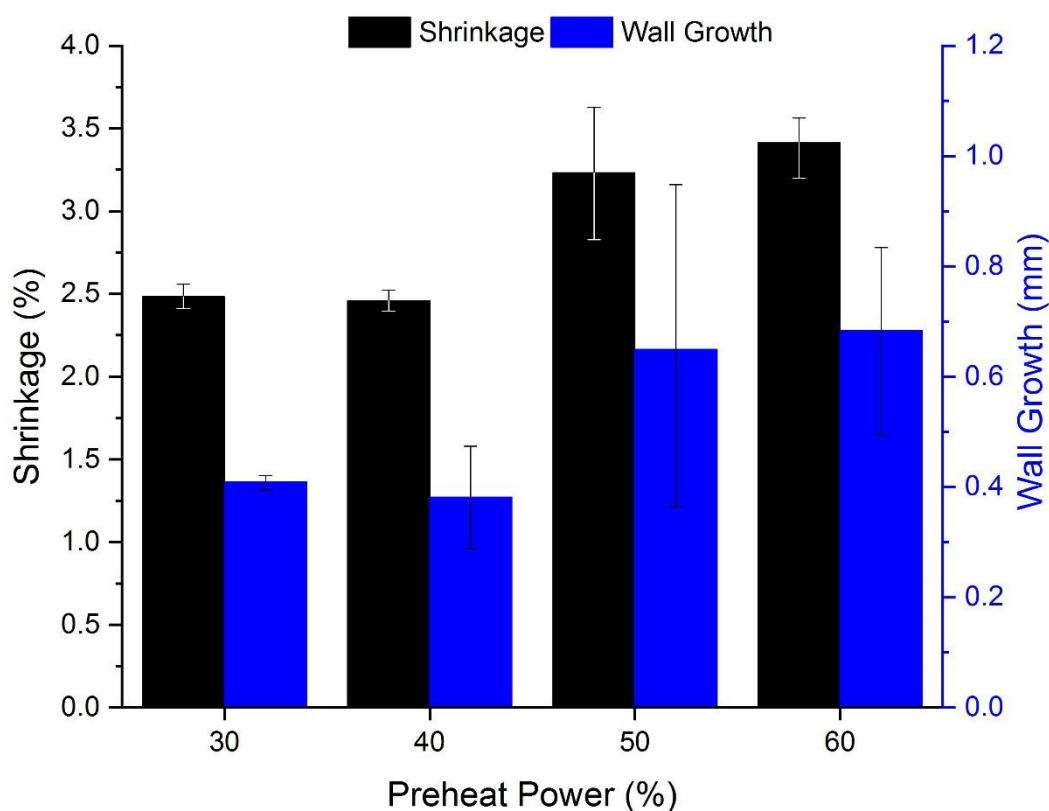


Figure 4.17 A graph showing the effect of preheat power on wall growth and shrinkage. The error bars included are range bars.

It can be observed in Figure 4.17 an increase in shrinkage with increase in preheat power, this trend is also observed in the wall growth of parts manufactured at varying preheat powers.

From the data shown in Figures 4.15 - 4.17 it can be observed there is a small effect on shrinkage when altering grey level, preheat power and sinter speed. A general relationship can be drawn, which states that more energy leads to an increase in wall growth and higher shrinkage. Shrinkage in other polymer sintering processes is known to be affected by energy input (114), and this trend is therefore to be expected.

The minimum reported wall growth reported in this work is 0.64 mm which is significantly higher than the standard for Nylon 12 in HSS which is 0.4 mm. This is likely due to the broad melt peak of CP22 PP and therefore the possibility of sintering occurring without the use of IR absorbing ink. An increase in energy input also leads to an increase in temperature, further increasing the likelihood of this occurring.

#### 4.5.2 Part density

The density was calculated from the rectangular blocks, these pieces were measured in 4.5.1 and weighed using an OHAUS Pioneer PA64C Analytical Balance accurate to 4 decimal points of a gram. A minimum of three blocks were used to calculate density, except for the mid-point which are an average of multiple builds.

Figures 4.18 - 4.2 show how density is affected by the variance of grey level, sinter speed and preheat power.

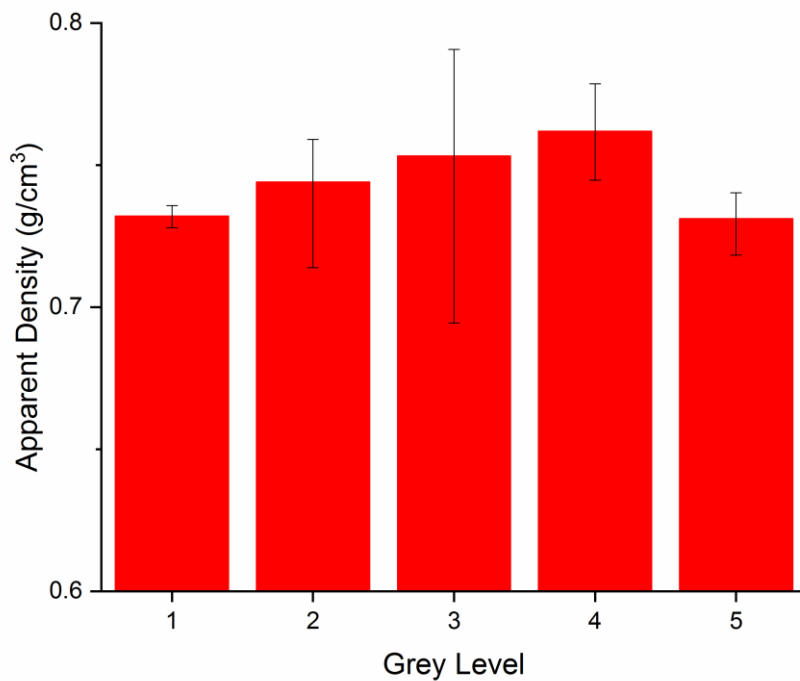


Figure 4.18 The effect of grey level on the density of parts. The error bars included are range bars.

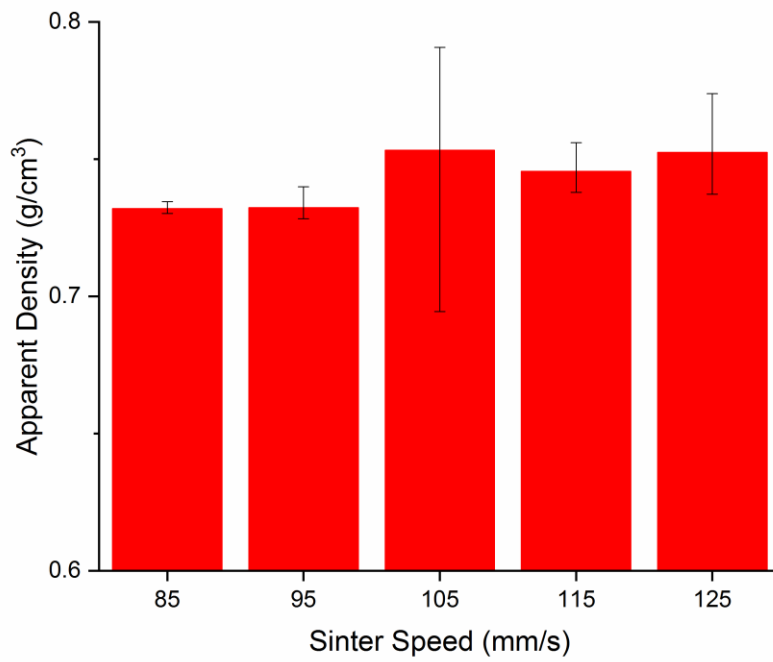


Figure 4.19 The effect of sinter speed on the density of HSS parts. The error bars included are range bars.

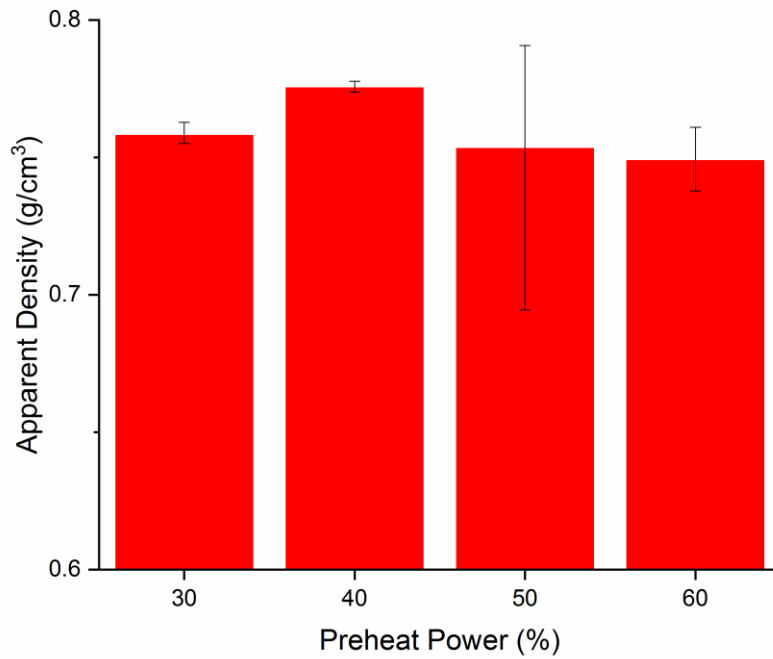


Figure 4.20 The effect of preheat power on the density of HSS parts. The error bars included are range bars.

From the data in Figures 4.18 - 4.2 there is no apparent trend of bulk density of the parts against change in grey level, sinter speed and preheat power. Gibson *et al.* (62) showed higher energy density led to an increase in part density in laser sintering, which subsequently led to improved mechanical properties. Density however is quite often unrepeatable from build to build therefore cannot be relied on as an indicator of mechanical properties.

Part density could be further explored by calculating the relative density of these parts by comparison of a sample manufactured with zero porosity. This sample could be created by pressing a film and then evaluating the density of this film. Along with SEM or other microscopy of the fracture surfaces would illustrate the porosity of the parts. This however was not carried out in this thesis, learning is possible though as a comparison between the parts measured is has been shown. This demonstrates the effect of the machine parameters on the density of parts. In summary a relative comparison has been made although and absolute comparison was not carried out.

#### 4.5.3 Tensile properties

Tensile properties were measured according to ASTM D638-14(115), ASTM D638-14 Type I tensile test pieces were manufactured, see Section 4.2 and part size was recorded according to Figure 4.12. A Tinius Olsen H5K-S with a model 500LC laser extensometer with Horizon software was used to test the tensile test specimens. The speed of test was 5 mm/min according to the ASTM unless stated otherwise, with the specimens rupturing between 0.5 to 5 min of testing time. Reflective tape was attached on the gauge length at an initial distance of 50 mm apart for the laser in the laser extensometer to detect and hence record the extension. The gauge width and thickness were used to calculate the tensile properties. To calculate the tensile properties of the parts stress and strain are plotted, as shown in Figure 4.21. The equation for stress is shown in Equation 4.1 and the equation for strain is shown in Equation 4.2.

$$\text{Stress} = \frac{\text{Force}}{\text{Area}} \quad 4.1$$

$$\text{Strain} = \frac{\text{Extension}}{\text{Original Length}} \quad 4.2$$

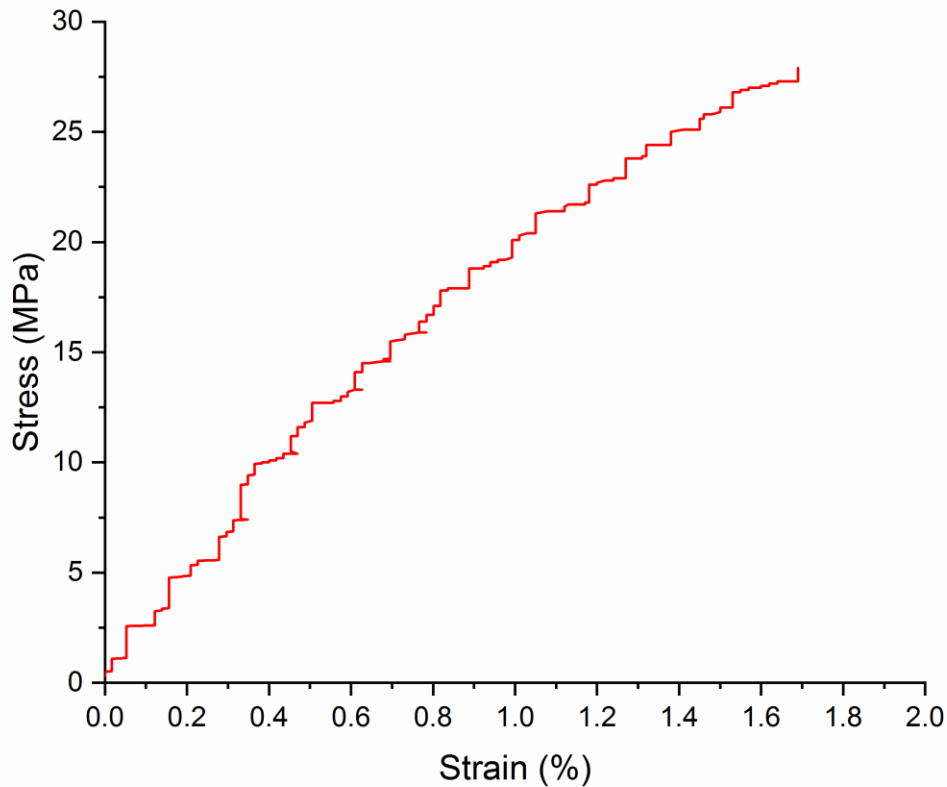


Figure 4.21 Stress strain curve of one tensile specimen in build **G3S3P4c**.

Figure 4.21 shows the sample tested failed whilst deforming elastically. This is not the typical method of failure for a polypropylene. The tensile properties reported are: Ultimate Tensile Strength (UTS) (MPa), Elongation at Break (EaB) (%) and Young's Modulus (YM) (MPa), as is standard in Additive Manufacturing. The UTS was calculated by the maximum stress that the sample undergoes before failure. The EaB is the strain of the specimen before it fractures. Young's Modulus is the relationship between stress and strain (see 4.3), whilst in the elastic region and the relationship is linear.

$$\text{Young's Modulus} = \frac{\text{Stress}}{\text{Strain}} \quad \mathbf{4.3}$$

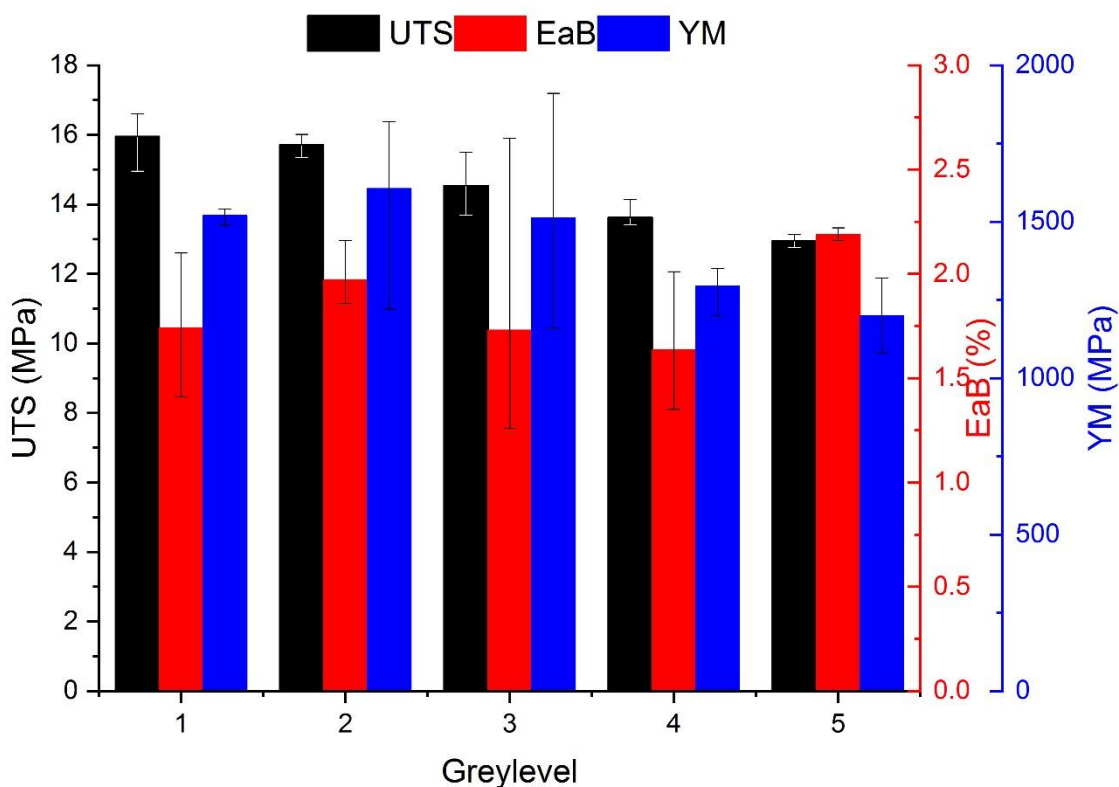


Figure 4.22 The effect of grey level on tensile properties (UTS, EaB and YM). The error bars included are range bars.

As seen in Figure 4.22 there is a trend in UTS as grey level varies, where an increase in grey level correlates to a decrease in UTS. A possible hypothesis for the mechanical property decreasing is there is sufficient energy for the part to melt with a low amount of infrared absorbing ink deposited. Therefore any further RAM printed can lead to excessive heat energy being absorbed, which could lead to the powder degrading and therefore causing the mechanical properties to deteriorate. Work in the literature by Noble *et al.* (55) demonstrated a similar effect of an excess of IR absorbing ink leading to a reduction of mechanical properties, with the most obvious trend observed for UTS. In this work a clear trend is not seen for EaB or YM due to large range bars for the data, therefore it will be examined further in Section 4.6.

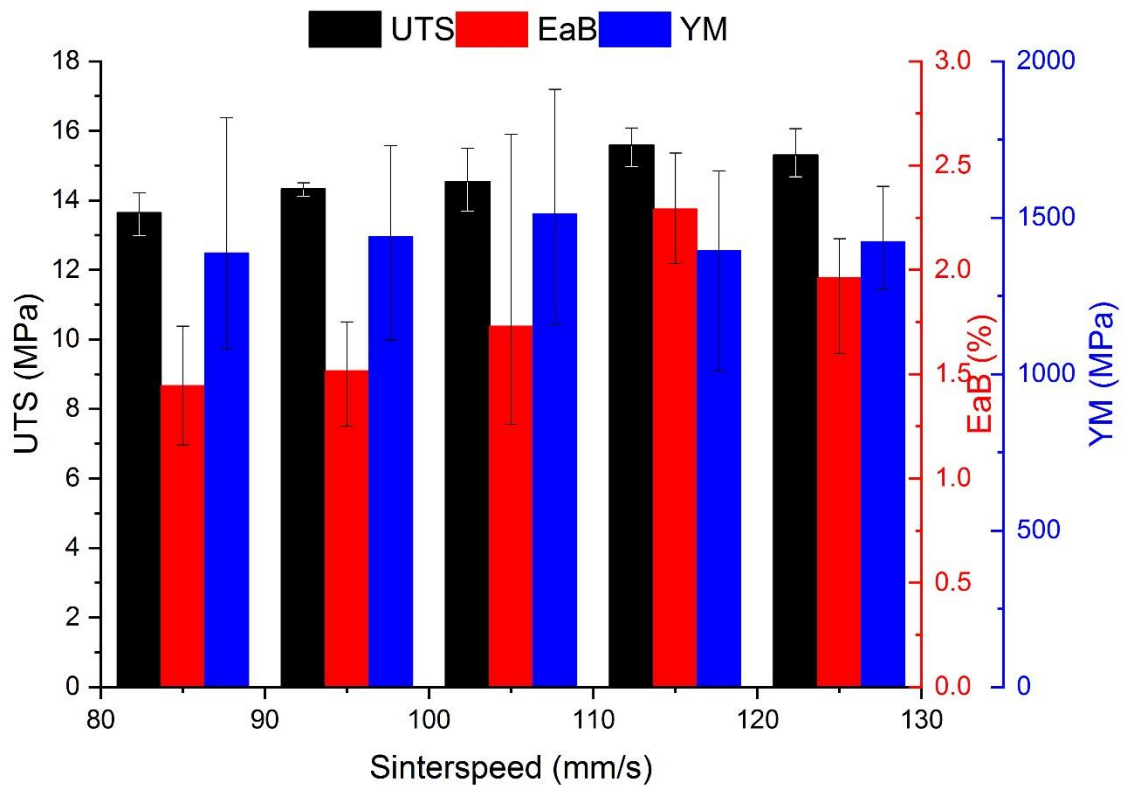


Figure 4.23 The effect of sinter speed on tensile properties (UTS, EaB and YM). The error bars included are range bars.

Figure 4.23 shows that as sinter speed increases the energy input via the sinter lamp decreases both UTS and EaB increase. However at the parameters used it was not possible to build parts at a faster sinter speed than 125 mm/s, as any increase in speed resulted in a critical loss of energy in the build causing the tensile test pieces to curl and the build to fail. The range bars for the UTS against sinter speed slightly overlap but a trend is observable. With regards to EaB, a significant difference can be observed between the extremes, but not between mid-point parameters. As it was difficult to observe a trend further examination will be carried out. Varying sinter speed showed no significant effect on YM, due to the large error present in YM measurement. If a trend is present for the UTS and EaB it is when energy decreases the mechanical properties increase, as higher energy leads to polymer degradation. Although enough energy needs to be inputted into the system for sintering to occur, without subsequent curling.

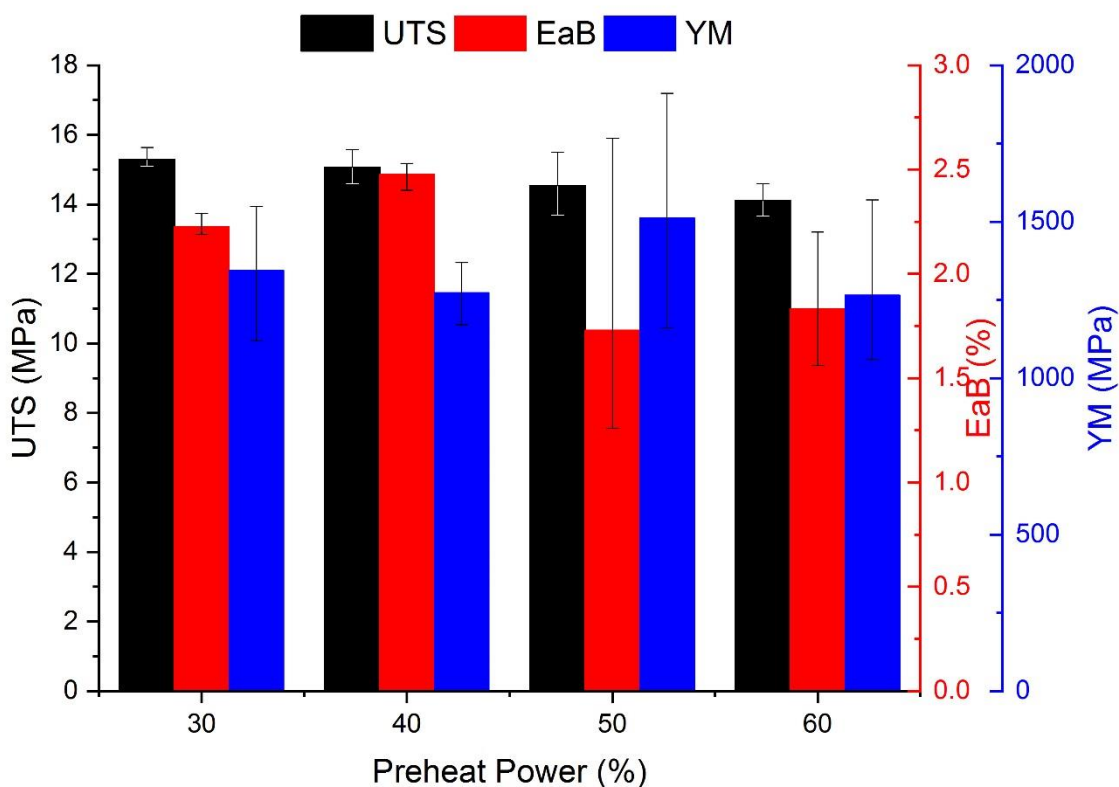


Figure 4.24 The effect of preheat power on tensile properties (UTS, EaB and YM). The error bars included are range bars.

The tensile data from the variation of preheat power is shown in Figure 4.24. There are no clear trends of UTS, EaB and YM altering as preheat power is varied. This can be expected as the preheat power is where the lamp is passed over freshly deposited powder, hence does not directly affect the sintering of the powder layer. Although the preheat lamp and hence the preheat power does impact the energy into the system so can cause the build bed to curl or fully sinter leading to build failure.

In this section it has been suggested that as more energy is input into the system the PP may degrade and the properties measured decrease. Two methods of measuring polymer degradation are Gel Permeation Chromatography (GPC) and Thermogravimetric Analysis (TGA). GPC is a technique that measures molecular weight as carried out latter in Section 5.3.3, however due to the solubility of PP is an expensive and not widely available technique. Due to these reasons it was used only for the powder ageing work where literature had demonstrated a molecular weight change when Nylon was used in LS.

TGA can measure the decomposition temperature of a polymer powder by heating a sample whilst recording its mass, as described in Section 5.3.3. When the mass begins to decrease it is due to the polymer beginning to decompose. The experimental method used for TGA is described in Section

5.3.3, a TGA trace for CP22 PP powder is shown in Figure 4.25. As can be seen the polymer begins to degrade at a temperature in the region of 300 °C.

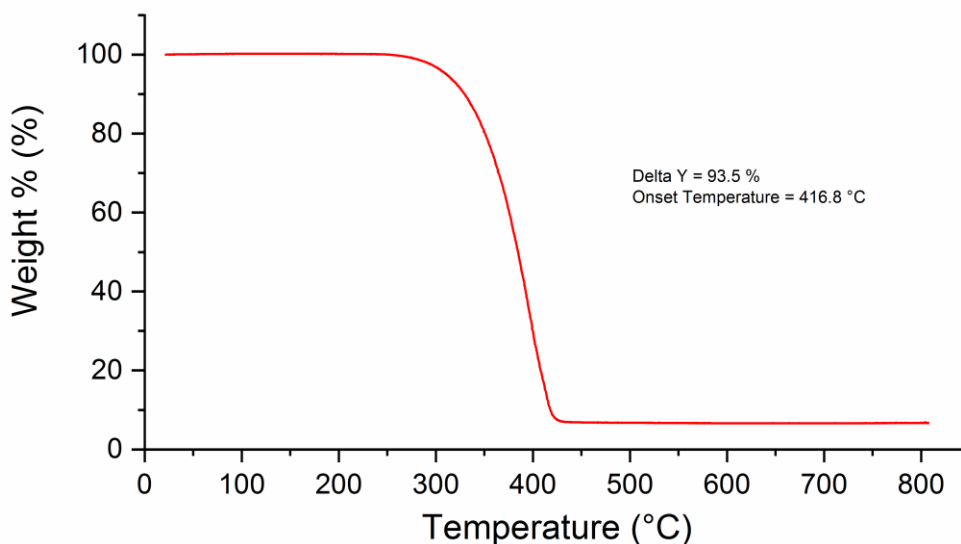


Figure 4.25 Thermogravimetric Analysis trace of CP22 PP powder.

A method to determine if the polymer in the part had decomposed would have been to calculate the decomposition temperature or the molecular weight from a sample of the part manufactured. If the molecular weight or decomposition temperature decreases as the part properties decrease this would have been clear evidence. This relationship has not previously been shown in literature, but would be a good contribution to the field.

#### 4.5.4 Melt characteristics of parts

A method used previously in literature is to relate enthalpy of melt of part to the crystallinity of the part (34). Percentage crystallinity was calculated by dividing the enthalpy of melting of a measured sample by the enthalpy of a 100 % crystalline material. Due to the lack of a 100 % crystalline material the enthalpies of the samples can be compared for learning. The samples were measured using the same method as the powder as described in Section 4.1.3, except part was used in comparison to powder. An example of a DSC trace for sample is shown in Figure 4.26, this trace is for **G3S3P4C**.

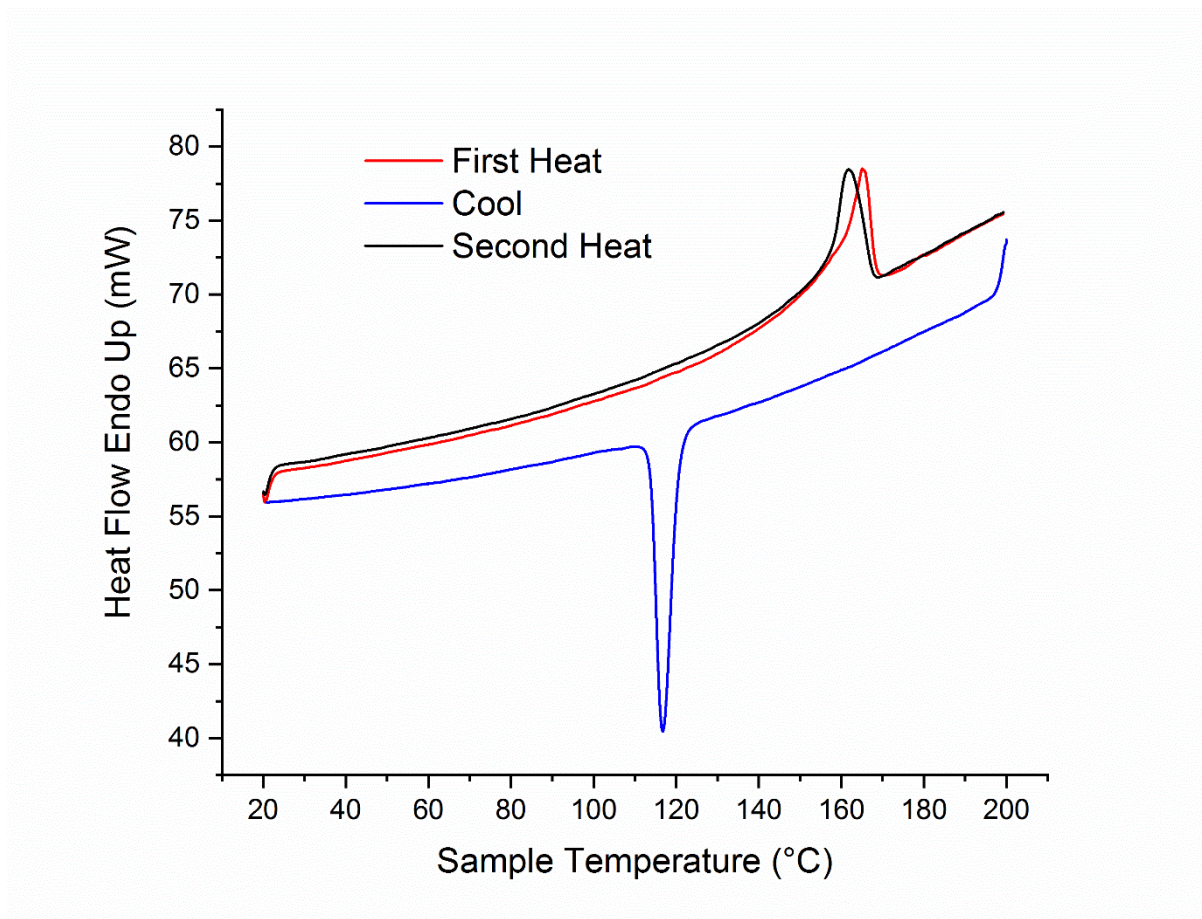


Figure 4.26 DSC trace of part in G3S3P4C build.

The enthalpy of melt or recrystallisation is calculated by the area under the peak. The melt curve although at a different temperature has a similar general shape for both the 1<sup>st</sup> melt and the 2<sup>nd</sup> melt. The difference in the temperature and change in enthalpy is due to the different thermal histories of the polymer, being as a formed part versus going through a DSC cycle.

Literature for Nylon parts has shown multiple peaks in the DSC melt as there are different crystalline structures present in the same sample (34, 58). As the temperature is increased different crystalline structures lose their uniformity at different temperatures hence a multi-peak. PP is also a polymorphic polymer and can have different crystalline structures. However, as shown in Figure 4.26 there is no evidence of this occurring. Therefore during the HSS process the material undergoes a full melt and no residual crystallinity is obtained.

#### 4.6 Further discussion

It should be noted that the inability of processing CP22 PP at build bed and overhead temperatures other than 150 °C demonstrates the major importance of this factor in HSS processing of CP22 PP.

However, in some of the analysis presented in the previous section, the lack of repeatability in the datasets makes it difficult to identify specific trends. To assist in deconvoluting this one way Analysis Of Variance (ANOVA) of the complete data sets was carried out. The ANOVA test determines if there are any statistically significant differences between the means of at least two groups of data. The post-hoc test then tests each individual set of data against every other set to determine if they are statistically significant. The ANOVA was carried out at a 0.05 significance level (95 % probability) and then a post-hoc Scheffe test(112) was carried out to compare data. The statistical analysis was carried out using Origin software, the results of this analysis was compiled into Table 4.12. The results in this Chapter will be discussed further in comparison to other materials tested in Chapter 8.

Table 4.12 One way analysis of variance the effect of various parameters on tensile properties and shrinkage and wall growth. The result of the ANOVA is shown with tests which should significance highlighted in green and then followed by post-hoc tests to demonstrate which data sets were significantly different from each other. The numbers in the table signify the two levels of parameters examined, e.g. in grey level shrinkage 2 1 is the comparison between the data for the grey level 1 compared to the data for grey level 2.

One way ANOVA set tested	Is it significant at 0.05 level?	Post Hoc test - Scheffe tests									
<b>Dimensional accuracy</b>											
Greylevel Shrinkage	Yes	2 1	3 1	3 2	4 1	4 2	4 3	5 1	5 2	5 3	5 4
Greylevel Wall Growth	Yes	2 1	3 1	3 2	4 1	4 2	4 3	5 1	5 2	5 3	5 4
Sinter Speed Shrinkage	Yes	95 85	105 85	105 95	115 85	115 95	115 105	125 85	125 95	125 105	125 115
Sinter Speed Wall Growth	Yes	95 85	105 85	105 95	115 85	115 95	115 105	125 85	125 95	125 105	125 115
Preheat Shrinkage	Yes	40 30	50 30	50 40	60 30	60 40	60 50				
Preheat Wall Growth	Yes	40 30	50 30	50 40	60 30	60 40	60 50				
<b>Mechanical properties</b>											
Greylevel UTS	Yes	2 1	3 1	3 2	4 1	4 2	4 3	5 1	5 2	5 3	5 4
Greylevel EaB	No	2 1	3 1	3 2	4 1	4 2	4 3	5 1	5 2	5 3	5 4
Greylevel YM	No	2 1	3 1	3 2	4 1	4 2	4 3	5 1	5 2	5 3	5 4
Sinter Speed UTS	Yes	95 85	105 85	105 95	115 85	115 95	115 105	125 85	125 95	125 105	125 115
Sinter Speed EaB	Yes	95 85	105 85	105 95	115 85	115 95	115 105	125 85	125 95	125 105	125 115
Sinter Speed YM	No	95 85	105 85	105 95	115 85	115 95	115 105	125 85	125 95	125 105	125 115
Preheat UTS	Yes	40 30	50 30	50 40	60 30	60 40	60 50				
Preheat EaB	Yes	40 30	50 30	50 40	60 30	60 40	60 50				
Preheat YM	No	40 30	50 30	50 40	60 30	60 40	60 50				
<b>Legend</b>		Significant		Not significant							

Table 4.12 shows the summary of the ANOVA testing of the shrinkage and wall growth data. The ANOVA results show there is significance for all the size data. However a more thorough examination shows the size data for the grey level parameter set has only a few data points which are significant whereas sinter speed shrinkage and wall growth and preheat shrinkage show difference in the data across several parameter levels. This indicates that sinter speed is critical in the wall growth of parts produced, whilst preheat power and sinter speed both have a marked effect on the shrinkage of parts produced. The effect of ink quantity is less significant.

The effect of grey level on tensile properties was shown in Figure 4.22 and a trend of UTS decreasing with grey level is shown; however there were no other clear trends. This is supported by the statistical analysis carried out in Table 4.11. This variance in mechanical properties with grey level has been shown previously in research by Noble *et al.*(55). It might also be expected that trends would be observed for EaB and YM, however as seen in this work the difference in the impact of the parameters is not large enough to induce a significant effect compared to the reproducibility shown. The lack of a significant trend does not indicate that there is no effect of these parameters, but that if there is any effect it has been obscured by the lack of repeatability within the system.

No apparent effect of sinter speed on YM can be observed in Figure 4.23, whilst there is an apparent trend of UTS and EaB increasing with increasing sinter speed. This is again supported by the statistical analysis. The statistics also demonstrate especially for the UTS variance between the data for a majority of data sets. The lack of trend for YM is due to the low precision often observed for AM parts. The effect of lamp power has previously been studied to a limited extent by Majewski *et al.*(54) where an increase in lamp energy demonstrated an increase in mechanical properties at two different levels. Although this previous work does not directly correlate with this research it does however show a consistent trend, despite the use of a different machine and powder feedstock. The lack of clear trends observed for the effect of preheat power on mechanical properties is supported by the statistical analysis carried out in Table 4.12.

#### 4.7 Summary

This work has shown it is possible to process polypropylene in HSS. CP22 PP has processed in HSS with similar mechanical properties to those quoted on the LS data sheet.

However, as shown in this research the CP22 PP has a very tight processing window, as emphasised by the difficulty in ensuring repeatability of manufacture.

It has also been established that sinter speed plays a key role in determining both dimensional accuracy and mechanical properties. Grey level has also been identified as important where dimensional accuracy is key.

Next steps will be to establish the ability to reuse unsintered powder (crucial from a cost and sustainability perspective). Other grades of LS polypropylene will also be investigated to determine whether the narrow processing window observed here is a characteristic of PP itself, or of the specific grade tested here.



## Chapter 5 The effect of powder age in High Speed Sintering of polypropylene

### 5.1 Introduction

It was demonstrated in Chapter 4 that it is possible to manufacture parts using PP as a powder feedstock in HSS, thus confirming that there is no fundamental material property preventing it being compatible with the HSS process. However, Fast Moving Consumer Goods (FMCGs) require low cost and sustainability in their production, meaning there is a clearly defined need for the reduction of excess in the manufacture of parts. During the HSS process, unsintered powder is used as support for the manufacture of parts(2); if this powder cannot be reused then waste and hence cost is added to the process, meaning the cost and environmental impact may be too high for the use in FMCGs.

During the HSS process, unsintered powder is subjected to elevated temperatures for extended periods of time, which creates the potential for changes to occur which may be detrimental to the material's use in subsequent builds. The ageing of powder feedstock has been shown for Nylon powders in LS. Gornet *et al.* (116) demonstrated a change in mechanical properties with the effect of ageing, with tensile strength decreasing and elongation at break decreasing. This was attributed to the change in melt flow index which is an indicator for the molecular weight of the polymer tested. However, this effect has yet to be investigated in HSS or for PP in LS or HSS, and will therefore be investigated here.

The effect of powder age on part production using HSS will be studied. The aged powder will be examined to understand any changes in the parts manufactured.

### 5.2 Part manufacture via High Speed Sintering

The powder used in this research was CP22 PP from Diamond Plastics as used in Chapter 4. The only variable of interest in this section was the powder age, hence the machine parameters were kept constant. The parts manufactured were ASTM D638 Type I tensile test pieces with rectangular blocks as described in Section 4.2, and produced using the same build layout. The machine parameters are shown in Table 5.1 and are the same as the mid-point parameters examined previously. These parameters were used as they had been shown to provide reasonably consistent build success.

Table 5.1 Machine parameters used for the production of parts to assess the effect of powder age.

Parameter	Level
Preheat Power (%)	50
Sinter Power (%)	100
Preheat Speed (mm/s)	60
Sinter Speed (mm/s)	105
Recoater Vibration (%)	100
Feed Hopper Fill Frequency	11
Feed Hopper Fill Duration (s)	1.25
Grey level	3
Build Bed (°C)	150
Build Overhead (°C)	150
Layer Thickness (µm)	100

After each build the surrounding powder around the parts was collected and passed through a course sieve to break up any large aggregates, before being processed in the HSS system as a separate powder 'grade'. This process is shown in Figure 5.1.

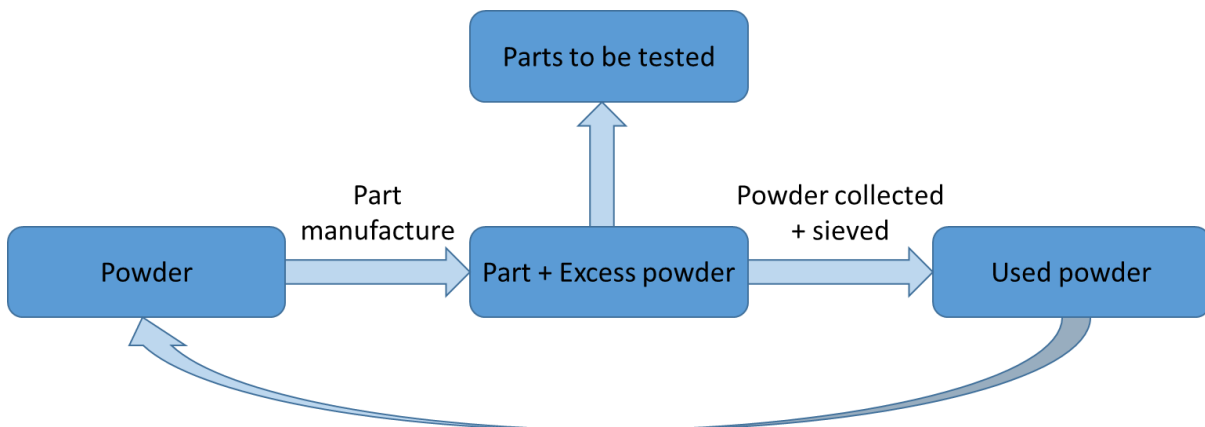


Figure 5.1 Flow chart demonstrating the process of powder age in HSS.

New powder from the supplier was described as virgin, with the powder recovered from these builds classified as used 1. Subsequent powder grades were named used 2 to used 6, following the same convention, and providing seven grades of powder to assess. Powder was collected from builds using the same generation and mixed together to form a feedstock of powder of that particular age. In order to generate enough powder for each subsequent build, multiple builds were required in each grade; previous initial work had led to a supply of used 1 and used 2 powder which reduced the number of builds required to produce enough used powder for the builds used.

The same classification for builds as described in Table 4.5 was used where builds were complete, partially complete (1 test piece failed) or failed due to curl. Table 5.2 shows the number of builds attempted with each age of powder and the success rate. The deposition of the powder as powder age increased was not observed to change and remained good.

*Table 5.2 The powder age of builds and the successfulness of builds at different powder ages.*

<b>Powder age</b>	<b>Number of builds complete</b>	<b>Number of partially complete</b>	<b>Failed</b>	<b>Total number of builds</b>
Virgin	4	2	5	11
Used 1	1	5	1	7
Used 2	1	5	1	7
Used 3	5	0	1	6
Used 4	4	0	0	4
Used 5	2	0	0	2
Used 6	1	0	0	1

Table 5.2 shows the builds carried out in this work, which shows that builds using highly aged powder led to a higher build success rate. In order to understand the potential reasons for this, and to determine any effect on part quality, a series of powder characterisation tests were conducted.

### 5.3 Powder characterisation

#### 5.3.1 Powder flow

The tapped bulk density and powder flow of the powder was measured for three samples of each powder grade, using the same methods described in Section 4.1.1, although three repeats were run for each sample. It was not possible to measure the density or flowability of the used 6 powder as there was insufficient quantities to carry out the test after parts were manufactured. Figures 5.2 and 5.3 show how the powder grade affects the packing and hence the tapped density and the powder flow of the aged particles.

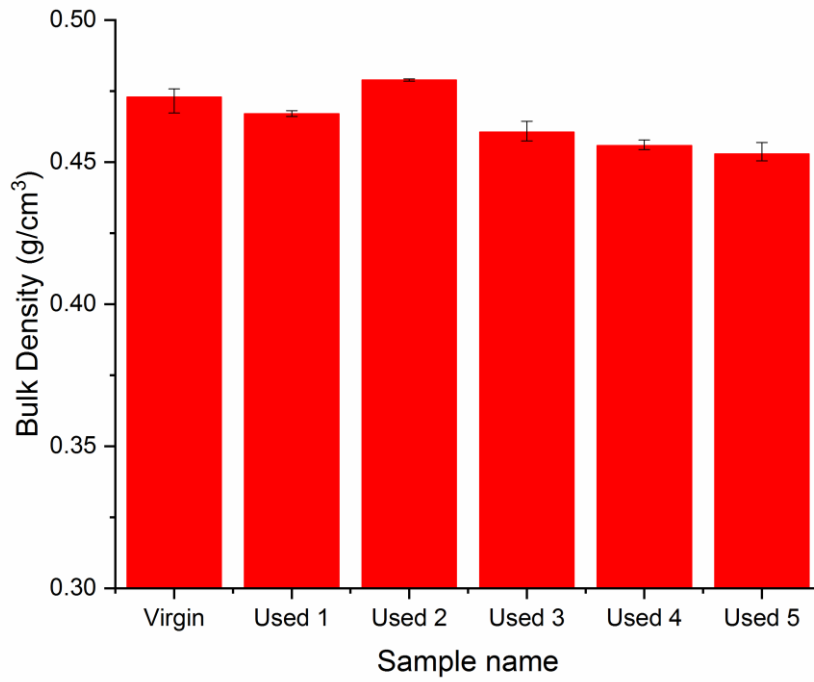


Figure 5.2 The effect of powder ageing on the bulk tapped density of CP22 PP powder. The error bars included are range bars.

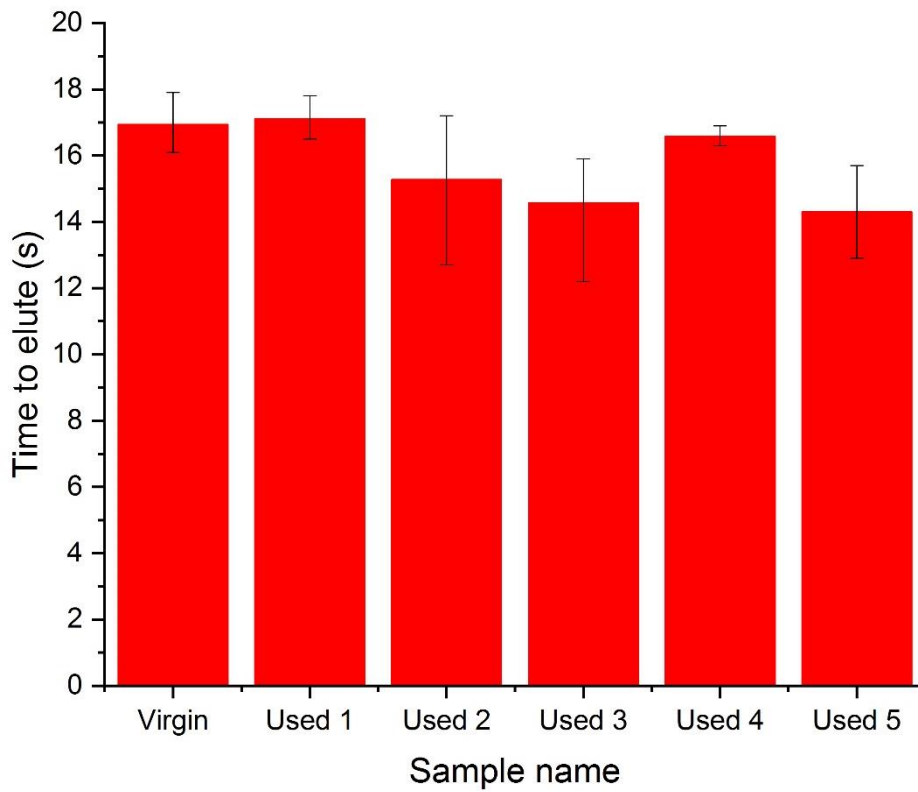


Figure 5.3 The effect of powder age on the flowability of CP22 PP powder. The error bars included are range bars.

From Figure 5.2 a slight trend can be observed whereby tapped density decreases as the powder has been through the HSS process more. The powder flow results shown in Figure 5.3 demonstrate an increase in flowability of the powder as it has been processed in the HSS system more, although it should be noted the large range bars in the data make it difficult to state a statistically significant effect.

### 5.3.2 Particle size and morphology

Particle size and shape are also known to have an effect on powder packing and flow, hence the impact of powder age on these was also investigated.

#### Particle size

Using the Malvern Mastersizer 3000 as described in Section 4.1.2, the particle size and shape of the PP powder grades were measured. Ten measurements were taken for each sample and this was repeated three times with different samples of each powder grade. Each powder feedstock used to manufacture parts was analysed as well as the remaining unused powder from the final generation build creating eight generations of powder (virgin to used 7). Figure 5.4 shows the averaged particle size traces of the aged powders overlaid, with the D(10), D(50) and D(90) reported in Table 5.3 and Figure 5.5.

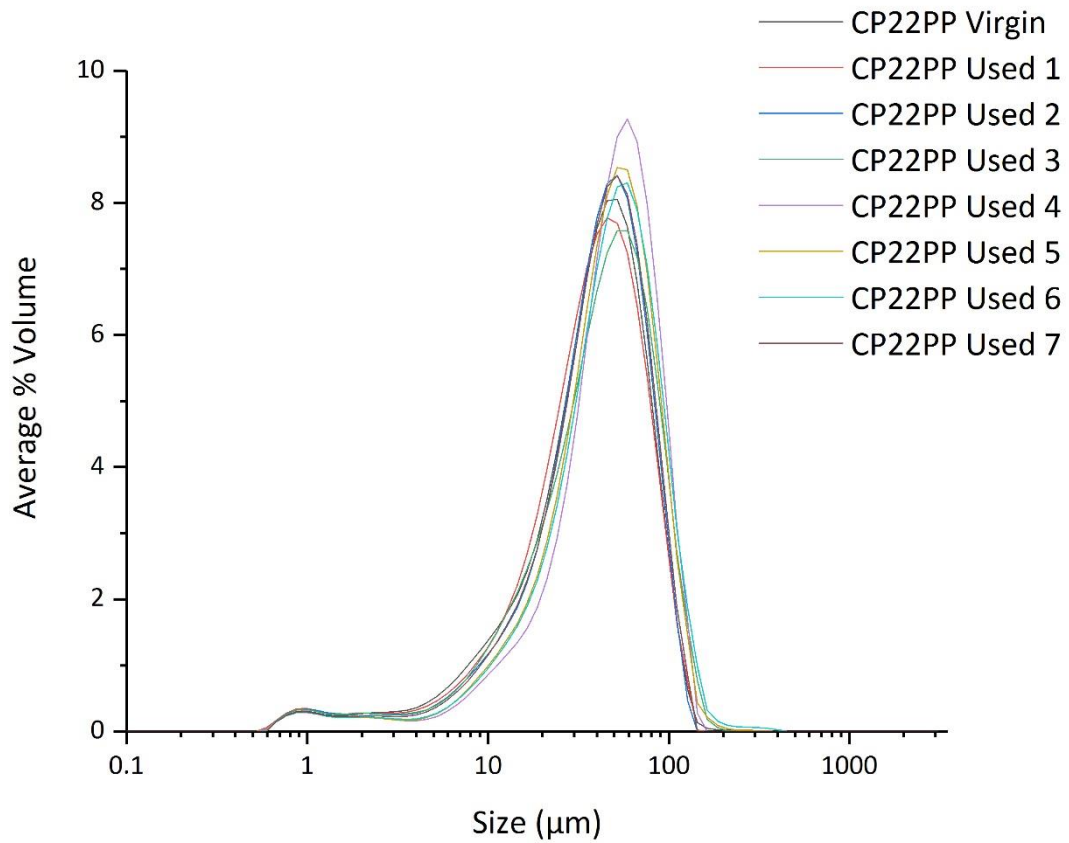


Figure 5.4 Particle size trace of aged PP powders from laser diffraction.

Table 5.3 shows the averaged particle sizes of the various aged CP22 PP powder. D(10) represents the maximum diameter of the smallest 10 % of particles, D(50) is the mean particle diameter and D(90) is the maximum diameter of the smallest 90 % of particles.

Table 5.3 Particle size breakdown of different powder ages of PP.

Sample name	D(10) (μm)	D(50) (μm)	D(90) (μm)
Virgin	11.0	39.9	82.8
Used 1	12.4	42.8	81.9
Used 2	12.1	43.8	89.6
Used 3	12.2	43.9	90.8
Used 4	14.6	49.3	97.8
Used 5	13.9	45.7	90.3
Used 6	15.0	49.3	98.0
Used 7	14.4	48.7	99.1

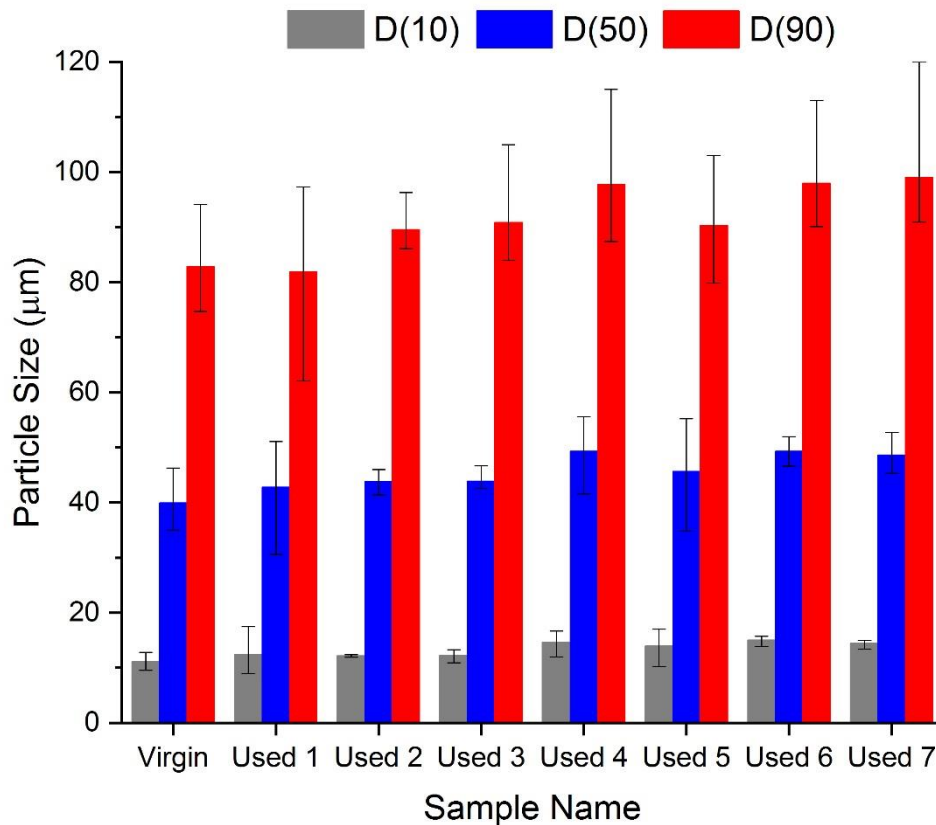


Figure 5.5 Particle size of ageing PP powders portrayed by the D(10), D(50) and D(90) of each powder. The error bars included are range bars.

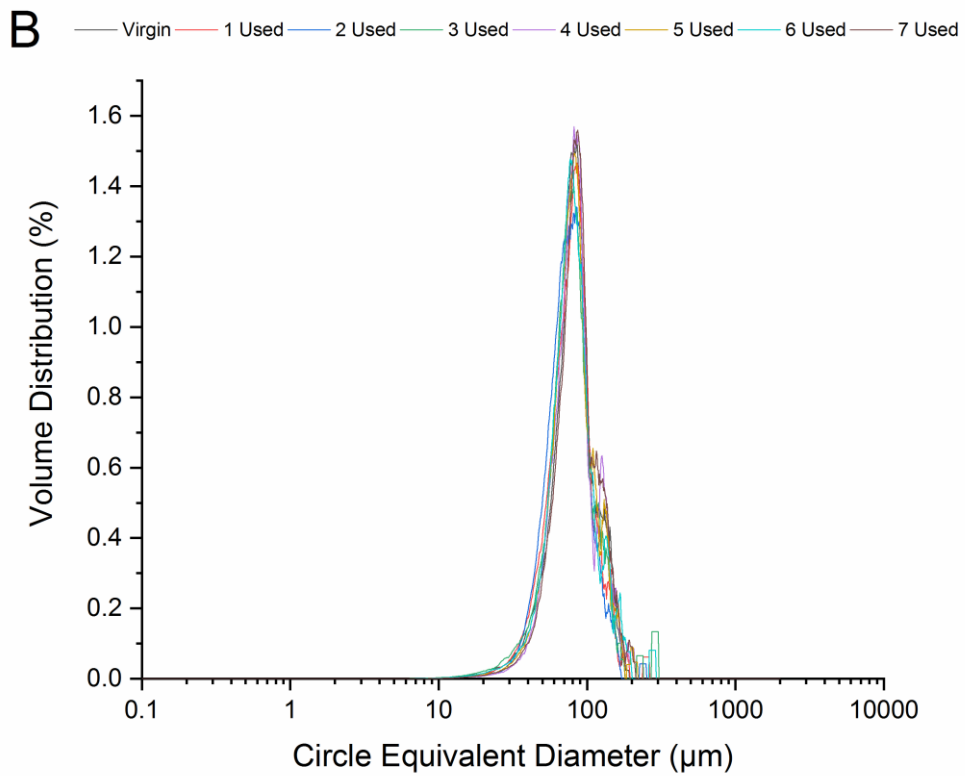
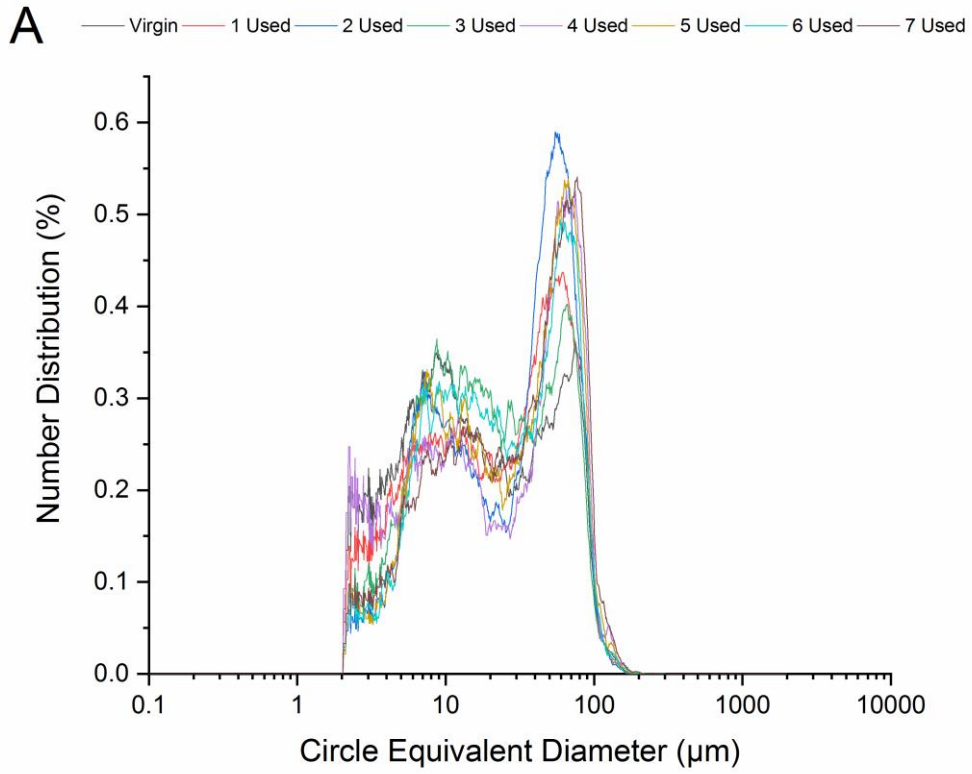
It was observed that the aged powder tended towards having a larger particle size; this is most likely caused by the loss of smaller particles during the deposition and powder removal stages of the HSS process. There are two drivers for this to occur; small particles are the most likely to become airborne and lost from the feedstock, when sieving the powder to break up large aggregates, placing the powder in the hopper of the machine and the deposition of the powder of the build. The other possible driver could be small particles selectively sintering as their small nature requires less thermal energy for them to melt.

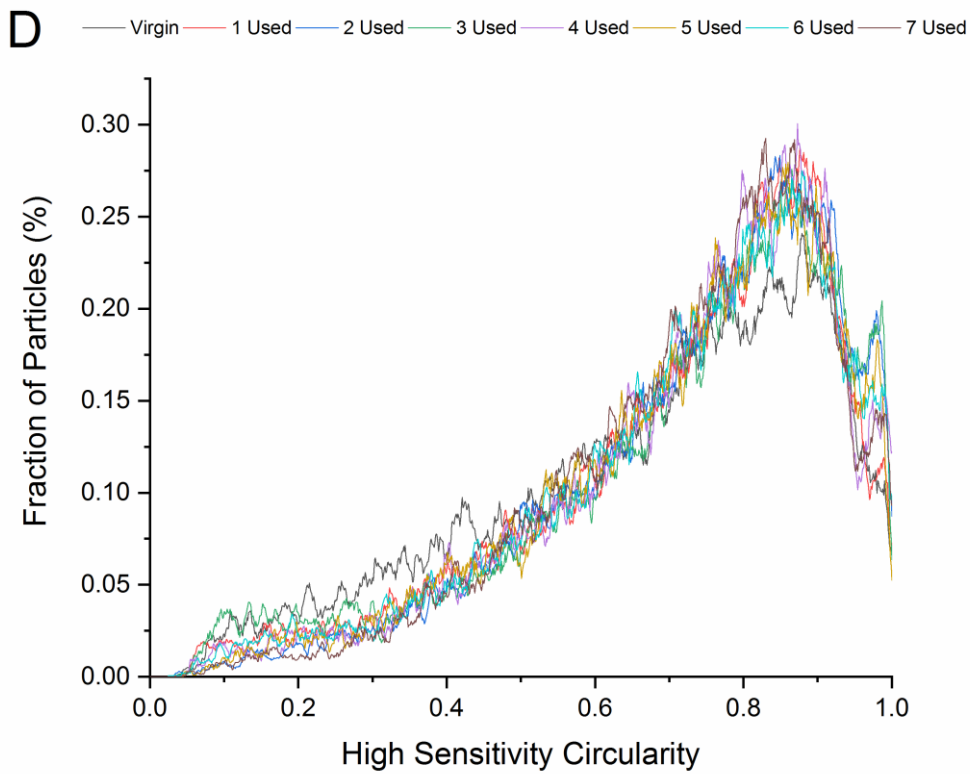
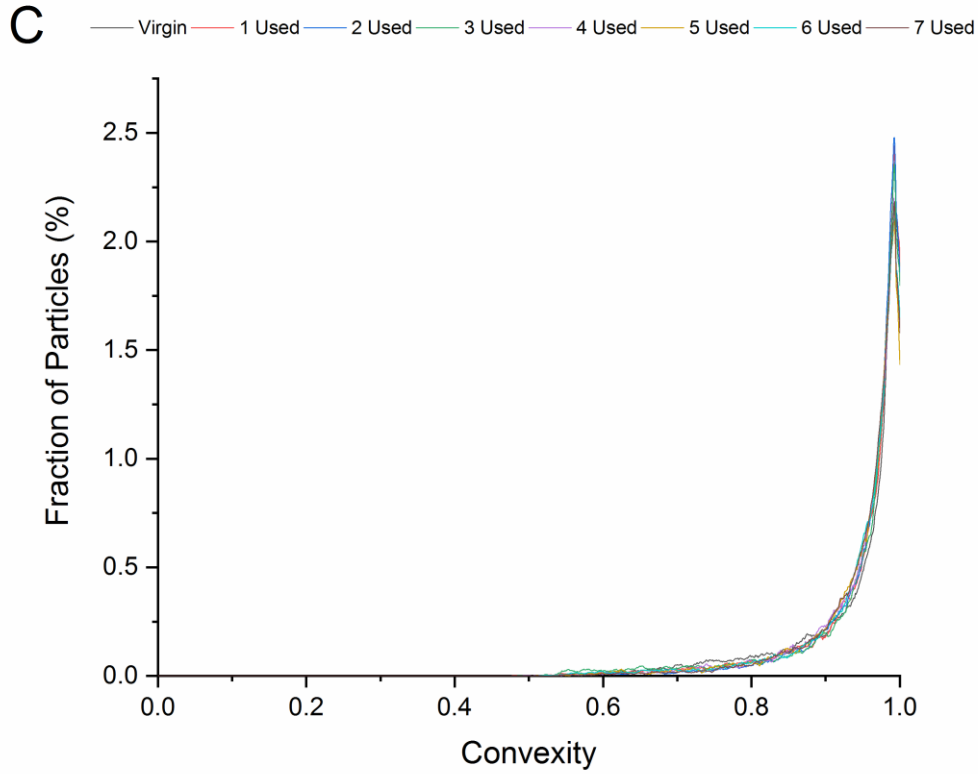
#### Particle Shape

A Malvern Morphogi G3 was used to measure the particle size and shape as the powder experienced more iterations through the HSS machine (Figure 5.6). Table 5.4 is a repeat of Table 4.3 for ease in describing the parameters measured.

Table 5.4 Parameters measured by image analysis and their descriptions and equations (109).

Measured Variable	Description	Equation
Circle Equivalent Diameter (CE Diameter) - Number Distribution	Diameter of a circle with the same area as the projected area of the particle image measured as a number distribution (number of particles).	
Circle Equivalent Diameter (CE Diameter) - Volume Distribution	Diameter of a circle with the same area as the projected area of the particle image measured as a volume distribution (the volume contribution of the particles). This is similar to traces obtained via laser diffraction.	
Convexity	A measurement of how 'spiky' a particle is, as the value tends to zero the particle becomes more 'spiky'. Hence as the value tends to 1 the particle is smoother.	$\text{Convexity} = \frac{\text{Convex hull perimeter}}{\text{Perimeter of particle}}$
High Sensitivity Circularity (HS Circularity)	The ratio of a particle area to the square of its perimeter, where a perfect circle has a HS Circularity of 1 and a narrow rod has a HS circularity of near 0.	$\text{HS Circularity} = \frac{4 \times \pi \times \text{Area}}{\text{Perimeter}^2}$
Aspect Ratio (AR)	The ratio of width to length of the particle measured.	$\text{AR} = \frac{\text{Width}}{\text{Length}}$





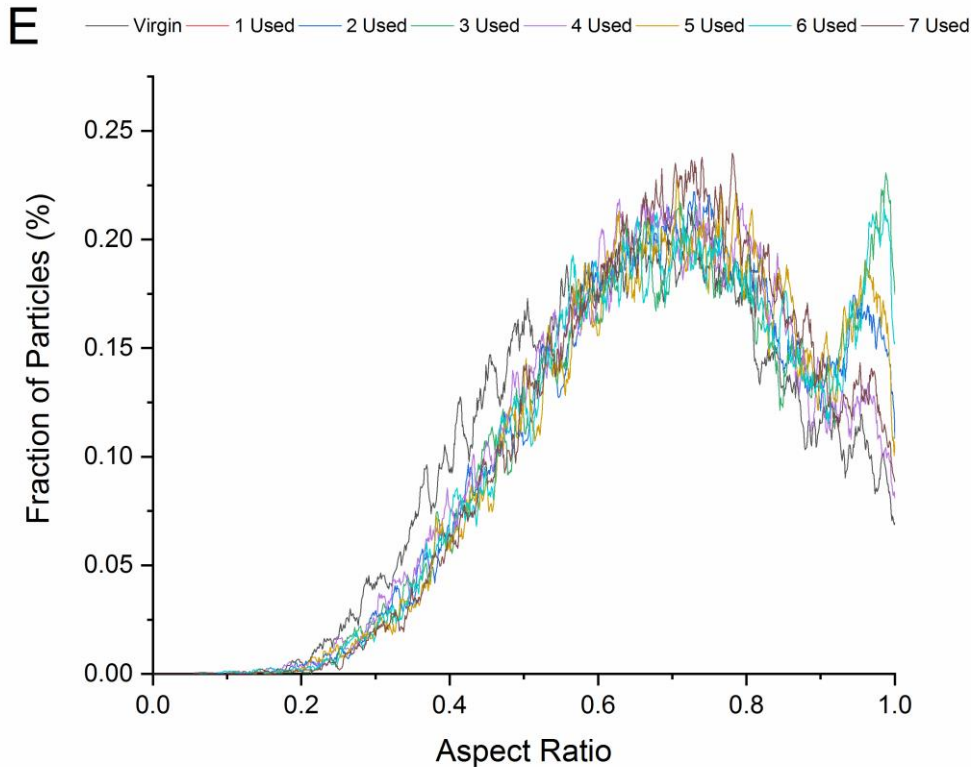


Figure 5.6 Image analysis traces showing size and shape of the various ages of CP22 PP powder. (A) Circle equivalent diameter against the number distribution of powder particles. (B) Circle equivalent diameter against the volume distribution of powder particles. (C) Convexity against fraction of powder particles. (D) High sensitivity circularity against fraction of powder particles. (E) Aspect ratio against fraction of powder particles.

Studying the traces shown in Figure 5.6, no clear trends were observed, although it can be seen that there are more virgin particles with low aspect ratio and high sensitivity circularity. This may indicate that the particles become more spherical in nature after being processed in the HSS system, possibly due to slight annealing of the powder, but subsequent increases are not observed with further powder grades.

Whilst it is not possible to draw any major conclusions in terms of powder size/shape changes, the powder flow changes observed are somewhat supported by the observation of the powder size increasing as larger particles would lead to better flow (73), and an increase in powder size would also lead to worse packing and hence a lower bulk tapped density. The slight change in particle shape leading to more circular powder particles would also lead to better powder flow. However, it is unlikely that any of these are the dominant reason for the changes in build success observed during this set of trials.

## 5.3.3 Chemical and thermal properties

Molecular Weight

Previous work using Nylon 12 on powder age has shown change in molecular weight of the polymer (117, 118), with the molecular weight and the dispersity of the Nylon increasing with used powder. Therefore the molecular weight and the dispersity of the various aged PP were measured using Gel Permeation Chromatography (GPC).

Molecular weight determination was carried out by GPC externally by Smithers Rapra. An Agilent PL GPC220 with 3 Agilent Technologies PLgel Olexis guard plus (300 mm, 13  $\mu$ m) columns in a 1,2,4-trichlorobenzene with anti-oxidant solvent at a flow rate of 1.0 mL/min at 160 °C using refractive index and differential pressure detectors were used for testing. Calibration was carried out using polystyrene calibrants and Mark-Houwink parameters were used to equivocate to linear polypropylene (119). Two samples were measured for each powder age and averaged. Three parameters were recorded for each polymer – the number average molecular weight ( $M_n$ ), weight average molecular weight ( $M_w$ ) and dispersity ( $\mathcal{D}$ ), as described in Table 5.5.

*Table 5.5 Parameters measured by Gel Permeation Chromatography to define molecular weight, where  $M_i$  is the molecular weight of a polymer chain and  $N_i$  is the number of chains of that molecular weight.  $M_w$  is reported as a small number of small polymer chains can have a large effect on  $M_n$  although little to no effect on the properties measured of the polymer.*

Measured Parameter	Symbol	Description	Equation
Number average molecular weight	$M_n$	The total weight of the polymer, divided by the total number of molecules.	$M_n = \frac{\sum N_i M_i}{\sum N_i}$
Weight average molecular weight	$M_w$	$M_w$ takes into consideration the molecular weight of each polymer chain into calculating the overall molecular weight of the polymer.	$M_w = \frac{\sum N_i M_i^2}{\sum N_i M_i}$
Dispersity	$\mathcal{D}$	The distribution of molecular weight of the polymers.	$\mathcal{D} = \frac{M_w}{M_n}$

*Table 5.6  $M_w$ ,  $M_n$  and  $\mathcal{D}$  of CP22 PP powders at various powder ages.*

Sample	$M_w$	$M_n$	$\mathcal{D}$
Virgin	171000	41500	4.1
Used 1	173000	40800	4.3
Used 2	169000	43000	3.9
Used 3	171000	43200	4.0
Used 4	167000	38800	4.3
Used 5	170000	39400	4.3
Used 6	171000	39800	4.3
Used 7	170000	41000	4.2

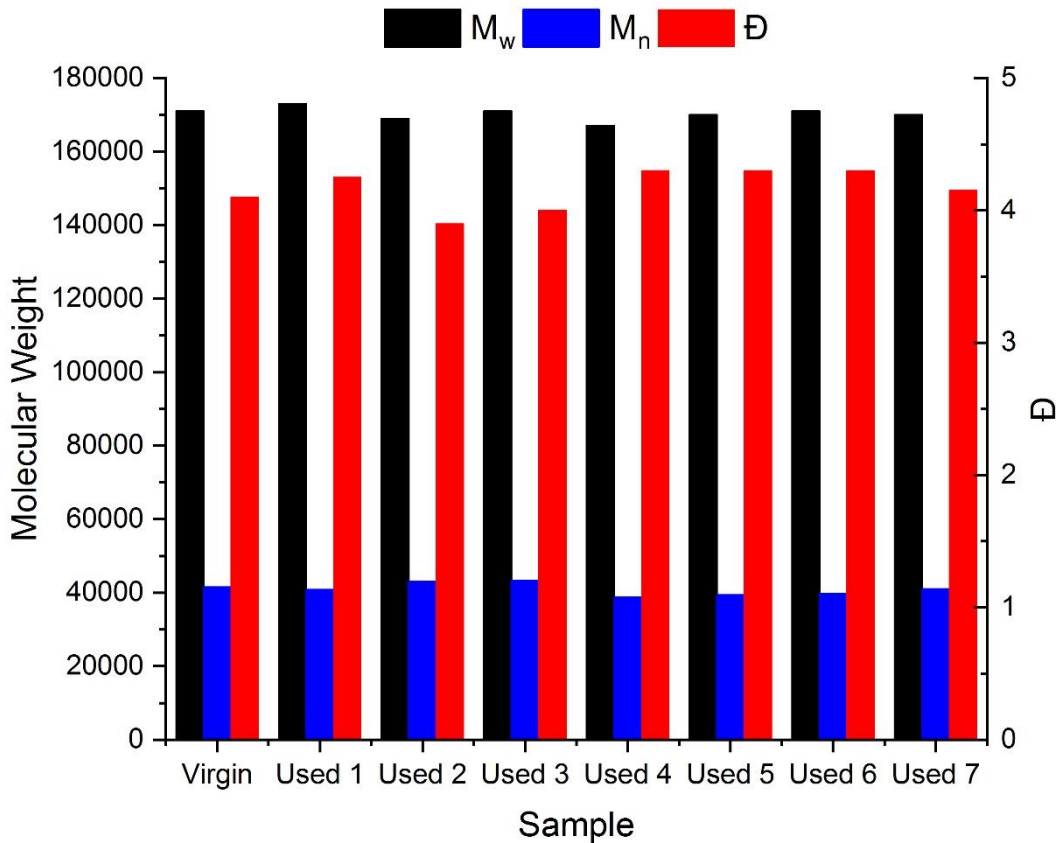


Figure 5.7 The effect of powder age in PP powders on number average molecular weight, weight average molecular weight and dispersity.

Table 5.6 and Figure 5.7 show that, unlike the reported literature for Nylon 12, the PP tested showed only minor molecular weight change as the powder was aged in the HSS process. Nylon can undergo reactions at high temperatures which increases the molecular weight of the polymer (120). Whereas PP does not have the same chemical groups, the lack of the amide group, which allow this reaction to occur. The chemical structures of both polypropylene and Nylon 12 are shown in Figure 5.8. Polypropylene is a chain growth polymer where by free radical polymerisation a polymer chain is grown. In contrast to Nylon which is step growth condensation polymer where water is a side product of the polymerisation.

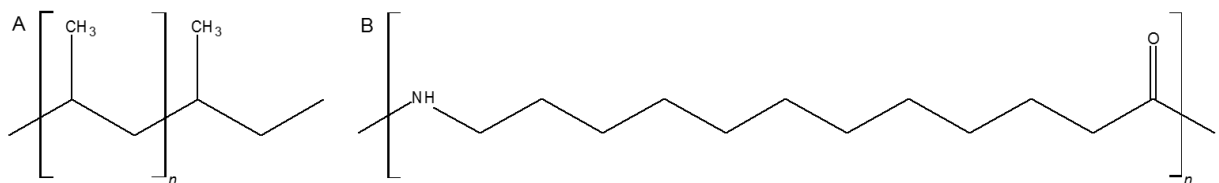


Figure 5.8 The chemical structure of A. polypropylene and B. Nylon 12.

The degradation mechanism of PP is via a radical chain reaction, initiated by a free radical (121). The rate of this reaction is increased at an elevated temperature as used in the HSS process. However as shown in Figure 5.7 this is not observed. Although this could occur in the part where the polymer experiences a higher temperature.

#### Decomposition behaviour

Thermogravimetric analysis (TGA) is an analysis technique which involves heating a sample in a controlled manner to well above the decomposition temperature of the material and measuring the mass loss, providing information regarding the decomposition temperature of the polymer where it breaks down into gases. The remaining mass gives information on the amount of additives added to the material by the supplier before the material is received, as additives such as glass beads and fumed silicas which act as flow agents do not decompose, at these temperatures (78, 110).

A Pyris 1 TGA was used to carry out thermogravimetric analysis whereby a sample of powder was heated and its mass recorded during the process using an accurate in built balance. The operating procedure was heating of a  $5 \pm 1$  mg sample in a ceramic crucible from 20 °C to 800 °C at 10 °C/min in a N<sub>2</sub> atmosphere, as this is standard procedure for TGA. Three repeats were measured for virgin, used 3, used 4 and used 6, and for the remaining grades a single measurement was made. The parameters examined were the % residual of material remaining and the onset of decomposition temperature, both calculated using the Pyris software for the TGA. The onset of decomposition of the material is calculated by the temperature at which a straight line from the baseline of the curve intercepts with a tangential line where the curve has a point of inflection, this value acts as a means of comparison between TGA curves, as shown in Figure 5.9. The percentage residual was calculated by the percentage change in mass of the sample.

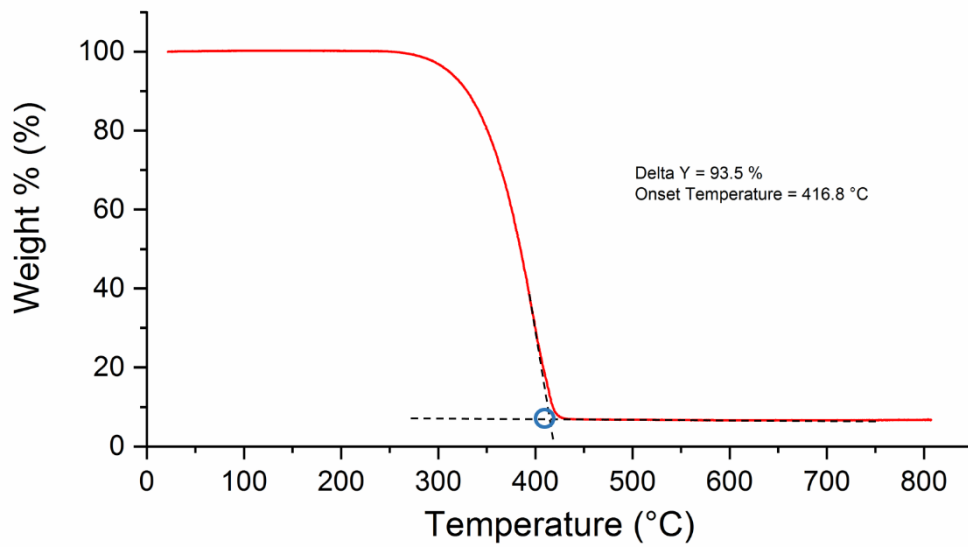


Figure 5.9 Example of onset temperature (°C) and percentage residual for virgin CP22 PP.

The onset temperature for each polymer powder tested was averaged and reported in Figure 5.10. The residual percentage is equal to one minus the delta y measured (5.1), these were also averaged and reported in Figure 5.10.

$$\text{Residual Percentage} = 1 - \delta y$$

**5.1**

Where  $y$  is the percentage of original mass of the sample from the TGA.

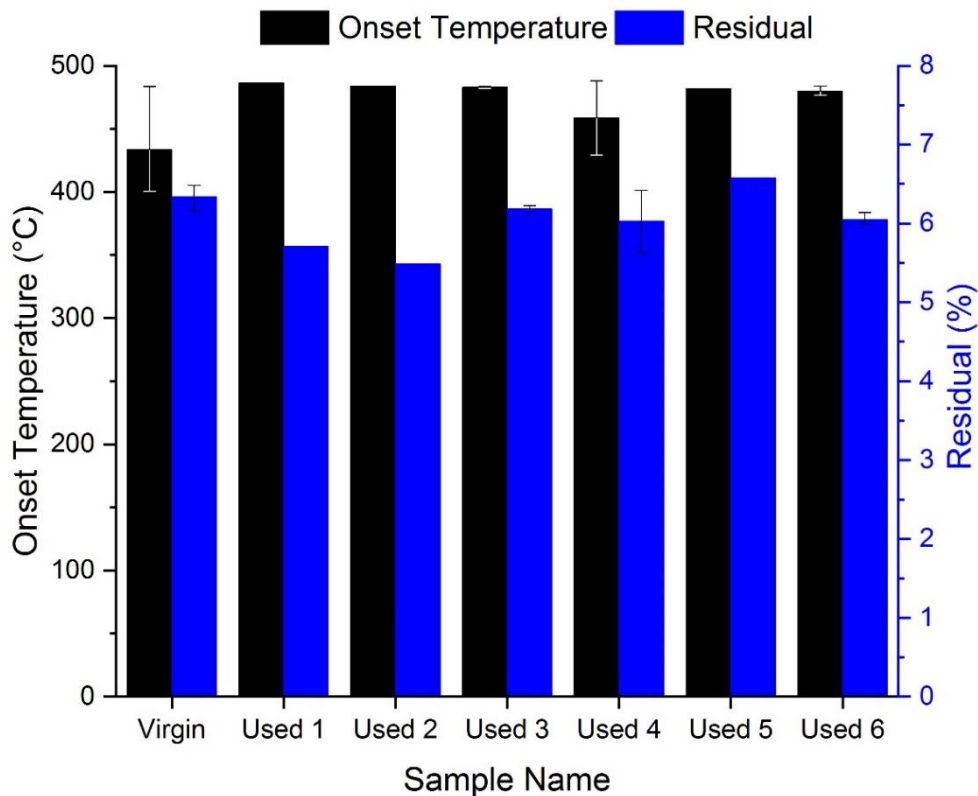


Figure 5.10 The effect of powder age on decomposition temperature and residual mass. The error bars included are range bars.

It can be seen that there is no obvious trend in the onset temperatures or residual mass, and that the lowest decomposition temperature of the polymer is still well above the operating temperature of the HSS process. This indicates that powder decomposition is unlikely to be the cause of the changes in processability reported in Section 5.2.

The inorganic remains causing the residual mass are most likely the flow agents, residual carbon and other additives added to the powder, which were previously identified as being present in the CP22 PP powder in Section 4.1.2 and Figure 4.6. Flow agents are often fumed silicas (78) which are light and have the possibility of being lost to the powder feedstock during general handling and sieving. However, there is no evidence of these changing, meaning the flowability change seen in Section 5.3.1 is unlikely to be caused by a variation in the quantity of flow agent.

#### Thermal properties

Differential Scanning Calorimetry (DSC) was used to measure additional thermal properties, specifically the melt and recrystallisation temperatures and enthalpies. Temperatures were calculated

from maxima or minima of the peak, whereas the enthalpy was calculated from the area under the curve.

A PerkinElmer DSC 8000 was used. A sample  $7 \text{ mg} \pm 2 \text{ mg}$  was placed in an aluminium sample pan, which was crimped and placed in the DSC sample furnace with an empty crimped sample pan placed in the reference furnace. The samples were subjected to a temperature cycle as follows:

1. Held at  $20 \text{ }^\circ\text{C}$  for 1 min.
2. Heated from  $20 \text{ }^\circ\text{C}$  to  $200 \text{ }^\circ\text{C}$  at  $10 \text{ }^\circ\text{C}/\text{min}$ .,
3. Held at  $200 \text{ }^\circ\text{C}$  for 1 min.,
4. Cooled from  $200 \text{ }^\circ\text{C}$  to  $20 \text{ }^\circ\text{C}$  at  $10 \text{ }^\circ\text{C}/\text{min}$ .,
5. Held at  $20 \text{ }^\circ\text{C}$  for 1 min.,
6. Heated from  $20 \text{ }^\circ\text{C}$  to  $200 \text{ }^\circ\text{C}$  at  $10 \text{ }^\circ\text{C}/\text{min}$ .

This temperature cycle was chosen as  $10 \text{ }^\circ\text{C}/\text{min}$  is a standard rate used in literature (111) and  $20 \text{ }^\circ\text{C}$  to  $200 \text{ }^\circ\text{C}$  were selected as this range included temperatures from room temperature to above melt temperature but without reaching temperatures which would cause degradation of the polymer. The hold steps were used to ensure the full temperature range was obtained. A second heat cycle was included in this analysis compared to the DSC carried out in Section 4.1.3.

A second heat cycle is sometimes used in DSC analysis to analyse the thermal history of the polymer being examined. This is because the previous thermal history of the polymer is unknown and by heating and then cooling at a controlled rate the thermal history of the polymer is known and then can be compared between polymers if required (122). The thermal history imparted to the sample is controlled in the cooling step (Step 4). An example DSC trace is shown in Figure 5.11; these traces were then analysed using the Pyris software to output the temperatures and enthalpies of the peaks.

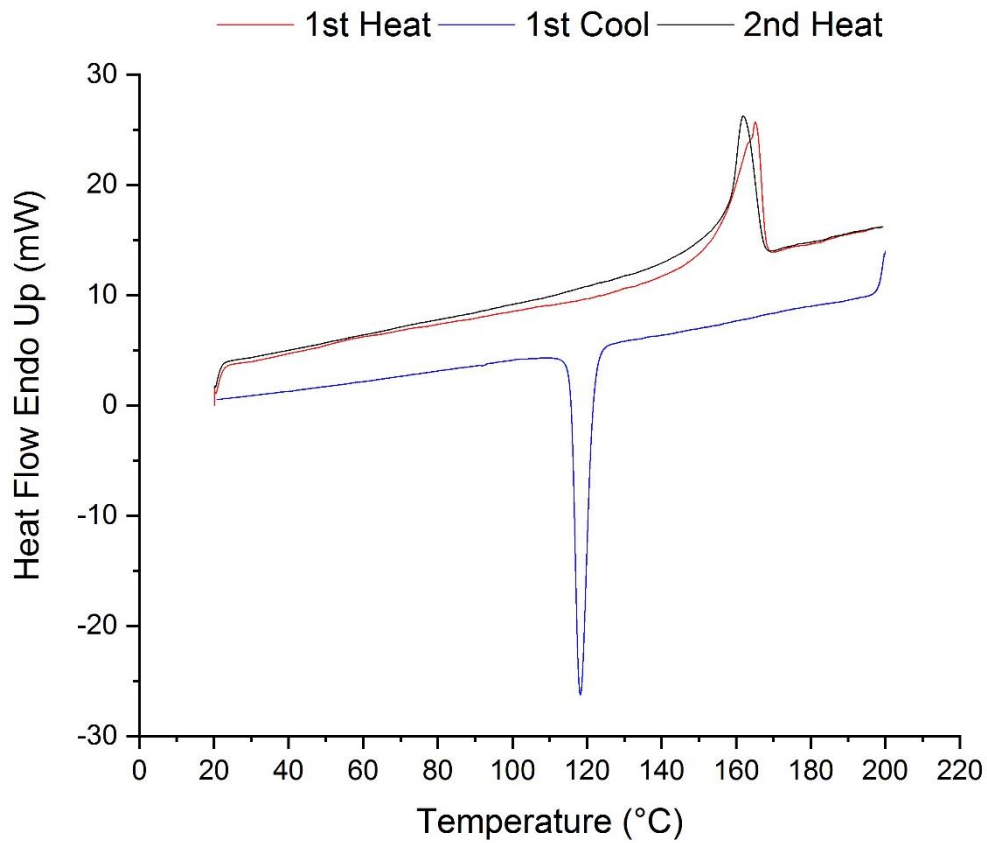


Figure 5.11 DSC trace of virgin PP showing the 1st and 2nd heat and 1st cool cycle.

The melt and recrystallisation temperatures for each aged powder were calculated using Pyris software and then compiled into Figure 5.12. The melt and recrystallisation enthalpies were also calculated using the Pyris software and compiled into Figure 5.13.

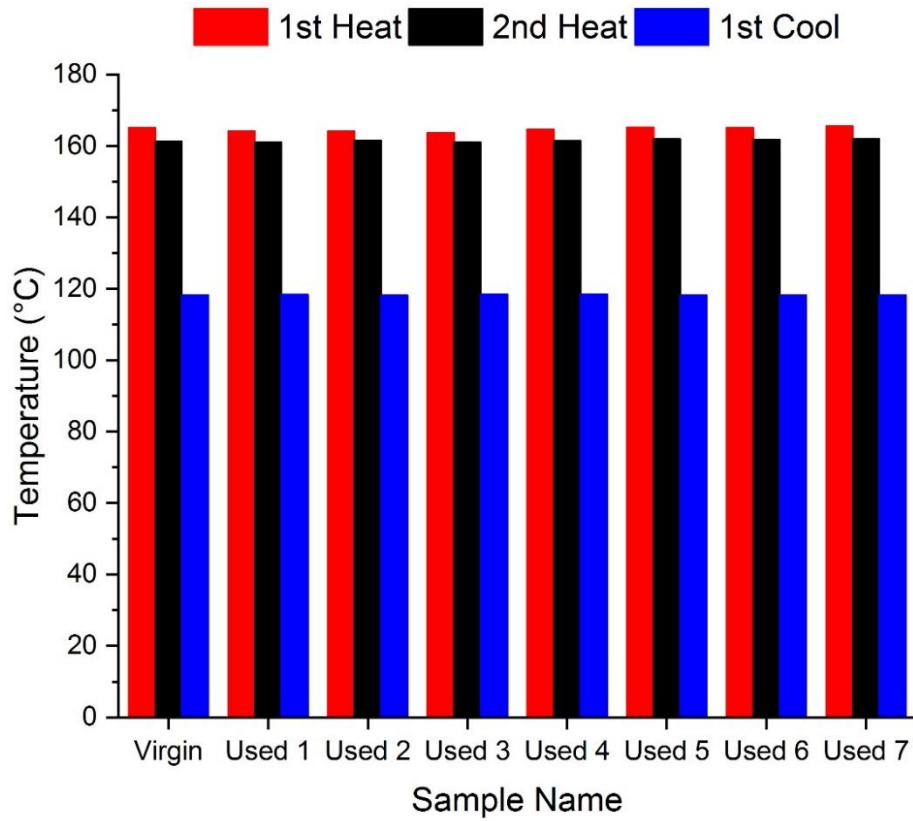


Figure 5.12 Melt and recrystallisation temperatures of various aged PP powders.

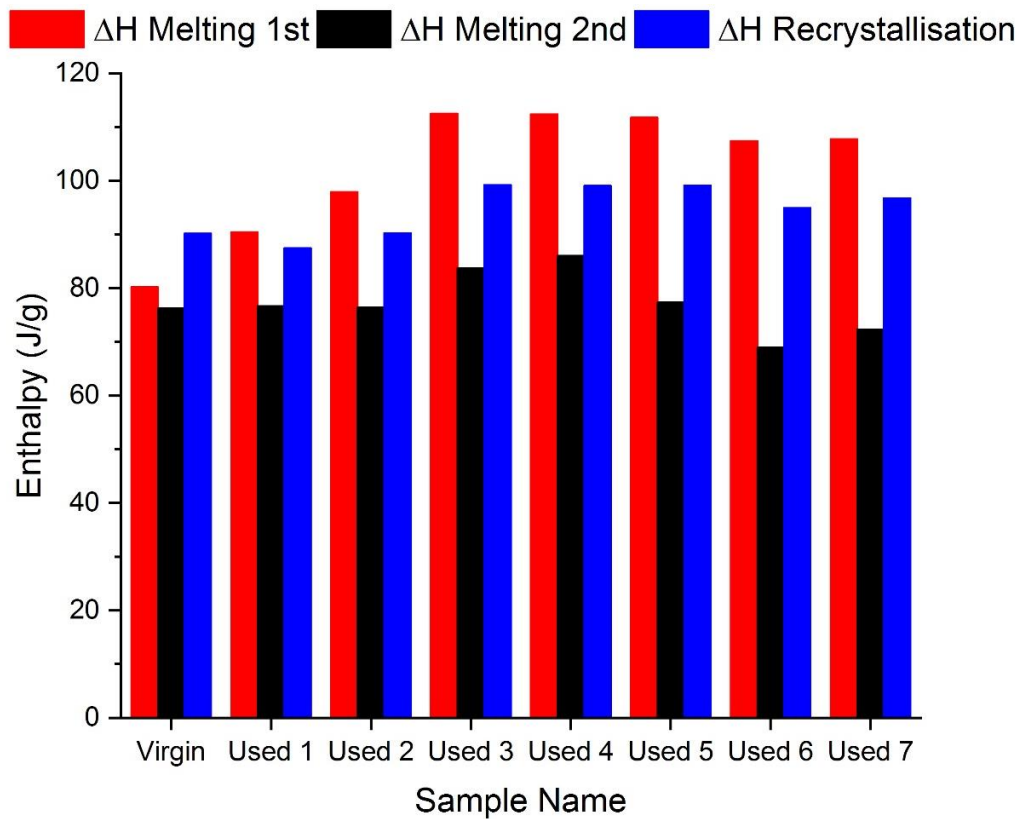


Figure 5.13 Melt and recrystallisation enthalpies of various aged PP powders.

As can be seen in Figure 5.12, there is no apparent change in the melt or recrystallisation temperatures with variation in powder age. However, there is alteration in the enthalpies as the CP22 PP becomes aged. The enthalpy of melting is directly proportional the crystallinity of a sample, meaning there is a change in crystallinity with powder age.

Figure 5.13 shows an increase in melt enthalpy (and therefore in crystallinity) with powder age, until the used 3 powder at which point no further change is observed. These observations show the PP powder increases in crystallinity until the powder has been processed in the HSS machine three times and hence been thermally cycled three times and then plateaus. There are no clear trends for the second melt and the recrystallisation enthalpies where the polymer has then experienced similar thermal histories.

#### 5.3.4 Powder characterisation summary

The analysis carried out in this section has shown the powder changes after being processed in the HSS process. Powder flow increases as the particle size and shape of the CP22 PP becomes more conducive to good flowability and the amount of flow agent does not change as measured by TGA.

The molecular weight and the melt and recrystallisation temperatures do not change after the powder particles are aged, however the crystallinity of the polymer is observed to alter; this is another potential cause for the changes in processability observed in the trials reported in this section. The chemical difference between PP and previously examined Nylon in LS literature is key. As discussed they undergo different degradation mechanisms and therefore perform differently in powder bed fusion.

### 5.4 Characterisation of parts

In order to determine whether the changes in processability identified previously also indicate changes in mechanical properties, parts were manufactured as described in 5.2, using each of the powder ages assessed in Section 5.3.

#### 5.4.1 Part size

Part dimensions were measured and used to calculate shrinkage and wall growth also described in Section 4.5.1. Figure 5.14 shows the effect of powder age on shrinkage and wall growth of HSS parts.

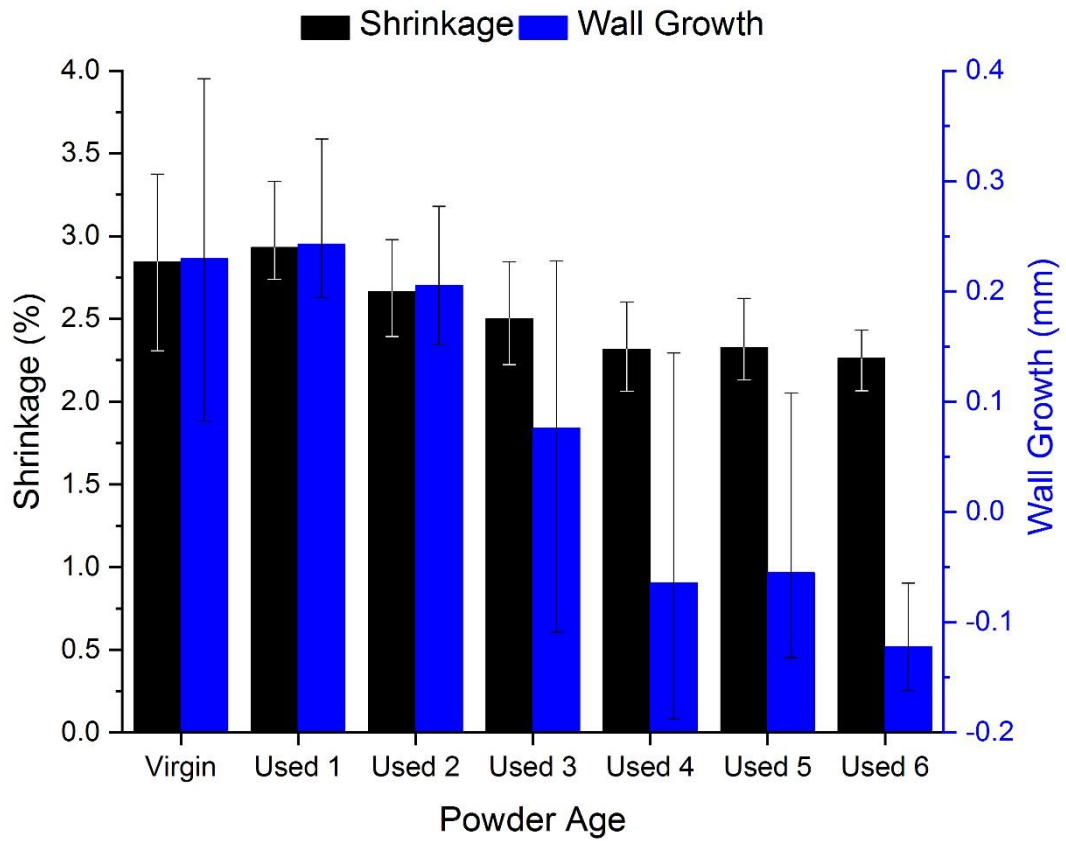


Figure 5.14 The effect of powder age on shrinkage and wall growth of HSS PP parts. The error bars included are range bars.

The effect of powder age on shrinkage and wall growth is shown in Figure 5.14, where both parameters appear to decrease as the powder becomes more aged (examined later in Section 5.5).

#### 5.4.2 Part density

Part density was calculated from rectangular blocks as described in Section 4.5.2. Figure 5.15 shows the effect of powder age on part density, where it can be seen that a decrease in part density occurs as the powder used as feedstock is aged.

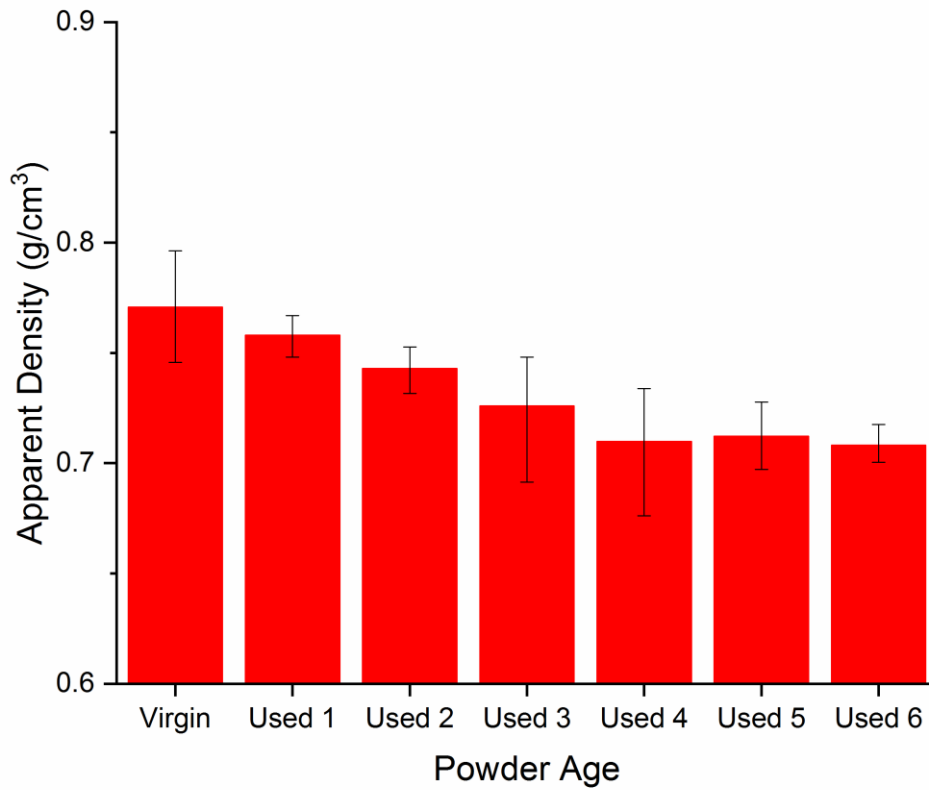


Figure 5.15 The effect of powder age on part density. The error bars included are range bars.

#### 5.4.3 Tensile properties

Tensile properties were measured as described in Section 4.5.3 using ASTM D638-14. The tensile properties measured were Ultimate Tensile Strength (UTS), Elongation at Break (EaB) and Young's Modulus (YM), as shown in Figure 5.16.

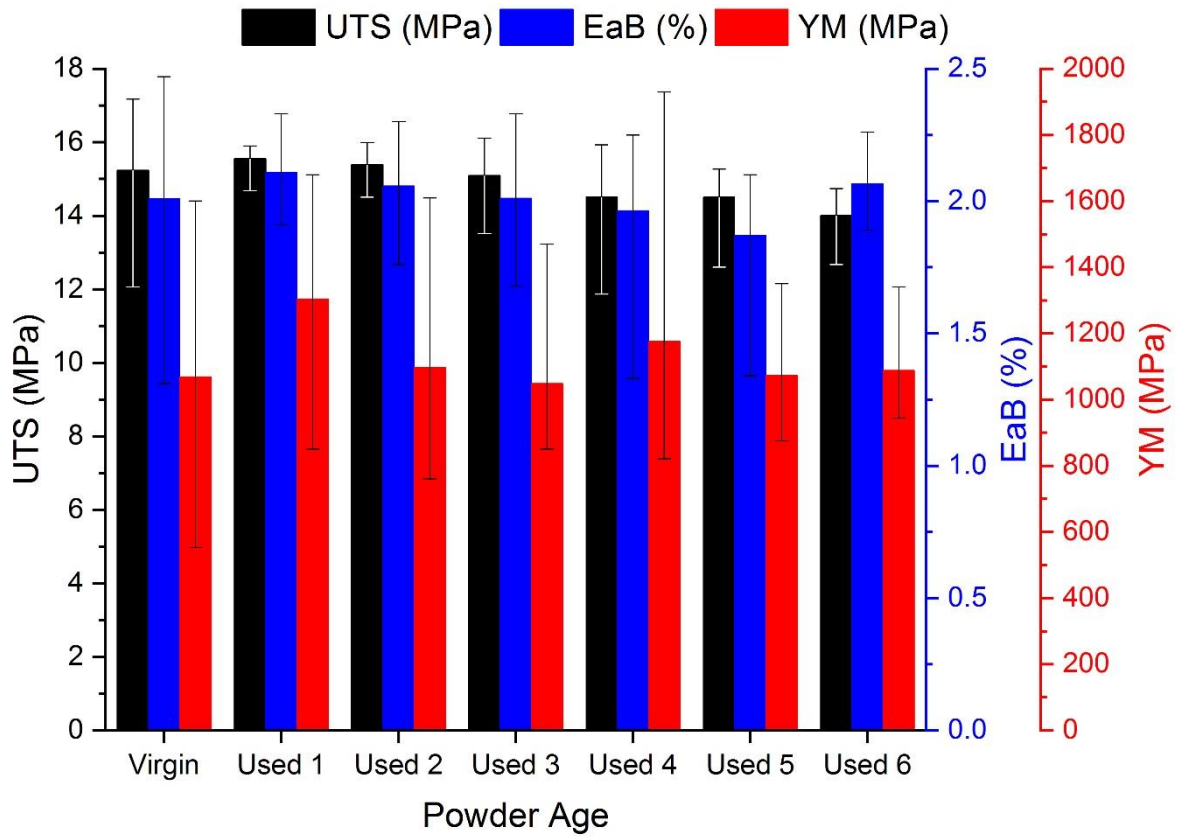


Figure 5.16 The effect of powder age on tensile properties including; UTS, EaB and YM. The error bars included are range bars.

There are no obvious trends in tensile properties with powder age, although this will be examined statistically in Section 5.5.

### 5.5 Further discussion

Due to the lack of repeatability in some of the data present in both Figures 5.14 and 5.16 (as evidenced by large, and often overlapping, range bars), an ANOVA test was used to assess differences between data sets as described in Section 4.6; the results of these tests are compiled in Table 5.7.

Table 5.7 One way analysis of variance the effect of powder age on tensile properties and shrinkage and wall growth. The result of the ANOVA is shown with tests which should significance highlighted in green and then followed by post-hoc tests to demonstrate which data sets were significantly different from each other. The numbers in the table signify the two levels of parameters examined, e.g. 1U V is the comparison between powder of virgin age compared to powder of used 1 age.

One way ANOVA set tested	Is it significant at 0.05 level?	Post Hoc test - Scheffe tests
<b>Dimensional accuracy</b>		
Powder Age Shrink	Yes	1U V   2U V   2U 1U   3U V   3U 1U   3U 2U   4U V   4U 1U   4U 2U   4U 3U   5U V   5U 1U   5U 2U   5U 3U   5U 4U   6U V   6U 1U   6U 2U   6U 3U   6U 4U   6U 5U
Powder Age Wall	Yes	1U V   2U V   2U 1U   3U V   3U 1U   3U 2U   4U V   4U 1U   4U 2U   4U 3U   5U V   5U 1U   5U 2U   5U 3U   5U 4U   6U V   6U 1U   6U 2U   6U 3U   6U 4U   6U 5U
<b>Mechanical properties</b>		
Powder Age UTS	Yes	1U V   2U V   2U 1U   3U V   3U 1U   3U 2U   4U V   4U 1U   4U 2U   4U 3U   5U V   5U 1U   5U 2U   5U 3U   5U 4U   6U V   6U 1U   6U 2U   6U 3U   6U 4U   6U 5U
Powder Age EaB	No	1U V   2U V   2U 1U   3U V   3U 1U   3U 2U   4U V   4U 1U   4U 2U   4U 3U   5U V   5U 1U   5U 2U   5U 3U   5U 4U   6U V   6U 1U   6U 2U   6U 3U   6U 4U   6U 5U
Powder Age YM	No	1U V   2U V   2U 1U   3U V   3U 1U   3U 2U   4U V   4U 1U   4U 2U   4U 3U   5U V   5U 1U   5U 2U   5U 3U   5U 4U   6U V   6U 1U   6U 2U   6U 3U   6U 4U   6U 5U
<b>Legend</b>		Significant      Not Significant

The statistical analysis displayed in Table 5.7 shows that there is a statistically significant effect of powder age on dimensional accuracy, but not for mechanical properties.

The trend observed with density of parts decreasing as powder is aged can be explained by the fact that the powder used to manufacture the parts is larger and has a lower tapped bulk density. Therefore, when the powder is sintered there is less powder present, meaning less dense parts can be manufactured.

Although density and mechanical properties are related, they often show a relatively 'noisy' correlation. Given the relatively small change seen here, and the quite messy data, it means we don't see a clear correlation. Molecular weight was shown not to alter as powder was more used more and therefore the change in mechanical properties seen by Gornet *et al.*(116) and Zarringhalam *et al.*(118) was not observed.

## 5.6 Conclusions

The research carried out in this chapter has shown CP22 PP can be reused without significant degradation of mechanical properties, which is likely to be crucial for the use of PP in FMCGs, where cost and sustainability are key.

However, although Chapters 4 and 5 have demonstrated that polypropylene can be processed in HSS, the mechanical properties of CP22 PP parts are unlikely to be acceptable for use in FMCGs. Further grades of PP have therefore been studied in order to determine whether PP can be reliably processed with acceptable mechanical properties, and whether conclusions can be made as to the properties of the PP which will lead to a successful outcome.



## Chapter 6 Processability of alternative polypropylene grade XX00199PP (pre-commercial)

### 6.1 Introduction

The work presented in Chapter 4 demonstrated that it is possible to process polypropylene (PP) in the High Speed Sintering (HSS) process. However the mechanical properties of these parts were not sufficient for end use parts for Fast Moving Consumer Goods (FMCGs), and the process window of the CP22 material was small. This in turn led to the repeatability of the process being low. Other grades of PP will therefore be tested, in order to determine whether PP in general is not suitable for use in the HSS process or whether the CP22 PP is specifically problematic.

A pre-commercial grade of PP designed for use in Additive Manufacturing (AM) will be characterised. This powder will then be trialled in HSS to analyse the effect of various parameters in HSS on the dimensional and mechanical properties of parts produced.

### 6.2 Characterisation of raw materials

A pre-commercial grade of polypropylene, XX00199PP, under development for use in Laser Sintering (LS) was supplied by A. Schulman. XX00199PP was fully characterised to allow future comparisons between the polypropylenes tested.

#### 6.2.1 Powder flow

The tapped bulk density was measured using the same method described in Section 4.1.1. Table 6.1 shows the tapped density of virgin XX00199PP powder.

*Table 6.1 Tapped bulk density of XX00199PP for each run and average. Standard deviation is shown in brackets.*

Run	Density of XX00199PP (gcm <sup>-3</sup> )
1	0.454
2	0.455
3	0.452
<b>Average</b>	<b>0.45 (0.002)</b>

Powder flow assessment was attempted using the same cone apparatus as used in Section 4.1.1. However, in this case the powder did not flow through the orifice, meaning this test was not possible. Although this test was not possible the powder flowed well in the HSS process and good powder deposition was observed, forming an even powder layer on the build bed. This suggests that, although

the powder flow of this material is not as high as for the more standard PA 2200, it is sufficient to allow processing.

### 6.2.2 Particle size and morphology

Particle size was measured by laser diffraction using a mastersizer as described in Section 4.1.2. The volume distribution against size trace for XX00199PP is shown in Figure 6.1. The averages of the three samples measured are reported in Table 6.2; D(10) represents the maximum diameter of the smallest 10 % of particles, D(50) is the mean particle diameter and D(90) is the maximum diameter of the smallest 90 % of particles.

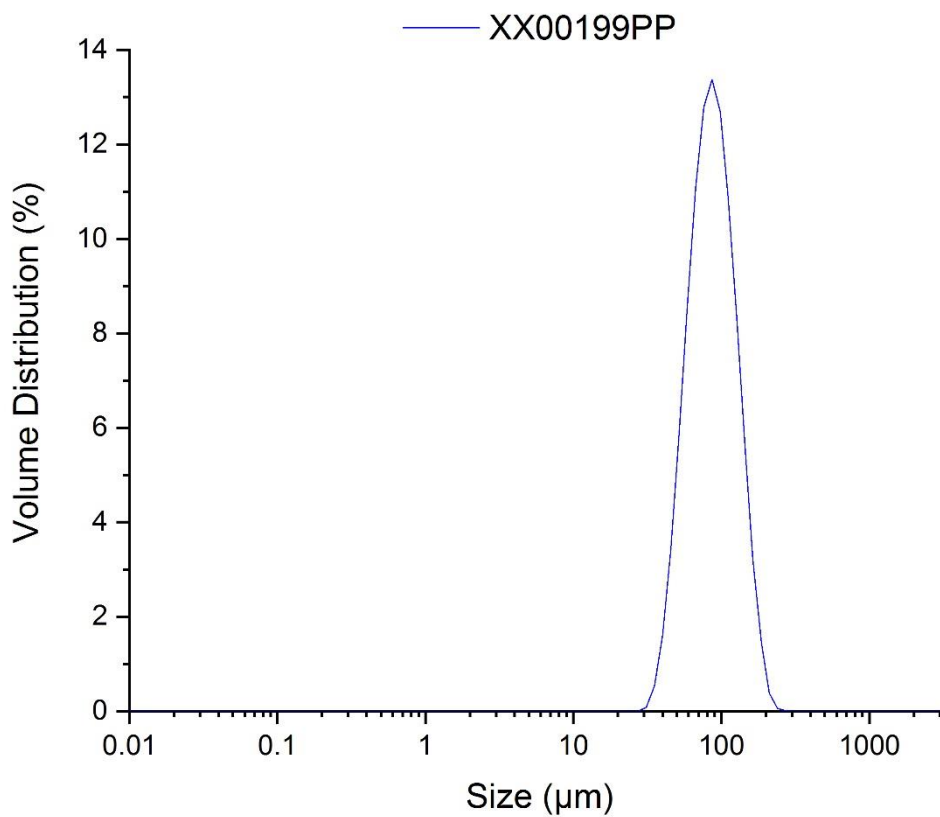


Figure 6.1 Mastersizer trace of XX00199PP.

Table 6.2 Particle size breakdown of XX00199PP.

Material	D(10) (µm)	D(50) (µm)	D(90) (µm)
XX00199PP	56.5	92.5	149.3

The characterisation of XX00199PP will allow future comparison to other PP tested in this research.

Image analysis was also used to measure particle size and also particle shape; a Malvern Morpholgi G3 was used to carry out this analysis as described in Section 4.1.2. The size and shape data traces are shown in Figure 6.2.

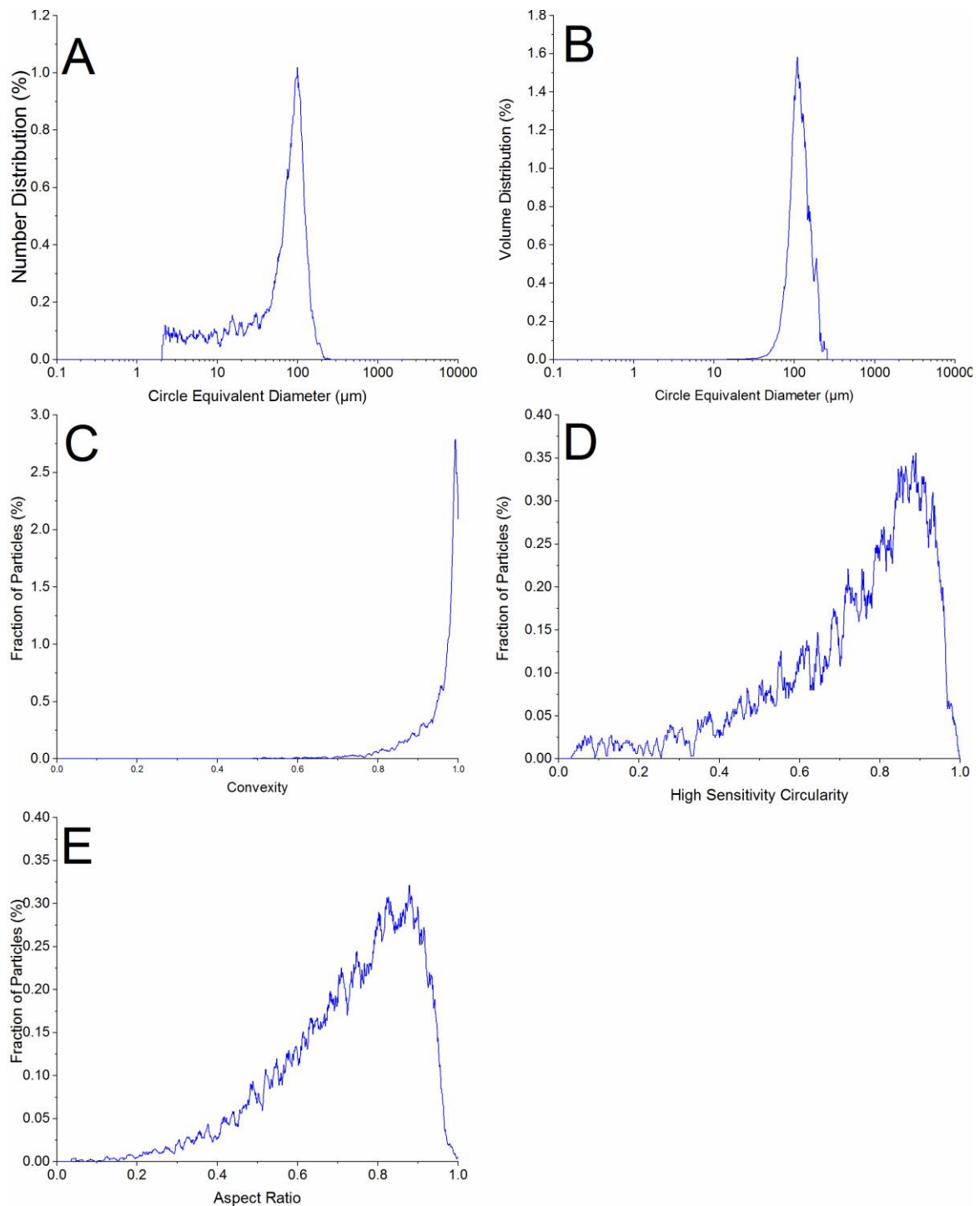


Figure 6.2 Image analysis traces showing size and shape of the CP22 PP powder. (A) Circle equivalent diameter against the number distribution of powder particles. (B) Circle equivalent diameter against the volume distribution of powder particles. (C) Convexity against fraction of powder particles. (D) High sensitivity circularity against fraction of powder particles. (E) Aspect ratio against fraction of powder particles.

Figure 6.2 **A** shows a large component of large particles in the number distribution, which would normally be expected to lead to good powder flow. Discussions of the reasons this is not the case will be made in Chapter 8.

The XX00199PP powder was also examined using Scanning Electron Microscopy (SEM), using the same method of sample preparation and equipment as in Section 4.1.2. Figure 6.3 shows SEM images of XX00199PP at a high and low magnification. The shape of the polymer powder particles in the SEM micrograph are not smooth and indicate grinding of the polymer, during its manufacture. However, there is no evidence of additives with substantially different shape.

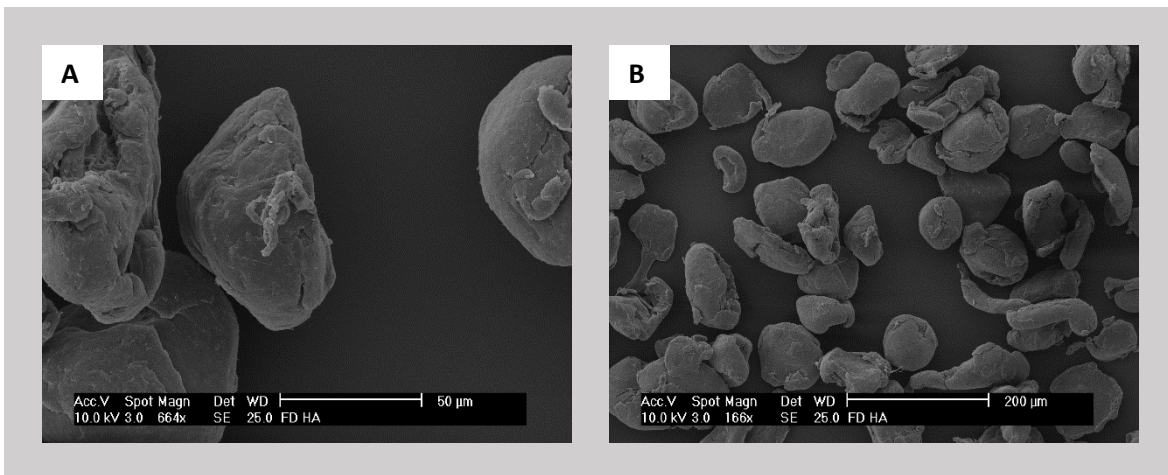


Figure 6.3 SEM of XX00199PP (A&B) used high and low magnification respectively.

### 6.2.3 Thermal properties

The thermal properties of XX00199PP were also examined to give information on suitable parameter settings as well as allowing comparison to other PP powders.

Differential Scanning Calorimetry (DSC) was carried out to determine the melt and recrystallisation temperature of the PP powder to aid in setting the build bed and overhead temperatures. The same method presented in Section 4.1.3 was used. This method involved using a PerkinElmer DSC 8000 and heating and cooling at a controlled rate of 10 °C/min; the DSC trace is shown in Figure 6.4.

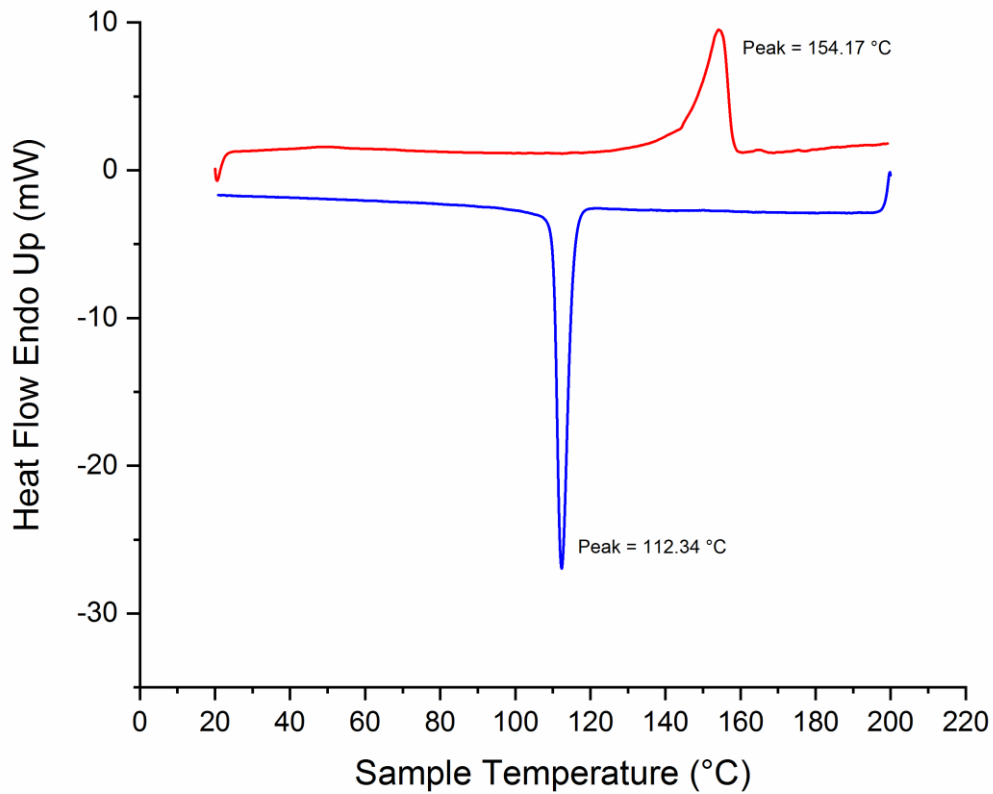


Figure 6.4 DSC curve of XX00199PP; temperature scan at 10 °C/min.

The peak melt of XX00199PP is 154 °C and the peak recrystallisation temperature was measured as 112 °C, this information was used in Section 6.4 to set the initial build parameters for this material.

Thermogravimetric analysis was also carried out on XX0199PP to allow later comparisons between PP powders; this analysis was as described in Section 5.3.3 where the powder sample was heated in a N<sub>2</sub> atmosphere at a controlled rate and the mass loss was measured. An example curve is shown in Figure 6.5. Three runs were made for the material and these are displayed in Table 6.3 and averaged.

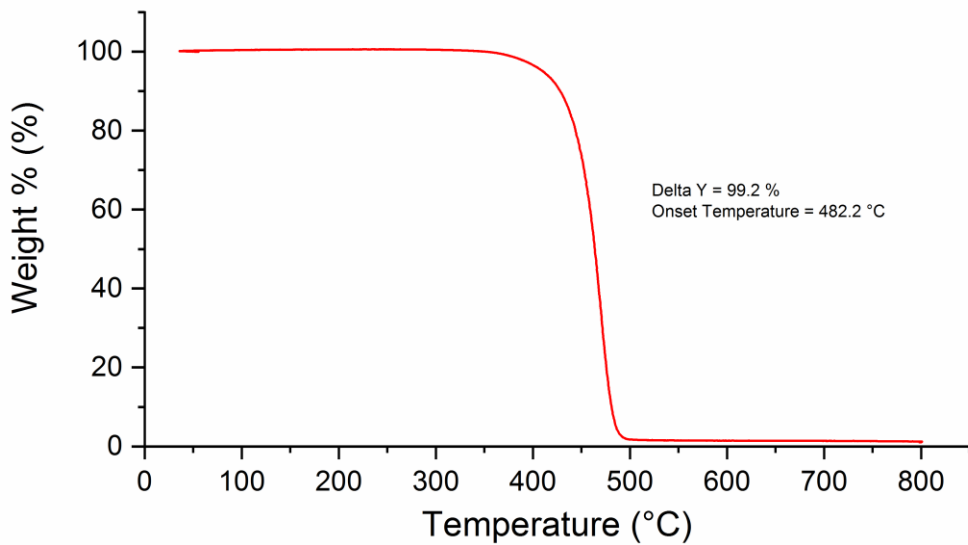


Figure 6.5 Thermogravimetric Analysis trace of XX00199PP powder.

Table 6.3 TGA results for XX00199PP including; onset temperature and residual mass. Standard deviation is shown in brackets.

Sample name	Onset temperature (°C)	Residual mass (%)
XX00199PP 1	482.22	0.8426
XX00199PP 2	475.95	2.4111
XX00199PP 3	479.06	2.7039
<b>Average</b>	<b>479.08 (3.14)</b>	<b>1.99 (1.00)</b>

The onset temperature and residual mass will be used in Chapter 8 to compare the different grades of PP used in this research.

### 6.3 Part manufacture via High Speed Sintering

The same strategy was used to manufacture parts using XX00199PP as the powder feedstock as used for CP22PP, this method was described in Section 4.2. The HSS machine was voxeljet's 'alpha' VX200 HSS machine, the builds manufactured were same build files used previously five ASTM D638 Type I tensile test specimens and four rectangular blocks to test part density.

### 6.4 Identification of initial processing parameters

There are several parameters which can be altered for the manufacture of HSS parts; these parameters are: preheat power, sinter power, preheat speed, sinter speed, recoater vibration, feed hopper fill duration and frequency, grey level, build bed and overhead temperature and layer thickness, see Table 6.4.

Table 6.4 High Speed Sintering parameters for the attempted processing of XX00199PP.

Parameter	Range
Preheat Power (%)	30 - 100
Sinter Power (%)	100
Preheat Speed (mm/s)	70
Sinter Speed (mm/s)	60 - 140
Recoater Vibration (%)	100
Feed Hopper Fill Frequency	12
Feed Hopper Fill Duration (s)	1.25
Grey level	1 – 5
Build Bed (°C)	130 - 144
Build Overhead (°C)	130 - 144
Layer Thickness (µm)	100

The initial attempt at processing XX00199PP used a parameter set which had previously manufactured parts using CP22 PP as shown in Table 6.5.

Table 6.5 Parameter set attempted to process XX00199PP which had previously manufactured CP22 PP powder into HSS parts.

Parameter	Setpoint
Preheat Power (%)	50
Sinter Power (%)	100
Preheat Speed (mm/s)	70
Sinter Speed (mm/s)	105
Recoater Vibration (%)	100
Feed Hopper Fill Frequency	12
Feed Hopper Fill Duration (s)	1.25
Grey level	3
Build Bed (°C)	144
Build Overhead (°C)	144
Layer Thickness (µm)	100

The build using the parameter set displayed in Table 6.5 failed due to the whole build bed sintering. Therefore it was necessary to identify alternative parameters to process XX00199PP in HSS, as outlined below.

#### 6.4.1 Build bed temperature

Build bed and overhead temperature is the temperature to which the build area is heated to. The mid-point parameters used in Section 4.3 were a build bed temperature of 150 °C a difference of 13 °C from the DSC measurement. Therefore a build bed temperature of 141 °C would be suggested.

#### 6.4.2 Preheat power

An initial value of 50 % for pre-heat power was selected as this is standard in HSS and was used previously in Sections 4.3.1 and 5.2.

#### 6.4.3 Sinter power

100 % sinter power was used throughout the builds as the lamp's spectral output is most aligned to the absorption spectra of the lamp at 100 % power, and this is the power level previously used for the CP22 PP material.

#### 6.4.4 Preheat speed

Preheat speed is the speed the carriage moves across the build bed for the new layer deposition as well as the preheat lamp. This speed was fixed at 70 mm/s the standard in VX200 HSS machine as at this speed a good even powder deposition was acquired. This is different from the value set in previous work (see Section 4.3.3), this is due to the orifice on the HSS machine for powder deposition changing and hence the rate at which the powder flowed out altered therefore a speed of 70 mm/s maintained a good powder deposition, this speed was kept constant throughout the work on XX0019PP.

#### 6.4.5 Sinter speed

An initial sinter speed of 100 mm/s was chosen to be the starting sinter speed of the range selected to assess the effect of sinter speed on properties.

#### 6.4.6 Grey level

Previous work with Nylon 12 on this machine had indicated a grey level of 2 or 3 to give good part properties, and the work on CP22 PP showed that the highest mechanical properties were observed at a grey level of 1 or 2. A grey level of 2 was therefore selected as a start-point here.

### 6.5 Effect of processing parameter variation

Various builds were attempted, within the range stated previously in Table 6.5. The results of these builds were classified into the same five categories as used previously; these categories are shown in Table 6.6 which is a copy of Table 4.5.

*Table 6.6 Build classifications and the explanation of the terms used, where the builds classified by the first two terms were then further tested. Compared to the other build classifications which were described and could not be further tested.*

<b>Classification</b>	<b>Explanation</b>
Complete	All test pieces were manufactured and post processed, then analysed.
Complete but 1 test piece failed	All but one test pieces were manufactured and post processed, the remaining pieces were then analysed. The piece that was not complete failed due to localised curl on the single piece.
Failed due to powder removal	The manufacture of parts was completed but the excess powder around the parts was sintered to the extent it could not be removed by reasonable post processing.
Failed due to build bed sintered	The build bed became fully sintered before the beginning of printing ink (during the 50 pad layers), therefore the build was abandoned at this point.
Failed due to curl	During a point of the manufacture of test pieces they underwent curl and caused the build area to fail.

Four variables were altered, and were changed independently to assess the effect of each parameter on the properties of the parts manufactured. This method was chosen as it was previously used in Chapter 4, as well as the reasoning laid out in 4.4.1.

The build name notation used is very similar to the notation used in Chapter 4, with the addition of the prefix **B** to signify the build bed and overhead temperature. Therefore, the build name notation is **B\_G\_S\_P\_**, where **B** is the build bed and overhead temperature, **G** is the amount of ink used (grey level), **S** is the sinter speed where the lowest number is the fastest sinter speed and hence the least energy input and **P** is the preheat power with the highest number being the highest preheat power.

### 6.5.1 Build bed temperature

From the DSC trace and the application of CP22PP in HSS in Section 4.4.2 an initial temperature for the build bed and overhead was selected to be 140 °C. However, for XX00199PP to process at 140 °C a fast sinter speed was required (140 mm/s, **B3G2S1P2**) or powder removal was not possible due to the overheating of parts as seen in **B3G2S5P2**. Therefore, the build bed temperature was lowered to 135 °C and then 130 °C. It was also shown that at a low bed temperature more energy was required through the sinter lamp. This was demonstrated by **B1G2S8P2**, where parts were manufactured at a low build bed temperature but slow sinter lamp speed was needed.

The builds used to compare the effect of build bed and overhead temperature are highlighted in Table 6.7. It should be noted the sinter speed is not constant across these builds, this is due to a lower build bed temperature requiring more input energy from the sinter lamp and a higher build temperature requiring less energy from the sinter lamp for the build to succeed.

Table 6.7 Build parameters where build bed and overhead temperature was varied. The builds highlighted are those used for comparison of build bed temperature.

Build Name	Powder	Grey Level	Sinter Speed (mm/s)	Preheat Power (%)	Build Bed and Overhead (°C)	Complete?
<b>B1G2S5P2</b>	XX00199PP	2	100	50	130	Failed due to curl
<b>B1G2S7P2a</b>	XX00199PP	2	80	50	130	Failed due to curl
<b>B1G2S7P2b</b>	XX00199PP	2	80	50	130	Failed due to curl
<b>B1G2S8P2</b>	XX00199PP	2	70	50	130	Complete
<b>B1G2S9P2a</b>	XX00199PP	2	60	50	130	Failed due to build bed sintered
<b>B1G2S9P2b</b>	XX00199PP	2	60	50	130	Failed due to build bed sintered
<b>B2G2S1P2</b>	XX00199PP	2	140	50	135	Complete but 1 test piece failed
<b>B2G2S2P2</b>	XX00199PP	2	130	50	135	Complete
<b>B2G2S3P2</b>	XX00199PP	2	120	50	135	Complete
<b>B2G2S4P2</b>	XX00199PP	2	110	50	135	Complete
<b>B2G2S5P2</b>	XX00199PP	2	100	50	135	Complete
<b>B2G2S6P2</b>	XX00199PP	2	90	50	135	Complete but 1 test piece failed
<b>B2G2S7P2</b>	XX00199PP	2	80	50	135	Complete
<b>B3G2S1P2</b>	XX00199PP	2	140	50	140	Complete
<b>B3G2S5P2</b>	XX00199PP	2	100	50	140	Failed due to powder removal

### 6.5.2 Grey level

Varying the amount of ink deposited was attempted as shown in Table 6.8, however it was not possible to manufacture parts with a grey level of 1 or 5, therefore only grey levels of 2 and 3 are compared. A deterioration of properties was observed from a grey level of 2 to 3 (see Section 6.6) and failure at a grey level 5 led to a grey level of 4 not being examined.

Table 6.8 Build parameters where grey level was varied.

Build Name	Powder	Grey Level	Sinter Speed (mm/s)	Preheat Power (%)	Build Bed and Overhead (°C)	Complete?
<b>B2G1S4P2</b>	XX00199PP	1	110	50	135	Failed due to curl
<b>B2G2S4P2</b>	XX00199PP	2	110	50	135	Complete
<b>B2G3S4P2</b>	XX00199PP	3	110	50	135	Complete
<b>B2G5S4P2</b>	XX00199PP	5	110	50	135	Failed due to curl

Builds attempted using a grey level of 1 or 5 failed due to curl. At a grey level of 1 the parts fail due to curl because the lack of energy absorbed by the ink is enough to cause the parts to sinter but they then cool below the recrystallisation temperature and curl. At the higher grey level it is likely that the

large amount of relatively cold ink printed onto the surface of the sintered piece leads to it cooling below the recrystallisation temperature of the polymer and hence curls.

### 6.5.3 Sinter speed

Table 6.9 demonstrates how sinter speed was varied, where the highlighted rows show the builds with parts used to compare the effect of sinter speed on properties. The build bed temperature was kept the same except for at the slowest sinter speed where it was not possible to keep the build bed temperature constant and hence it was reduced to 130 °C.

*Table 6.9 Build parameters where sinter speed was varied. The builds highlighted are those which parts were used for the comparison of sinter speed.*

Build Name	Powder	Grey Level	Sinter Speed (mm/s)	Preheat Power (%)	Build Bed and Overhead (°C)	Complete?
<b>B2G2S1P2</b>	XX00199PP	2	140	50	135	Complete but 1 test piece failed
<b>B3G2S1P2</b>	XX00199PP	2	140	50	140	Complete
<b>B2G2S2P2</b>	XX00199PP	2	130	50	135	Complete
<b>B2G2S3P2</b>	XX00199PP	2	120	50	135	Complete
<b>B2G2S4P2</b>	XX00199PP	2	110	50	135	Complete
<b>B1G2S5P2</b>	XX00199PP	2	100	50	130	Failed due to curl
<b>B2G2S5P2</b>	XX00199PP	2	100	50	135	Complete
<b>B3G2S5P2</b>	XX00199PP	2	100	50	140	Failed due to powder removal
<b>B2G2S6P2</b>	XX00199PP	2	90	50	135	Complete but 1 test piece failed
<b>B1G2S7P2a</b>	XX00199PP	2	80	50	130	Failed due to curl
<b>B1G2S7P2b</b>	XX00199PP	2	80	50	130	Failed due to curl
<b>B2G2S7P2</b>	XX00199PP	2	80	50	135	Complete
<b>B1G2S8P2</b>	XX00199PP	2	70	50	130	Complete
<b>B2G2S8P2</b>	XX00199PP	2	70	50	135	Failed due to build bed sintered

### 6.5.4 Preheat power

Preheat power, the lamp percentage power during the preheat stroke, was also examined. When the preheat power was varied the other parameters were required also to be changed to allow the production of testable parts at different preheat powers. The alteration of the other parameters being required it was not possible to effectively assess the preheat power and hence it was kept constant at 50 %.

### 6.5.5 Summary of the effect of processing parameter variation

It is apparent that the level of each parameter has an effect on the other parameters which can be used to successfully manufacture parts. This is clearly demonstrated by **B1G2S5P2**, **B2G2S5P2** and **B3G2S5P2** where; at the **B1** level the build failed due to curl, at the **B2** level the build was complete

and at the **B3** level the build failed as the powder from the parts could not be removed. However, at other sinter speeds the parts were manufactured successfully at the **B1** and **B3** level (**B3G2S5P2** and **B3G2S1P2**). A summary of all builds is shown in Table 6.10.

*Table 6.10 Summary table of builds attempted, with build parameters with build name. **B** indicates the build bed temperature, **G** the grey level, **S** sinter speed where lower **S** value indicates a higher speed and therefore less energy input and **P** the preheat power. Small letters indicate repeat at same parameter set and capitals are used where bed and overhead temperature are non-standard.*

Build Name	Grey Level	Sinter Speed (mm/s)	Preheat Power (%)	Build Bed and Overhead (°C)
<b>B1G2S5P2</b>	2	100	50	130
<b>B1G2S7P2a</b>	2	80	50	130
<b>B1G2S7P2b</b>	2	80	50	130
<b>B1G2S8P2</b>	2	70	50	130
<b>B1G2S9P2a</b>	2	60	50	130
<b>B1G2S9P2b</b>	2	60	50	130
<b>B2G1S4P2</b>	1	110	50	135
<b>B2G2S1P2</b>	2	140	50	135
<b>B2G2S2P2</b>	2	130	50	135
<b>B2G2S3P2</b>	2	120	50	135
<b>B2G2S4P2</b>	2	110	50	135
<b>B2G2S5P2</b>	2	100	50	135
<b>B2G2S6P2</b>	2	90	50	135
<b>B2G2S7P2</b>	2	80	50	135
<b>B2G2S8P2</b>	2	70	50	135
<b>B2G3S4P2</b>	3	110	50	135
<b>B2G5S4P2</b>	5	110	50	135
<b>B3G2S1P2</b>	2	140	50	140
<b>B3G2S5P2</b>	2	100	50	140

## 6.6 Part characterisation

### 6.6.1 Part size

Part size was used to calculate wall growth and shrinkage as described in Section 4.5.1. The effect of parameter variation on shrinkage and wall growth of parts manufactured using XX00199PP as feedstock for HSS was studied. Figure 6.6 shows how shrinkage and wall growth are affected as the bed temperature is varied.

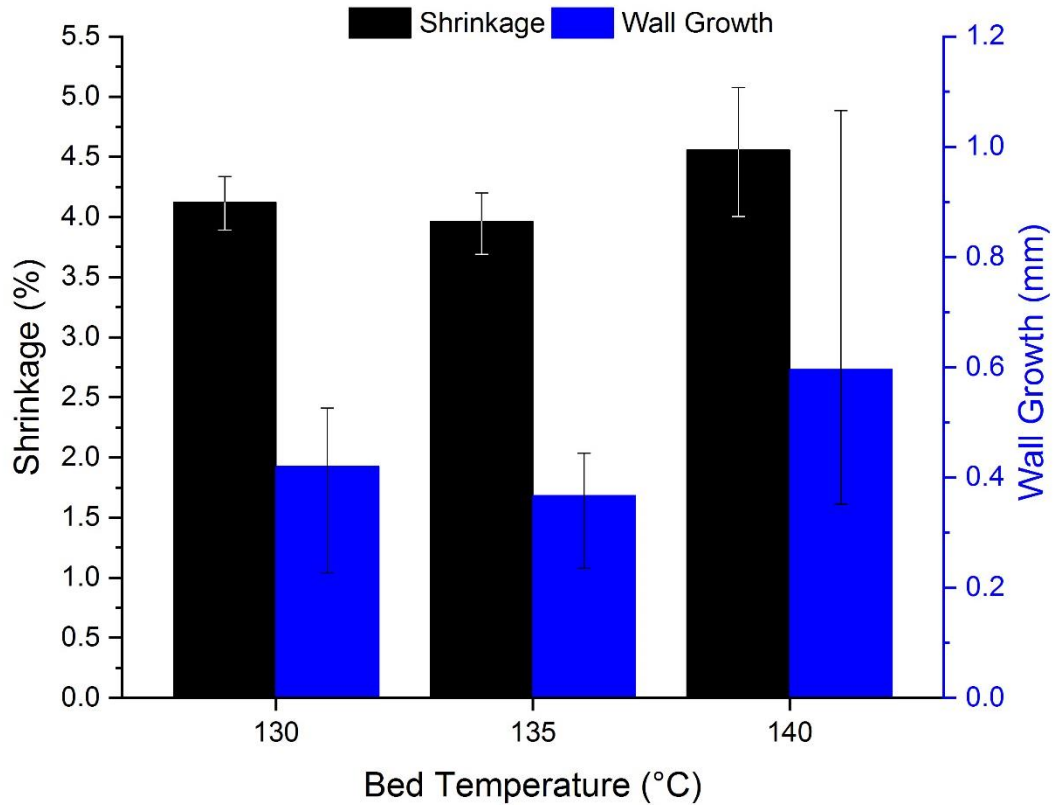


*Figure 6.6 The effect of bed temperature on shrinkage and wall growth on XX00199PP parts. The error bars included are range bars.*

From Figure 6.6 there appears to be an increase in wall growth and shrinkage at the highest level of build bed temperature. However, it should be noted that the builds used for this comparison also required the sinter speed to be decreased at low build bed temperature and increased at high build bed temperature to allow builds at different build bed temperatures to be completed. Therefore, it may be possible that the difference in sinter speed has affected the possible trend in build bed temperature.

The effect of grey level on shrinkage and wall growth was studied in Figure 6.7, at grey level 2 and 3.

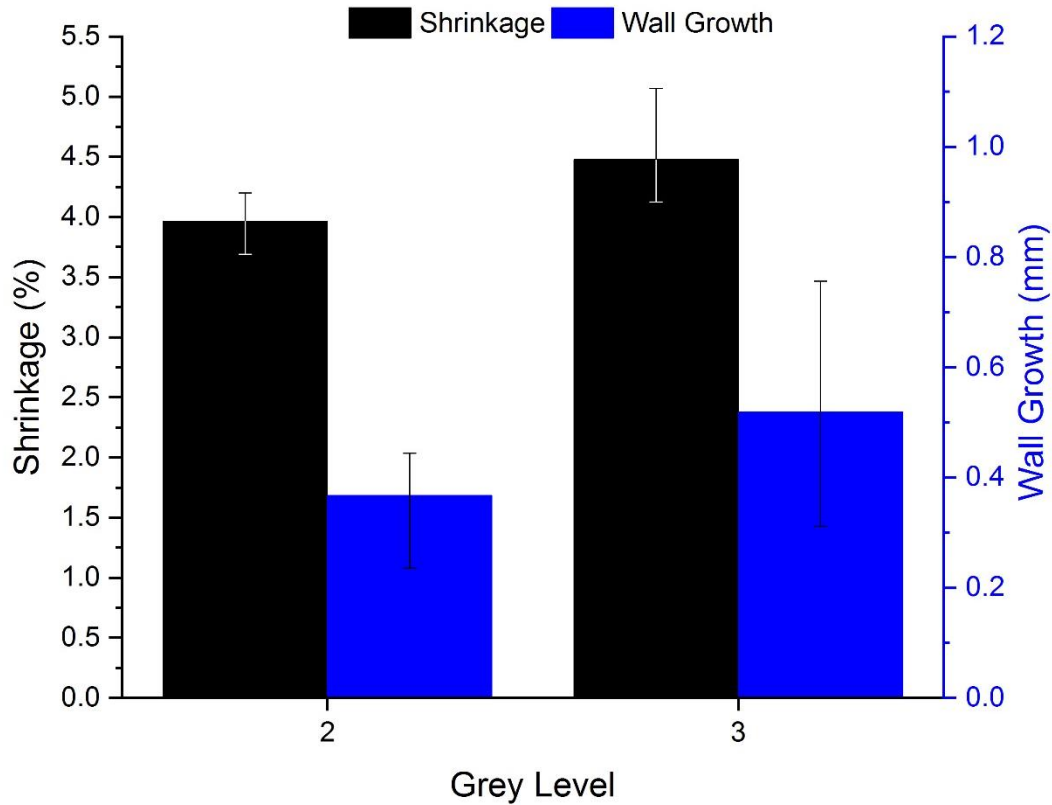


Figure 6.7 The effect of grey level on shrinkage and wall growth on XX00199PP parts. The error bars included are range bars.

Figure 6.7 shows an apparent increase in shrinkage and wall growth as greyscale is increased, although the lack of repeatability of the results means makes it difficult to state this with a high level of confidence. This effect is likely to be due to the part sintering more as the local temperature is increased for the IR ink, therefore decreasing the part volume and hence increasing shrinkage.

The effect of varying the sinter speed on the shrinkage and wall growth of parts is shown in Figure 6.8. The overall length dimension for the builds at 100 mm/s and 120 mm/s (**B2G2S5P2** and **B2G2S3P2**) were inadvertently tensile tested before the overall length was recorded hence the shrinkage and wall growth of the parts could not be calculated.

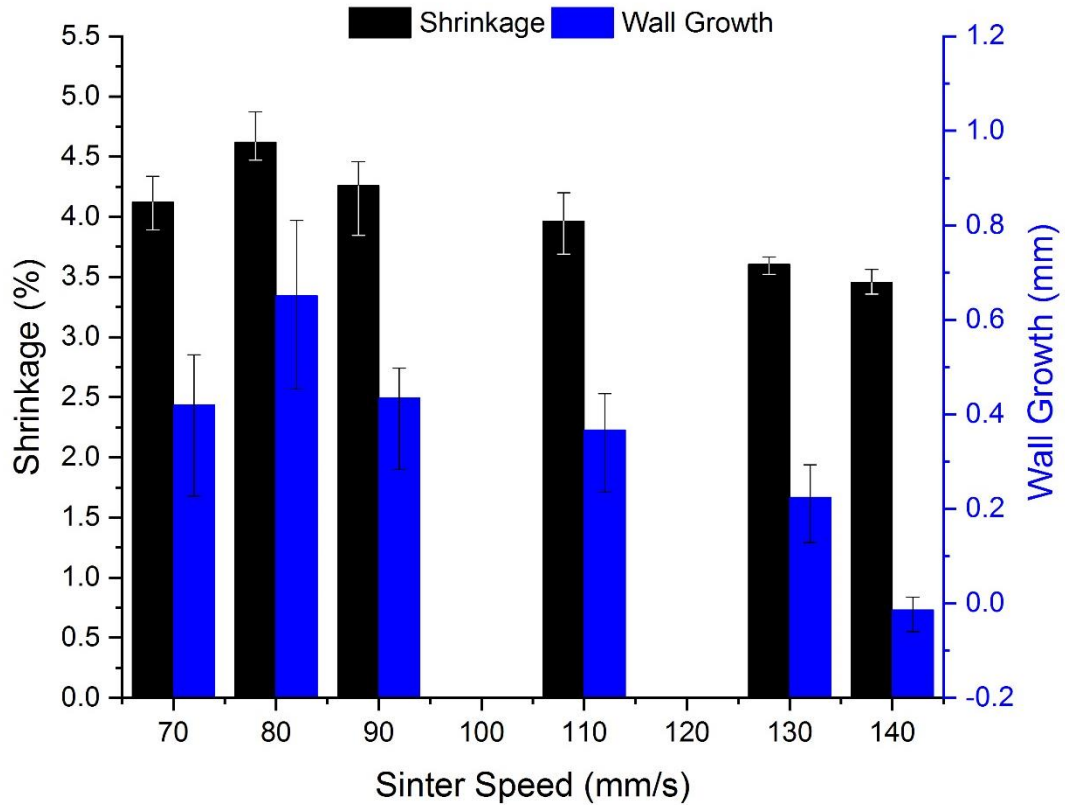


Figure 6.8 The effect of sinter speed on shrinkage and wall growth on XX00199PP parts. The error bars included are range bars.

Figure 6.8 demonstrates a decrease in shrinkage and wall growth as the sinter speed is increased (energy input from the sinter lamp is decreased). This trend is contradicted by the build at 70 mm/s, where lower shrinkage and wall growth were observed. This is most likely due to the lower build bed and overhead temperatures required to process XX00199PP in HSS at this sinter speed.

### 6.6.2 Part density

The same method to calculate part density as described in Section 4.5.2 was employed. Figures 6.9 – 6.11 demonstrate how density is affected by build bed temperature, grey level and sinter speed.

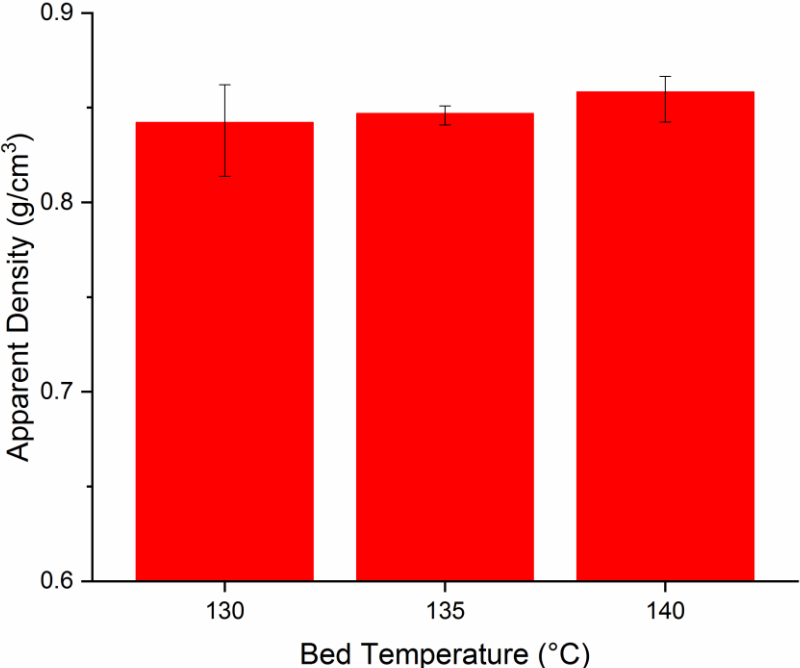


Figure 6.9 The effect of build bed temperature on part density of XX00199PP parts. The error bars included are range bars.

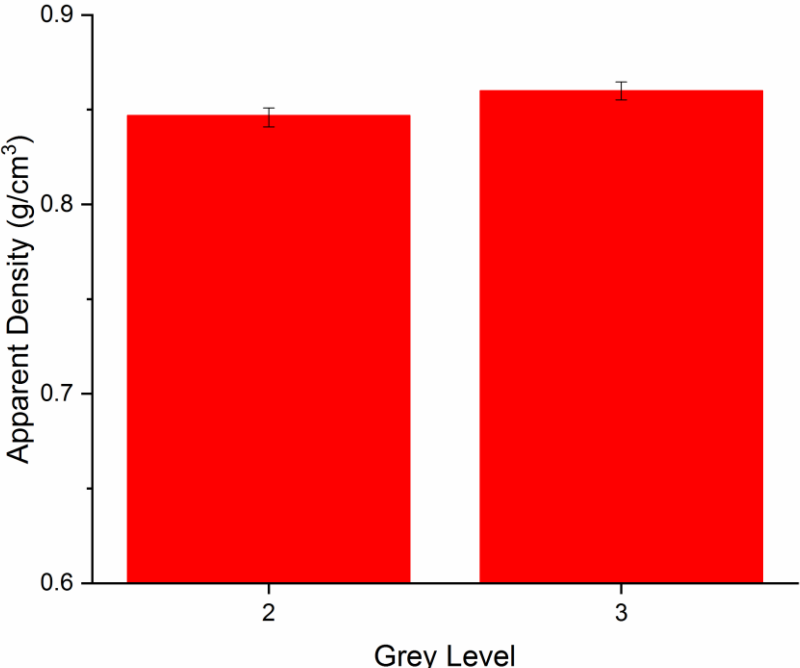


Figure 6.10 The effect of grey level on part density of XX00199PP parts. The error bars included are range bars.

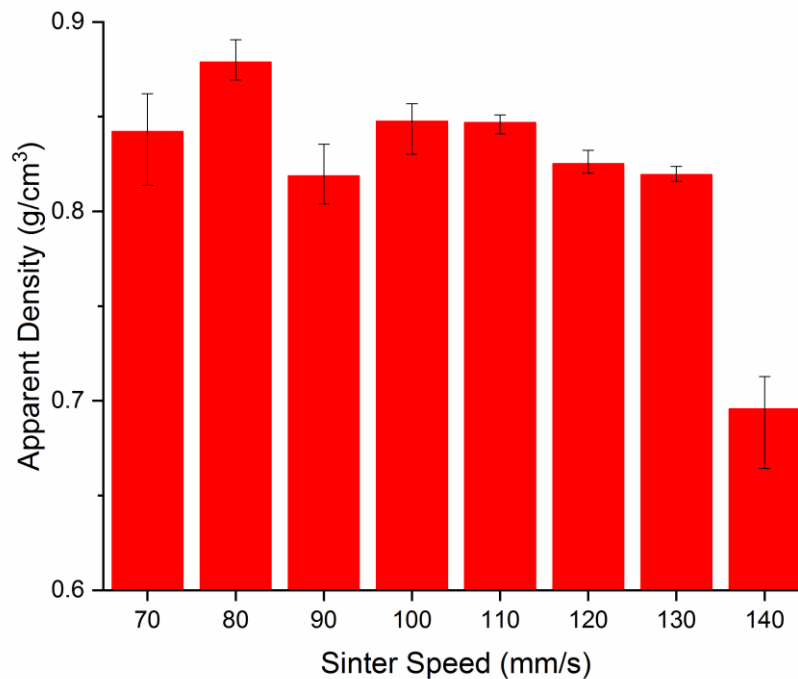


Figure 6.11 The effect of sinter speed on part density of XX00199PP parts. The error bars included are range bars.

From Figures 6.9 – 6.11 a small increase in density was perceived, but not large enough to have any practical effect. The part density of the build at 140 mm/s is significantly lower suggesting a more porous part which may show weaker tensile properties, see 6.6.3. As the polymer used is the same therefore the method of reducing the density is inclusion of pores. However, due to the use of Vernier callipers to calculate volume error could be generated using these. This general trend is supported by literature (62) as discussed in 5.5.2. Although not carried out in this research methods to characterise the porosity of the parts are possible. Archimedes, pycnometry, SEM and Micro-CT are methods to calculate porosity of parts.

### 6.6.3 Tensile properties

The tensile test pieces manufactured were ASTM D638-14 Type I specimens and were tested in accordance with the ASTM (115), as described in Section 4.5.3. The effect of build bed and overhead temperature is shown in Figure 6.12.

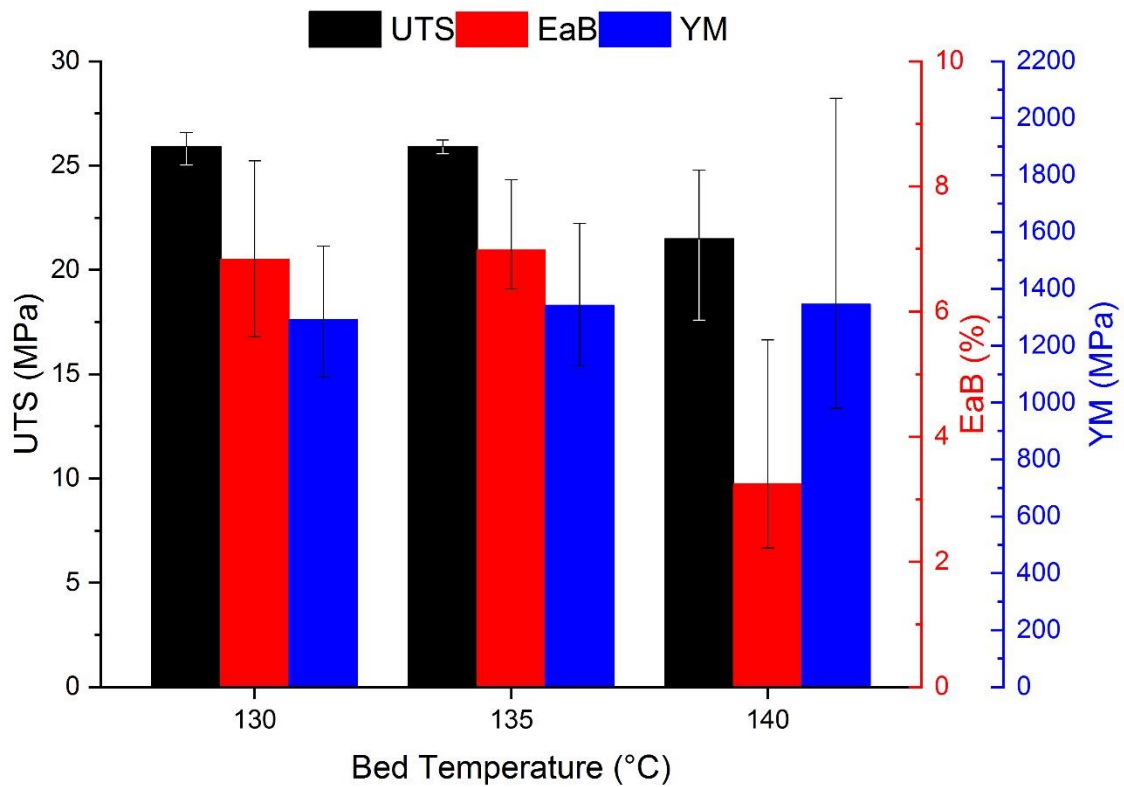


Figure 6.12 The effect of build bed temperature on the mechanical properties of HSS parts using XX00199PP as the powder feedstock. The error bars included are range bars.

As seen in Figure 6.12 there is no discernible difference in the mechanical properties of parts manufactured at a bed temperature of 130 °C and 135 °C. However, at 140°C the parts exhibited different mechanical properties, which will be discussed in Section 6.7.

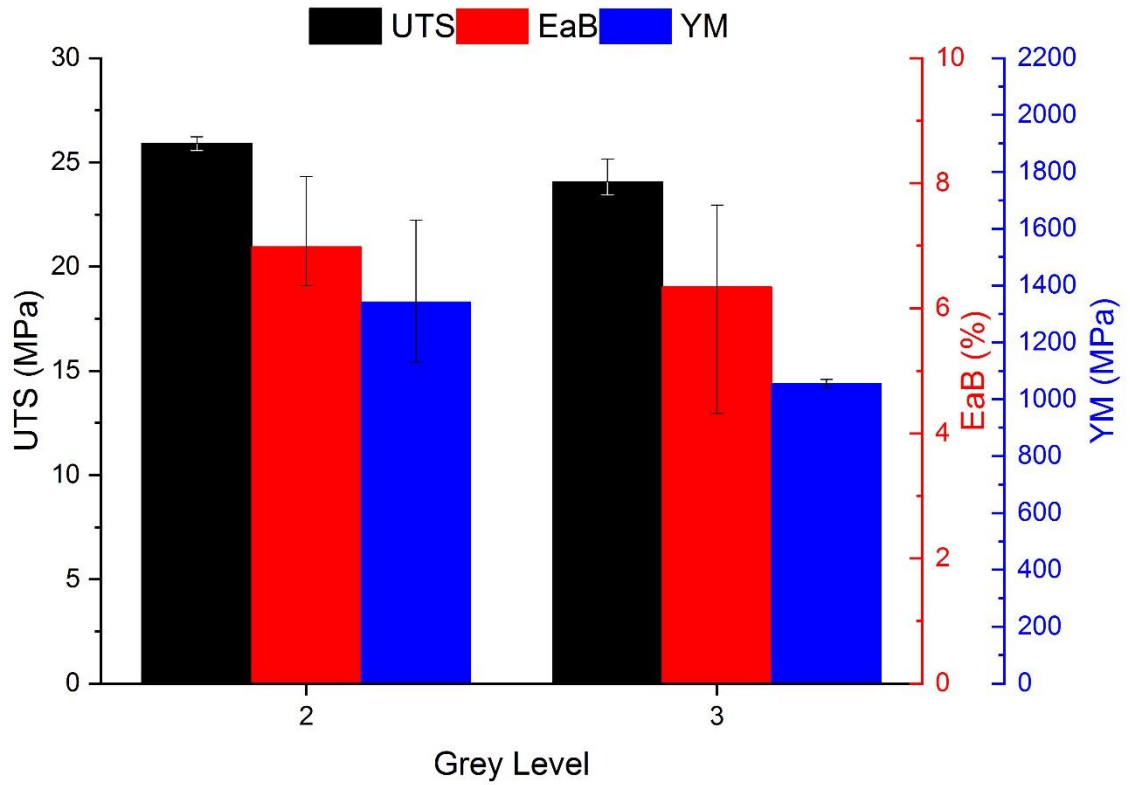


Figure 6.13 The effect of grey level on the mechanical properties of XX00199PP parts manufactured via HSS. The error bars included are range bars.

Figure 6.13 shows an apparent decrease in all the measured mechanical properties as the grey level was increased from 2 to 3, which will be examined further in Section 6.7.

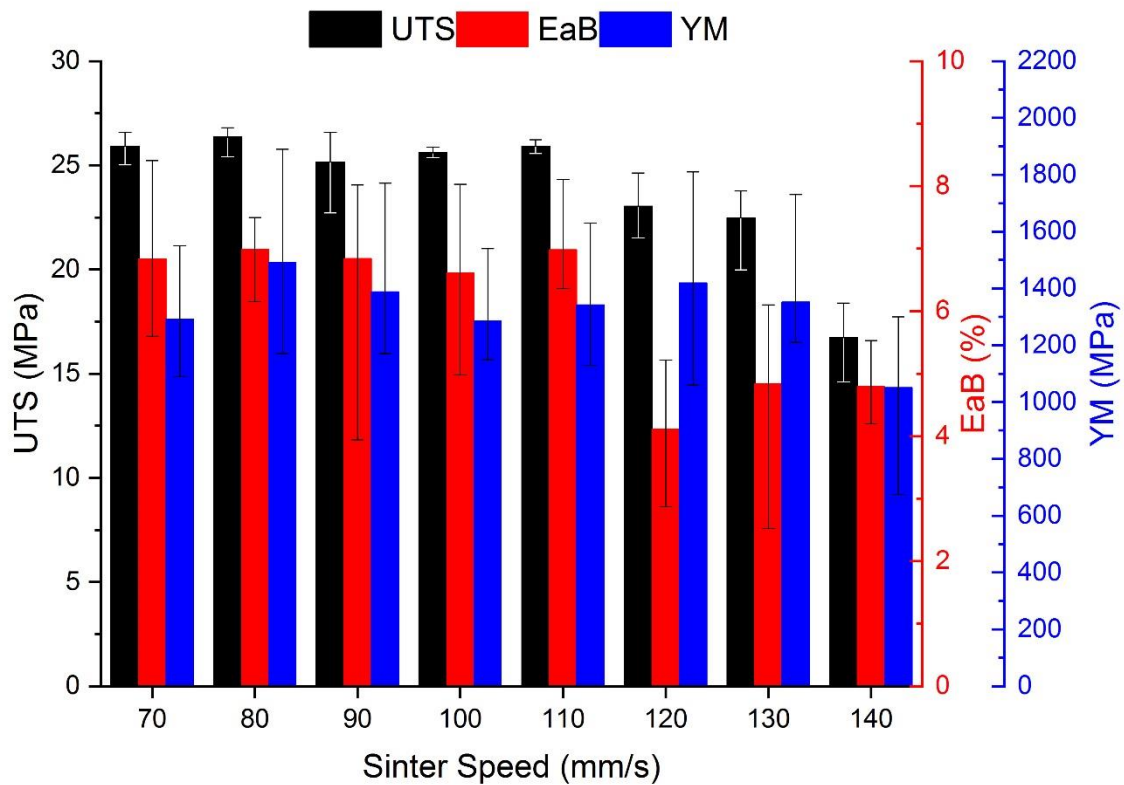


Figure 6.14 The effect of sinter speed on the mechanical properties of parts manufactured using XX00199PP via HSS. The error bars included are range bars.

As shown in Figure 6.14, UTS remains relatively constant until the sinter speed increases past 110mm/s, at which point the UTS begins to decrease. EaB again shows relatively consistent performance over a range of increasing sinter speed, before exhibiting a sharp drop from 120 mm/s upwards. No discernible trend was observed for YM as sinter speed was varied, when error the error as shown in the graphs is considered.

### 6.7 Further discussion

As previously, the large amount of variability in the results obtained meant it was difficult in some cases to identify which trends were significant. ANOVA was used to determine statistical differences between the data as described in Section 4.6, and the results are shown in Table 6.11.

Chapter 6 - Processability of alternative polypropylene grade XX00199PP (pre-commercial)

Table 6.11 One way analysis of variance the effect of various parameters on tensile properties and shrinkage and wall growth. The result of the ANOVA is shown with tests which should significance highlighted in green and then followed by post-hoc tests to demonstrate which data sets were significantly different from each other. The numbers in the table signify the two levels of parameters examined, e.g. in build bed temperature shrinkage 135 130 is the comparison between the data for the build bed temperature at 130 °C compared to the data for build bed temperature at 135 °C.

One way ANOVA Set Tested	Is it significant at 0.05 level?	Post Hoc test - Scheffe tests														
<b>Dimensional accuracy</b>																
Build Bed Temperature Shrinkage	Yes	135 130	140 130	140 135												
Build Bed Temperature Wall Growth	Yes	135 130	140 130	140 135												
Grey Level Shrinkage	Yes	3 2														
Grey Level Wall Growth	No	3 2														
Sinter Speed Shrinkage	Yes	80 70	90 70	90 80	110 70	110 80	110 90	130 70	130 80	130 90	130 110	140 70	140 80	140 90	140 110	140 130
Sinter Speed Wall Growth	Yes	80 70	90 70	90 80	110 70	110 80	110 90	130 70	130 80	130 90	130 110	140 70	140 80	140 90	140 110	140 130
<b>Mechanical properties</b>																
Build Bed Temperature UTS	Yes	135 130	140 130	140 135												
Build Bed Temperature EaB	Yes	135 130	140 130	140 135												
Build Bed Temperature YM	No	135 130	140 130	140 135												
Grey Level UTS	Yes	3 2														
Grey Level EaB	No	3 2														
Grey Level YM	Yes	3 2														
Sinter Speed UTS	Yes	80 70	90 70	90 80	100 70	100 80	100 90	110 70	110 80	110 90	110 100	120 70	120 80	120 90	120 100	120 110
		130 70	130 80	130 90	130 100	130 110	130 120	140 70	140 80	140 90	140 100	140 110	140 120	140 130		
Sinter Speed EaB	Yes	80 70	90 70	90 80	100 70	100 80	100 90	110 70	110 80	110 90	110 100	120 70	120 80	120 90	120 100	120 110
		130 70	130 80	130 90	130 100	130 110	130 120	140 70	140 80	140 90	140 100	140 110	140 120	140 130		
Sinter Speed YM	No	80 70	90 70	90 80	100 70	100 80	100 90	110 70	110 80	110 90	110 100	120 70	120 80	120 90	120 100	120 110
		130 70	130 80	130 90	130 100	130 110	130 120	140 70	140 80	140 90	140 100	140 110	140 120	140 130		
<b>Legend</b>		Significant		Not Significant												

The results show a significant effect of all parameters on dimensional accuracy, with the exception of the effect of changes in grey level on wall growth. In general the dimensional accuracy of parts was shown to decrease as the energy input into the system increases.

No trend was observed for any of the parameters examined for YM except grey level; this is likely due to the large error of YM in AM parts. Grey level was only tested at two levels in this work due to the difficulty of manufacturing parts at other quantities of IR absorbing ink.

From the statistical test data it is apparent sinter speed has a significant effect on the UTS of parts manufactured, but no effect on EaB and YM. When sinter speed was increased and hence less energy was input via the sinter lamp, the UTS decreased. This is due to powder particles in the part not sintering together as fully and hence requiring less tensile force to break the specimens. This is also supported by the part density measurements which show a decrease in density with an increase in sinter speed, indicating a potential increase in porosity of the parts. The variability in the results for the UTS measurements is also much smaller which means a trend is clear compared to the large variability in EaB and YM which may mask possible trends.

For parts to be built at different build bed temperatures it was necessary to change the sinter speeds for parts to be manufactured. At lower build bed temperatures it was necessary to put more sinter lamp energy into the system to stop builds from curling. At high build bed temperatures it was necessary to remove energy input from the sinter lamp by increasing the sinter speed to stop builds failing due to inability of powder removal or the whole bed sintering without the addition of the IR ink. Therefore when comparing the build bed temperatures there will be an effect from the sinter lamp on the properties occurring simultaneously.

The mechanical properties where the build bed temperature was varied are significantly different when the 135 °C level is compared to the 140 °C level. For manufacture to be possible at the 140 °C level a sinter speed of 140 mm/s was used, when a sinter speed of 140 mm/s was used at the 135 °C build bed temperature parts had significantly lower mechanical properties than those at a speed of 130 mm/s. Therefore it is not possible to judge the effect of build bed temperature accurately when XX00199PP is used as a powder feedstock for HSS.

## 6.8 Conclusions

Sinter speed and grey level have been shown again to have a key role in the mechanical properties and dimensional accuracy of parts produced. Build bed temperature is difficult to vary without also changing the other parameters used to manufacture parts and hence has been shown again to be critical in the processing of PP in HSS.

XX00199PP was processable at different build bed temperatures, sinter speeds and grey levels. This range of processing parameters is wider than those for CP22 PP although this will be compared in detail in Chapter 8. The mechanical properties of XX0199PP are also higher than CP22PP, although arguably still not sufficient for the use in FMCGs.

The following Chapter will present the results of the third Polypropylene grade tested in the HSS system.



## Chapter 7 Processability of alternative polypropylene grade AdSint (commercial)

### 7.1 Introduction

In order to provide a further comparison with the materials tested previously, a final polypropylene grade was investigated here.

### 7.2 Characterisation of raw materials

A grade of PP designed for the Laser Sintering process, AdSint PP, was sourced from Advanc3D Materials GmbH. The AdSint PP powder was characterised using the same methods described in Section 4.1.

#### 7.2.1 Powder flow

The tapped bulk density was measured using the same method as described in Section 4.1.1. Table 7.1 shows the tapped density of AdSint PP powder.

*Table 7.1 Tapped bulk density of AdSint PP for each run and average.*

Run	Density of AdSint PP ( $\text{gcm}^{-3}$ )
1	0.438
2	0.443
3	0.439
<b>Average</b>	<b>0.44 (0.003)</b>

Powder flow measurement was again attempted using the method described in Section 4.1.1. However, as with the XX00199PP material, when the powder was loaded into the cone and the removable stop was removed the powder did not flow. It was therefore not possible for this test to be performed. Although the powder did not flow through the orifice in the cone on the testing apparatus, the powder again flowed sufficiently to form an even powder layer during deposition on the HSS equipment. The difference in the powder flows of the PP powders tested will be discussed in Chapter 8.

#### 7.2.2 Particle size and morphology

Particle size was measured by laser diffraction using a mastersizer as described in 4.1.2. The mastersizer trace for AdSint PP is shown in Figure 7.1. The averages of the three samples measured are reported in Table 4.2; D(10) represents the maximum diameter of the smallest 10 % of particles,

D(50) is the mean particle diameter and D(90) is the maximum diameter of the smallest 90 % of particles.

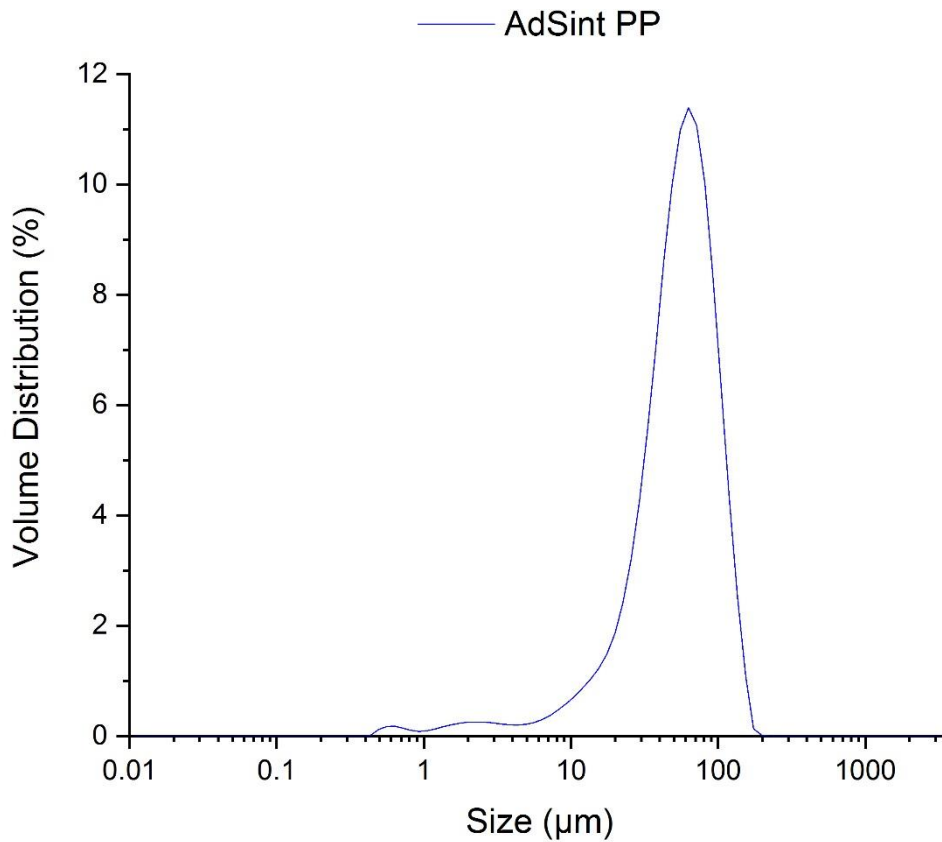


Figure 7.1 Mastersizer trace of AdSint PP.

Table 7.2 Particle size breakdown of AdSint PP.

Material	D(10) (µm)	D(50) (µm)	D(90) (µm)
AdSint PP	21.8	58.0	105.3

From the volume distribution against size trace (Figure 7.1) and the summary table (Table 4.2), it is observed there is a large component of small particles which would provide an explanation for the poor powder flow observed during flow testing, but may also lead to better packing as small particles could fill gaps between larger particles.

As previously, a Malvern Morphogi G3 was used to record additional information regarding particle shape, as described in Section 4.1.2. The size and shape traces are shown in Figure 7.2.

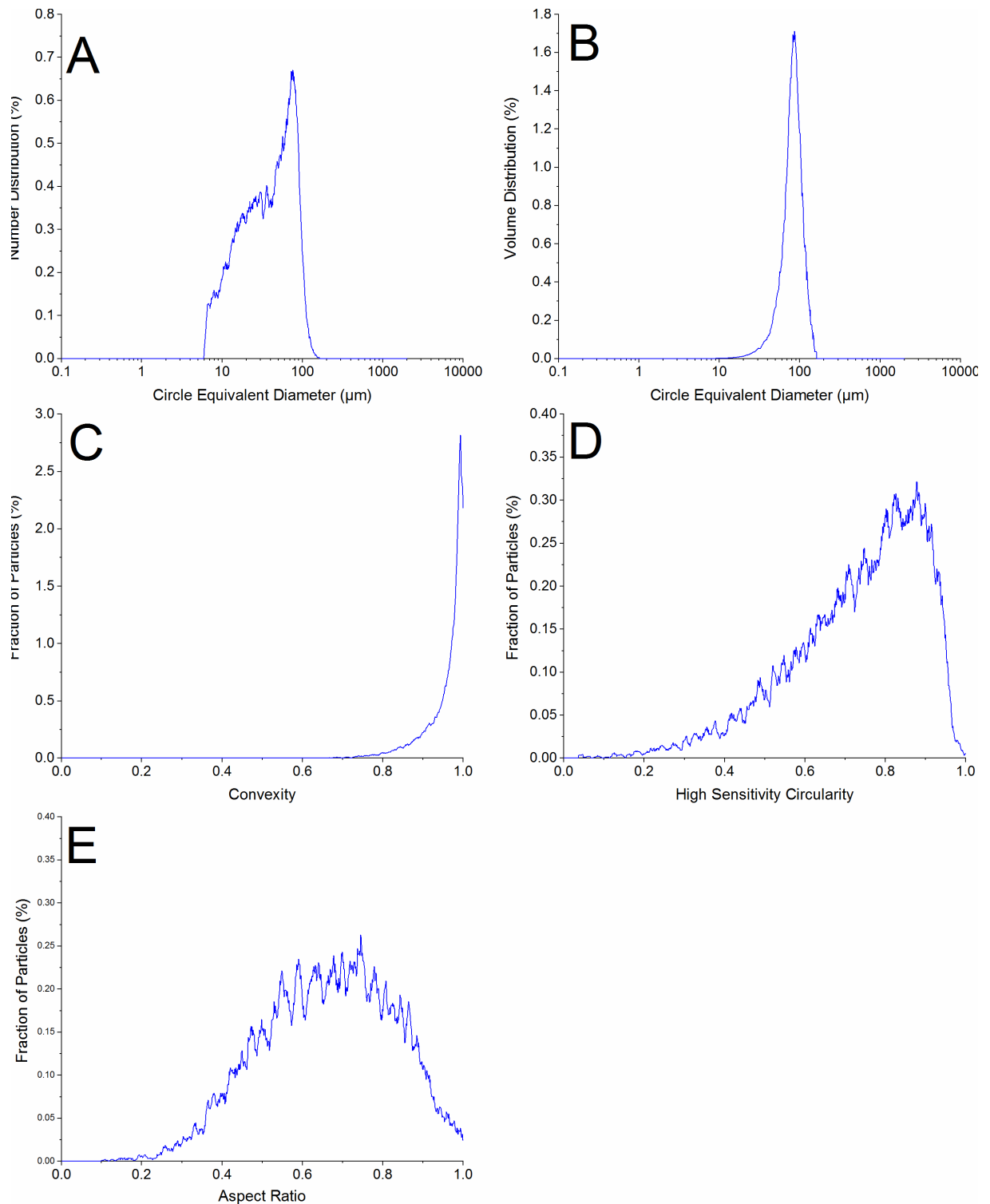


Figure 7.2 Image analysis traces showing size and shape of the CP22 PP powder. (A) Circle equivalent diameter against the number distribution of powder particles. (B) Circle equivalent diameter against the volume distribution of powder particles. (C) Convexity against fraction of powder particles. (D) High sensitivity circularity against fraction of powder particles. (E) Aspect ratio against fraction of powder particles.

Figure 7.2 (A) the number distribution of particle size shows there are a large amount of small particles; this will be further compared to the other powders characterised in Chapter 8. The AR (E)

also shows there are a wide range of powder aspect ratios and the particles are 'squashed' in their appearance.

Scanning Electron Microscopy (SEM) was also used to characterise the AdSint PP powder, the same method as described in Section 4.1.2 was used. Figure 7.3 shows AdSint PP particles at a low and high magnification.

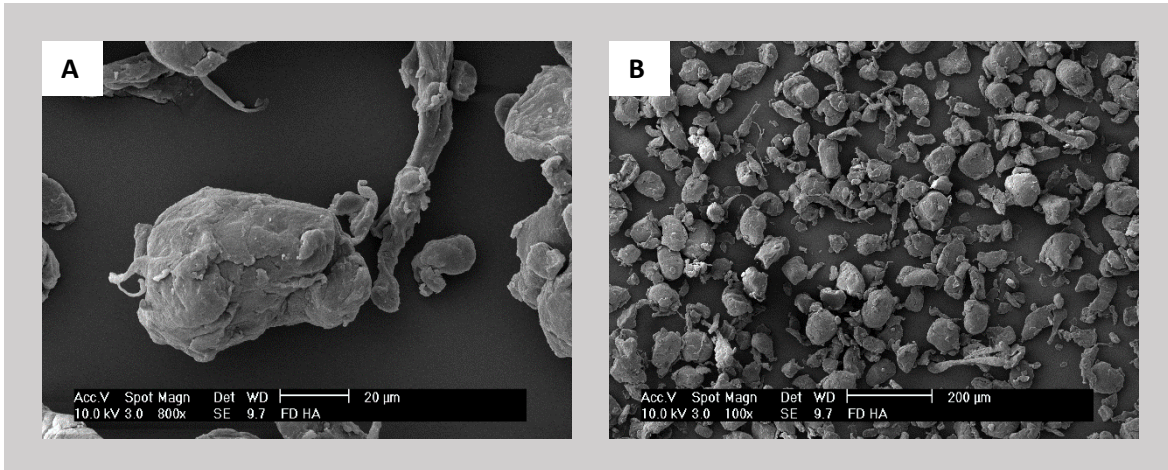


Figure 7.3 SEM images of AdSint PP (A&B), using high and low magnification respectively.

From the microscopy images (Figure 7.3) it is difficult to gain an object sense of shape as the number of particles sampled is small. This is the primary reason for using the image analysis Morpholgi G3 as a much larger sample size is used.

### 7.2.3 Thermal properties

Thermal properties of AdSint PP were also measured using Differential Scanning Calorimetry (DSC) and Thermogravimetric Analysis (TGA), to allow comparison to the other powders studied as well as identify initial HSS parameters.

DSC was used to measure the melt and recrystallisation temperatures of the AdSint PP powder. The method used is described in Section 4.1.3, where the powder was heated and cooled at a rate of 10 °C/min. Pyris software was then used to identify the peak temperatures for melting and recrystallisation as shown in Figure 7.4.

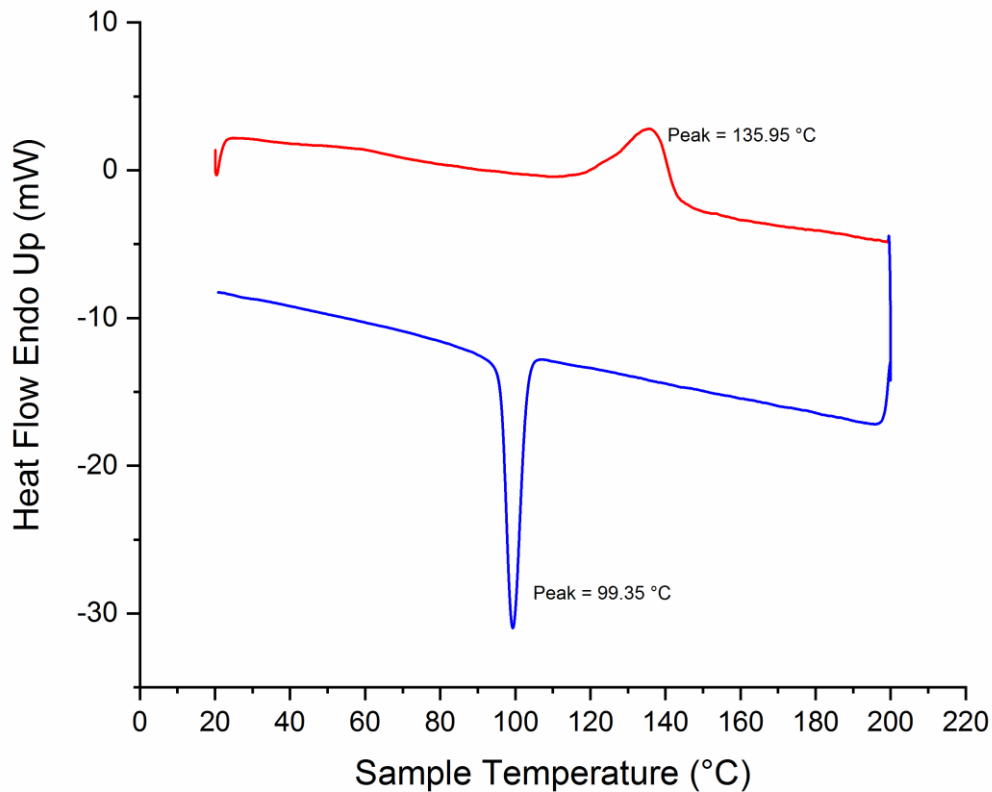


Figure 7.4 DSC curve of AdSint PP; temperature scan at 10 °C/min.

The peak melt temperature was shown to be 136 °C and the peak recrystallisation temperature at 99 °C; this information will be used to set the build parameters. The melt temperature of iso-tactic PP is 164 °C (76), however as demonstrated by the DSC trace the melting temperature of AdSint PP is lower. This suggests AdSint may be a copolymer with ethylene inclusion into the polymerisation. The addition of ethylene to propylene during polymerisation to manufacture a copolymer is often used in the plastics industry, where the addition of ethylene units reduce the strength of the polymer but increase the malleability of the polymer and is often used where high impact resistance is required (76, 94). PP copolymer is often identified by having a lower crystallinity and melt temperature as demonstrated by AdSint PP compared to the other grades tested. The low melt temperature of AdSint PP limits its use in some applications where elevated temperatures are required; however, this is not the case for FMCGs so the use of AdSint PP remains viable.

A copolymer in comparison to a homopolymer can have different material properties. These include; mechanical properties where the copolymer has higher elongation but a lower strength. A copolymer also has a lower melt temperature than the homopolymer, therefore the processing temperature in HSS being lower. Branching of the polymer is likely to have a large effect on the crystallinity of the

polymer powder feedstock. However, the differing side chains in a co-polymer are likely to lead to the packing being not as ordered and therefore reducing the crystallinity. These smaller side chains are also likely to reduce the melt viscosity of the polymer as the chains will be able to move past each other with less entanglement. Although, molecular weight will have a larger effect and be the determining factor. These differences are therefore expected to change the processing in HSS (see Section 7.4) as well as the mechanical properties (see Section 7.6).

TGA was used to analyse the decomposition temperature of the PP as well as the residual inorganics remaining after the polymer was burned off. The same method was used as described in Section 5.3.3, an example curve is shown in Figure 7.5. The data obtained from the TGA is presented in Table 7.3 and averaged.

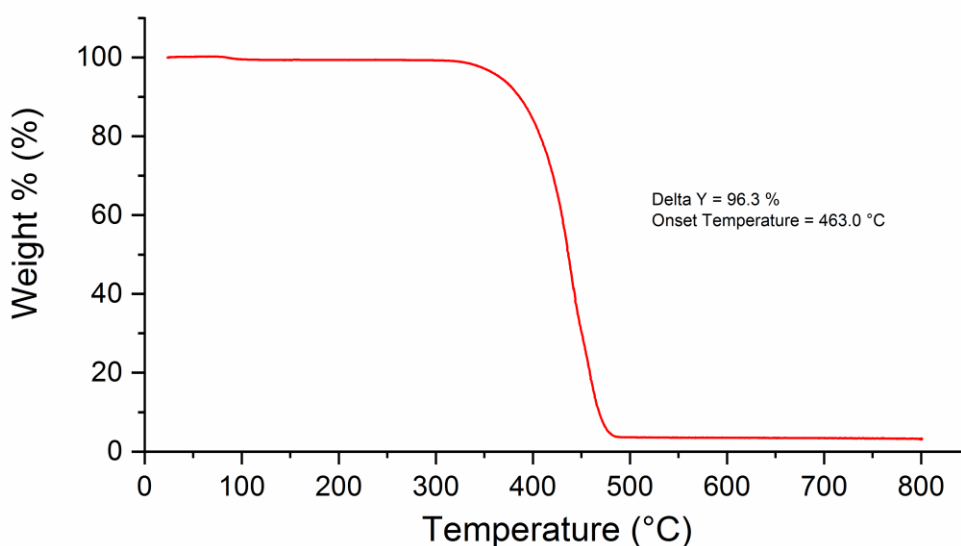


Figure 7.5 Thermogravimetric Analysis trace of AdSint PP powder.

Table 7.3 TGA results for AdSint PP, including; decomposition onset temperature and residual mass percentage.

Sample name	Onset temperature (°C)	Residual mass (%)
AdSint PP 1	463.02	3.7069
AdSint PP 2	478.35	3.3722
AdSint PP 3	444.73	2.1084
<b>Average</b>	<b>462.03 (16.83)</b>	<b>3.06 (0.84)</b>

### 7.3 Part manufacture via High Speed Sintering

AdSint PP was used to manufacture parts via HSS, using the strategy described in Sections 4.2 and 6.3.

Figure 7.6 shows parts from a successful build using AdSint PP in HSS.

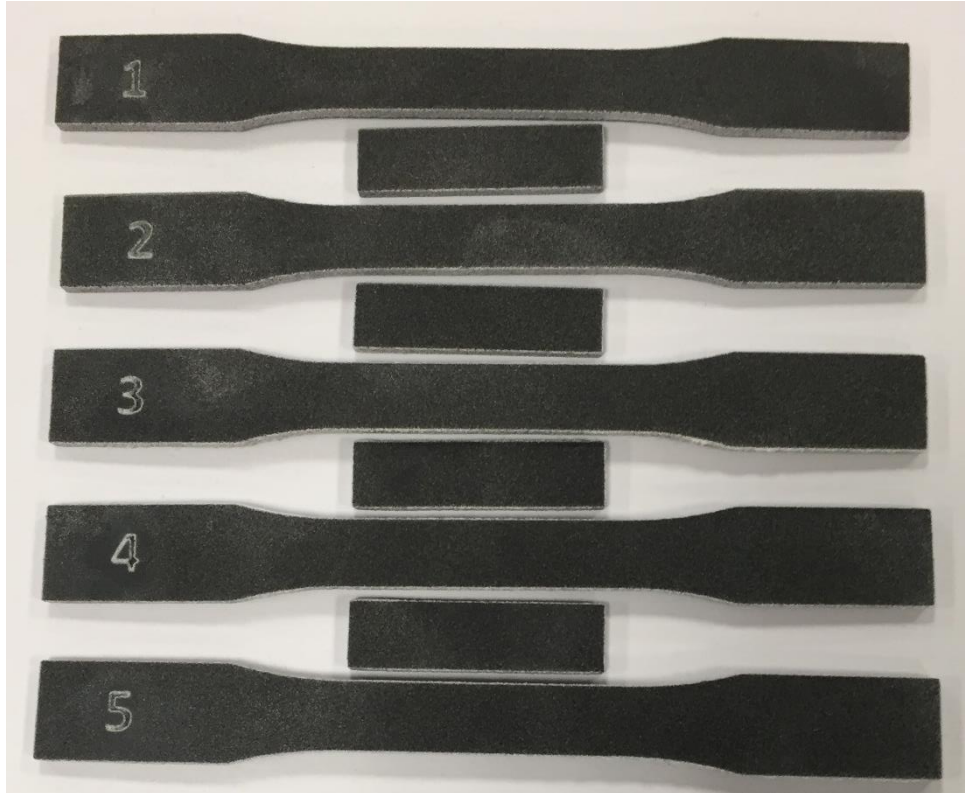


Figure 7.6 Photo of parts using AdSint PP in HSS.

### 7.4 Identification of initial processing parameters

Table 7.4 shows the parameter ranges attempted for the AdSint material.

Table 7.4 High Speed Sintering parameters for the attempted processing of AdSint PP.

Parameter	Range
Preheat Power (%)	0 - 100
Sinter Power (%)	100
Preheat Speed (mm/s)	70
Sinter Speed (mm/s)	60 - 100
Recoater Vibration (%)	100
Feed Hopper Fill Frequency	12
Feed Hopper Fill Duration (s)	1.25
Grey level	1 - 7
Build Bed (°C)	110 - 118
Build Overhead (°C)	110 - 118
Layer Thickness (µm)	100

It was not possible to process AdSint PP at the same parameters as used for the other grades of polypropylene powders tested. This is supported by the difference in the DSC traces of the various PP powders. Due to the previous parameters sets not being appropriate for the use of AdSint PP as a powder feedstock for HSS, it was necessary to identify initial processing parameters for the powder, as outlined below.

#### 7.4.1 Build bed temperature

Previously a difference of roughly 13 °C between the melt peak from DSC (Figure 7.4) and the build bed temperature was used to set the build bed temperature. However, as shown in the DSC trace (Figure 7.4) the melt peak of AdSint PP is broad, therefore a difference of 13 °C would still be above the onset of melt temperature. An initial build bed temperature of 110 °C was therefore set to allow manufacture below the melt onset temperature but above the recrystallisation onset temperature.

#### 7.4.2 Preheat power

Previous work used a preheat power level of 50 %; this level was also selected as the initial level for the work using AdSint PP as a powder feedstock.

#### 7.4.3 Sinter power

The sinter power has remained constant at 100% throughout this research and remained set at this level for the AdSint PP material trials.

#### 7.4.4 Preheat speed

The preheat speed remained at 70 mm/s (see Section 6.4.4). The preheat speed is intrinsically linked to the powder deposition and at this speed a good even powder deposition was obtained. This speed was not altered in this research.

#### 7.4.5 Sinter speed

This parameter was used as a variable to change the amount of input energy into the system during the sinter stroke. The initial build bed temperature used in this research was 110 °C and various sinter speeds were trialled for this build temperature to be usable and this was found to be 70 mm/s. Therefore when build bed temperature was varied to allow a wider range of parameters to be used the sinter speed was then varied around this initial level.

#### 7.4.6 Grey level

As discussed in Section 6.4.6 the initial grey level was set at the same level as the work on XX00199PP at a grey level of 2. This grey level was then varied to assess the effect of ink quantity on the properties of the PP parts manufactured.

## 7.5 Effect of processing parameter variation

Several builds were attempted using AdSint PP as the powder feedstock; the ranges for the parameters used are shown in Table 7.4. The same classification system was used as previously. These categories are shown in Table 7.5, which is a copy of Table 4.5.

*Table 7.5 Build classifications and the explanation of the terms used, where the builds classified by the first two terms were then further tested. Compared to the other build classifications which were described and could not be further tested.*

Classification	Explanation
Complete	All test pieces were manufactured and post processed, then analysed.
Complete but 1 test piece failed	All but one test pieces were manufactured and post processed, the remaining pieces were then analysed. The piece that was not complete failed due to localised curl on the single piece.
Failed due to powder removal	The manufacture of parts was completed but the excess powder around the parts was sintered to the extent it could not be removed by reasonable post processing.
Failed due to build bed sintered	The build bed became fully sintered before the beginning of printing ink (during the 50 pad layers), therefore the build was abandoned at this point.
Failed due to curl	During a point of the manufacture of test pieces they underwent curl and caused the build area to fail.

The same four variables as studied previously (build bed temperature, grey level, sinter speed and preheat power) were altered and their effect was studied on the properties of the parts manufactured. These parameters were altered one at a time around the mid-point parameters. This method was chosen as it was previously used in Chapter 4 and 6, as well as the reasoning laid out in 4.4.1.

The same build notation defined in Section 6.5 was used. The build notation used is **B\_G\_S\_P\_**, where **B** is the build bed and overhead temperature, **G** is the amount of ink used (grey level), **S** is the sinter speed where the lowest number is the fastest sinter speed and hence the least energy input and **P** is the preheat power with the highest number being the highest preheat power. The lower case letters indicate a repeat.

### 7.5.1 Build bed temperature

From the onset of the powder melt measured by DSC the initial build bed temperature was set to 110 °C. However it was not possible to manufacture parts at a sinter speed which would allow the sinter speed to be varied later in this research, although a build was completed at a sinter speed of 70 mm/s whilst using a build bed temperature of 110 °C. Table 7.6 shows the builds attempted where build bed temperature was varied.

The build bed temperature was increased in two degree steps. At a build bed temperature of 118 °C powder removal was not possible, due to this a mid-point of 114 °C was chosen to use as basis for variation of other variables.

*Table 7.6 Build parameters where build bed and overhead temperature was varied. The builds highlighted are those used for comparison of build bed temperature.*

Build Name	Powder	Grey Level	Sinter Speed (mm/s)	Preheat Power (%)	Build Bed and Overhead (°C)	Complete?
<b>B1G2S3P4</b>	AdSint PP	2	80	50	110	Failed due to curl
<b>B1G2S4P4</b>	AdSint PP	2	70	50	110	Complete
<b>B2G2S3P4</b>	AdSint PP	2	80	50	112	Complete
<b>B3G2S3P4a</b>	AdSint PP	2	80	50	114	Complete
<b>B3G2S3P4b</b>	AdSint PP	2	80	50	114	Complete
<b>B3G2S3P4c</b>	AdSint PP	2	80	50	114	Complete
<b>B4G2S3P4</b>	AdSint PP	2	80	50	116	Complete
<b>B5G2S3P4</b>	AdSint PP	2	80	50	118	Failed due to powder removal

**B3G2S3P4a-c** are three repeat builds which are mid-point builds and will be used when the various parameters tested are altered.

### 7.5.2 Grey level

Table 7.7 shows the build parameters when the grey level was varied, whereby all the successful builds were used to analyse the effect of grey level.

*Table 7.7 Build parameters where grey level was varied.*

Build Name	Powder	Grey Level	Sinter Speed (mm/s)	Preheat Power (%)	Build Bed and Overhead (°C)	Complete?
<b>B3G1S3P4</b>	AdSint PP	1	80	50	114	Complete
<b>B3G2S3P4a</b>	AdSint PP	2	80	50	114	Complete
<b>B3G2S3P4b</b>	AdSint PP	2	80	50	114	Complete
<b>B3G2S3P4c</b>	AdSint PP	2	80	50	114	Complete
<b>B3G3S3P4</b>	AdSint PP	3	80	50	114	Complete
<b>B3G4S3P4</b>	AdSint PP	4	80	50	114	Complete
<b>B3G5S3P4</b>	AdSint PP	5	80	50	114	Complete
<b>B3G7S3P4</b>	AdSint PP	7	80	50	114	Failed due to powder removal

The build attempted at a grey level of 7 failed, due to the inability to remove the powder from the parts manufactured. During this build ink bleeding was observed from the location where it was

printed. This is likely to have caused the ink to flow further and cause the excess powder to sinter, joining the gaps between parts and therefore rendering powder removal impossible.

### 7.5.3 Sinter speed

Table 7.8 shows the various builds where the sinter speed was varied. All the builds shown in Table 7.8 were used to compare the effect of sinter speed on part properties except **B3G2S5P4** where parts were manufactured but could not be tested due to powder removal not being possible.

*Table 7.8 Build parameters where sinter speed was varied. The naming notation **S1** is the fastest sinter speed and hence the least input energy from the sinter lamp in accordance with the other naming notations.*

Build Name	Powder	Grey Level	Sinter Speed (mm/s)	Preheat Power (%)	Build Bed and Overhead (°C)	Complete?
<b>B3G2S1P4</b>	AdSint PP	2	100	50	114	Complete
<b>B3G2S2P4</b>	AdSint PP	2	90	50	114	Complete
<b>B3G2S3P4a</b>	AdSint PP	2	80	50	114	Complete
<b>B3G2S3P4b</b>	AdSint PP	2	80	50	114	Complete
<b>B3G2S3P4c</b>	AdSint PP	2	80	50	114	Complete
<b>B3G2S4P4</b>	AdSint PP	2	70	50	114	Complete
<b>B3G2S5P4</b>	AdSint PP	2	60	50	114	Failed due to powder removal

### 7.5.4 Preheat power

As discussed in 7.4.2 the initial preheat power was set to 50 % and this value was then altered. Levels of 30, 40, 60 and 70 % were selected to show the effect of small changes in the preheat power and 0 and 100 % were selected to show the extremes. Table 7.9 shows the builds where preheat power was altered; all the successful builds were used to study the effect of preheat power on part properties. At a preheat power of 100 % the full build bed sintered and hence no parts were produced that could then be tested.

Table 7.9 Build parameters where the preheat power was varied.

Build Name	Powder	Grey Level	Sinter Speed (mm/s)	Preheat Power (%)	Build Bed and Overhead (°C)	Complete?
<b>B3G2S3P1</b>	AdSint PP	2	80	0	114	Complete
<b>B3G2S3P2</b>	AdSint PP	2	80	30	114	Complete
<b>B3G2S3P3</b>	AdSint PP	2	80	40	114	Complete
<b>B3G2S3P4a</b>	AdSint PP	2	80	50	114	Complete
<b>B3G2S3P4b</b>	AdSint PP	2	80	50	114	Complete
<b>B3G2S3P4c</b>	AdSint PP	2	80	50	114	Complete
<b>B3G2S3P5</b>	AdSint PP	2	80	60	114	Complete
<b>B3G2S3P6</b>	AdSint PP	2	80	70	114	Complete
<b>B3G2S3P7</b>	AdSint PP	2	80	100	114	Failed – build bed fully sintered

### 7.5.5 Summary of the effect of processing parameter variation

Build bed and overhead temperature, grey level, sinter speed and preheat power have been varied whilst using AdSint PP as a powder feedstock for HSS. It was not possible to manufacture at all the parameters attempted. It was also observed again that the combination of parameters have an effect on the success of builds, e.g. **B1G2S3P4** with a sinter speed of 80 mm/s and a build bed temperature of 110 °C failed but a decrease in sinter speed to 70 mm/s in **B1G2S4P4** allowed a build to be completed. Table 7.10 is a summary table of the builds attempted using AdSint PP as a powder feedstock for HSS.

Table 7.10 Summary table of builds attempted, with build parameters with build name. **B** indicates the build bed and overhead temperature, **G** indicates the grey level, **S** sinter speed where lower **S** value indicates a higher speed and therefore less energy input and **P** the preheat power. Small letters indicate repeat at same parameter set. Cells highlighted are the centre point repeats used.

Build Name	Grey Level	Sinter Speed (mm/s)	Preheat Power (%)	Build Bed and Overhead (°C)
<b>B1G2S3P4</b>	2	80	50	110
<b>B1G2S4P4</b>	2	70	50	110
<b>B2G2S3P4</b>	2	80	50	112
<b>B3G2S3P4a</b>	2	80	50	114
<b>B3G2S3P4b</b>	2	80	50	114
<b>B3G2S3P4c</b>	2	80	50	114
<b>B4G2S3P4</b>	2	80	50	116
<b>B5G2S3P4</b>	2	80	50	118
<b>B3G1S3P4</b>	1	80	50	114
<b>B3G3S3P4</b>	3	80	50	114
<b>B3G4S3P4</b>	4	80	50	114
<b>B3G5S3P4</b>	5	80	50	114
<b>B3G7S3P4</b>	7	80	50	114
<b>B3G2S1P4</b>	2	100	50	114
<b>B3G2S2P4</b>	2	90	50	114
<b>B3G2S4P4</b>	2	70	50	114
<b>B3G2S5P4</b>	2	60	50	114
<b>B3G2S3P1</b>	2	80	0	114
<b>B3G2S3P2</b>	2	80	30	114
<b>B3G2S3P3</b>	2	80	40	114
<b>B3G2S3P5</b>	2	80	60	114
<b>B3G2S3P6</b>	2	80	70	114
<b>B3G2S3P7</b>	2	80	100	114

## 7.6 Characterisation of parts

### 7.6.1 Part size

Part size was measured to calculate dimensional accuracy including wall growth and shrinkage as described in Section 4.5.1. The effect of varying the build parameters on shrinkage and wall growth of parts manufactured using AdSint PP was examined. The first parameter examined was the bed temperature and its effect on shrinkage and wall growth is shown in Figure 7.7.

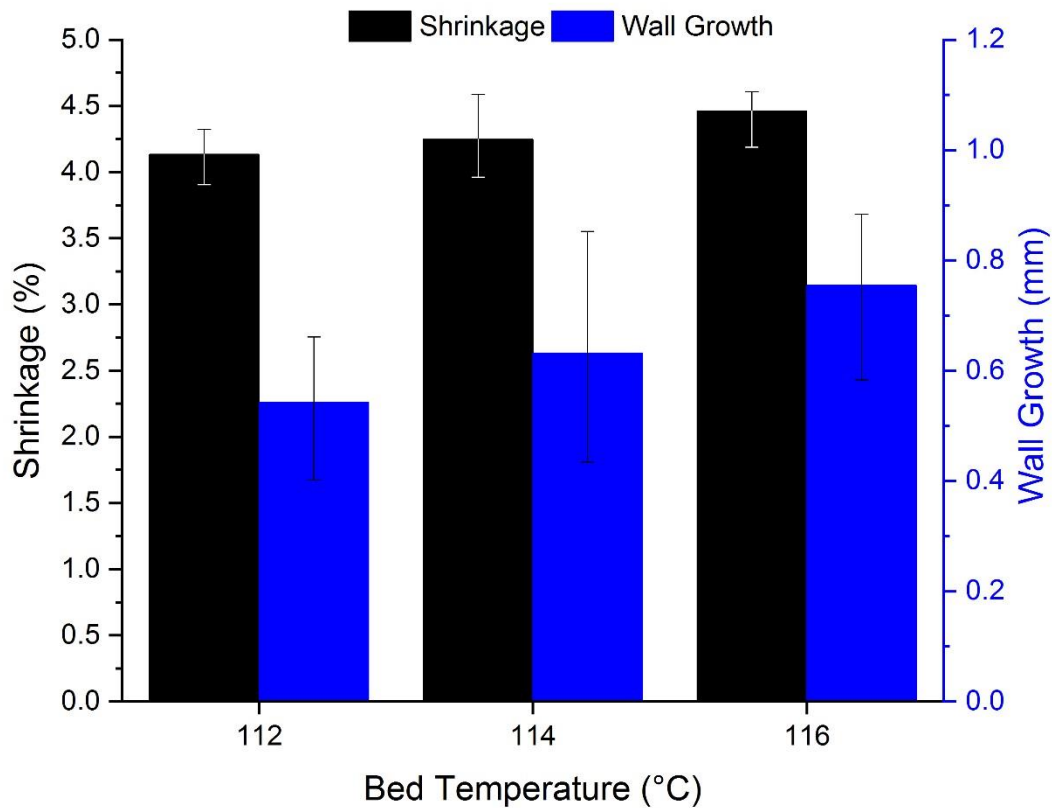


Figure 7.7 The effect of build bed temperature on shrinkage and wall growth of AdSint PP parts. The error bars included are range bars.

There is an apparent trend shown in Figure 7.7 of shrinkage and wall growth increasing as the build bed temperature increases, which will be further discussed in Section 7.7. This is the trend that would be expected as higher temperature would lead to further melting of the powder particles therefore a smaller volume of part and hence more shrinkage. The increase in wall growth is due to powder particles sintering surrounding the print area more easily due to the bed temperature being closer to the melt temperature of the powder.

The effect of grey level on the dimensional accuracy of parts was also studied, as shown in Figure 7.8.

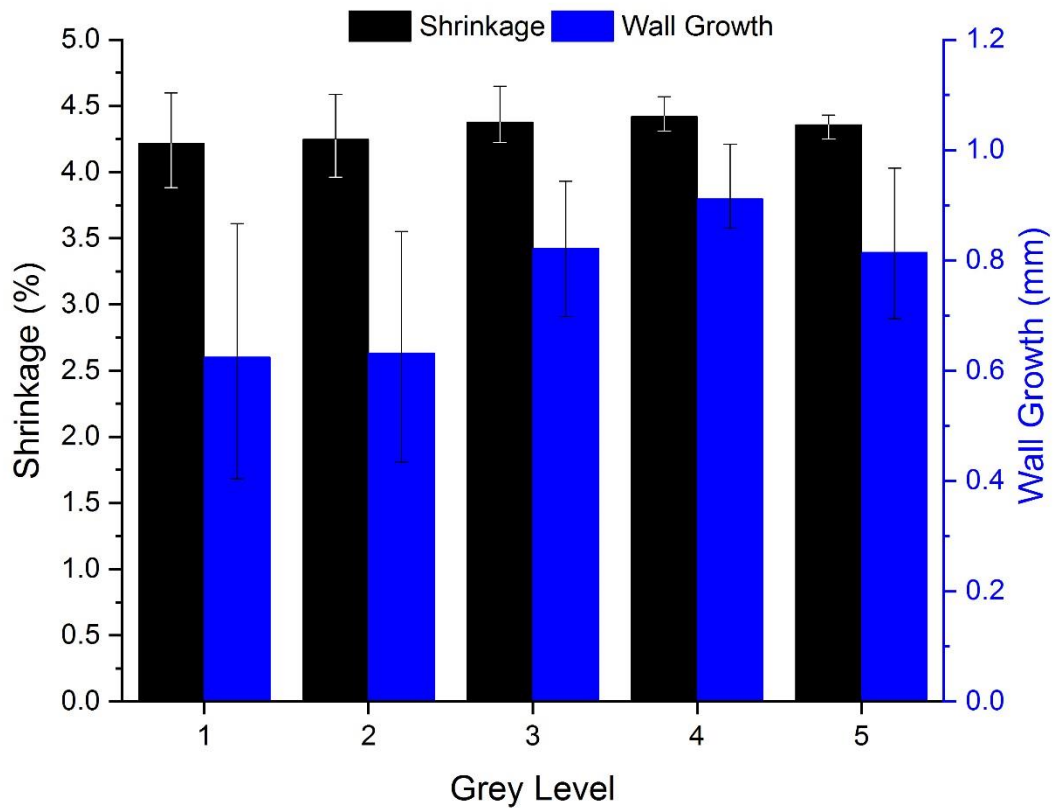


Figure 7.8 The effect of grey level on shrinkage and wall growth of AdSint PP parts. The error bars included are range bars.

Figure 7.8 as above with the effect of build bed temperature, again showing a general trend of increasing shrinkage and wall growth as grey level is increased. This will also be discussed further in Section 7.7. If shrinkage is increasing the reason for this is more of the powder is melting and hence fills a smaller volume and therefore shrinks more. Wall growth increase is likely to be caused by a combination of factors; with more ink the printed area is likely to increase in temperature and surrounding powder will sinter. The other factor being more ink is present and therefore can flow to a wider area, which is not necessarily the targeted printed area and cause additional sintering to occur, leading to increased wall growth.

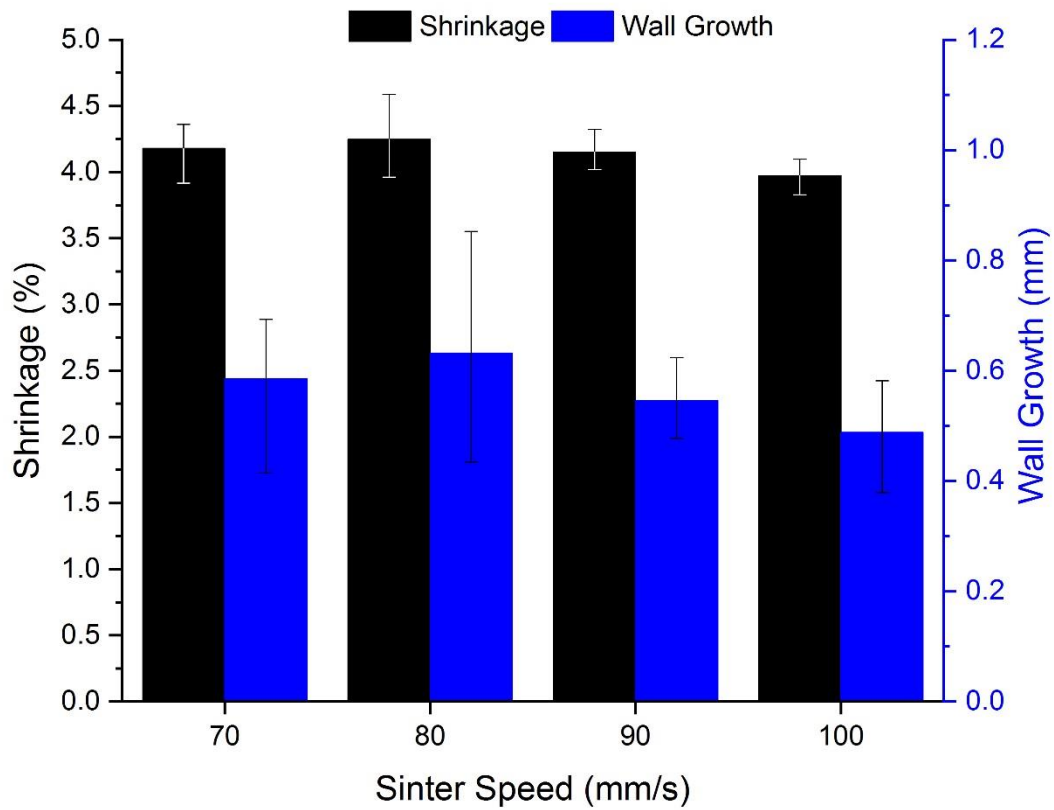


Figure 7.9 The effect of sinter speed on the shrinkage and wall growth of AdSint PP parts. The error bars included are range bars.

The impact of sinter speed on the wall growth and shrinkage of parts is shown in Figure 7.9. There is no clear trend observed, although this will be examined statistically in Section 7.7. The expected trend would be a decrease in wall growth and shrinkage as sinter speed is increased (e.g. a decrease in sinter lamp energy).

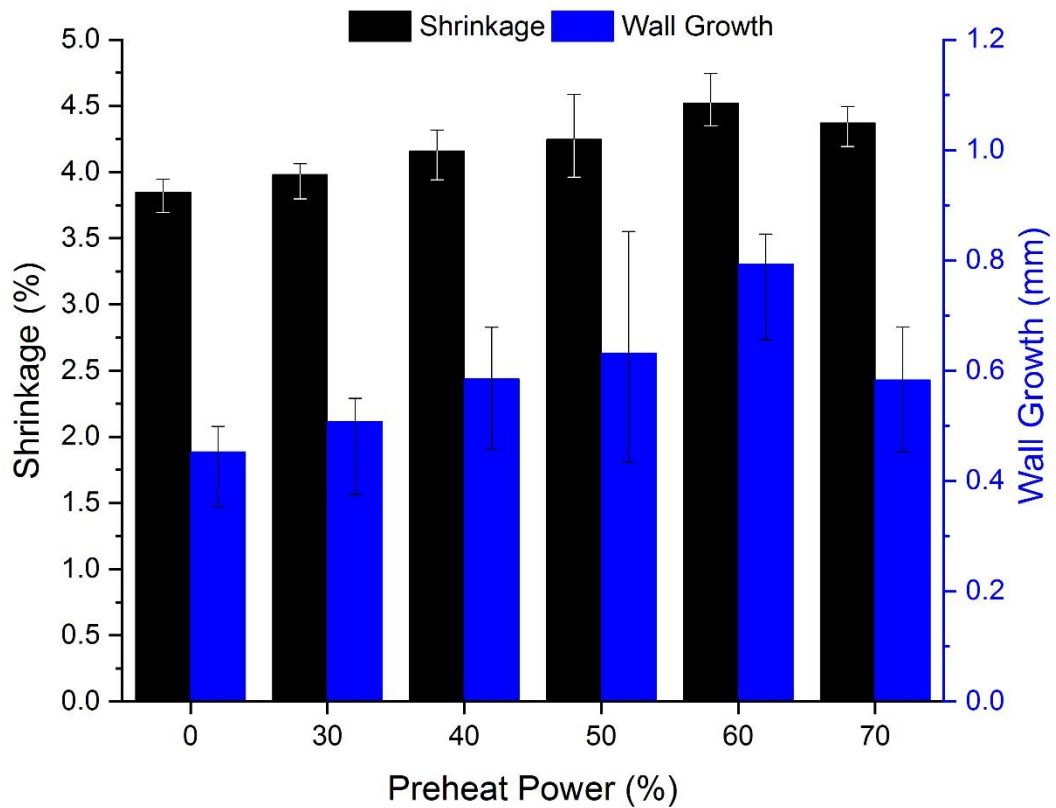


Figure 7.10 The effect of preheat power on the shrinkage and wall growth of AdSint PP parts. The error bars included are range bars.

Figure 7.10 shows the impact of preheat power on wall growth and shrinkage of the parts produced using HSS and the AdSint PP powder. The increased range bars of the preheat power at 50 % should be noted due to the use of three repeat builds for this parameter set. A general trend of shrinkage and wall growth increasing as preheat power is increased can be observed. This corresponds with the other trends observed for the dimensional accuracy, where an increase in input energy has led to an increase in both shrinkage and wall growth.

### 7.6.2 Part density

Part density was calculated using the method described in Section 4.5.2. Figures 7.11 - 7.14 demonstrate how density is affected by build bed temperature, grey level, sinter speed and preheat power.

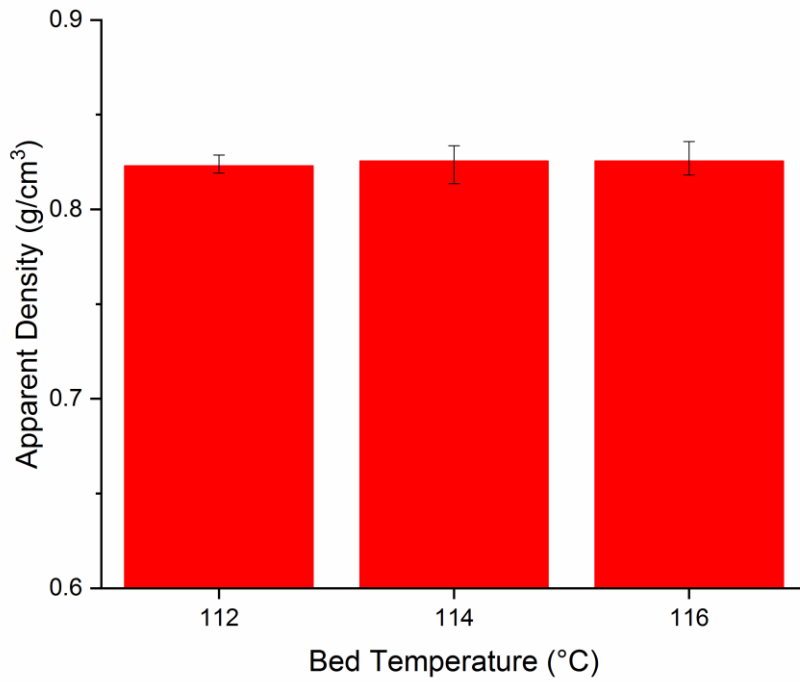


Figure 7.11 The effect of build bed temperature on part density of AdSint PP parts. The error bars included are range bars.

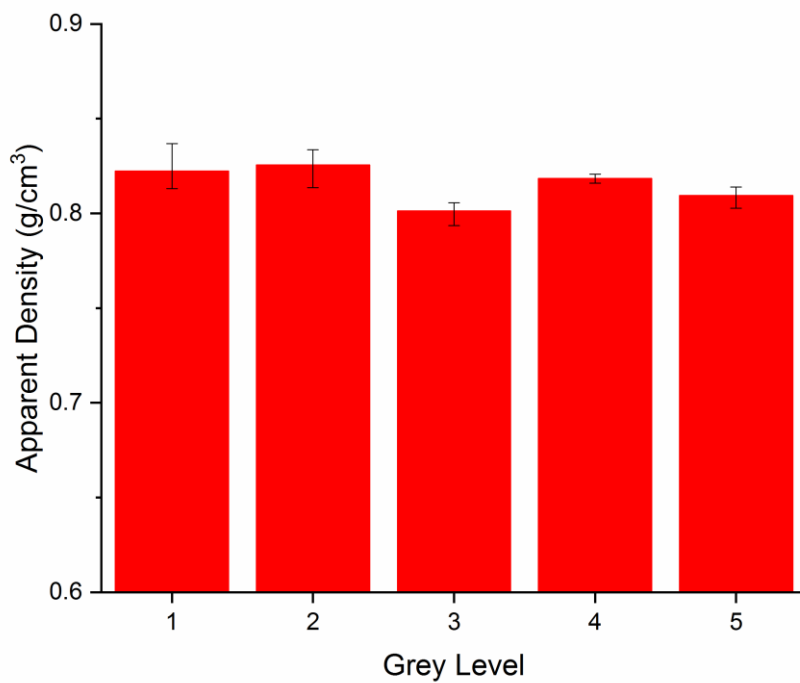


Figure 7.12 The effect of grey level on the part density of AdSint PP parts. The error bars included are range bars.

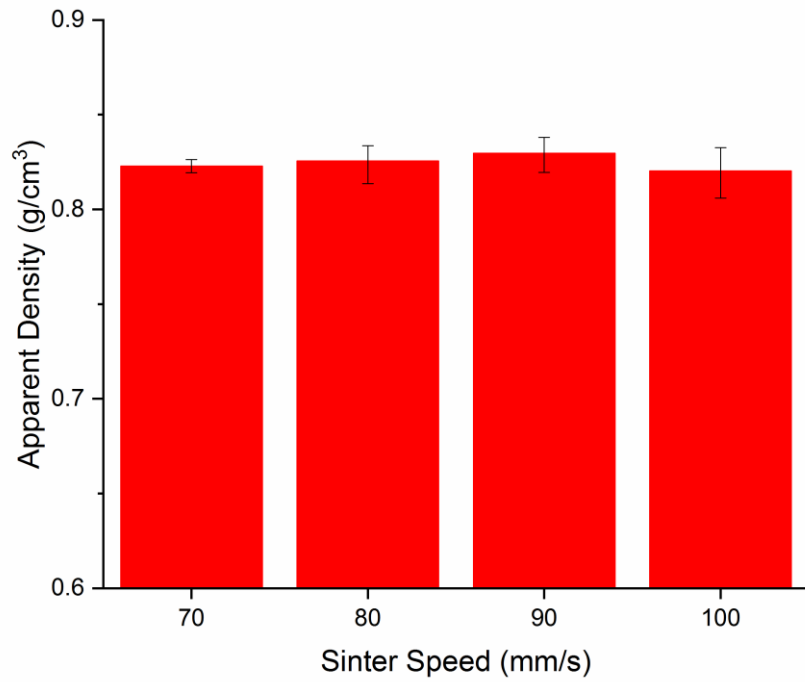


Figure 7.13 The effect of sinter speed on part density of AdSint PP parts. The error bars included are range bars.

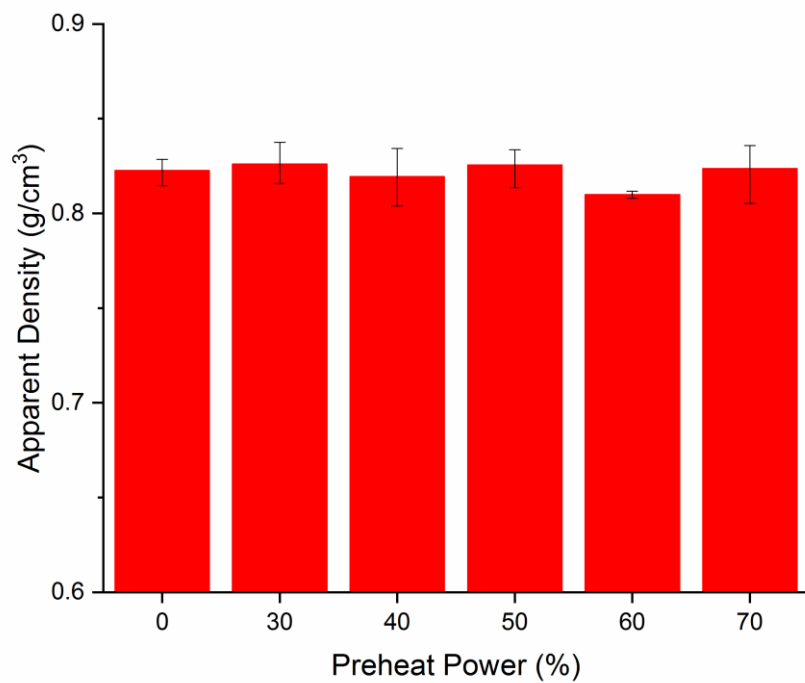


Figure 7.14 The effect of preheat power on part density of AdSint PP parts. The error bars included are range bars.

Figures 7.11 - 7.14 demonstrate the effect of the build parameters on the density of parts produced. No clear trends can be drawn where the build parameter is varied. As build bed temperature is increased there appears to be a small increase in density, however this falls within the small error described by the range bars shown. The little to no change in density is in agreement with the measurements for part shrinkage in 7.6.1 where a small increase in shrinkage would indicate a similarly small change in density, which is likely to be masked by any variability in the density measurement.

There is no significant trend in the density of parts produced against the parameters that have been varied, although there is a change in shrinkage and wall growth. Although this appears to be a contradiction it is possible due to the HSS process. As powder is deposited in the z-axis after the layer has been sintered to the fixed level of the rest of the powder bed.

### 7.6.3 Tensile properties

The tensile test pieces manufactured were ASTM D638-14 Type I specimens and were tested in accordance with the ASTM (115), as described in Section 4.5.3. A stress strain curve for a part in the **B3G2S3P4a** is Figure 7.15. In comparison to Figure 4.21 a much higher EaB is achieved as well as the shape of the curve significantly different where the part built using the AdSint Material showing a ductile nature. The effect of build bed and overhead temperature is shown in Figure 7.16.

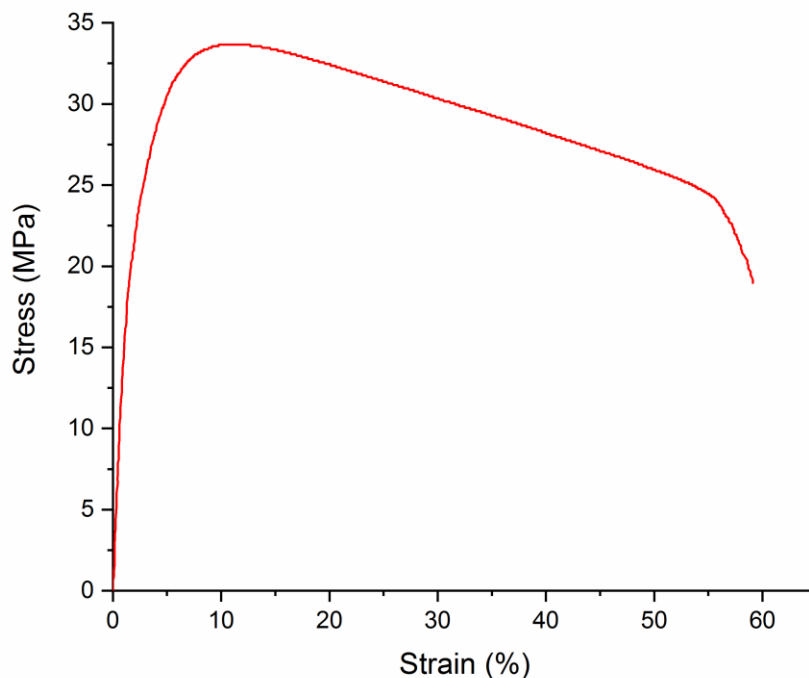


Figure 7.15 Stress strain curve of one tensile specimen in build **B3G2S3P4a**.

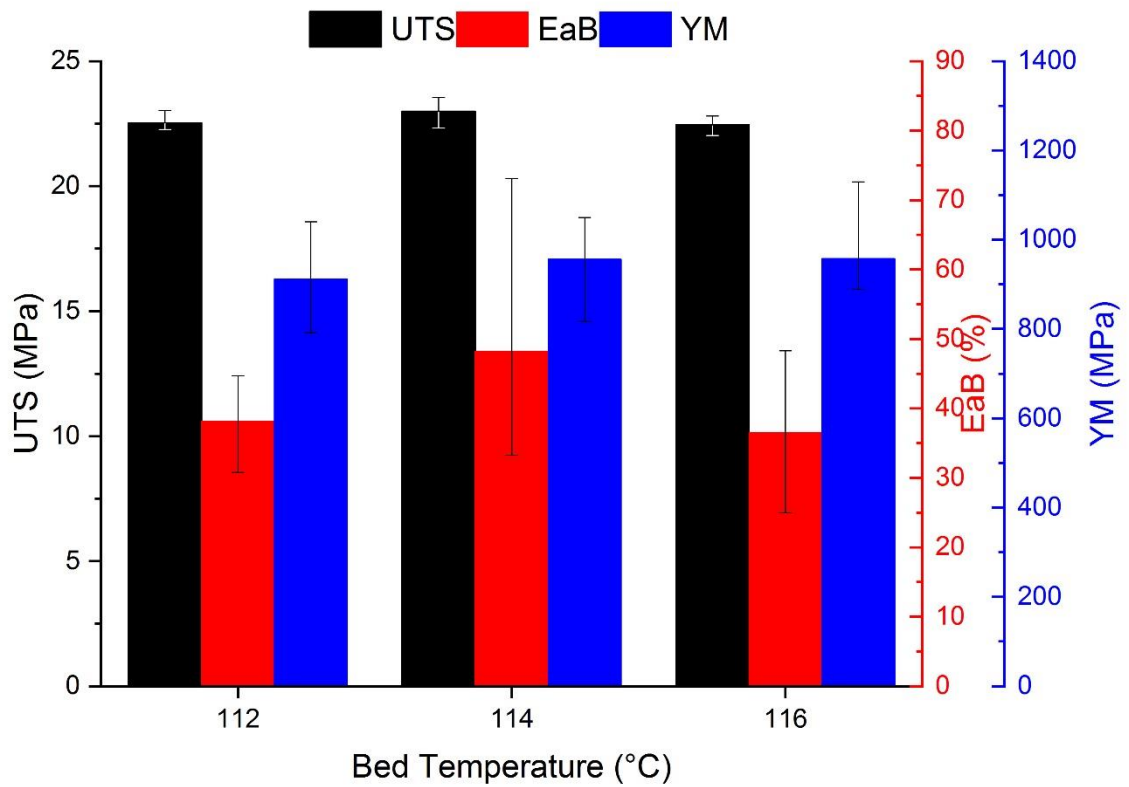


Figure 7.16 The effect of build bed temperature on the mechanical properties of HSS parts using AdSint PP as the powder feedstock. The error bars included are range bars.

Figure 7.16 shows no clear effect of the build bed temperature on the mechanical properties. The range of build temperatures where it was possible to manufacture AM parts was only 4 °C, however the other build parameters were kept constant. The 4 °C appears not to be large enough to show any differences in mechanical properties due to build bed temperature. The impact of grey level on the mechanical properties is shown in Figure 7.17.

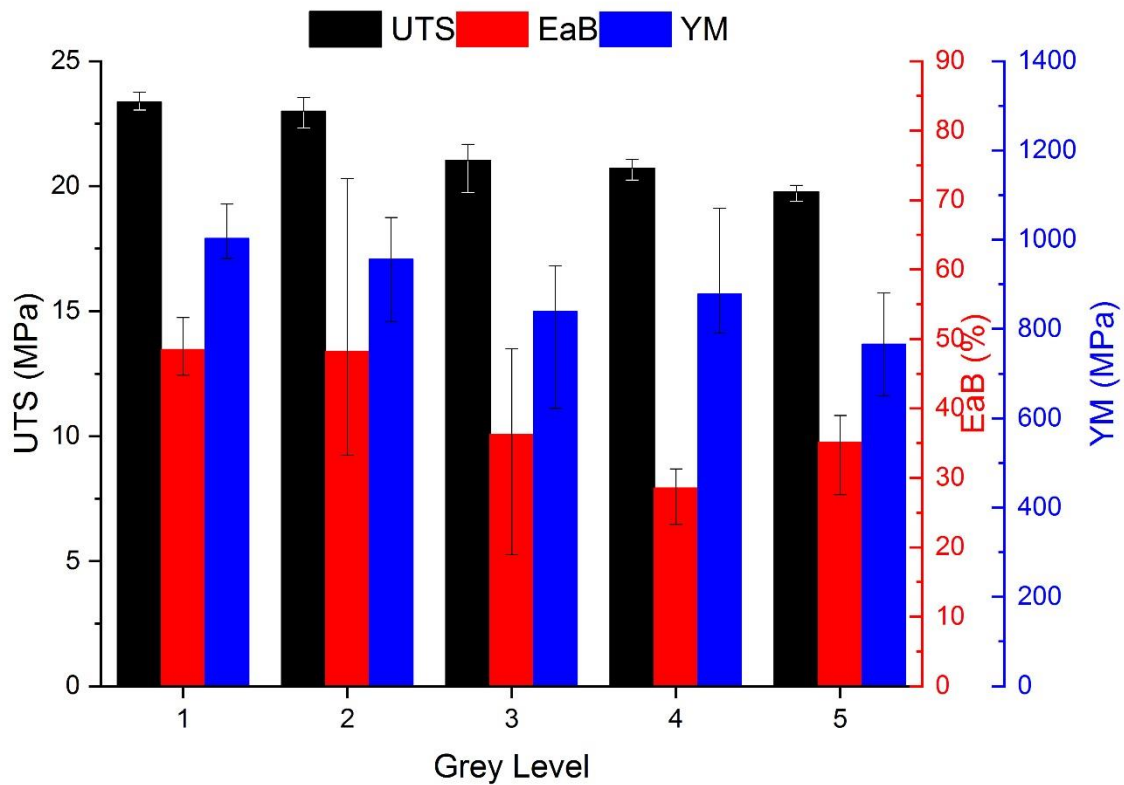


Figure 7.17 The effect of grey level on the mechanical properties of HSS parts using AdSint PP as a powder feedstock. The error bars included are range bars.

The apparent trend shown in Figure 7.17 is mechanical properties decreasing with increase in the amount of ink deposited on the powder bed (grey level). Possible reasons for the drop off in mechanical properties are that the increased amount of ink could lead to more possible fracture sites by acting as an inclusion between the sintering powder particles, or that the increased energy causing the material to overheat and degrade the polymer leading to lower mechanical properties as described by Ellis *et al.* (57). This degradation is different to it not being observed in Section 5.3.4, as the powder when melted undergoes a higher temperature than when it remains a powder. This can lead to degradation of the polymer in the part, where chain scission occurs (123), in contrast to oxidation which occurs when Nylon is processed. How sinter speed affects the mechanical properties is shown in Figure 7.18.

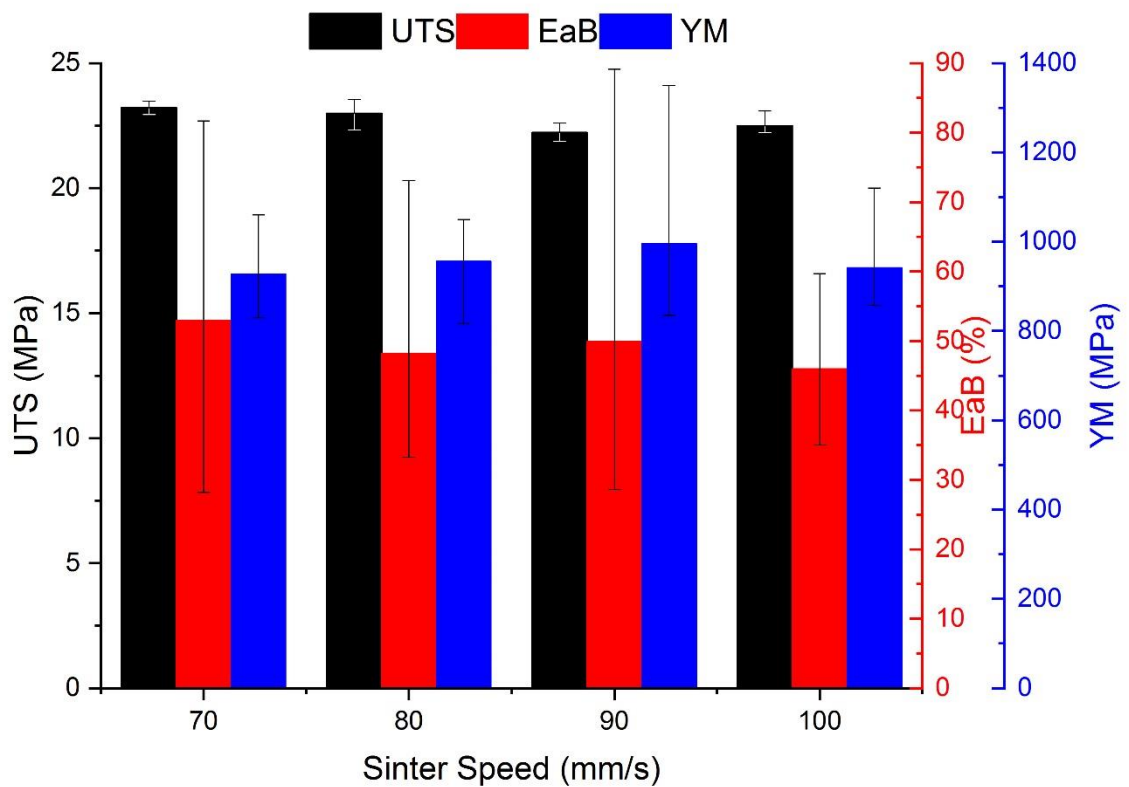


Figure 7.18 The effect of sinter speed on the mechanical properties of parts manufactured using AdSint PP as a powder feedstock for HSS. The error bars included are range bars.

The effect of sinter speed on mechanical properties is shown in Figure 7.18. No clear trends can be drawn from this data, due to the large error and the range bars shown in Figure 7.18. Statistical analysis will be carried out in Section 7.7 to assess whether there are any statistical differences between the data sets. A trend of higher mechanical properties at a slower sinter speed and hence more input energy from the sinter lamp would be expected, as shown for the other materials tested and discussed in Chapter 8, but this correlation is not clearly observed for the effect of sinter speed on mechanical properties.

Figure 7.19 shows the effect of preheat power on the mechanical properties of parts manufactured using AdSint PP.

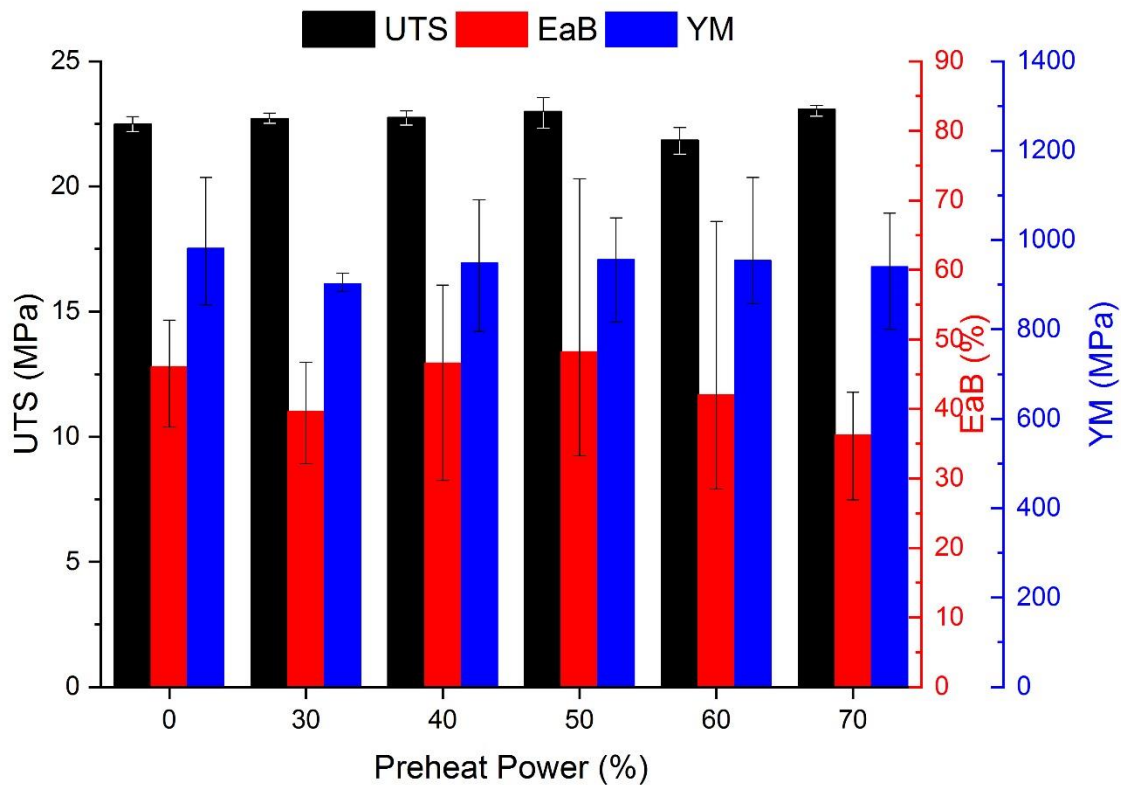


Figure 7.19 The effect of preheat power on the mechanical properties of AdSint PP parts manufactured using HSS. The error bars included are range bars.

EaB and YM show no apparent trend as the preheat power is varied, although this will be investigated further in Section 7.7.

The preheat power is one of the parameters along with the preheat speed (maintained as a constant in this work) which affects the amount of energy input from the sinter lamp on the preheat stroke after a fresh layer of powder is deposited on the build bed surface. Hence during this the IR lamp is passing over the powder bed where no IR absorbing ink is printed and should therefore have less effect on the build unless the powder is absorbing the IR energy from the lamp and heating. The **B3G2S3P7** build at 100 % preheat power did however cause the whole bed to sinter, indicating that the powder must therefore absorb some of the IR energy without the absorbing ink present.

#### 7.6.4 Melt characteristics of parts

As described in Section 4.5.4, the melt and recrystallisation characteristics of parts were measured. The melt and recrystallisation enthalpies were calculated as well as the temperatures at which these occur were recorded. These were then plotted against the machine parameters in Figures 7.20 – 7.23.

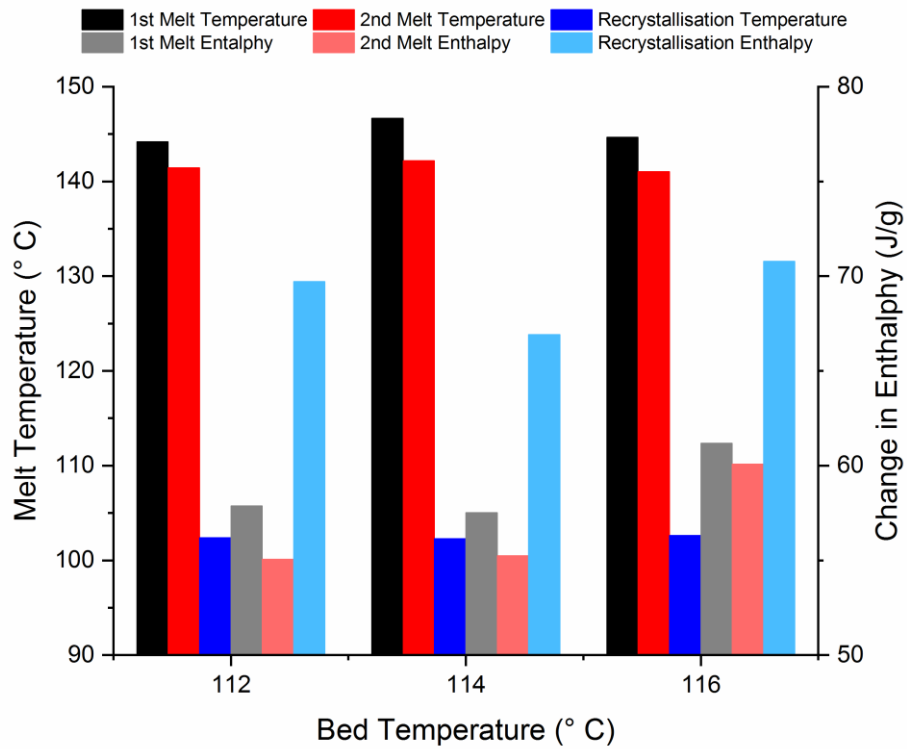


Figure 7.20 Graph showing the melt and recrystallisation temperatures and enthalpies of AdSint PP parts compared to bed temperature.

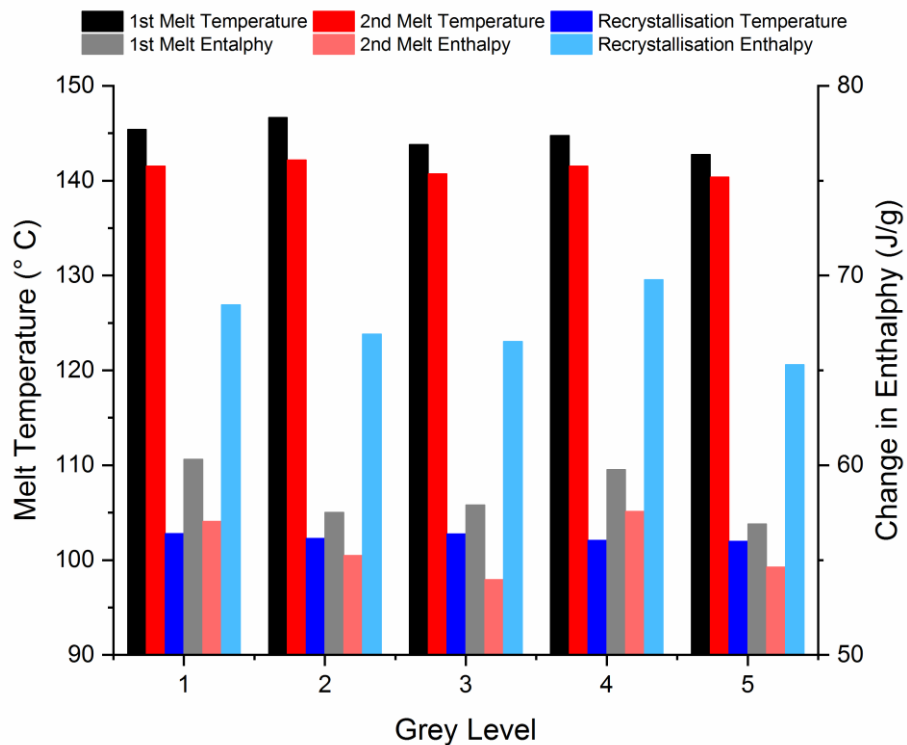


Figure 7.21 Graph showing the melt and recrystallisation temperatures and enthalpies of AdSint PP parts compared to grey level.

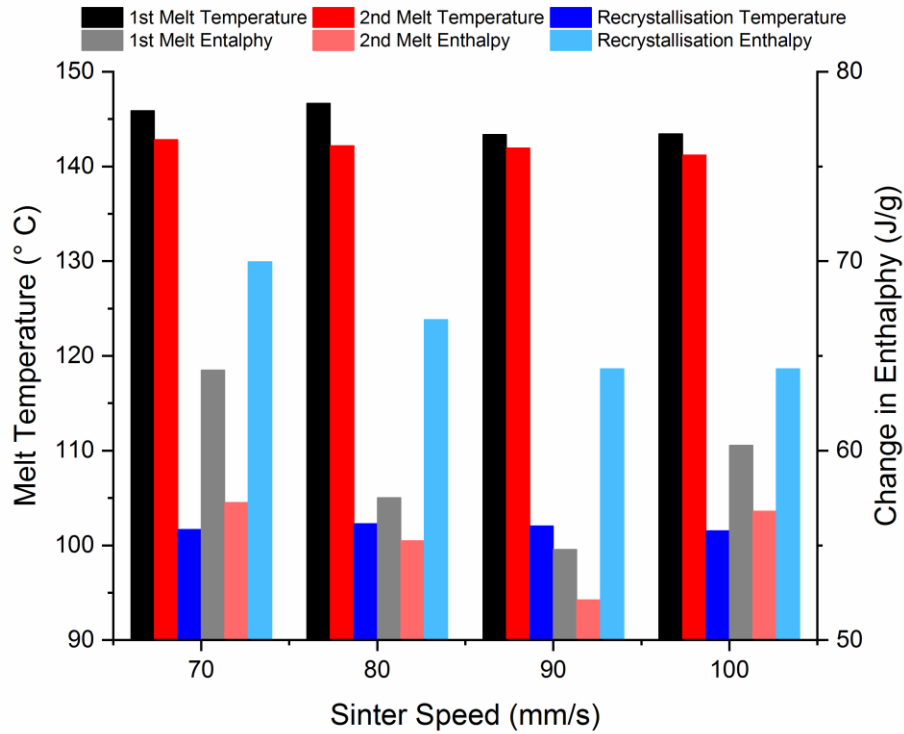


Figure 7.22 Graph showing the melt and recrystallisation temperatures and enthalpies of AdSint PP parts compared to sinter speed.

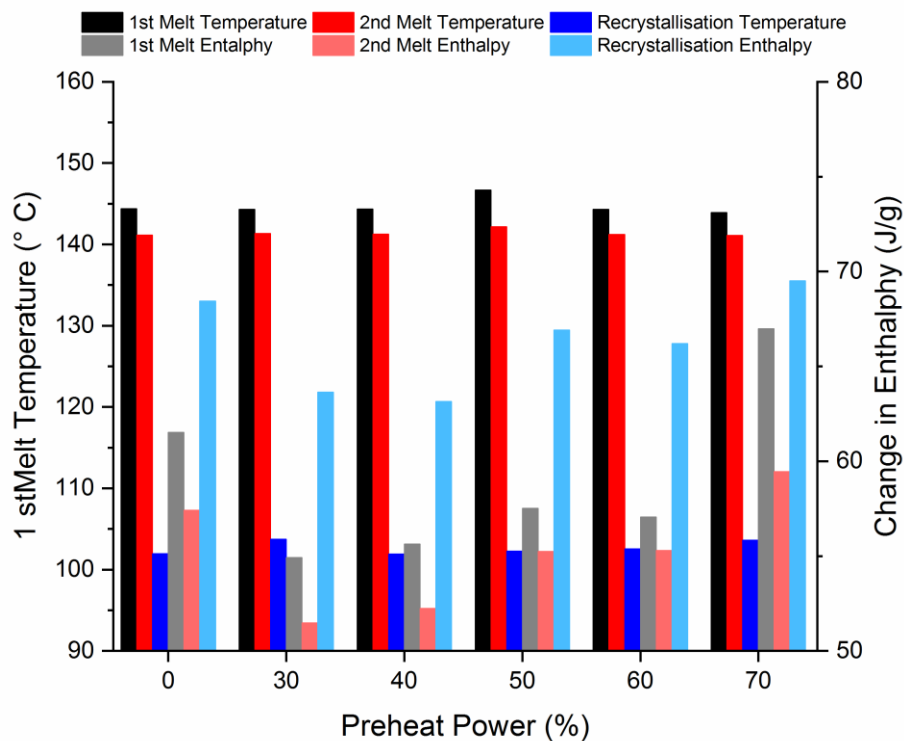


Figure 7.23 Graph showing the melt and recrystallisation temperatures and enthalpies of AdSint PP parts compared to preheat power.

As discussed in Section 4.5.4 an increase in enthalpy of the part indicates an increase in crystallinity. In the Figures above there is no obvious trend as the machine parameters are varied for melt and recrystallisation temperatures or enthalpies. As shown above there can be n clear trend drawn from the enthalpy data, a larger sample database would allow this relationship to be clarified or ruled out. However with this data set no clear conclusions can be drawn. In Section 8.3, a comparison of enthalpy vs mechanical properties is made.

As well as manufacturing test specimens other geometries were possible as shown below in Figure 7.24. The bottle demonstrates that over hangs and different shapes and volumes are also possible. Furthermore in Figure 7.25, lattice structures were manufactured although powder removal was difficult.



*Figure 7.24 Hollow bottle manufactured using AdSint PP in HSS.*



*Figure 7.25 Lattice structure manufactured using HSS using AdSint PP as a powder feedstock.*

### 7.7 Further discussion

In order to fully determine which parameters have the greatest influence on dimensional accuracy and mechanical properties, one way Analysis Of Variance (ANOVA) was used to determine statistical differences between the data as described in Section 4.6. The results of this are shown in Table 7.11.

Chapter 7 - Processability of alternative polypropylene grade AdSint (commercial)

Table 7.11 One way analysis of variance the effect of various parameters on tensile properties and shrinkage and wall growth. The result of the ANOVA is shown with tests which should significance highlighted in green and then followed by post-hoc tests to demonstrate which data sets were significantly different from each other. The numbers in the table signify the two levels of parameters examined, e.g. in build bed temperature shrinkage 114 112 is the comparison between the data for the build bed temperature at 114 °C compared to the data for build bed temperature at 112 °C.

One way ANOVA set tested	Is it significant at 0.05 level?	Post Hoc test - Scheffe tests															
<b>Dimensional accuracy</b>																	
Build Bed Temperature Shrinkage	Yes	114 112	116 112	116 114													
Build Bed Temperature Wall Growth	No	114 112	116 112	116 114													
Grey Level Shrinkage	No	2 1	3 1	3 2	4 1	4 2	4 3	5 1	5 2	5 3	5 4						
Grey Level Wall Growth	Yes	2 1	3 1	3 2	4 1	4 2	4 3	5 1	5 2	5 3	5 4						
Sinter Speed Shrinkage	Yes	80 70	90 70	90 80	100 70	100 80	100 90										
Sinter Speed Wall Growth	No	80 70	90 70	90 80	100 70	100 80	100 90										
Preheat Shrinkage	Yes	30 0	40 0	40 30	50 0	50 30	50 40	60 0	60 30	60 40	60 50	70 0	70 30	70 40	70 50	70 60	
Preheat Wall Growth	Yes	30 0	40 0	40 30	50 0	50 30	50 40	60 0	60 30	60 40	60 50	70 0	70 30	70 40	70 50	70 60	
<b>Mechanical properties</b>																	
Build Bed Temperature UTS	No	114 112	116 112	116 114													
Build Bed Temperature EaB	No	114 112	116 112	116 114													
Build Bed Temperature YM	No	114 112	116 112	116 114													
Grey Level UTS	Yes	2 1	3 1	3 2	4 1	4 2	4 3	5 1	5 2	5 3	5 4						
Grey Level EaB	Yes	2 1	3 1	3 2	4 1	4 2	4 3	5 1	5 2	5 3	5 4						
Grey Level YM	Yes	2 1	3 1	3 2	4 1	4 2	4 3	5 1	5 2	5 3	5 4						
Sinter Speed UTS	Yes	80 70	90 70	90 80	100 70	100 80	100 90										
Sinter Speed EaB	No	80 70	90 70	90 80	100 70	100 80	100 90										
Sinter Speed YM	No	80 70	90 70	90 80	100 70	100 80	100 90										
Preheat UTS	Yes	30 0	40 0	40 30	50 0	50 30	50 40	60 0	60 30	60 40	60 50	70 0	70 30	70 40	70 50	70 60	
Preheat EaB	No	30 0	40 0	40 30	50 0	50 30	50 40	60 0	60 30	60 40	60 50	70 0	70 30	70 40	70 50	70 60	
Preheat YM	No	30 0	40 0	40 30	50 0	50 30	50 40	60 0	60 30	60 40	60 50	70 0	70 30	70 40	70 50	70 60	
<b>Legend</b>		Significant		Not Significant													

After all of the parameters were examined; the build bed temperature, grey level, sinter speed and preheat power showed a statistically significant effect on the dimensional accuracy of parts manufactured, but none of these induced consistent variation between different parameters. It can therefore be concluded that these parameters may have become more important if the process window were able to be opened up, but are not major factors at the current time.

A statistically significant effect on mechanical properties was observed for altering grey level, sinter speed and preheat power, but not build bed temperature. Where UTS was the most consistent measure and supported by the correlation observed by the post hoc tests showing a relationship as both sinter speed and grey level were varied. The preheat power also shows a significant difference between several post hoc test but these are all between a single data set at 60 mm/s, hence no trend can be inferred. As with dimensional accuracy the effect on mechanical properties by the parameters varied may be more obvious if it was possible to extend the process window and be able to access a wider range of parameters.

## 7.8 Conclusions

Bed temperature is a critical parameter as a restricted range of build bed temperatures was available to process the material. However the AdSint PP material has been shown to process reliably by repeat builds in the processing range. The grey level has also been shown to be critical in affecting the mechanical properties of parts, where a large amount of ink has led to lower properties. The effect of sinter speed and preheat power have also been studied.

AdSint PP has been shown to have significantly higher EaB than the other PP powders analysed, and this EaB would be sufficiently high to produce FMCGs with AdSint PP.

The analysis of the AdSint PP powder and the parts manufactured using the same powder has been carried out. This analysis will be now used to compare the three grades of PP used in this research, CP22 PP, XX00199PP and AdSint PP, in an attempt to understand the factors affecting processability and part quality. The characterisation of the powder will aid in comparison of the parts manufactured using the different powder feedstocks.

## Chapter 8 Discussion

### 8.1 Introduction

Three different grades of PP have been characterised for use within the HSS process; CP22 PP, XX00199 PP and AdSint PP (analysed in Chapters 4, 6 and 7 respectively). In this chapter the results will be compared across all three powders, in an attempt to draw conclusions regarding the reasons for differences in their performance.

### 8.2 Ease of processing

All three grades of PP CP22 PP, XX00199PP and AdSint PP were processed in High Speed Sintering and were able to produce parts suitable for mechanical property testing. However the processability of the materials varied substantially between the three powder grades.

The CP22 PP grade of PP was very sensitive to changes in build bed temperature and was only processable at a single build bed temperature. At this temperature the repeatability of the builds remained poor, as demonstrated by the attempts to repeat mid-point builds; two out of four builds attempted using the same parameters on a single day failed whilst the others were completed without issue.

The XX00199PP and the AdSint PP materials both demonstrated the ability to be built using a wider build bed and overhead temperature range, as well as the ability to build repeatedly within this range. This indicates that the CP22 material has a more restricted processing window, and is more susceptible to variations in process parameters. The thermal properties of the PP powders were previously analysed to give information on the initial set temperature for sintering, however comparison between these values may also help to explain the difference in process windows.

#### 8.2.1 Thermal properties

Differential Scanning Calorimetry (DSC) as described in Section 5.3.3 was used to calculate the melt and recrystallisation temperatures and enthalpies, as shown in Table 8.1.

*Table 8.1 Summary table of the melt and recrystallisation temperatures and enthalpies of the PP powders tested.*

Sample Name	Melt Temperature (°C)	Recrystallisation Temperature (°C)	$\Delta H$ Melting (J/g)	$\Delta H$ Recrystallisation (J/g)
CP22 PP	165.15	118.25	80.21	-90.18
XX00199 PP	154.17	112.34	80.00	-91.23
AdSint PP	135.95	99.35	65.19	-75.44

The difference between the melt and recrystallisation temperature is approximately; 47 °C, 42°C and 35 °C for CP22 PP, XX00199PP and AdSint PP respectively, which would indicate that the CP22 PP would have the widest process window. However, as shown in processing this difference does not increase the processability of the material. Therefore there is another reason for the difference in the processing of these grades of PP powder in HSS. The DSC curves for each polymer are shown in their respective chapters, see Figures 4.8, 6.4 and 7.4. The DSC curve for CP22 PP (Figure 4.9) and the curve for the XX00199PP (Figure 6.4) have a very similar shape, this is in comparison to the curve for AdSint PP (Figure 7.4), which is broader and has a lump on the curve before the peak melt temperature. The difference observed between the grades of PP indicates a difference between the first two grades of PP investigated and the AdSint PP material.

The enthalpy results show very similar enthalpies for the CP22 PP material and the XX0199 PP whereas the AdSint PP has lower enthalpy values. Enthalpy has previously been used to calculate percentage crystallinity and hence degree of particle melt (124). Percentage crystallinity was calculated by dividing the enthalpy of the sample by the enthalpy of a 100 % crystalline sample. However due to the lack of information provided by the powder suppliers this calculation was not possible hence enthalpy values will be compared as an indicator of crystallinity.

The enthalpy of the AdSint PP material is less than the two other PPs tested, whilst the other two grades of PP have very similar enthalpy values. If this were the cause of the lack of processability, it would be expected that the CP22 PP and the XX0199PP would have equally poor processability. However, as the XX0199PP has a similar enthalpy to the CP22 PP, but exhibits a much greater processability this is unlikely to be the cause.

### 8.2.2 Flow agent

Another possible reason for the differing performance of the polymer powders is the amount of flow agent used in the different grades of PP. The effect of flow agent has previously been studied by Lexow *et al.* (75). The research demonstrated the capability of cryo-grinding a PP powder and then addition of a flow agent the powder was then sinterable in LS.

#### Powder flow

Measurement of the powder flow of three grades of PP was attempted, as described in Section 4.1.1. However although CP22 PP and a Nylon grade used as a reference sample flowed freely through the test apparatus the other two grades of PP did not and hence no quantitative measure was made. As discussed in 4.1.1, the apparatus used to measure powder flow in this thesis was not ideal. Ideally a machined metal cone with the same dimensions would allow powder flow to be better investigated. Similar to the apparatus used for Hall or Carney flow tests but developed for polymers used in powder

bed fusion. Further investigations of the size and shape of the powders were attempted to explain this difference.

*Particle size and morphology*

Powder particle size and shape have previously been demonstrated to have an effect on powder flow (72-74); hence it would be reasonably expected for the CP22 PP to have the shape and size to lead to the best powder flow, as the only measurable powder flow using the apparatus available was for CP22 PP.

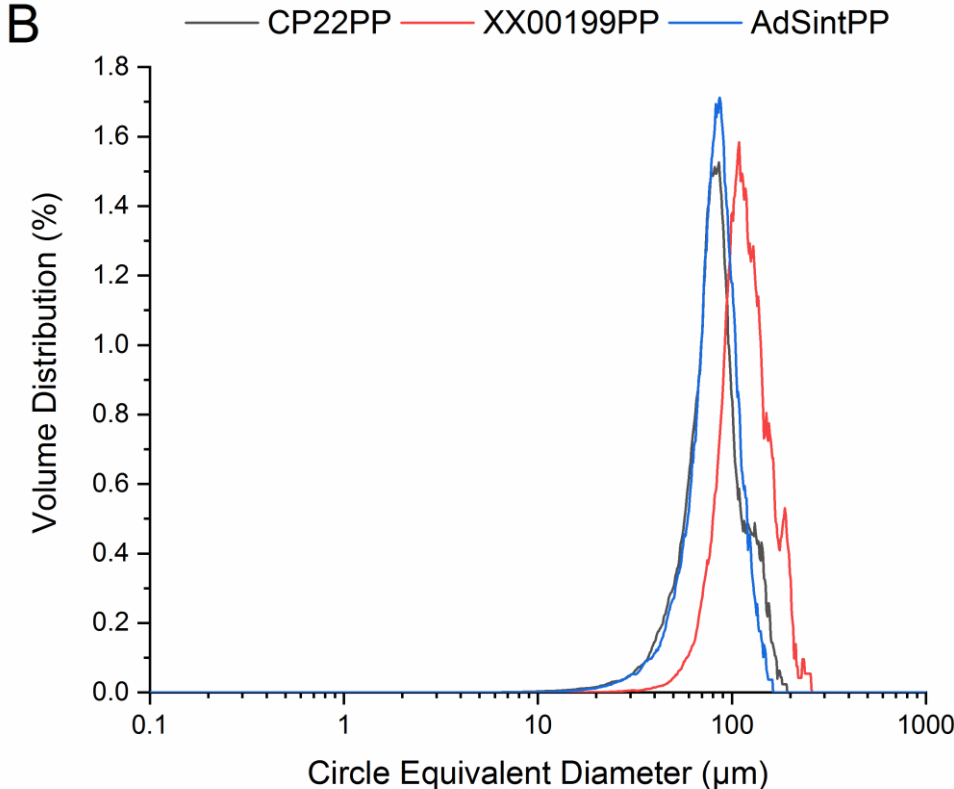
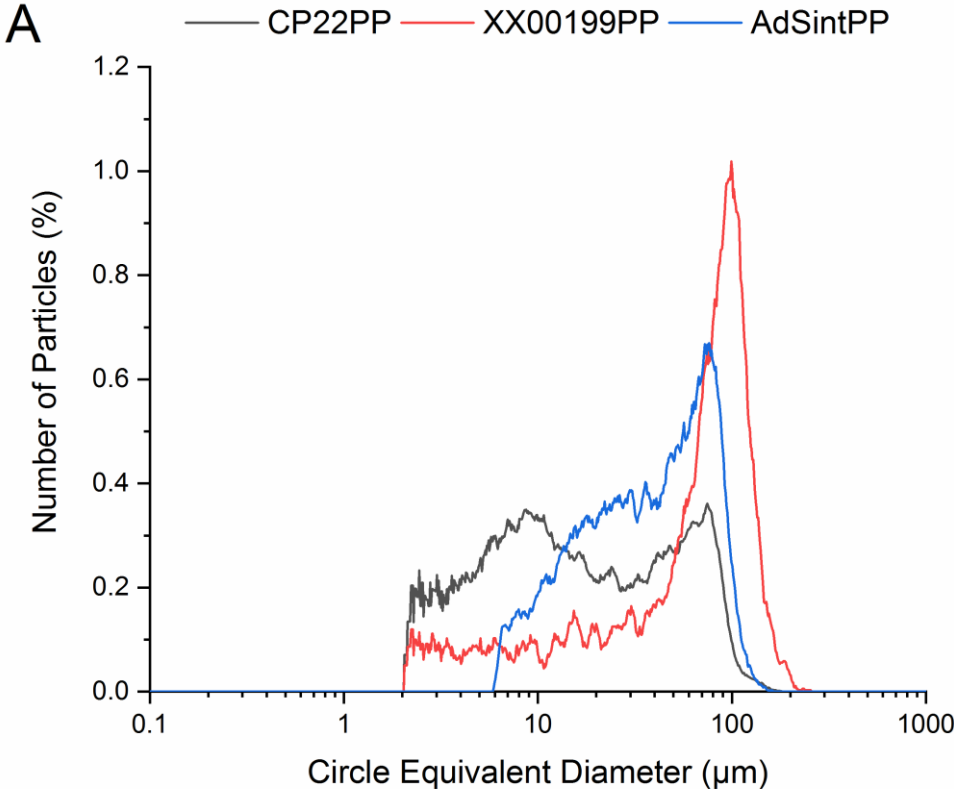
In this research particle size and shape were studied using laser diffraction and image analysis, Table 8.2 is a summary table of the particle size and shape parameters recorded.

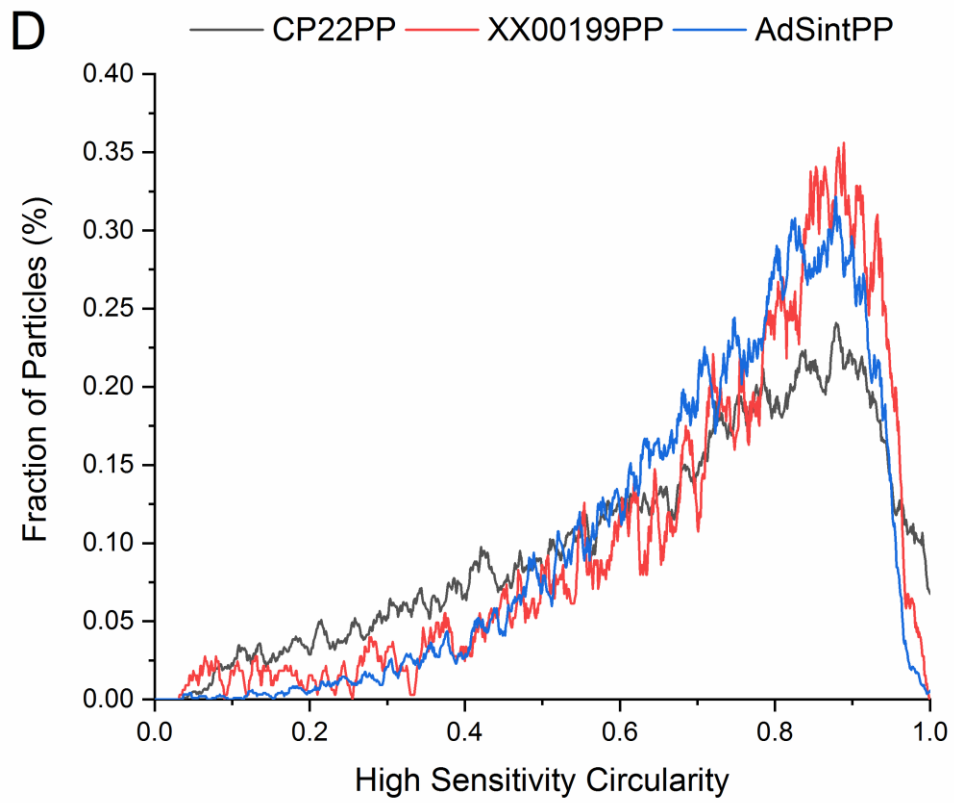
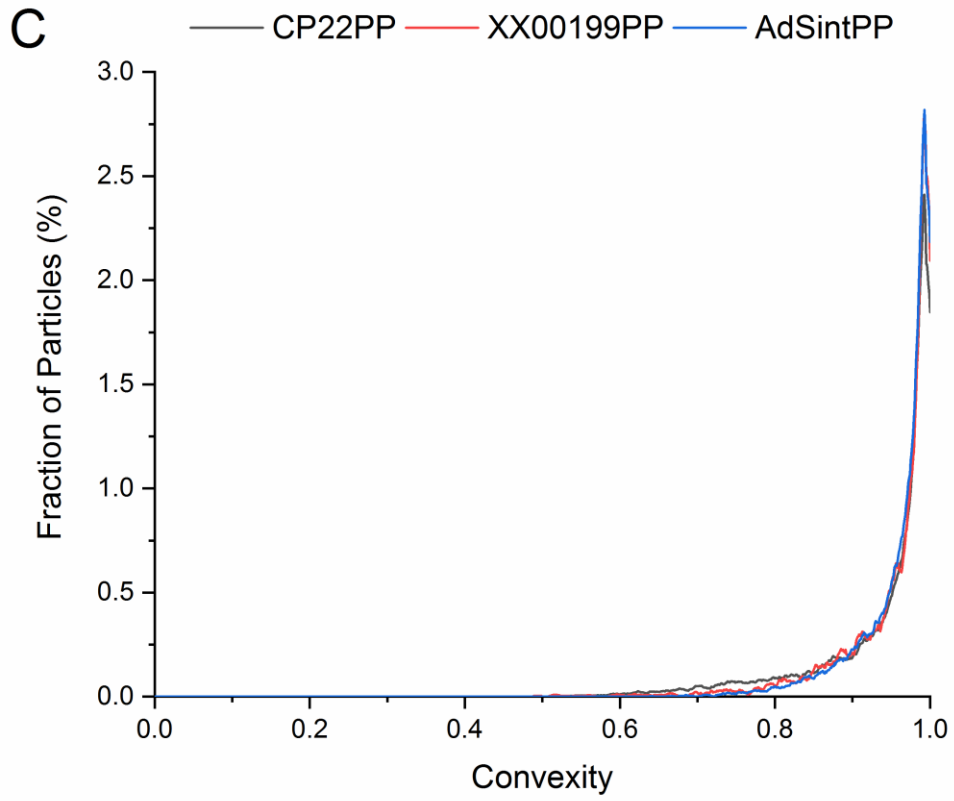
*Table 8.2 Particle size and shape information for the three PP powders tested.*

Sample Name	Laser Diffraction			Image Analysis			
	D (10) ( $\mu\text{m}$ )	D (50) ( $\mu\text{m}$ )	D (90) ( $\mu\text{m}$ )	CE Diameter Mean - Number Distribution ( $\mu\text{m}$ )	Convexity Mean	HS Circularity Mean	Aspect Ratio Mean
CC22 PP	11.0	39.9	82.8	34.69	0.94	0.674	0.656
XX00199 PP	56.5	92.5	149.3	76.73	0.95	0.733	0.686
AdSint PP	21.8	58.0	105.3	44.6	0.96	0.731	0.661

A comparison of the particle shape traces is shown in Figure 8.1. The CP22 PP powder has the smallest particle size of the PP powders tested with the XX00199PP having a much larger average particle size and the AdSint PP falling between the two. The smallest particles observed for both CP22 PP and the XX00199PP were 2  $\mu\text{m}$  which is roughly the minimum size which this technique can measure whereas the AdSint PP material has no particles smaller than 6  $\mu\text{m}$ .

The CP22 PP material displayed the highest quantity of small particles, whereas the AdSint PP has more particles at a large particle size, and the XX00199PP material has a large amount of large particles and a relatively continuous amount of particles within the range of 2 – 20  $\mu\text{m}$ .





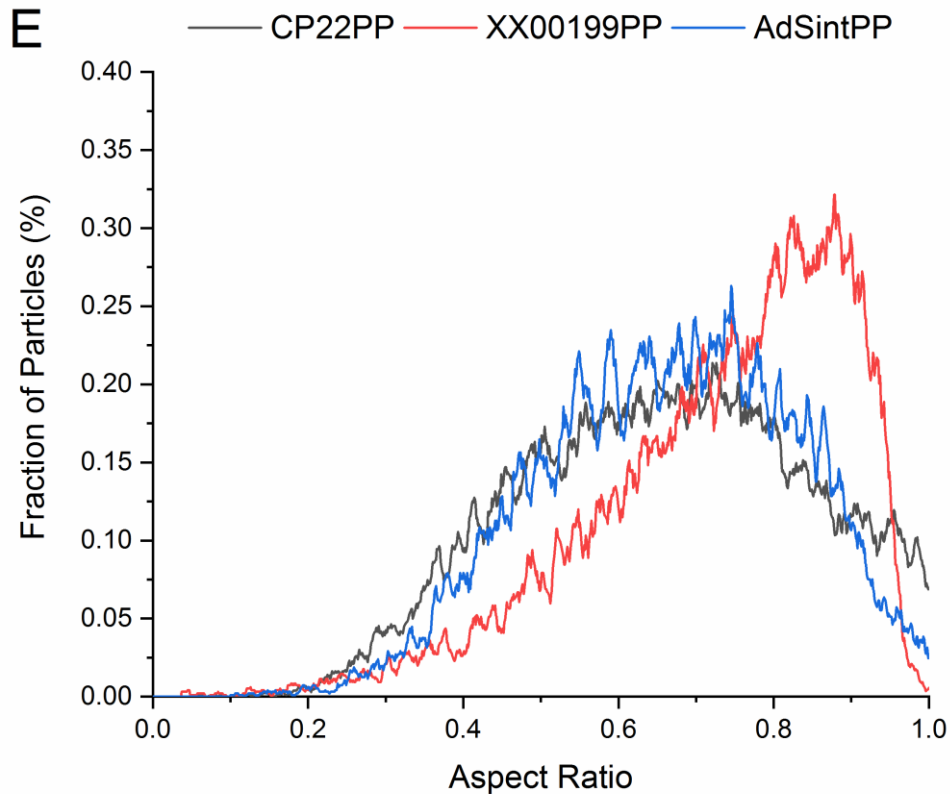


Figure 8.1 Image analysis traces showing size and shape of the CP22 PP, XX00199PP and AdSint PP powder to allow comparison. (A) Circle equivalent diameter against the number distribution of powder particles. (B) Circle equivalent diameter against the volume distribution of powder particles. (C) Convexity against fraction of powder particles. (D) High sensitivity circularity against fraction of powder particles. (E) Aspect ratio against fraction of powder particles.

The shape parameters of the PP powders were also studied. The only mean average to change significantly between the powders is the High Sensitivity Circularity (HS Circularity) which is affected by both changes in the overall form and the surface roughness of the particles. HS Circularity (D) was noted to be significantly lower for CP22PP compared to the other powders tested. This is also seen in the distribution shown in Figure 8.1.

On the graph of convexity (C), a measurement of surface roughness, it is difficult to see a difference in the powders however it can be observed at a convexity of roughly 0.75 that there is a larger contribution from the CP22 PP than the other powders tested. This is probably the driving force for the HS circularity to be different for the powders which is a more sensitive measure than convexity.

AdSint PP and the CP22 PP have similar AR (E) distributions compared to XX00199PP which has a larger contribution of particles at a higher AR. This is likely due to the processing of the XX00199PP before it was received to be used.

These differences in size and shape distributions are most likely caused by the powderisation process for each material. Powders for AM can be manufactured by different processes, these processes are protected by the manufacturers of the powders therefore it is difficult to confirm the process used for each powder. One method would be to polymerise the powder and then grind to the appropriate size, the alternative method would be to precipitate out the polymer similar to that used in production of Nylon polymer powder of the required size (97).

The contribution of the shape and size would be expected to lead to the XX0199PP having the best powder flow followed by the AdSint PP then the CP22PP material (73). However, this was not the case here with CP22 PP demonstrating the highest powder flow as discussed above. Therefore there must also be another parameter affecting the powder flow.

It is common practice in polymer powder bed fusion (PBF) processes to include some sort of flow agent, and it is possible that this may be the cause of the processability differences seen here. Flow agents often used include; fumed silicas, glass spheres, hydroxyapatite and calcium carbonate which are all inorganic materials and often small to aid with flow.

#### Thermogravimetric analysis

Thermogravimetric Analysis (TGA) was used to analyse the decomposition temperature and the residual mass of the powders, as described in Section 5.3.3. A summary of the TGA results is shown in Figure 8.2.

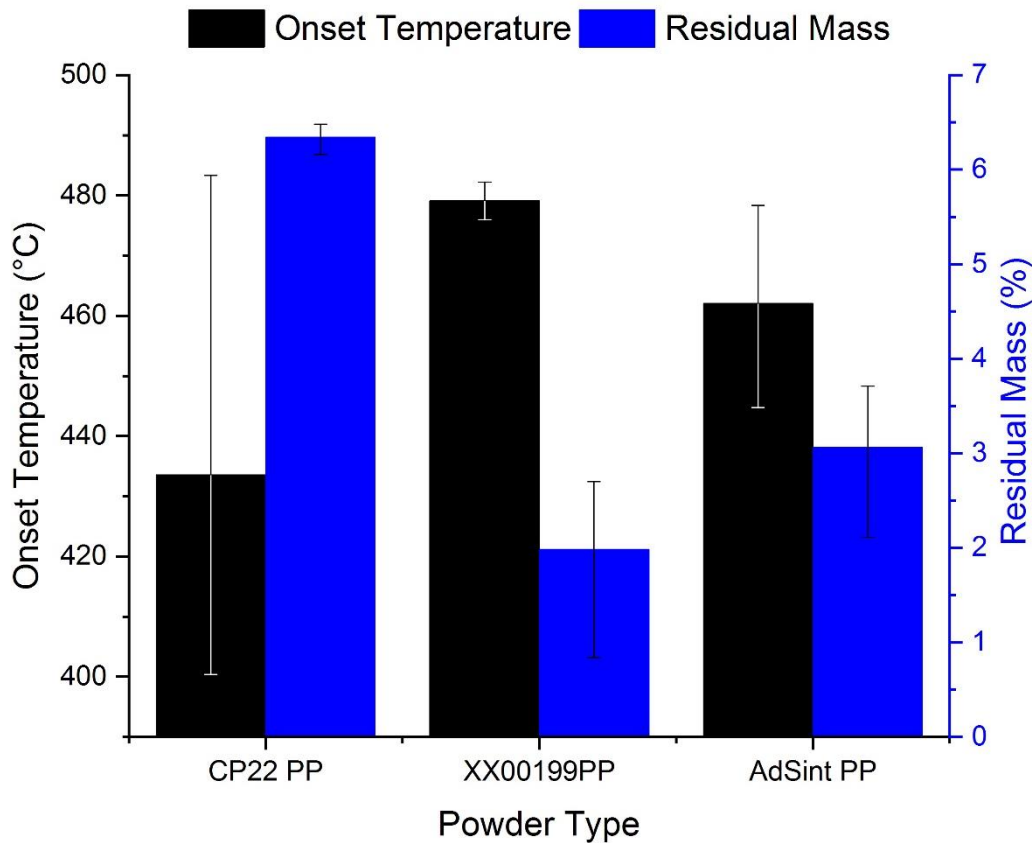


Figure 8.2 TGA results of the PP powders, showing decomposition onset temperature and residual mass. The error bars included are range bars.

It can be observed that there is no significant difference in the onset temperature between the three materials, when error is considered. This temperature is also significantly higher than the operating temperature of HSS. However, the residual mass percentage does offer some insight into the powders. The residual mass is the remaining inorganic material after the polymer decomposes at a high temperature, with at least some of this likely to be flow agent.

It can be seen that the CP22 PP material contains the highest level of inorganic material, indicating the inclusion of a high quantity of flow agent may be the reason for the high flow. However, there is some evidence both published and anecdotal that high levels of flow agent can affect the sintering process. Norazaman *et al.* (78) showed the effect of flow agent on the mechanical properties on parts, at a level of 0.5 % the mechanical properties decreased. Therefore even if only a small quantity of these residuals is a flow agent, there could be a large effect on processability and mechanical properties.

The amount of flow agent is one of the differences between the PP powder grades assessed, and is considered to be a likely reason for the different performances in processability observed. This should be investigated as part of further work to build on this thesis, see Section 9.2. The difference in

chemical composition of the polymers with AdSint PP likely a copolymer is also likely to be a key factor in the differing performance.

### 8.3 Mechanical properties of parts

Parts were manufactured using all three PP powders used in the HSS process; Figure 8.3 shows a comparison of the mechanical properties and densities of parts produced. The mid-point machine parameters identified as most reliable have been used for this discussion. The parameters used for comparison are shown in Table 8.3.

*Table 8.3 Builds used to compare general mechanical properties of parts manufactured using CP22 PP, XX00199PP and AdSint PP via HSS.*

Powder	Build Bed and Overhead (°C)	Grey Level	Sinter Speed (mm/s)	Preheat Power (%)
CP22 PP	150	3	105	50
XX00199 PP	135	2	110	50
AdSint PP	114	2	80	50

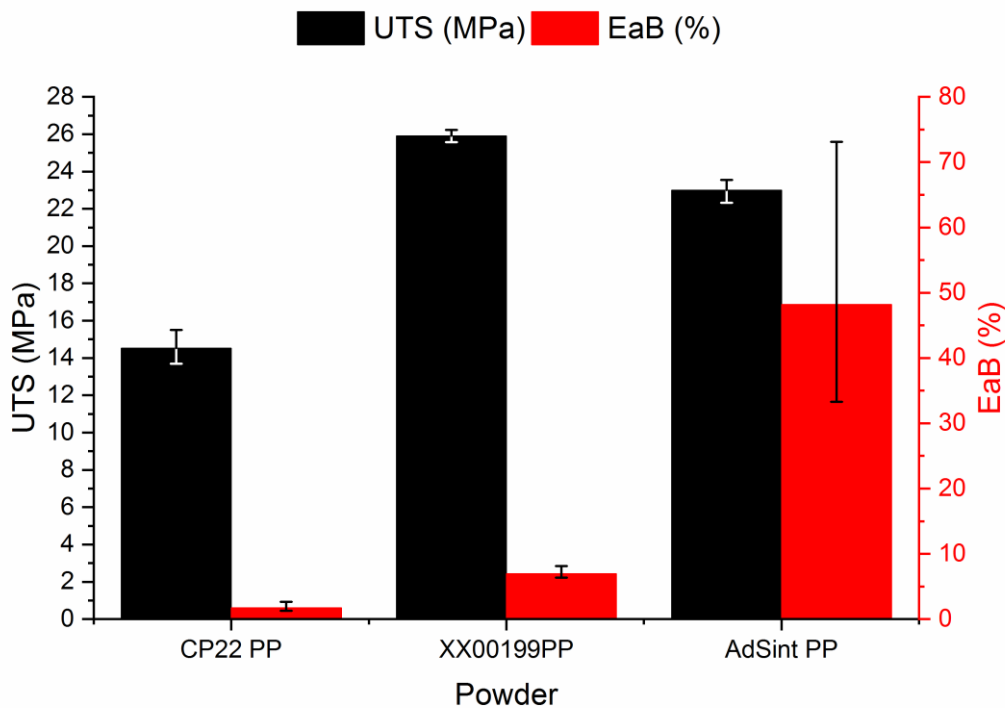


*Figure 8.3 Summary of the UTS and EaB of parts manufactured using different PP powders. The error bars included are range bars.*

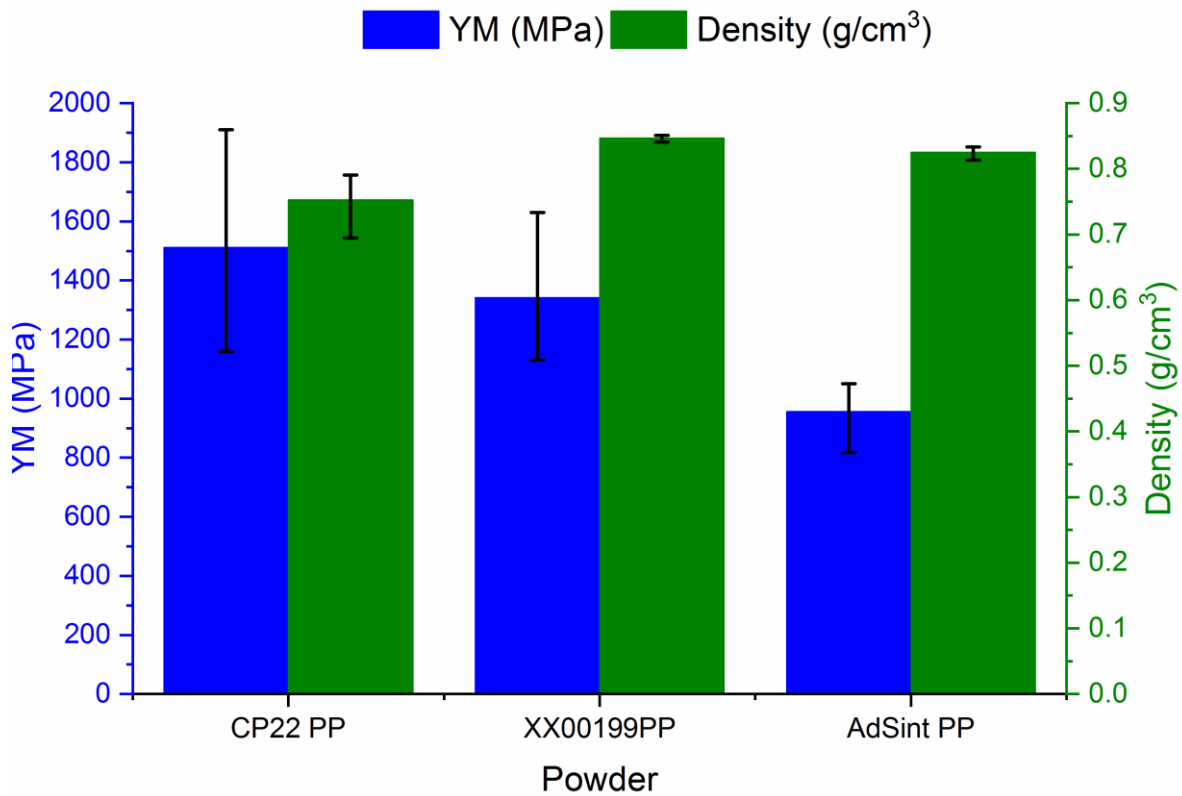


Figure 8.4 Summary of the YM and Apparent density of parts manufactured using different polymer powder feedstocks. The error bars included are range bars.

Figure 8.3 and Figure 8.4 shows the differences in mechanical properties between the powders tested. The maximum mechanical properties from a single build are also included in Table 8.4 to aid comparison.

Table 8.4 The highest properties achieved for the various powders selected from the build with the highest EaB (most significant for FMCGs). The standard deviation is shown in brackets.

Powder	UTS (MPa)	EaB (%)	YM (MPa)	Density (gcm <sup>-3</sup> )
CP22 PP	15.59 (0.43)	2.29 (0.23)	1394 (247)	0.768 (0.008)
XX00199PP	25.9 (0.28)	6.99 (0.68)	1342 (188)	0.847 (0.004)
AdSint PP	23.39 (0.17)	59.33 (13.65)	977 (65)	0.828 (0.003)

The UTS of parts manufactured using XX00199PP were demonstrated to be the strongest with a small but significant decrease to parts from the AdSint PP then a large decrease to CP22 PP parts. An increase in EaB was observed between XX00199pp from CP22 PP but much larger increase was shown using the AdSint PP material. Although it was possible to improve EaB by varying the parameters used to manufacture the parts it was not possible to get EaB values in the same magnitude as the AdSint

PP grade. Similar YM values were measured for the CP22 PP and XX0199PP however a markedly lower level was measured for the AdSint powder.

### 8.3.1 Part density

Part density has been shown in literature (53) to affect the mechanical properties and was therefore further investigated here. The density of parts shows small differences with different PP powders, Figure 8.5 shows the tapped bulk density measured using the same technique for the different grades of PP tested.

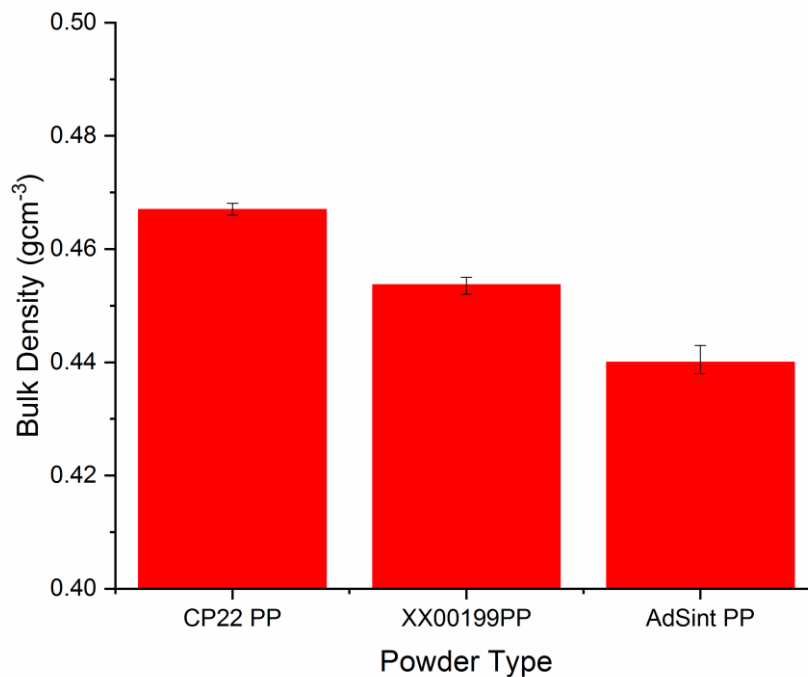


*Figure 8.5 Tapped bulk density of CP22 PP, XX00199PP and AdSint PP. The error bars included are range bars.*

It can be seen that the CP22 PP grade has the highest bulk density, which would be expected to lead to a higher part density as it would mean there is more sinterable material present for parts to be manufactured with (106). However, the part density as shown in Figure 8.3 was markedly lower for the CP22 PP than the other grades of polypropylene, which is in contrast to the bulk tapped density. This demonstrates the importance of the processability of the polymer, as a higher density bulk powder does not necessarily lead to denser parts (125). The powders may also have different true densities due to the polymer chemistries which they have. This comes from the polymer chains packing differently due to the chemical groups, branching and molecular weight varying.

### 8.3.2 Elongation at Break

Elongation at Break (EaB) is the most important mechanical property for the use of AM in FMCGs, and is traditionally low for AM when compared to more traditional manufacturing techniques. Although parts do not undergo high forces, wear and tear means EaB is critical.

AdSint PP parts possessed substantially higher EaB value in comparison to XX00199PP and CP22 PP. From the DSC results it is shown that the AdSint PP has a markedly reduced melt and recrystallisation temperature and enthalpy, Table 8.1. As discussed in Section 7.2.3 these changes suggest the AdSint PP is a PP copolymer of polypropylene and polyethylene (126), which has the effect of increasing the EaB of the material(94). The lower crystallinity of a PP copolymer compared to the homopolymer leads to more amorphous regions and hence higher EaB but less stiff and therefore a lower YM (76). Another possible reason for the difference between the EaB in the AdSint PP and the CP22 PP is the inclusion of flow agent as discussed above, where the addition of excess flow agent has previously been demonstrated to decrease the mechanical properties of HSS parts (78). Although if the flow is not sufficient a poor surface finish may be obtained, which would lead to crack propagation sites leading to poor mechanical properties.

The XX0199PP grade is also shown to have a significantly lower quantity of additives than CP22 PP grade; although it shows some increase in EaB it is not as large as observed for the AdSint PP material. The CP22 PP has a peak melt temperature indicative of a commercially available iso-tactic PP (76). The XX0199PP is more difficult to identify although, two possible routes leading to a retarded melt temperature are a different tacticity (127, 128) or thermal treatment of the polymer such as annealing during the grinding process to form a powder. This thermal process could lead to a different melt temperature, but not change the mechanical properties substantially. The thermal treatment is more likely as the tacticity change would likely lead to a lower crystallinity (76) in comparison to the CP22 PP which is not observed via DSC measurement. The decrease in crystallinity would lead to a more malleable material with a higher EaB (76). Therefore the difference between the CP22 PP and the XX00199PP most likely is due to the difference in additives, whereas the difference between the AdSint PP and XX0199 PP is more likely due to the polymer itself. A method of testing this would be to post dose the AdSint PP and the X00199 PP with flow additives, then observe the processability and mechanical properties in the HSS process.

In previous research in LS and HSS mechanical properties have been linked to the crystallinity and the degree of particle melt of parts (57, 58). Majewski *et al.* (58) demonstrated a clear linear trend of material properties (UTS and EaB) increasing as crystallinity decreased (enthalpy decreased) until a

full melt was obtained (calculated by DSC and comparison to literature). The trends fitted by Ellis *et al.* (57) are more arbitrary and no data provided relating to the goodness of fit.

The relationship between enthalpy of melting and crystallinity was discussed in Section 8.2.1; where increase in enthalpy represents an increase in crystallinity. The enthalpy of melting ( $\Delta H$ ) was calculated for the central tensile test specimen, compared with the mechanical properties of that test piece. The enthalpy of parts was compared to the mechanical properties of the CP22 PP parts and the AdSint PP parts as these showed the most extreme properties. The relationship between EaB and crystallinity is shown in Figures 8.5 and 8.6.

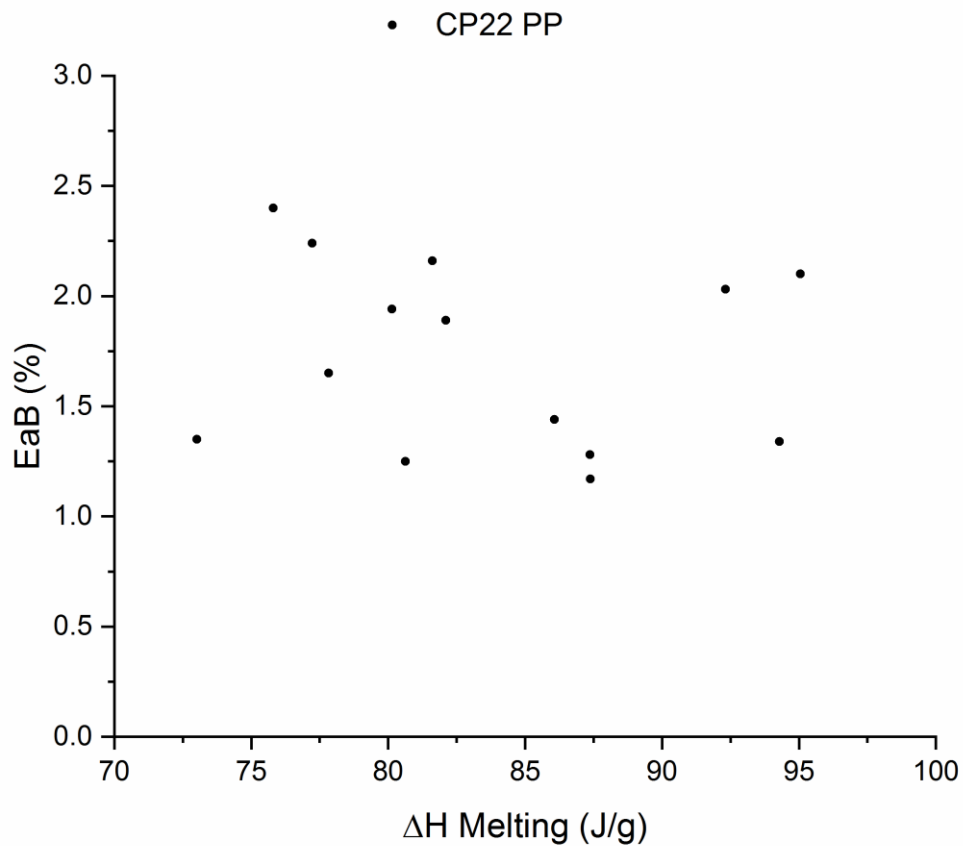


Figure 8.6 Relationship of enthalpy of melting against the EaB of parts manufactured using CP22 PP.

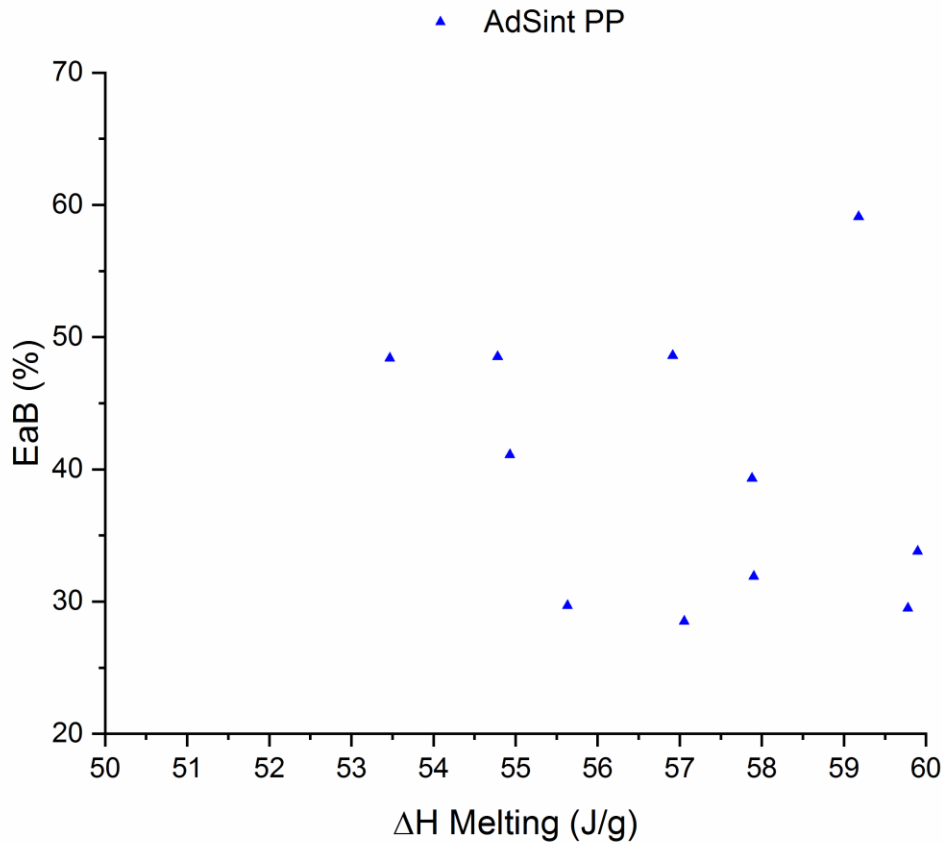


Figure 8.7 Relationship of enthalpy of melting against the EaB of parts manufactured using AdSint PP.

The data sets for AdSint PP and CP22 PP show the expected overall trend with a lower melt enthalpy leading to higher EaB. A linear fit was applied to the data to test if there is a trend present. However, there is no trend within the data sets a linear fit was attempted but it is clear there is no linear trend. R squared (as measure of fit goodness) values are 0.053 for the CP22 PP and 0.026 for the AdSint PP, where a low value of R squared explains little of the variance of the data. The AdSint PP and the CP22 PP although both PP they likely have different chemical composition therefore care should be taken when comparing the polymers.

### 8.3.3 Ultimate Tensile Strength

The Ultimate Tensile Strength (UTS) of the parts were measured, where a higher crystallinity would normally indicate a higher UTS for manufactured parts (76). This was observed for the XX0199PP compared to the AdSint PP where the XX0199PP had a maximum UTS of 25.90 MPa and a melt enthalpy of 80.21 J/g for the powder in comparison to the AdSint PP's maximum UTS of 23.39 MPa and a melt enthalpy of 65.19 J/g. This did not hold true for the CP22 PP, suggesting that the poor sintering nature of this material led to a more dominant negative effect.

As with EaB (see Section 8.3.2) the UTS of parts was compared to the crystallinity of parts by plotting the enthalpy of melting against the UTS of both CP22 PP and AdSint PP in Figure 8.8.

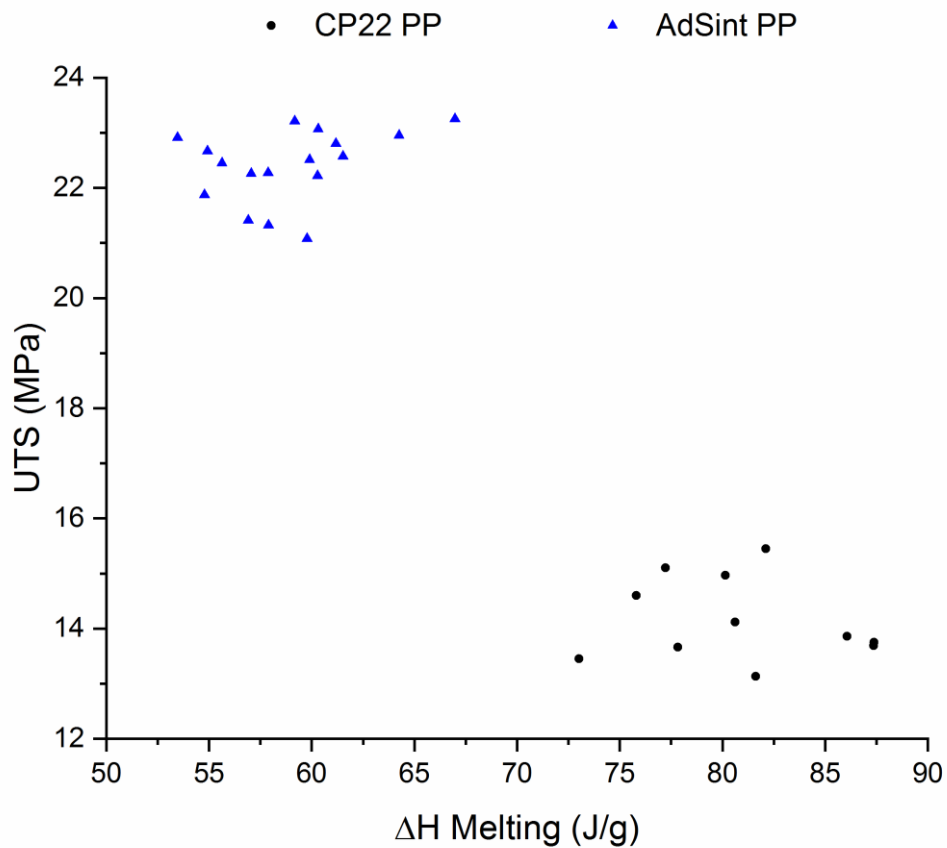


Figure 8.8 Relationship of enthalpy of melting against the UTS of parts manufactured using CP22 PP and AdSint PP.

The overall trend of the CP22 PP having a higher enthalpy of melting but lower UTS is unexpected but as discussed above is likely due to the poor processing. There is no trend shown in the data sets demonstrated by the low values of R squared of 0.108 and 0.120 for the CP22 PP and the AdSint PP respectively.

#### 8.3.4 Young's Modulus

Young's Modulus (YM) was also measured to observe the stiffness of the parts manufactured, with the CP22 PP and XX0199PP not showing any marked difference in their stiffness. However as expected from the crystallinity and polymer differences (129), discussed in Section 8.3.2, the AdSint PP demonstrated a lower YM. The CP22 PP and XX0199PP had YM values of 1394 MPa and 1342 MPa and melt enthalpy values of 80.21 J/g and 80.00 J/g respectively in comparison to AdSint with a YM 977 MPa of and melt enthalpy of 65.19 J/g.

The crystallinity of the parts represented by the enthalpy of melting was compared to the stiffness of the parts represented by the YM, see Figure 8.9.

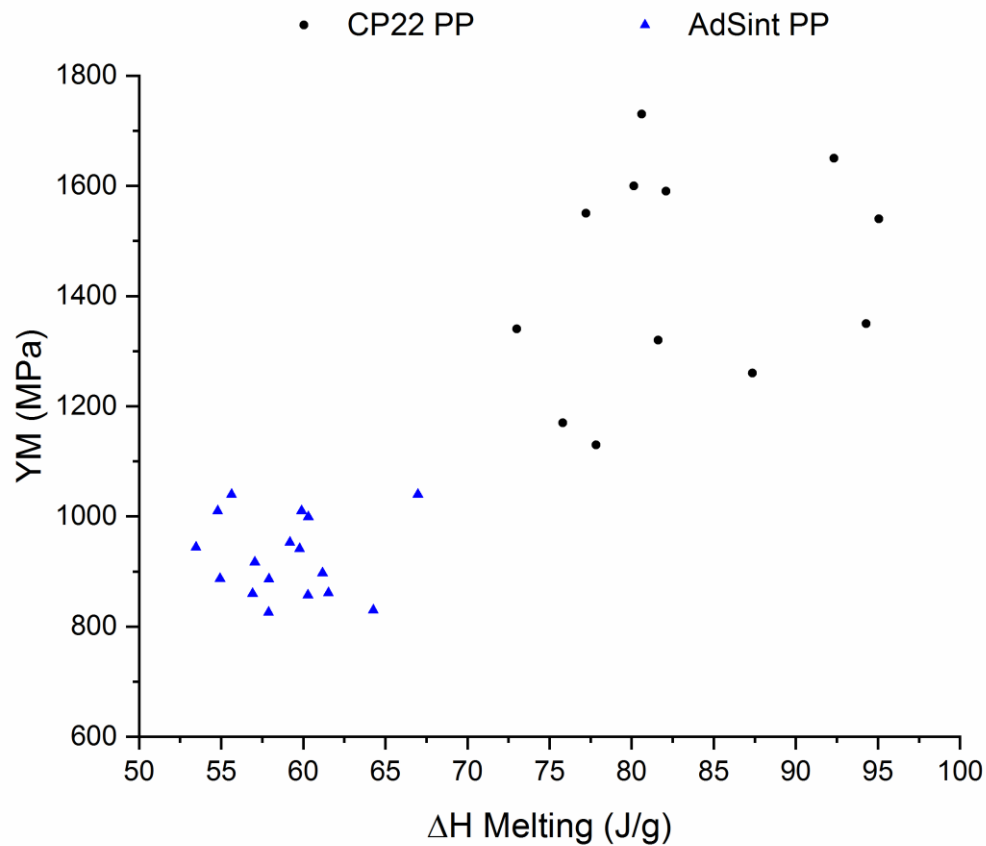


Figure 8.9 Relationship of enthalpy of melting against YM of parts manufactured using CP22 PP and AdSint PP.

Comparison between the data sets shows as expected a higher enthalpy of melting led to an increase in YM. However, in the data sets no trend was observed as represented by the low R squared values of 0.099 and 0.0005 for the CP22 PP and AdSint PP respectively. With more data it may be possible to understand if crystallinity affects the mechanical properties within the specific powder data set.

#### 8.4 Effect of build parameters

In addition to differences in processability and mechanical properties, differences were observed in the effect of build parameter variations and will be discussed here; build bed and overhead temperature, grey level, sinter speed and preheat power.

##### 8.4.1 Build bed and overhead temperature

Build bed temperature has been shown to be critical in the manufacture of parts. Using CP22 PP as a powder feedstock only one temperature was available to process at. XX00199PP allowed a wider build

bed temperature to be used (10 °C), although to process across this range it was required to alter the other parameters used due to dependence of the process parameters on each other, in order to compensate for the energy differences in the process. The AdSint PP material allowed processing across a 6 °C process window, and within a 4 °C window when keeping all build parameters constant. A reason for this is the AdSint PP material is less crystalline than the other PP powders and hence the driving force for parts to fail via curl is less strong. This has clear implications for processability, especially where rigid control of parameters proves difficult. The ability to continue building where temperatures and energy input varies may be advantageous.

For CP22 PP the processing window was found to be extremely narrow and hence repeat builds at identical parameter levels were inconsistent in their success. In contrast the XX00199PP material showed a much wider processing window and the AdSint PP produced multiple repeats.

Although different build bed temperatures were accessible using XX00199PP as a powder feedstock due to the requirement to simultaneously alter the sinter speed no clear correlation can be determined. The AdSint PP displayed increased shrinkage and wall growth as the build bed temperature was increased.

Build bed temperature has been shown to be critical in the processing of all the grades of PP tested. However, from this research the altering of the build bed temperature in this processable range has displayed little effect on the part properties. This is in contrast to previous work by Majewski *et al.* (54) and Hopkinson *et al.* (22) using Nylon as a powder feedstock for HSS. Where all mechanical properties measured increased with increase in build bed temperature, which is also observed in LS with multiple materials by various authors (48, 62). This difference is most likely due to the range being too narrow to observe any significant changes caused by the change in build bed temperature.

#### 8.4.2 Grey level

Various levels of grey level were used to manufacture PP parts, XX00199PP was only processable at two levels (2 and 3) contrasting to CP22 PP and AdSint PP which were both processed at five levels 1-5. Possible reasons for this difference include interaction of the ink with the powder surface causing different flow of the ink hence altering the process. There may be differences in wetting of the ink on the powder surface caused by differences in polarity or surface energy, but these should be studied in further work.

A generic trend of wall growth increasing as grey level was increased is apparent in the dimensional accuracy graphs (Figures 4.15, 6.7 and 7.8) and, although this trend was not always statistically significant the same apparent trend was observed for all powders. This is likely due to the IR absorbing

ink flowing further than intended, hence causing surrounding powder to sinter and increase the wall growth of the measured parts.

The effect of grey level on mechanical properties was studied. For all the grades of PP powders studied a clear relationship was observed, as grey level was increased the UTS decreased, although little or no change was at the lowest grey level. The increase in ink amount could lead to the residuals left by the ink becoming crack propagation sites, therefore lowering the strength of the parts. Alternatively the additional energy input could lead to the polymer degrading and the molecular weight decreasing which would lead to a lower UTS. The EaB did not appear to have a correlation to varying the grey level, whereas in some cases YM showed a decrease with increasing ink amounts.

#### 8.4.3 Sinter speed

The higher the sinter speed, the shorter length of time the IR absorbing ink is exposed to the IR radiation, meaning less heating energy is inputted into the system. This has the opposite effect to increasing the sinter power as studied in other HSS research with various materials (44, 54, 78) or increasing the energy density in a Laser Sintering (LS) (48, 86), but maintaining a constant emission spectrum.

As sinter speed was increased and hence less energy was input via the sintering lamp wall growth and shrinkage decreased, which has been observed previously in HSS (44). Although this was clearly demonstrated for the CP22 PP and XX00199PP an obvious relationship was not observed for the AdSint PP, although high sinter speeds over 100 mm/s were not assessed for this material. Less input energy from the sinter lamp in general leads to greater dimensional accuracy as discussed previously.

CP22 PP shows an increase in mechanical properties as sinter speed is increased, with this correlation most obvious for the UTS measurement although it is also observed for the EaB parameter. This is an apparent contradiction to the relationship observed for the XX0199PP and to a lesser extent the AdSint PP material where an increase in sinter speed led to lower mechanical properties and UTS in particular.

Increasing mechanical properties as energy input from the sinter lamp is increased has previously been observed in HSS (54, 78) and is what would be expected. A trend of fracture strength and EaB plateauing and decreasing with a higher energy density was observed at the highest level of input energy by Caulfield *et al.* (53), where the authors found this was due to the powder being damaged by excess heat from the laser. This was supported by SEM micrographs. It is therefore possible that the CP22 PP is being overheated at the slowest sinter speeds and therefore better mechanical properties are measured at lower sinter lamp energy input levels. Majewski *et al.* (54) demonstrated a more significant increase in mechanical properties as build bed temperature was increased

compared to as sinter power was increased. The CP22 PP was run at a similar sinter speed however required a much higher build bed temperature (see Table 8.3) and possessed a similar decomposition temperature as measured by TGA therefore is more likely to undergo degradation during sintering.

#### 8.4.4 Preheat power

No clear relationship was observed between the preheat power level and the properties of parts produced. As there is a layer of powder between the IR radiation output by the lamp and the IR absorbing ink, the lamp power does not affect the part properties in the ranges tested. However it has been shown the preheat power is critical in the manufacture of parts, where incorrect preheat power leads to either curl when the newly deposited powder causes the part to recrystallise and curl then fail or sinter the powder bed and fail.

UTS has been shown to be the most sensitive measure to the altering of build parameters in HSS, and has shown the greatest repeatability. Demonstrated by having the smallest error bars shown in the graphs plotted.

Two of the powders (CP22 PP and XX00199PP) tested in this work result in relatively brittle parts, with low EaB. A small variability in the results therefore leads to a large percentage error, meaning observing and stating correlations with any level of confidence is more difficult. Large error is also often observed for the Young's Modulus of AM parts.

Build bed temperature and preheat power have been demonstrated to have an effect on the ability to process PP powders in HSS, especially build bed temperature. However neither of the parameters have affected the properties of parts produced when they were altered. Increasing the amount of IR absorbing ink by increasing the grey level leads to a decrease in mechanical properties after a level of 2. Sinter speed was shown to effect the properties of parts produced as it was changed, but this change was dependent on the powder used.

The overall energy input into the system has been shown to be critical. When energy is taken out by reducing the energy input from one variable it can be compensated by increasing the energy using another parameter. Rather than classifying the energy input from each parameter, it has been shown to be prudent to consider the energy input cumulatively rather than as individual energy inputs. This would be similar to LS where energy density is used as a cumulative energy measure from the different machine parameters. As discussed in Section 4.4.1, a design of experiment would be ideal to show the parameter dependence in HSS. However this was not possible to complete the builds at the required parameter levels.

The work carried out in this thesis has examined three different grades of PP, which worked with varying levels of success and various explanations have been offered for the differences observed. The following chapter will draw this research together and provide final conclusions and recommendations for further work.

## Chapter 9 Conclusions and further work

### 9.1 Conclusions

This work has shown, for the first time, that it is possible to process polypropylene within the High Speed Sintering process. Table 9.1 demonstrates the mechanical properties observed for PP using differing manufacture manufacturing methods, it should be noted that it was not possible to compare the same material across techniques.

*Table 9.1 Mechanical properties of PP in different manufacturing techniques, data from Polymer Handbook (82, 94) for IM. The LS data is from Kleijnen et al.(111). The HSS data is from this thesis, standard deviations are shown for work carried out in this thesis.*

Material	UTS (MPa)	EaB (%)	YM (MPa)
Injection Moulded PP	35.5	150	1380
CP22 PP in LS	12.5	1.0	1990
CP22 PP in HSS	25.9 (0.28)	6.99 (0.68)	1342 (188)
AdSint PP in HSS	23.39 (0.17)	59.33 (13.65)	977 (65)

As shown above in Table 9.1 when the same material was used in both LS and HSS, higher UTS and EaB were obtained using the HSS process. This is likely due to the powder particles being sintered together more completely than was obtained in the LS process.

Through testing on three separate PP materials it has been identified that several key characteristics have a major effect on processability and mechanical properties, with only one of the grades producing parts with mechanical properties which may be suitable for the production of FMCGs. Key conclusions from this study are as follows:

- Effect of material selection.

AdSint PP was the best performing grade of PP tested, with mechanical properties of UTS of 23.4 MPa (SD 0.17), EaB of 59.3 % (SD 13.7) and YM of 977 MPa (SD 65). This was an increase of 2591 % in EaB from the other commercial PP (CP22) and an increase of 849 % from a pre-commercial grade (XX0199PP). The chemical structure of the AdSint PP material was suggested to be different from the other grades of PP with a lower crystallinity and melt temperature therefore producing different material properties as well as mechanical properties in the end parts.

- Effect of processing parameters.

The processing windows of the AdSint PP and the XX0199PP grade were found to be significantly larger than the CP22PP, which is likely to be due to the difference in quantity of flow additives of the material.

In general, increasing input energy led to an increase in mechanical properties, where UTS was the mechanical property most affected. Build bed temperature was demonstrated to have a large effect on the processing of PP to find a viable process window, however no obvious effect was observed on the mechanical properties. This is due to the CP22 PP material only being processable at one bed temperature, the XX00199PP required other parameters to be varied to be able to change the temperature. This means the AdSint PP material is the most robust to process variations. The effect of processing parameters has been shown, and this result for PP in HSS tallies with previous literature as discussed in Section 2.3.1 as more lamp energy was input mechanical properties increased.

The grey level (amount of IR absorbing ink) was also varied and its effect studied. Above a certain point, an increase in grey level led to a decrease in mechanical properties. This phenomenon was also observed for Nylon by Noble *et al.*(55). Potential reasons for this have been identified as excess ink causing localised overheating and degradation of the polymer or more inclusions in the part acting as potential fracture sites.

The effect of the sinter speed was also studied, where different correlations were observed for the different PP powders. The CP22 PP showed an increase in mechanical properties as sinter speed was increased, whereas XX0199PP and to a lesser extent AdSint PP showed a decrease in mechanical properties as sinter speed was increased. This is because the energy input into the system markedly more for CP22 PP in comparison to the other grades and is hence likely overheating and degrading.

- Effect of additives.

The size distribution and shape of the CP22 PP grade would indicate poor powder flowability, but this was the only grade to exhibit a positive result during flow tests. It was therefore theorised that this grade contained a relatively large quantity of flow agent. Evidence from TGA analysis and SEM images supports this theory, and explains the differences between the PP grades tested. Published literature and other anecdotal evidence suggests that this is a likely reason for the differences observed in mechanical properties and processability.

- Effect of powder age.

It was demonstrated that one grade of PP can be reused with no requirement for refreshing with virgin powder, without significant degradation of mechanical properties. The reasoning for this lack of change compared to Nylon was due to the chemical reactivity difference between PP and Nylon. This has significant cost and sustainability implications, enabling unsintered powder to be reused to a greater extent than in other HSS materials such as Nylon-12.

- Practical significance.

PP was identified as an appropriate material for investigation in HSS with respect to the FMCG industry because due to its possibility of good mechanical properties, low cost and compatibility with HSS. This work has shown that the choice of PP grade has a significant effect on processability and mechanical properties. Of the materials investigated, AdSint PP is the most appropriate choice currently for the production of FMCGs via HSS, partly through its higher mechanical properties, and partly due to its greater ease of processing. The learning developed from this work should also help the assessment of future grades of PP as they become available.

This work has demonstrated the use of PP in HSS. As well as this contribution other significant portions of work have been achieved; these include a thorough investigation into commodity thermoplastics and the opportunity to be used in HSS, see Section 3.2.5. A process has been described to assess polymers in HSS, see Figure 3.1. In addition to this multiple grades of PP have been assessed and compared to find the reasons for the processing differences between the grades as discussed in Chapter 8. The first investigation into powder ageing has also been carried out in HSS was in Chapter 5, where no significant change in mechanical properties were observed as the powder aged unlike shown for nylon in LS.

## 9.2 Recommendations for future work

As this was the first time PP has been investigated in HSS, there remain several areas for further work, as discussed here.

- Effect of crystallinity.

Through characterisation of the starting materials it was apparent the best performing material was significantly different to the other materials tested in certain areas such as melting and recrystallisation temperatures and enthalpies. This in turn suggests that the AdSint PP is a copolymer.

A different way of modifying these parameters is by changing the tacticity from a commercial iso-tactic polymer to a polymer which has more syndiotactic or atactic nature which would change the crystallinity of the polymer powder feedstock. Crystallinity is known to have an effect on processing and mechanical properties in PBF systems, and it would therefore be of interest to study how the crystallinity of PP affects the properties and processing in HSS.

- Further study of the effect of flow agent and other additives.

There are various grades of PP available commercially; however these grades do not come in a form usable in powder bed fusion (PBF). To convert them into usable forms powders often go through a

grinding process leading to poor powder size and shape distributions, which in turn leads to poor flow as observed in materials such as CP22 PP and work by Lexow *et al.* (75). Flow agents are therefore often added to counter this effect, although there is some evidence to suggest that the quantity of these should be minimised. The study of the effect of flow agent on the mechanical properties of PP parts in HSS is therefore crucial to ensure good quality powders and parts. In particular, identifying the optimum level of flow agent to aid processability but maintain high quality parts would provide a valuable addition to current knowledge.

In addition, the only research in HSS to date on flow agents has been the effect of fumed silica (78), but it may be possible to use a range of flow agents including glass, hydroxyapatite and calcium carbonate as well as different grades of silica powders (72).

- Powder aging for a range of PP materials.

It has been demonstrated that powder age had little to no effect on the properties of parts produced using CP22 PP as the powder feedstock. However further confirmation is needed as to whether this is due to the specific material grade, or is true for PP in general. Future work should therefore include the study of powder age on other grades of PP.

- Finer study of the effect of grey level.

In this research grey level was assessed in discrete levels due to the use of drop per dot system in employed by the printheads used. The utilisation of this system would allow the manufacture of parts using smaller increments of ink volume increase to sinter parts. With further knowledge of this effect parts could be manufactured with functional grading with different mechanical properties in different areas of the part where the amount of ink used was varied to alter the properties.

- Surface finish and post-processing of HSS PP parts.

The focus of this study was on processability and mechanical properties when using PP in the HSS process. However, surface finish is also a key consideration for end-use parts, and should be investigated through surface roughness measurements. Post-processing is a necessary requirement for parts manufactured using HSS, and powder removability should also be investigated in order to confirm that a sufficient level can be reached ensure suitability for end-use parts. The ability of other post-processing techniques such as surface polishing and colouring of parts will also be of interest moving forwards.

Further general areas for future work in HSS include a study into factors relating to temperature in HSS. These include what is the peak temperature of black ink, when the lamp passes over the printed

area in HSS? Development of a method to quantify the energy input via the differing mechanisms in HSS, to input energy into the system. Akin to energy density and energy melt ratio in LS, see Section 2.3. Investigation into if a finer control of temperature allows processing of materials with a narrower process window as well as an increase in repeatability of results.

HSS uses an infrared absorbing ink and infrared lamps to heat the powder to cause the powder to selectively sinter. The interaction of this ink with the powder has not previously been researched. How the ink interacts with powders is likely to change with different powder materials and surface treatments of the powders, as the wetting of the ink will change dependant on the powder. This wetting will drive how the powder flows across the powder and therefore how the ink absorbs IR energy and then imparts it to the powder.



## Chapter 10 References

1. ASTM. Standard Terminology for Additive Manufacturing Technologies. ASTM F2792-12A: ASTM International; 2012.
2. Gibson I, Rosen DW, Stucker B. Additive manufacturing technologies: Springer; 2010.
3. Wohlers T. Wohlers Report 2017: 3D Prnting and Additive Manufacturing State of the Industry Annual Worldwide Progress Report. Wohlers Associates, Inc; 2017.
4. Wohlers T. Wohlers Report 2015: 3D Prnting and Additive Manufacturing State of the Industry Annual Worldwide Progress Report. Wohlers Associates, Inc; 2015.
5. Crookston JJ, Long AC, Bingham GA, Hague RJM. Finite-element modelling of mechanical behaviour of rapid manufactured textiles. Proceedings of the Institution of Mechanical Engineers, Part L: Journal of Materials Design and Applications. 2008;222(1):29-36.
6. Johnson A, Bingham GA, Wimpenny DI. Additive manufactured textiles for high-performance stab resistant applications. Rapid Prototyping Journal. 2013;19(3):199-207.
7. Hopkinson N, Gao Y, McAfee DJ. Design for environment analyses applied to rapid manufacturing. Proceedings of the Institution of Mechanical Engineers, Part D: Journal of Automobile Engineering. 2006;220(10):1363-72.
8. Khajavi SH, Partanen J, Holmström J. Additive manufacturing in the spare parts supply chain. Computers in Industry. 2014;65(1):50-63.
9. Porsche. Classic parts from a 3D printer Porsche Newsroom: Porsche; 2018 [updated 12/2/2018. Available from: <https://goo.gl/xXZp8A>.
10. GE Reports. 3D -Printing Flight: The Journey Begins 2017 [Available from: <https://gereports.ca/3d-printing-flight-journey-begins/#>.
11. Molitch-Hou M. Adidas uses Carbon's 3D printing to mass-produce Futurecraf 4D shoes engineering.com: engineering.com; 2017 [Available from: <https://www.engineering.com/3DPrinting/3DPrintingArticles/ArticleID/14691/Adidas-Uses-Carbons-3D-Printing-to-Mass-Produce-Futurecraft-4D-Shoes.aspx>.
12. BMW. MINI Yours customised; from the original to the personalised unique special BMW Press2017 [Available from: <https://www.press.bmwgroup.com/global/article/detail/T0276990EN/mini-yours-customised:-from-the-original-to-the-personalised-unique-special?language=en>.
13. Collins English Dictionary. HarperCollins Publishers; 2018.
14. Wohlers T. Wohlers Report 2015: 3D Prnting and Additive Manufacturing State of the Industry Annual Worldwide Progress Report; History of Additive Manufacturing. Wohlers Associates, Inc; 2015.
15. Images produced by Theo Doncaster, The University of Sheffield.
16. Mearian L. Review: Formlabs Form1+ 3D printer offers mind blowing precision. Computerworld. 2015 May 19, 2015.
17. Lumb D. The Top Nine Consumer 3-d Printers For Every Budget. 2013.
18. Camillo J. 3D-Printed Tools aid Assemblers at VW Autoeuropa Plant Assembly Magazine2018 [Available from: <https://www.assemblymag.com/articles/94387-d-printed-tools-aid-assemblers-at-vw-autoeuropa-plant>.
19. Prater TJ, Bean QA, Beshears RD, Rolin TD, Werkheiser NJ, Ordonez EA, et al. Summary report on phase I results from the 3D printing in zero g technology demonstration mission, volume I. 2016.
20. Sachs EM, Haggerty JS, Cima MJ, Williams PA. Three-dimensional printing techniques. Google Patents; 1993.
21. Hopkinson N, Dicknes P. Analysis of rapid manufacturing—using layer manufacturing processes for production. Proceedings of the Institution of Mechanical Engineers, Part C: Journal of Mechanical Engineering Science. 2003;217(1):31-9.
22. Hopkinson N, Erasenthiran P. High speed sintering - early research into a new rapid manufacturing process. Solid Freeform Fabr Symp Proc. 2004:312-20.

23. Erasenthiran P, Hopkinson N. Method and apparatus for combining particulate material. Google Patents; 2005.
24. MAPP Hub. Large Volume, Multi-Material High Speed Sintering Machine MAPP Hub Website2017 [Available from: <https://mapp.ac.uk/projects/large-volume-multi-material-high-speed-sintering-machine>].
25. Yusoff WAYW. An investigation of the “orange peel” phenomenon: Cardiff University; 2007.
26. HP Development Company. Technical white paper: HP Multi Jet Fusion technology2016 22 September 2017:[7 p.].
27. O'Connor HJ, Dickson AN, Dowling DP. Evaluation of the mechanical performance of polymer parts fabricated using a production scale multi jet fusion printing process. Additive Manufacturing. 2018;22:381-7.
28. Morales-Planas S, Minguella-Canela J, Lluma-Fuentes J, Travieso-Rodriguez JA, García-Granada A-A. Multijetfusion Manufacturing Parameters for Watertightness, Strength and Tolerances. Preprints. 2018(2018070308).
29. Sintermask GmbH. Media Release fabbster.com/2015 [
30. Khoshnevis B, Asiabanpour B, Mojdeh M, Palmer K. SIS – a new SFF method based on powder sintering. Rapid Prototyping Journal. 2003;9(1):30-6.
31. Blueprinter. Blueprinter website blueprinter-powder-3dprinter.co.uk/2015 [
32. Baumers M, Tuck C, Hague R. Selective Heat Sintering Versus Laser Sintering: Comparison Of Deposition Rate, Process Energy Consumption And Cost Performance. 26th Annual International Solid Freeform Fabrication Symposium, SFF 2015; Austin, Texas2015.
33. Kruth JP, Mercelis P, Van Vaerenbergh J, Froyen L, Rombouts M. Binding mechanisms in selective laser sintering and selective laser melting. Rapid Prototyping Journal. 2005;11(1):26-36.
34. Zarringhalam H, Majewski C, Hopkinson N. Degree of particle melt in Nylon-12 selective laser-sintered parts. Rapid Prototyping Journal. 2009;15(2):126-32.
35. Khalil Y, Hopkinson N, Kowalski A, Fairclough JPA. Influence Of Laser Power on Morphology And Properties Of Laser-Sintered UHMWPE. 27th Annual International Solid Freeform Fabrication Symposium, SFF 2016; Austin, Texas2016. p. 814 - 33.
36. Fox L, Ellis A, Hopkinson N. Use of an Alternative Ink in the High Speed Sintering Process. 26th Annual International Solid Freeform Fabrication Symposium, SFF 2015; Austin, Texas2015.
37. Bellehumeur CT. Polymer sintering and its role in rotational molding: McMaster University; 1997.
38. Narkis M, Rosenzweig N. Polymer powder technology: Wiley; 1995.
39. Vasquez M, Hopkinson N, Haworth B. Laser sintering processes: practical verification of particle coalescence for polyamides and thermoplastic elastomers. Annu Tech Conf Soc Plast Eng. 2011;69th(Vol. 3):2458-62.
40. Ellis A, Hadjiforados A, Hopkinson N, Reinhold I. Speed and Accuracy of High Speed Sintering. NIP & Digital Fabrication Conference. 2015;2015(1):303-6.
41. Fahad M, Hopkinson N. Evaluation and comparison of geometrical accuracy of parts produced by sintering-based additive manufacturing processes. The International Journal of Advanced Manufacturing Technology. 2017;88(9):3389-94.
42. Ellis A, Brown R, Hopkinson N. The effect of build orientation and surface modification on mechanical properties of high speed sintered parts. Surface Topography: Metrology and Properties. 2015;3(3):034005.
43. Thomas HR, Hopkinson N, Erasenthiran P. High speed sintering - continuing research into a new rapid manufacturing process. Solid Freeform Fabr Symp Proc. 2006:682-91.
44. Majewski CE, Oduye D, Thomas HR, Hopkinson N. Effect of infra-red power level on the sintering behaviour in the high speed sintering process. Rapid Prototyping Journal. 2008;14(3):155-60.
45. Ajoku U, Saleh N, Hopkinson N, Hague R, Erasenthiran P. Investigating mechanical anisotropy and end-of-vector effect in laser-sintered nylon parts. Proceedings of the Institution of Mechanical Engineers, Part B: Journal of Engineering Manufacture. 2006;220(7):1077-86.

46. Norazman F, Smith P, Hopkinson N. Spectral Analysis of Infrared Lamps for Use in the High Speed Sintering Process. 27th Annual International Solid Freeform Fabrication Symposium, SFF 2016; Austin, Texas 2016.
47. Rouholamin D, Hopkinson N. Understanding the efficacy of micro-CT to analyse high speed sintering parts. *Rapid Prototyping Journal*. 2016;22(1):152-61.
48. Ho HCH, Gibson I, Cheung WL. Effects of energy density on morphology and properties of selective laser sintered polycarbonate. *Journal of Materials Processing Technology*. 1999;89-90:204-10.
49. Khalil Y, Kowalski A, Hopkinson N. Influence of energy density on flexural properties of laser-sintered UHMWPE. *Additive Manufacturing*. 2016;10:67-75.
50. Starr TL, Gornet TJ, Usher JS. The effect of process conditions on mechanical properties of laser-sintered nylon. *Rapid Prototyping Journal*. 2011;17(6):418-23.
51. Beal VE, Paggi RA, Salmoria GV, Lago A. Statistical evaluation of laser energy density effect on mechanical properties of polyamide parts manufactured by selective laser sintering. *Journal of Applied Polymer Science*. 2009;113(5):2910-9.
52. Williams JD, Deckard CR. Advances in modeling the effects of selected parameters on the SLS process. *Rapid Prototyping Journal*. 1998;4(2):90-100.
53. Caulfield B, McHugh PE, Lohfeld S. Dependence of mechanical properties of polyamide components on build parameters in the SLS process. *J Mater Process Technol*. 2007;182(1-3):477-88.
54. Majewski CE, Hobbs BS, Hopkinson N. Effect of bed temperature and infra-red lamp power on the mechanical properties of parts produced using high-speed sintering. *Virtual and Physical Prototyping*. 2007;2(2):103-10.
55. Noble C, Ellis A, Hopkinson N. Effect of Greyscale/Print Density on the Properties of High Speed Sintered Nylon 12. 25th Annual International Solid Freeform Fabrication Symposium, SFF 2014 2014.
56. Ellis A, Hartley L, Hopkinson N. Effect of Print Density on the Properties of High Speed Sintered Elastomers. *Metallurgical and Materials Transactions A*. 2015;46(9):3883-6.
57. Ellis A, Noble CJ, Hopkinson N. High Speed Sintering: Assessing the influence of print density on microstructure and mechanical properties of nylon parts. *Additive Manufacturing*. 2014;1-4(0):48-51.
58. Majewski CE, Zarringhalam H, Hopkinson N, editors. Effects of degree of particle melt and crystallinity in SLS Nylon-12 parts. 19th Annual International Solid Freeform Fabrication Symposium, SFF 2008; 2008.
59. Zarringhalam H. Investigation into crystallinity and degree of particle melt in selective laser sintering [PhD Theses]: Loughborough University; 2007.
60. Gao W, Zhang Y, Ramanujan D, Ramani K, Chen Y, Williams CB, et al. The status, challenges, and future of additive manufacturing in engineering. *Computer-Aided Design*. 2015;69:65-89.
61. Tontowi AE, Childs THC. Density prediction of crystalline polymer sintered parts at various powder bed temperatures. *Rapid Prototyping Journal*. 2001;7(3):180-4.
62. Gibson I, Shi DP. Material properties and fabrication parameters in selective laser sintering process. *Rapid Prototyping Journal*. 1997;3(4):129-36.
63. Ku CWJ, Gibson I, Cheung WL. Selective laser sintered Castform polystyrene with controlled porosity and its infiltration by red wax. 13th Annual International Solid Freeform Fabrication Symposium, SFF 2002; 2002; Austin Texas: University of Texas.; 2002.
64. Amel H. Investigating the Cyclic Performance of Laser Sintered Nylon 12 [Doctoral Thesis]: University of Sheffield; 2015.
65. Kruth J-P, Levy G, Schindel R, Craeghs T, Yasa E, editors. Consolidation of polymer powders by selective laser sintering. *Proceedings of the 3rd International Conference on Polymers and Moulds Innovations*; 2008.
66. Wohlers T. Wohlers Report 2014: 3D Printing and Additive Manufacturing State of the Industry Annual Worldwide Progress Report, German Edition. Wohlers Associates, Inc; 2014. p. 114.

67. 3D Systems Corporation. DuraForm® EX Plastic. [paramountind.com/selective-laser-sintering-material.html](http://paramountind.com/selective-laser-sintering-material.html): 3D Systems Corporation; 2008.
68. EOS GmbH - Electro Optical Systems. PA 2200 Balance 1.0 Data Sheet. [materialdatacenter.com](http://materialdatacenter.com): EOS GmbH; 2010.
69. Goodridge RD, Tuck CJ, Hague RJM. Laser sintering of polyamides and other polymers. *Progress in Materials Science*. 2012;57(2):229-67.
70. Schmid M, Amado A, Wegener K. Materials perspective of polymers for additive manufacturing with selective laser sintering. *J Mater Res*. 2014;29(17):1824-32.
71. Kruth JP, Wang X, Laoui T, Froyen L. Lasers and materials in selective laser sintering. *Assembly Automation*. 2003;23(4):357-71.
72. Berretta S, Ghita O, Evans KE, Anderson A, Newman C, editors. Size, shape and flow of powders for use in Selective Laser Sintering (SLS). *Proceedings of the 6th International Conference on Advanced Research in Virtual and Rapid Prototyping*; 2013 1-5 October, 2013; Leiria, Portugal: CRC Press.
73. Fu X, Huck D, Makein L, Armstrong B, Willen U, Freeman T. Effect of particle shape and size on flow properties of lactose powders. *Particuology*. 2012;10(2):203-8.
74. Berretta S, Ghita O, Evans KE. Morphology of polymeric powders in Laser Sintering (LS): From Polyamide to new PEEK powders. *European Polymer Journal*. 2014;59(0):218-29.
75. Lexow MM, Drummer D. New Materials for SLS: The Use of Antistatic and Flow Agents. *Journal of Powder Technology*. 2016;2016:9.
76. Brydson JA. *Plastics materials*. Seventh Edition ed: Elsevier; 1999.
77. Ellis A, Noble CJ, Hartley L, Lestrangle C, Hopkinson N, Majewski C. Materials for high speed sintering. *J Mater Res*. 2014;29(17):2080-5.
78. Norazman F, Hopkinson N. Effect of Sintering Parameters and Flow Agent on the Mechanical Properties of High Speed Sintered Elastomer. *Journal of Manufacturing Science and Engineering Special Issue: Additive Manufacturing (AM) and 3D Printing*. 2014.
79. Norazman F, Smith P, Ellis A, Hopkinson N. Smoother and stronger high speed sintered elastomers through surface modification process. *International Journal of Rapid Manufacturing*. 2017;6(2-3):155-69.
80. Schmidt M, Pohle D, Rechtenwald T. Selective laser sintering of PEEK. *CIRP Annals - Manufacturing Technology*. 2007;56(1):205-8.
81. Wegner A. New Polymer Materials for the Laser Sintering Process: Polypropylene and Others. *Physics Procedia*. 2016;83:1003-12.
82. Mark JE. *Polymer Data Handbook (2nd Edition)*: Oxford University Press; 2009.
83. Norazman F, Beaumont D, Zanten JV, Ellis A, Hopkinson N. The Effect of Surface Modification on Mechanical Properties of High Speed Sintered Elastomers. *14th Rapid Design, Prototyping & Manufacturing Conference Loughborough 2015*.
84. Plastic News. *Plastic News Resin Pricing* [plasticnews.com](http://plasticnews.com): Plastic News; 2015 [
85. Goodridge RD, Hague RJM, Tuck CJ. An empirical study into laser sintering of ultra-high molecular weight polyethylene (UHMWPE). *Journal of Materials Processing Technology*. 2010;210(1):72-80.
86. Khalil Y, Kowalski A, Hopkinson N. Influence of laser power on tensile properties and material characteristics of laser-sintered UHMWPE. *Manufacturing Rev*. 2016;3.
87. Rietzel D, Kuehnlein F, Drummer D. Characterization of new thermoplastics for additive manufacturing by selective laser sintering. *Annu Tech Conf - Soc Plast Eng*. 2010;68th:2247-53.
88. Rimell JT, Marquis PM. Selective laser sintering of ultra high molecular weight polyethylene for clinical applications. *J Biomed Mater Res*. 2000;53(4):414-20.
89. Zhu W, Yan C, Shi Y, Wen S, Han C, Cai C, et al. Study on the selective laser sintering of a low-isotacticity polypropylene powder. *Rapid Prototyping Journal*. 2016;22(4):621-9.
90. Wegner A, Ünlü T. POWDER LIFE CYCLE ANALYSES FOR A NEW POLYPROPYLENE LASER SINTERING MATERIAL. 2016.

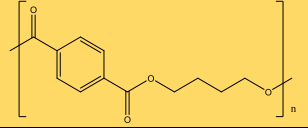
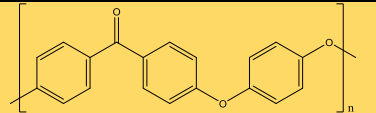
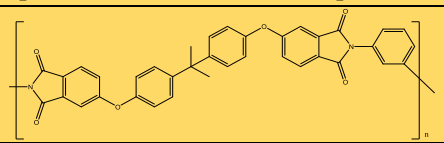
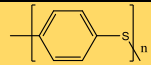
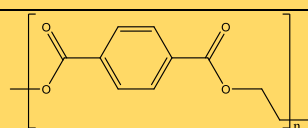
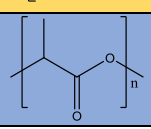
91. Kleijnen RG, Schmid M, Wegener K, Holzer CH, Payer M, editors. Nucleation and impact modification of polypropylene laser sintered parts. Polymer Processing Society Conference; 2015 21-25 September 2015; Graz, Austria: AIP Publishing.
92. Fiedler L, Correa LOG, Radusch H-J, Wutzler A, Gerken J. Evaluation of Polypropylene Powder Grades in Consideration of the Laser Sintering Processability. *Zeitschrift Kunststofftechnik / Journal of Plastics Technology*. 2007;3(4):1-14.
93. Drummer D, Rietzel D, Kuehnlein F. Development of a characterization approach for the sintering behavior of new thermoplastics for selective laser sintering. *Phys Procedia*. 2010;5(Pt. 2):533-42.
94. Hindle C. Polypropylene (PP): British Plastics Federation; 2018 [Available from: <http://www.bpf.co.uk/plastipedia/polymers/PP.aspx>].
95. Wegner A, Witt G, editors. Materials in Laser Sintering: Availability, Characteristics and New Developments. Inside 3D Printing Conference and EXPO; 2015; Berlin, Germany.
96. Zhu W, Yan C, Shi Y, Wen S, Liu J, Shi Y. Investigation into mechanical and microstructural properties of polypropylene manufactured by selective laser sintering in comparison with injection molding counterparts. *Materials & Design*. 2015;82:37-45.
97. Schmid M, Kleijnen R, Vetterli M, Wegener K. Influence of the Origin of Polyamide 12 Powder on the Laser Sintering Process and Laser Sintered Parts. *Applied Sciences*. 2017;7(5):462.
98. Drummer D, Wudy K, Kuehnlein F, Drexler M. Polymer blends for selective laser sintering: material and process requirements. *Phys Procedia*. 2012;39:509-17.
99. Geca P. Assessment of TPUs For Use in The Laser Sintering Process. 2016.
100. U.S. Pharmacopeia. <616> Bulk Density and Tapped Density of Powders. <http://www.usp.org/harmonization-standards/pdg/general-chapters/bulk-density-and-tapped-density-of-powers2012>.
101. Cooke A, Slotwinski J. Properties of metal powders for additive manufacturing: a review of the state of the art of metal powder property testing: US Department of Commerce, National Institute of Standards and Technology; 2012.
102. Amado A, Schmid M, Levy G, Wegener K. Advances in SLS powder characterization. *Group*. 2011;7(10):12.
103. Ziegelmeier S, Wöllecke F, Tuck C, Goodridge RD, Hague R, editors. Characterizing the bulk & flow behaviour of LS polymer powders2013 2013.
104. Rosser L. Design and manufacture of powder flow analysis equipment for Additive Manufacturing [MEng]: University of Sheffield; 2014.
105. Guo A, Beddow JK, Vetter AF. A simple relationship between particle shape effects and density, flow rate and Hausner ratio. *Powder Technology*. 1985;43(3):279-84.
106. Schmid M, Amado F, Levy G, Wegener K, editors. Flowability of Powders for Selective Laser Sintering (SLS) investigated by Round Robin Test. High Value Manufacturing: Advanced Research in Virtual and Rapid Prototyping; 2013 1-5 October 2013; Leiria, Portugal. CRC Press.
107. Grey RO, Beddow JK. On the Hausner Ratio and its relationship to some properties of metal powders. *Powder Technology*. 1969;2(6):323-6.
108. ISO. BS ISO 13320-2009 - Particle size analysis - Laser diffraction methods. 2009.
109. Malvern Instruments Ltd. Morphologi G3 User Manual. <https://www.malvernpanalytical.com/en/learn/knowledge-center/user-manuals/MAN0410EN2015>.
110. Potters Industries. Spheriglass® Solid Glass Microspheres. <http://www.thecarycompany.com/media/pdf/adobe/potters/Spheriglass-TDS.pdf>: Potters Industries LLC; 2013.
111. Kleijnen RG, Schmid M, Wegener K, Holzer CH, Payer M, editors. Nucleation and impact modification of polypropylene laser sintered parts2015 2016: AIP Publishing.
112. Field A. Discovering statistics using IBM SPSS statistics. Third Edition ed: sage; 2013.
113. Noble C. Investigating the effect of print density/greyscale on High Speed Sintered Nylon products' mechanical properties: The University of Sheffield; 2014.

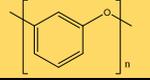
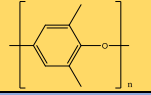
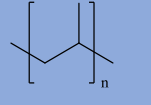
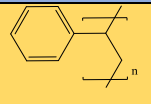
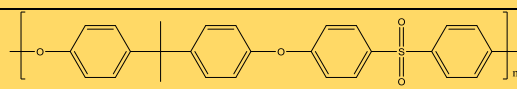
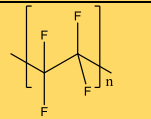
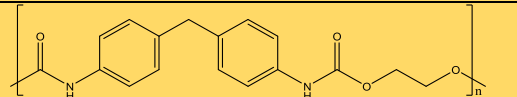
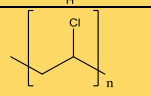
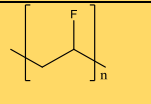
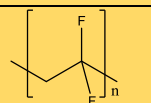
114. Soe SP, Evers DR, Setchi R. Assessment of non-uniform shrinkage in the laser sintering of polymer materials. *The International Journal of Advanced Manufacturing Technology*. 2013;68(1):111-25.
115. ASTM. Standard Test Method for Tensile Properties of Plastics. ASTM D638 – 14: ASTM International; 2014.
116. Gornet TJ, Davis KR, Starr TL, Mulloy KM, editors. Characterization of selective laser sintering materials to determine process stability. *Proceedings of the 13 th International Solid freeform fabrication symposium*; 2002; Austin, Texas.
117. Barry H, Neil H, David H, Xiaotao Z. Shear viscosity measurements on Polyamide-12 polymers for laser sintering. *Rapid Prototyping Journal*. 2013;19(1):28-36.
118. Zarringhalam H, Hopkinson N, Kamperman NF, de Vliieger JJ. Effects of processing on microstructure and properties of SLS Nylon 12. *Materials Science and Engineering: A*. 2006;435–436:172-80.
119. Young RJ, Lovell PA. *Introduction to polymers*: CRC press; 2011.
120. Chen FC, Griskey RG, Beyer GH. Thermally induced solid state polycondensation of nylon 66, nylon 6-10 and polyethylene terephthalate. *AIChE Journal*. 1969;15(5):680-5.
121. Qian S, Igarashi T, Nitta K-h. Thermal degradation behavior of polypropylene in the melt state: molecular weight distribution changes and chain scission mechanism. *Polymer Bulletin*. 2011;67(8):1661-70.
122. Mettler Toledo. *Thermal Analysis of Polymers, Selected Applications* 2013.
123. González-González VA, Neira-Velázquez G, Angulo-Sánchez JL. Polypropylene chain scissions and molecular weight changes in multiple extrusion. *Polymer Degradation and Stability*. 1998;60(1):33-42.
124. Zarringhalam H, Majewski C, Hopkinson N. Degree of particle melt in Nylon-12 selective laser-sintered parts. *Rapid Prototyping Journal*. 2009;15(2):126-32.
125. Hofland EC, Baran I, Wismeijer DA. Correlation of Process Parameters with Mechanical Properties of Laser Sintered PA12 Parts. *Advances in Materials Science and Engineering*. 2017;2017:11.
126. Ou C-F. The crystallization characteristics of polypropylene and low ethylene content polypropylene copolymer with copolyesters. *European Polymer Journal*. 2002;38(3):467-73.
127. Wang ZG, Wang XH, Hsiao BS, Phillips RA, Medellín-Rodríguez FJ, Srinivas S, et al. Structure and morphology development in syndiotactic polypropylene during isothermal crystallization and subsequent melting. *Journal of Polymer Science Part B: Polymer Physics*. 2001;39(23):2982-95.
128. Yamada K, Hikosaka M, Toda A, Yamazaki S, Tagashira K. Equilibrium Melting Temperature of Isotactic Polypropylene with High Tacticity: 1. Determination by Differential Scanning Calorimetry. *Macromolecules*. 2003;36(13):4790-801.
129. Kállay-Menyhárd A, Suba P, László Z, Fekete HM, Mester Á, Horváth Z, et al. Direct correlation between modulus and the crystalline structure in isotactic polypropylene. *Express Polymer Letters*. 2015;9(3):308-20.

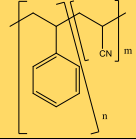
## Chapter 11 Appendix A

Table 11.1 A list of possible polymers for the use in HSS. Polymers identified by blue show a possibility to be used in HSS, polymers identified by yellow have a reason not to be used in HSS and this reason is highlighted in orange. Information collated from (82, 84).

Thermoplastic		Cost (£/kg)	Description	Melting Temperature (°C)	Formula
Acetal Copolymer		4.41-4.71	Lower crystallinity than Homo. Trade name includes: Tecaform	162-173	
Acetal Homo (POM)		5.02-5.22	Polyoxymethylene. Trade names include: Delfrin, Celcon, Ramtal, Duracon, Kepital and Hostaform	175	
Acrylic (PMMA)		4.24-4.41	Amorphous	Tg 106	
Acrylonitrile butadiene styrene (ABS)		4.04-40.7	Amorphous, carcogenic issues	105 Tg	
Cellulosics	Acetate	6.04	Likely to absorb in IR R = CH <sub>3</sub> CO or H	170 - 240	
	Butyrate	5.94	R = H or		
	Propionate	5.94	R = H or		
High Density Polyethylene (HDPE)		3.19-3.26	Little branching	130	
Linear Low Density Polyethylene (LLDPE)		3.02-3.15	High degree of short branches	122	""
Low Density Polyethylene (LDPE)		3.66-3.73	High degree of branching short and long	105 - 115	""
Nylon 6 Nylon 6.6		5.83-5.97 6.17-6.55	Would use Nylon 11/12. Nylon 12 is more than 4x more expensive than 6.6	220	

Thermoplastic	Cost (£/kg)	Description	Melting Temperature (°C)	Formula
Polycaprolactone (PCL)		Low melt temp	60	
Polycarbonate (PC)	7.39-8.24	May absorb in IR see N.I.R spectrum	155	
Polyester (PBT)	4.88-5.05	Not as strong or rigid as PET, IR	223	
Polyetherether ketone (PEEK)	152.63	IR issues	343	
Polyetherimide	29.85	Amorphous	Tg 216	
Polyphenylene sulfide	25.10-25.95		278-280	
Polyethylene terephthalate (PET)	3.02-3.09	Semi-crystalline but can get amorphous, IR	> 250	
Poly(lactic acid) (PLA)	9.78	PLLA 37% crystalline PDLA Increase crystallinity ↑ melt temp	150 - 160 173 - 178 PLLA	

Thermoplastic	Cost (£/kg)	Description	Melting Temperature (°C)	Formula
Polyphenylether (PPE)	4.17-6.34	IR	Tg 211 Tm 268	
Polyphenyloxide (PPO)		IR		
Polypropylene (PP)	3.26-3.36	Isotacticity gives hardness, Majority of PP is Iso Syndo is ≈ 30 % crystalline	171 Pure Iso 160 - 166 Com Iso 130 Syndo	
Polystyrene (PS)	3.90-4.04	Decomposes at lower temp than melt Amorphous	240	
Polysulfone	15.26-22.05	Amorphous	185	
Polytetrafluoroethylene (PTFE)	22.72-25.95		327	
Polyurethane Ester	7.22-7.53	Wide ranging however elastomer so not really useful	190-235	
Polyvinylchloride (PVC)	3.76-3.83	Few % crystalline, Decomposes at 140 °C	160-310	
Polyvinylfluoride (PVF)	In the region of PVDF	Fluorination is normally used to limit reactivity and increase temperature range.	200	
Polyvinylidene fluoride (PVDF)	24.42-25.78		175	

Thermoplastic		Cost (£/kg)	Description	Melting Temperature (°C)	Formula
Styrene-acrylonitrile (SAN)		4.75-5.56	Likely IR Issues	220-270	
Styrene-maleic anhydride (SMA)		6.07-6.21	Likely IR Issues	130-160	
TPE Polyester	Olefinic	4.07-4.58	Low crystalline materials give more elastomeric properties		
	Polyester	11.87-14.41			
	Styrenic	5.09-6.78			
UHMWPE		4.61-4.95	Very long chains n > 100,000	130-136	